

# **Development of Optically Stimulated Luminescence Techniques using Natural Minerals and Ceramics, and their Application to Retrospective Dosimetry**

**Lars Bøtter-Jensen**

**Abstract** This thesis summarises research and development of optically stimulated luminescence (OSL) and its applications by the author at Risø National Laboratory, up to 1999. These developments have been directed primarily at retrospective accident dosimetry and luminescence dating. Experimental investigations include the studies of OSL properties of the natural minerals quartz and feldspars and the artificial materials porcelain and aluminium oxide ( $\text{Al}_2\text{O}_3$ ).

Blue light emitting diodes and infrared laser diodes are shown to provide simple and practical alternatives to broad-band light and visible laser stimulation. The development of OSL apparatus designed for the rapid measurement of single grains of phosphors also opens up a new area of luminescence measurement, allowing the detailed examination of dose distributions within a multiple-grain sample. This is of particular importance to the studies of incompletely reset geological sediments, and to accident dosimetry measurements using unheated materials.

$\text{Al}_2\text{O}_3\text{:C}$  single crystals are tested as environmental OSL dosimeters for assessing both the natural background photon radiation dose rates in the field and the natural dose rates inside bricks collected for accident dose evaluation. Environmental doses of the order of few  $\mu\text{Gy}$  are measured with high precision. UV photo-stimulated luminescence spectra obtained from porcelain samples are used to confirm that the main component responsible for the OSL signal from porcelain is  $\text{Al}_2\text{O}_3$ .

OSL single-aliquot regenerative-dose (SAR) techniques are used with quartz extracted from Chernobyl bricks to determine the accrued dose after the accident. This has improved the measurement precision significantly, from about 5-6 % using traditional methods to now less than 2 %. Depth-dose profiles measured in Chernobyl bricks are compared with those obtained in the laboratory using different gamma sources and these comparisons show that the average energy of the accident radiation was lower than that of  $^{137}\text{Cs}$  photons. It is further demonstrated that doses lower than 50 mGy can be measured using the SAR method with a precision in the order of 2 %.

This thesis was submitted to the University of Copenhagen in September 1999.

Denne afhandling er af Det naturvidenskabelige Fakultet ved Københavns Universitet antaget til offentligt at forsvares for den naturvidenskabelige doktorgrad.

København den 7. September 2000

Henrik Jeppesen

Dekan

This thesis has been accepted by the Faculty of Science, University of Copenhagen, for public defence in fulfilment of the requirements for the degree of Doctor Scientiarum (Doctor of Science).

Copenhagen, 7. September 2000

Henrik Jeppesen

Dean

ISBN 87-550-2755-5

ISBN 87-550-2756-3 (Internet)

ISSN 0106-2840

Information Service Department, Risø, 2000

# Contents

## **Preface and Acknowledgements 5**

## **1 Introduction 9**

## **2 Thermally and Optically Stimulated Luminescence 11**

- 2.1 Introduction 11
- 2.2 Merits of OSL 16
- 2.3 Types of Optical Stimulation 21
- 2.4 Conclusions – TL and OSL 23

## **3 Development of OSL Measurement Technology 23**

- 3.1 Introduction 23
- 3.2 The Recent Instrument Platform 27
- 3.3 Development of Optical Stimulation Sources 31
- 3.4 Monochromators and Spectrometry 48
- 3.5 Development of Single Grain OSL Attachment Systems 55
- 3.6 Other OSL Measurement Systems 66
- 3.7 Conclusions - Instrumentation 70

## **4 OSL Characteristics of Quartz 70**

- 4.1 Introduction 70
- 4.2 The Quartz OSL Decay Curve 71
- 4.3 OSL Signals from Quartz using Different Stimulation Wavelengths 74
- 4.4 The Quartz OSL Response to Linearly Increasing Stimulation Power 78
- 4.5 Relation between TL and OSL Signals from Quartz 80
- 4.6 Luminescence Sensitivity Changes in Quartz as a Result of Annealing 82
- 4.7 Low-Dose OSL Properties of Quartz Extracted from Fired Materials 89
- 4.8 Conclusions - Quartz 93

## **5 OSL Characteristics of Feldspars 94**

- 5.1 Introduction 94
- 5.2 OSL Stimulation Characteristics of Feldspars 94
- 5.3 Emission Characteristics 96
- 5.4 Relation between TL and OSL Signals from Feldspars 99
- 5.5 Thermo-Optical Characteristics of Feldspars 103
- 5.6 Doped Feldspars with Enhanced IRSL Sensitivity 112
- 5.7 Conclusions - Feldspars 114

## **6 OSL Characteristics of Al<sub>2</sub>O<sub>3</sub>:C 114**

- 6.1 Introduction 114
- 6.2 TL Versus OSL from Al<sub>2</sub>O<sub>3</sub>:C 115
- 6.3 OSL Stimulation Characteristics of Al<sub>2</sub>O<sub>3</sub>:C 116
- 6.4 The OSL and TL Responses of Al<sub>2</sub>O<sub>3</sub>:C to Radiation Exposure 117
- 6.5 Low-Dose Field Measurements using Al<sub>2</sub>O<sub>3</sub>:C 119
- 6.6 The Temperature Dependence of OSL from Al<sub>2</sub>O<sub>3</sub>:C 120
- 6.7 Conclusions – Al<sub>2</sub>O<sub>3</sub>:C 124

## **7 OSL Characteristics of Porcelain 125**

- 7.1 Introduction 125

7.2	Samples and Experimental Details	125
7.3	The Origin of OSL from Porcelain	126
7.4	OSL Dose Response of Porcelain	132
7.5	Dose-Depth Profiles in Porcelain and the Effect of Transparency	133
7.6	Conclusions - Porcelain	135

## **8 Retrospective Dosimetry** 135

8.1	Introduction	135
8.2	Materials and Sampling	136
8.3	Sample Preparation and Experimental Details	138
8.4	Determining the Transient Accidental Dose	139
8.5	Development of Analytical Protocols	140
8.6	Retrospective Assessment of Environmental Dose Rates	157
8.7	Evaluation of Dose-Depth Profiles in Bricks	160
8.8	Retrospective Dosimetry - Conclusions	172

## **9 Concluding Remarks** 173

## **10 References** 175

# Preface and Acknowledgements

The idea of this thesis was conceived only recently and was stimulated by a series of recent events in my professional life. Because of these, I thought it would be worth while to write a review of the luminescence research and development carried out at Risø in the last few years.

The first event that inspired me to take stock and summarise luminescence research at Risø was the sudden death in 1997 of my long-standing friend and colleague Vagn Mejdahl. Vagn was the founder and former leader of the Nordic Laboratory for Luminescence Dating at Risø and his death ended an era for me and for many other people involved in luminescence dating. Early in my career, I was lucky enough that Vagn introduced me to the exciting and mysterious world of luminescence phenomena and I had the privilege to work closely with him for nearly a life time. Vagn had already introduced the use of thermoluminescence (TL) in personal dosimetry at Risø. Shortly after being employed there in 1966, I was asked to take over Vagn's position as the radiation health physicist responsible for personal dosimetry and health physics instrument calibration. This was to allow Vagn to devote himself entirely to the establishment of a thermoluminescence dating laboratory, an idea that he had been planning for a while, based on his experience of Martin Aitken's pioneering work at Oxford.

The dramatic and turbulent re-organisation of the departmental structure at Risø in the beginning of the 1990s required a marked reduction of the nuclear research areas. However, the strong collaboration between the Dating Laboratory and the Health Physics Group at Risø (of which I was the leader) during the introduction of the new optically stimulated luminescence (OSL) techniques in dosimetry and dating, conveniently pacified the Risø administration. Our introduction of OSL as a new research direction provoked interest among the management group, and resulted in the transfusion of new life into the Health Physics Instrument Development Group; it thus survived the re-organisation. The very close collaboration between the two laboratories over more than 30 years has resulted in, I think, some outstanding research and development in luminescence methods, instrumentation and measurement protocols. Particularly, the collaboration since 1991 in the development of OSL techniques for a variety of applications in dating and retrospective dosimetry has manifested itself in the large number of original papers published in the primary literature in recent years.

A second source of inspiration has been the experience I gained since the beginning of 1990s by collaborating closely with a number of outstanding scientists who worked in my laboratory at Risø over various periods, either as Ph.D students, postdoctoral fellows or guest scientists. I am extremely grateful to the following persons:

- 1) First of all to Geoff Duller who worked in my laboratory at various times from 1991 to the present, first as a Ph.D student, later as postdoctoral fellow and now as a very experienced research scientist. Geoff and I together pioneered the construction and testing of the first OSL prototype units at Risø and since then we have collaborated very closely in studying a large variety of OSL phenomena.
- 2) Nigel Poolton who worked with me at Risø as a postdoctoral fellow from 1992-1996. Together we worked especially in studies of the relationship between OSL characteristics of quartz and feldspars and their mineralogy.

- 3) Niels Agersnap Larsen whom I had the pleasure of supervising as a Ph.D student in my laboratory from 1994 to 1997. Niels was always a continuous source of inspiration and he contributed significantly to the physical explanation of a number of TL and OSL phenomena.
- 4) Nigel Spooner (and his wife Daniele Questiaux) who worked as a postdoctoral fellow in my laboratory from 1996-1997 and who (both) contributed to the introduction of OSL measurement protocols in retrospective dosimetry and the optimisation of optical filters in OSL measurements.
- 5) Brian Markey who worked in my laboratory as a postdoctoral fellow from 1995-1997 and who contributed especially to important instrument and software improvements to the benefit of our commercial activities.
- 6) Debabrata Banerjee, who worked at Risø as a postdoctoral fellow from 1997-1999. He contributed significantly to our research into improving measurement precision partly by introducing new single aliquot regeneration protocols in retrospective dosimetry.

I want to express my particular gratitude to Steve McKeever who worked as a guest professor in my laboratory for 6 months in 1996 and with whom I have since collaborated actively in a variety of OSL applications, using both experimental and theoretical approaches. The ever-stimulating impact of Steve's luminescence modelling in describing and explaining the experimental results from Risø has provided a source of exciting collaboration and has resulted in the publication of a number of joint papers.

I should also mention the privilege I have had in collaborating with a number of other luminescence researchers around the world. This has come about because of the somewhat unexpected success we have had in the commercialisation of the automated Risø luminescence dating reader. Over the years, this commercial activity has brought me in contact with a number of scientists from around the world with whom I have been able to exchange a lot of experience.

I also wish to express my very special gratitude to Andrew Murray. He became Vagn Mejdahl's successor as leader of the Nordic Laboratory for Luminescence dating at Risø in 1997. Andrew has since then been an inexhaustible source of new ideas and the collaboration with him has brought luminescence research at Risø, I think, into a leading position. In particular, his development of protocols for the single-aliquot regenerative-dose methods and single-grain luminescence analysis have improved the OSL techniques in dating and retrospective dosimetry significantly.

This thesis is a result of my close involvement in the development of OSL techniques and methods particularly since the mid 1990s. A large part of the work is based on the papers I have authored and co-authored, all of which have been published in international journals. The thesis is also intended to provide a technical reference which will, I hope be useful to students interested in OSL phenomena, techniques and methods, and especially in the application of OSL in retrospective dosimetry. The thesis reflects the development work carried out at Risø as a joint effort between me and my various collaborators. Therefore, in cases where the work refers to co-authored papers, I am grateful for these co-authors' written statements, saying that I contributed independently to the work. Let me also here express the hope that I managed to provide useful and productive scientific guidance to the several Ph.D students and postdoctoral fellows I have had the pleasure of supervising over the years.

I also wish to thank Leif Sarholt (University of Copenhagen) and Anders Damkjær (Head of Programme, Risø) for encouraging me to write up this thesis.

Finally, I want to express my genuine gratitude to my colleagues of the Instrument Development Group for their never-failing support. My special thanks

to Henrik Christiansen and Finn Willumsen for their excellent and genuinely pioneering development work with instrumental designs that made both our scientific and commercial activities so succesful, to Finn Jørgensen for his everlasting patience and skilful help with computer technology and for the production of all the figures, to Margit Nielsen for her enthusiastic and skilful help with our burdensome secretarial work and to Jørgen Jakobsen and Finn Pedersen for their excellent and skilful development work and for their many original contributions. The high-quality work carried out by all my colleagues in the instrument group has strongly contributed to transferring of so many scientific ideas into experimental practice. Without these people, the laboratory's reputation would not have been as strong as it is today.

Last but not least I want to thank my wife Marja for her patience and warm support.



# 1 Introduction

This thesis summarises the development work concerned with optically stimulated luminescence (OSL) techniques, methods and instrumentation carried out at Risø in recent years. Experimental investigations include the luminescence properties of natural materials such as quartz and feldspars and ceramic materials such as porcelain and aluminium oxide ( $\text{Al}_2\text{O}_3$ ) under stimulation with narrow-band infrared and visible (blue) as well as broad-band visible (blue-green) photon spectra.

The emphasis of much of the work was to investigate the OSL characteristics of a variety of materials with the aim of retrospectively assessing population doses after nuclear accidents in the past, by measuring the OSL signals from samples collected in the accident areas. The nuclear accident in Chernobyl in 1986 revealed serious public health problems, in that the radiation doses received by the majority of the local population were not known. Since no, or very little, dose monitoring equipment was in operation during the first phases of the nuclear release it was almost impossible to estimate immediately the doses to the different groups of people living around the power plant. In the time following the accident an increasing number of people suffered from radiation induced diseases; in particular, these personnel who had to help restoring the power plant and cleaning up immediately after the accident received large doses. Pilot studies had been carried out in connection with the use of nuclear weapons at Hiroshima in 1945 to retrospectively assess the accrued population doses received by the population using luminescence techniques with house bricks (Haskell et al, 1993). As a result, an EU supported project was initiated to investigate the use of retrospective dosimetry in the estimation of the accident doses to the population in Ukraine and Russia exposed to radiation after the nuclear accident in Chernobyl. The methods studied so far within the EU's third and fourth framework programmes (1992-1998) include (i) modelling based on dose rates measured with active dose rate meters just after the accident, (ii) biological dosimetry based on chromosome analysis of lymphocytes in blood and (iii) solid state dosimetry methods such as electron spin resonance (ESR) with tooth enamel and luminescence methods with ceramics. Risø participated in both framework programmes and suggested in 1992 the use of OSL (rather than TL) methods with ceramics to retrospectively assess accident doses. This was to use minerals extracted from bricks, pottery and porcelain items collected from domestic and industrial locations within the accident area.

The first of the following chapters deals with basic physical processes of different types of luminescence and the potential of using these phenomena in dosimetry. Then the principles of TL, continuous wave OSL, pulsed OSL and the general merits of OSL compared with those of TL are outlined. It is argued that OSL, due to its optical non-destructive nature, has several potential advantages over TL such as higher sensitivity, the possibility of repeated readouts and focused beam stimulation of small samples.

A comprehensive description of the OSL measurement systems developed at Risø over the last few years is then given, which includes a brief outline of the history of the luminescence instrument development. This chapter begins with the development of the automated TL reader and then considers the design and testing of different OSL attachments based on narrow-band infrared and blue light stimulation sources and broad-band (blue-green) stimulation light filtered from incandescent lamps. Recently available blue light emitting diodes (LEDs) have provided a simple and practical alternative to broad-band light and single line laser stimulation. Also recently developed infrared laser-diode stimulation

sources have been tested with excellent results. Different configurations of OSL apparatus developed for the measurements of single sand-sized grains have also been tested. These provide new scope for improved luminescence measurements with enhanced accuracy and should provide important information about poor bleaching and the variations in individual grain sensitivity.

Work carried out with monochromators specifically designed for use with the Risø luminescence reader demonstrated the desirability of routinely investigating both stimulation and emission characteristics of materials with the aim of determining the optimal energy windows within which OSL measurements are carried out.

After the summary of the equipment design, there follow chapters presenting the results of comprehensive investigations of OSL characteristics of quartz, feldspar, porcelain and aluminium oxide ( $\text{Al}_2\text{O}_3$ ). These materials are all relevant in retrospective dosimetry for measuring the accrued accident doses and the environmental dose rates. Stimulation spectra confirmed that using green light extending into the blue is more suitable for stimulating quartz,  $\text{Al}_2\text{O}_3$  and porcelain whereas 830-850 nm infrared light is suitable for excitation of feldspar due to the distinct resonance found in the infrared range for this particular material. The analysis of photo-stimulated luminescence (PL) spectra obtained by illumination of porcelain samples with UV light confirmed that the main component responsible for the OSL signal from porcelain is  $\text{Al}_2\text{O}_3$ ; this is known to be an extremely sensitive OSL dosimeter. Consequently,  $\text{Al}_2\text{O}_3\text{:C}$  single crystals were tested as environmental OSL dosimeters for assessing both the natural background photon radiation dose rates in the field and the natural dose rates inside bricks that were collected for dose evaluation. Environmental doses of the order of a few  $\mu\text{Gy}$ , which equals the natural background dose rate integrated over a few hours, have been measured with high precision.

Finally a broad description is given of OSL techniques applied in retrospective dosimetry. These include sample preparation and the determination of the background dose rate. New OSL measurement protocols based on the single-aliquot regenerative-dose technique are outlined which have improved the measurement precision significantly from typically 5-6 % to now less than 2 %. Depth-dose profiles are measured into brick materials to determine the energy of the radiation from fallout nuclides. Comparing these depth-dose profiles with those obtained in the laboratory using different gamma sources shows that the average energy of the accident radiation was lower than that of  $^{137}\text{Cs}$  photons. Typical data obtained from a variety of samples collected in the Chernobyl accident area further demonstrate that doses as low as 50 mGy can be measured, usually with a precision in the order of 2 %. It is concluded that the recent developments and improvements in OSL methods have made these preferred alternatives to TL techniques in the retrospective assessment of accident doses.

# 2 Thermally and Optically Stimulated Luminescence

## 2.1 Introduction

### 2.1.1 What is luminescence?

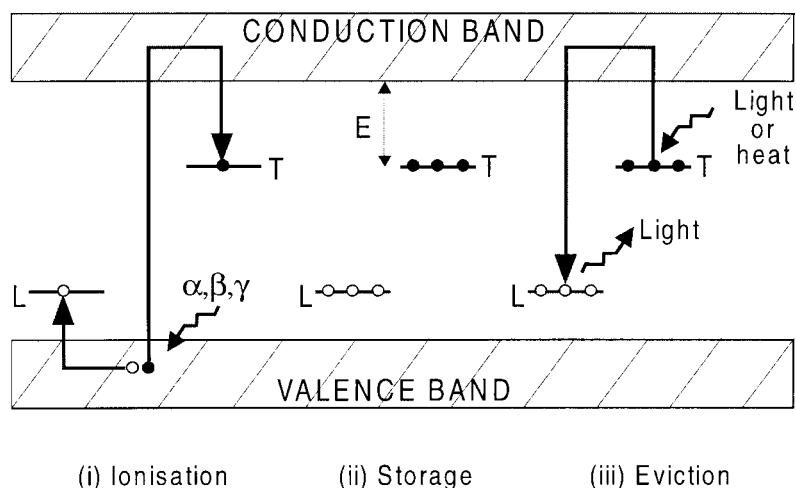
Any light emission is conditional on a preceding excitation of atoms or molecules from a lower to a higher energy state; the exciting energy may be thermal, as in an incandescent filament or non-thermal as is the case in a fluorescent tube. The different processes, by which non-thermal energy transforms into light, are all together called luminescence. Such processes have been used since the middle of this century either for radiation dosimetry, i.e. determination of the integrated radiation dose exposed to humans, or dating archaeological specimens and geological sediments. The assessment of the integrated radiation dose or the event to be dated are thus dependent on the setting to zero of the latent luminescence at some time in the past. This zeroing occurs through heating for some materials such as most radiation dosimeters, archaeological pottery, bricks and porcelain or by exposure to daylight for geological sediments. Subsequently, the latent luminescence signal builds up again through exposure to either radiation from man-made radiation sources or from the weak natural environmental background radiation. Radiation induced luminescence should be distinguished from other luminescence phenomena, e.g. photoluminescence, phosphorescence etc., which are not dose dependent and thus not relevant to dating or dosimetry.

Thus luminescence arises from stimulation, either thermal or optical, of minerals that have been previously exposed to ionising radiation. During exposure, radiation energy is accumulated and stored in the crystal lattice; this energy is stored in the form of electrons that have been trapped at defects in the lattice. During stimulation, the trapped charge is released and as a result the luminescence signal goes to zero. The energy diagrams for luminescence processes representing (i) ionisation due to exposure of a crystal to nuclear radiation, (ii) storage of radiation energy and (iii) stimulation, are given in Fig. 2.1.

### 2.1.2 Thermally stimulated luminescence

Thermally stimulated luminescence, usually termed thermoluminescence (TL), has been used extensively to measure nuclear radiation doses since the early 1950s (Daniels et al, 1953), following the commercial availability of sufficiently sensitive and reliable photomultiplier (PM) tubes. TL was subsequently applied to archaeological dating in the early 1960s (e.g. Aitken et al, 1964,; Aitken et al, 1968,; Mejdahl, 1969) and to geological dating in the beginning of the 1980s (e.g. Wintle and Huntley, 1980). Techniques and methods used in thermoluminescence dating are reviewed by Aitken (1985).

TL is usually observed by heating a sample at a constant rate to some temperature (e.g. 500°C) and recording the luminescence emitted as function of temperature. The TL signal is characterised by a so-called "glow curve", with distinct peaks occurring at different temperatures, which relate to the electron traps present in the sample. Defects in the lattice structure are responsible for these traps. A typical defect may be created by the dislocation of a negative ion, providing a negative ion vacancy that acts as an electron trap. Once trapped, an



T = Electron trap  
L = Luminescence center

Fig. 2.1. Energy-level representation of TL and OSL processes (based on Aitken 1998). (i) Ionisation due to exposure to nuclear radiation with trapping of electrons and holes at defects T and L, respectively. (ii) Storage of radiation energy during time; if leakage is negligible the lifetime of the electrons in the traps needs to be much longer than the storage time of the sample. This lifetime is dependent on the energy depth E of the trap below the conduction band. (iii) By heating or shining light onto the sample, electrons are evicted from the electron traps and some of these reach luminescence centres (L); if so, light (i.e. TL or OSL) is emitted as a result of the process of recombining into these centres.

electron will eventually be evicted by thermal vibrations of the lattice. As the temperature is raised these vibrations get stronger, and the probability of eviction increases so rapidly that within a narrow temperature range trapped electrons are quickly liberated. Some electrons then give rise to radiative recombinations with trapped "holes", resulting in emission of light (TL). A simplified diagram of a set up for measuring TL is shown in Fig. 2.2.a and a typical TL glow curve obtained from a sedimentary feldspar is shown in Fig. 2.2.b. The temperature peaks corresponding to different electron trap depths are clearly seen.

Although a TL glow curve may look like a smooth continuum, it is composed of a number of overlapping peaks derived from the thermal release of electrons from traps of different stabilities. The lifetime of electrons in deep traps is longer than that of electrons in shallow traps. Normally traps giving rise to glow peaks lower than 200°C are not useful for dosimetry as electrons can be drained from these traps over a prolonged time even at environmental temperatures. Stable glow peaks suitable for dosimetry usually occur at 300°C or higher. However, anomalous (i.e. unexpected) fading of high temperature glow peaks at room temperature has been observed in some feldspars. This is explained as a quantum mechanical tunnelling effect (Wintle, 1973).

Another complication in TL measurements is thermal quenching. Some high temperature peaks in quartz and feldspars are subject to thermal quenching pro-

processes, i.e. the increased probability of non-radiative recombination at higher temperatures (Wintle, 1975).

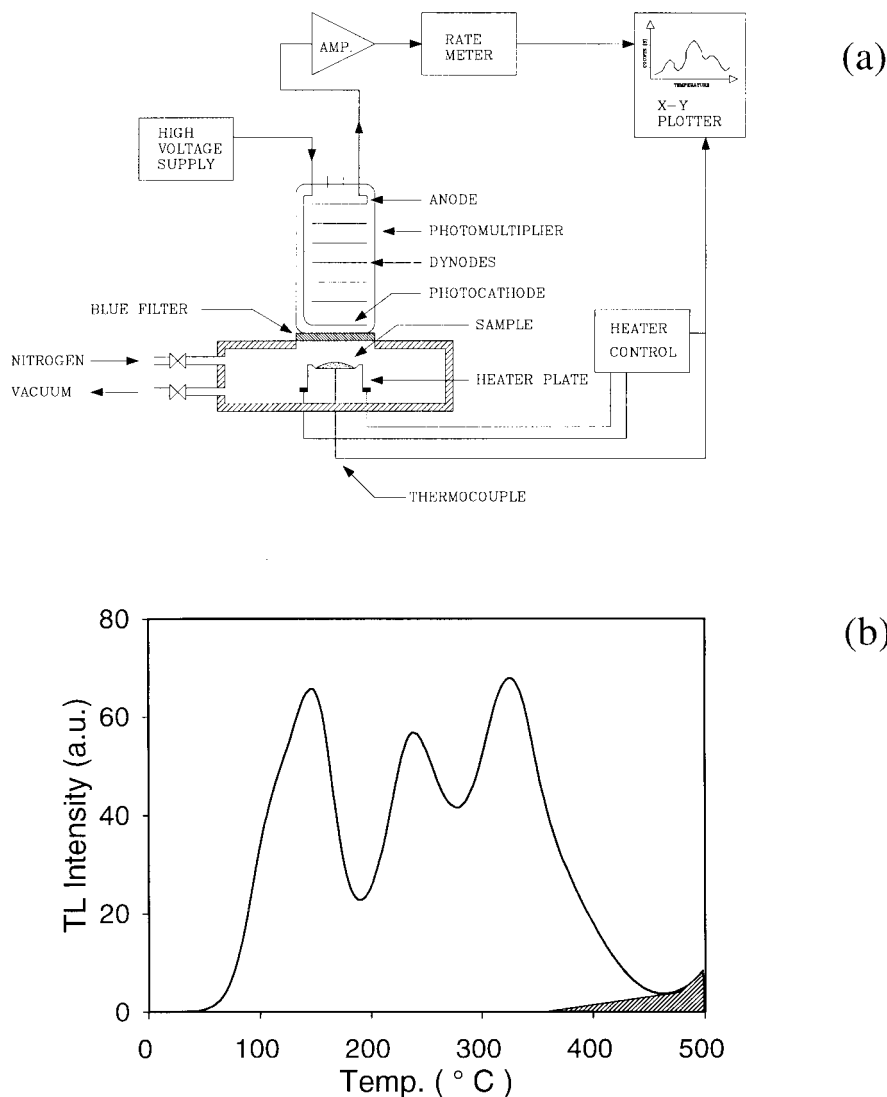


Fig. 2.2. (a) Simple diagram of a TL reader system with heater plate, photomultiplier detector and readout electronics (from Bøtter-Jensen, 1997).

(b) Typical TL glow curve from a sedimentary K-feldspar sample given a beta dose of 8 Gy in addition to the natural dose (approximately 200 Gy). The 150°C peak evident in this figure has been created by the recent beta dose; it is not usually evident in the natural signal as it has normally decayed away. The shaded area is the black body radiation observed when the sample is heated a second time with no additional irradiation (from Bøtter-Jensen, 1997).

### 2.1.3 Optically stimulated luminescence

Optically stimulated luminescence (OSL) arises from the recombination of charge which has been optically released from electron traps within the crystal. These traps may or may not be the same as those associated with the TL peaks. The electron population in the traps is the result of irradiation of the material, and thus the OSL intensity is related to the absorbed radiation dose. For experimental convenience OSL emitted during recombination of the detrapped charges is usually measured in a spectral region different from that of the exciting photons. Whereas the TL signal during heating appears as a curve (glow curve) with several temperature peaks representing the different trap levels, the OSL signal during exposure to the stimulation light is observed to decrease to a low level as the trapped charge is depleted (decay curve). The physical principles of OSL are thus closely related to those of TL. An immediate advantage of OSL over TL is that OSL is normally measured at or close to room temperature and thus results in less alteration of the crystal – i.e. it is less destructive. OSL also measures only the component of the trapped electron population that is most sensitive to light. In geological dating, this is important because this component is most likely to be emptied (or "reset") during transport prior to deposition and burial. A simplified diagram of a set up for measuring OSL is shown in Fig. 2.3a and a typical OSL decay curve obtained from a sedimentary (natural) quartz sample stimulated with broad-band (420-550 nm) blue-green light is shown in Fig. 2.3b.

The potential of OSL in dating applications was first identified by Huntley et al (1985), who used the green light from an argon laser (514 nm) to stimulate luminescence from quartz for dating sediments. Later studies characterised the OSL properties of quartz in more detail with a view to establishing the technique as a tool for dating and dosimetry ( e.g. Aitken and Smith, 1988; Aitken, 1990,; Godfrey-Smith et al., 1988; Rhodes, 1988). Hütt et al. (1988) discovered that infrared light (IR) could also be used for stimulation of luminescence in feldspars and subsequently Poolton and Bailiff (1989), Spooner et al. (1990) and Bøtter-Jensen et al. (1991) constructed units for stimulation based on systems of small IR light emitting diodes (LEDs). Broad-band emitters such as incandescent or arc lamps, in conjunction with selected filters, have also been used to produce both infrared and visible light stimulated luminescence from feldspar and quartz samples (e.g. Hütt and Jaek, 1989; Spooner and Questiaux, 1990, Bøtter-Jensen and Duller, 1992, Pierson et al., 1994).

The most frequently used natural minerals in luminescence dating are quartz and feldspar. Dating of archaeological and geological materials depends on the fact that, when mineral grains are concealed from daylight by burial, they begin to accumulate a trapped electron population. This results from exposure to the ionising radiation emitted by the decay of naturally occurring radionuclides present in the deposit. Some of the radioactivity is contained within the grains, but especially in quartz, the radiation dose is derived almost entirely from the surrounding material. If the flux of ionising radiation is constant, then the burial time of the grains can simply be determined by dividing the total dose that gave rise to the trapped electron population stored in the grains during burial by the dose rate, i.e.

$$\text{burial time} = \text{burial dose/dose rate}$$

In the laboratory a dose equivalent to the burial dose is measured, and this is referred to as the "equivalent dose" or  $D_e$ . Aitken (1998) has reviewed techniques and methods in optical dating.

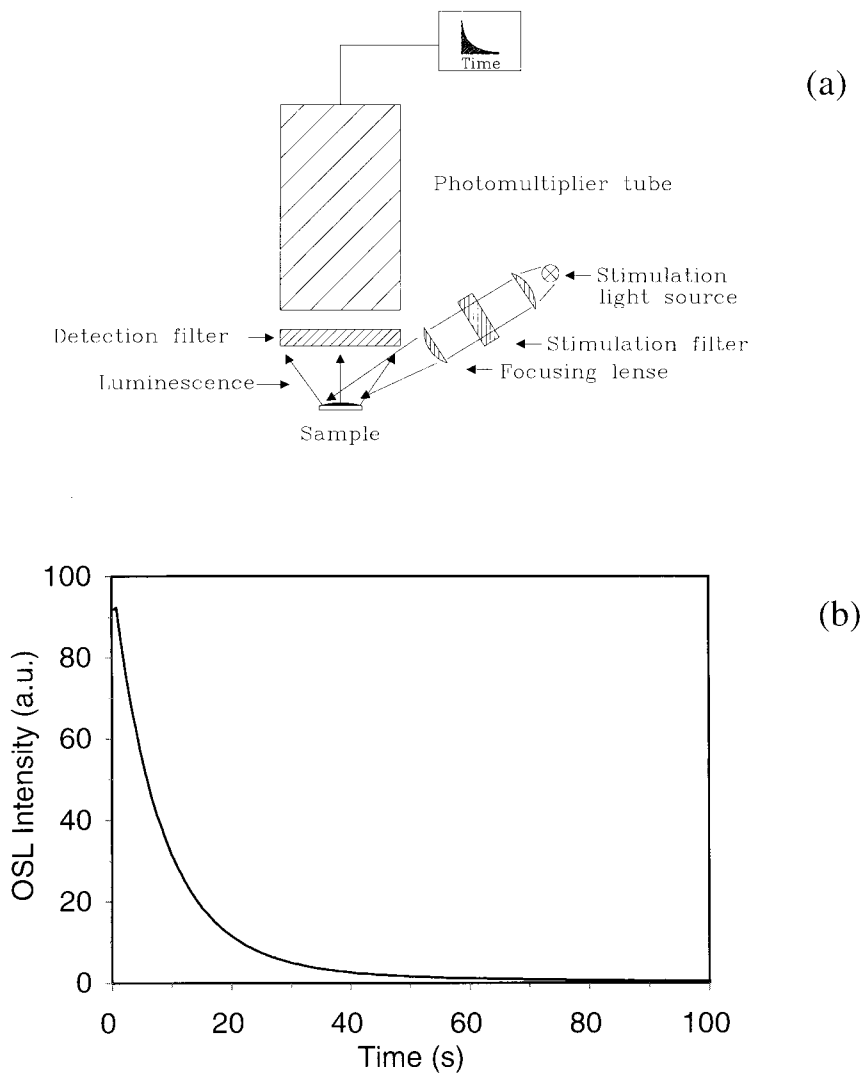


Fig. 2.3. (a) Simple diagram of an OSL system with stimulation light source, photomultiplier detector and readout electronics.

(b) Typical OSL decay curve obtained using green light stimulation on a sedimentary quartz sample.

Recently, luminescence techniques similar to those used in dating have been adopted for retrospective dose assessment i.e. reconstruction of radiation doses received by the general population after nuclear accidents. Typically, radiation doses are determined using luminescence measurements carried out on quartz and feldspar samples extracted from bricks, tiles, pottery, or porcelain items collected in radiation contamination areas such as Hiroshima and Chernobyl (e.g. Godfrey-Smith and Haskell, 1993; Haskell, 1993; Bailiff, 1995; Bøtter-Jensen, 1995; Bøtter-Jensen, 1996; Bøtter-Jensen et al. 1996). This application is described in detail in chapter 8.

## 2.2 Merits of OSL

### 2.2.1 OSL versus TL

In contrast to TL there is no widely accepted way of analysing the OSL decay curve and separately distinguishing the unstable and stable luminescence. It is usually considered necessary to employ a suitable thermal pre-treatment (pre-heat) to avoid unstable OSL in the measurement. The depletion of the OSL signal as a function of excitation illumination time indicates that the electron population in the OSL traps becomes progressively exhausted. It has been shown that the OSL decay curves for both quartz and feldspars show a slower decrease than corresponds to simple exponential decrease (e.g. Duller, 1991; Murray and Wintle, 1998). This raises the question whether only one, or more than one trap each having different eviction probability contribute to the total OSL signal (Duller and Bøtter-Jensen, 1993; Mc Keever et al, 1997, Murray and Wintle, 1998) or whether the non-exponential behaviour is due to re-trapping in other luminescence traps during optical stimulation. Because OSL only reads some of the traps (perhaps only one in quartz), it is likely to access a simpler physical system, and therefore one which is easier to model than TL.

Both TL and OSL processes can be explained by a "generic", phenomenological model for a luminescence dosimetric material, as illustrated in Fig.2.4 (from Bøtter-Jensen and McKeever, 1996). The model consists of a main dosimetric trap (level 2) from which electrons may be excited optically (in OSL) or thermally (in TL). Recombination of the released electrons with holes at recombination sites (level 4) produces the OSL or TL emission. In addition to the main dosimetric trap (or traps) almost all luminescence materials can be expected to contain shallow trapping levels (level 1) which cannot store trapped charge over long periods at ambient temperatures. Although such levels are normally not directly exploited in most dosimetry applications they do contribute to the overall character of the luminescent behaviour of the material. Additionally, one can expect the existence of deep, thermally disconnected traps; i.e. traps too deep to be thermally drained during normal TL applications (level 3). Such deep traps contribute to sensitisation and non-linear growth of the TL signal with dose and such complex dose-response curves are often difficult to model and interpret. Although such deep traps may be inaccessible thermally, the optical release of charge from these states using short wavelength high-energy light as the stimulation source is a real possibility in many materials. This immediately points to a further potential advantage of OSL over TL – namely, the possibility of using the deep traps as a source of dosimetric information.

Fig. 2.4 schematically shows a comparison of the main types of transition occurring during TL and OSL. In Fig. 2.4a transition *a* represents the thermal excitation of electrons from the dosimetric trap, producing TL via the recombination transition *b*. However, during this process electrons are also transferred to deep states (transition *c*) and these are lost from the recombination process. Transition *c* also gives rise to the non-linear growth of TL with dose. Thus TL includes several loss processes due to re-trapping or recombination events. In contrast, OSL has potentially a smaller number of loss processes (Fig. 2.4.b). Following optical stimulation, *a*, recombination occurs, *b*, to yield the OSL signal. Although re-trapping, *c*, into deeper traps may occur one also has the potential, via a suitable choice of wavelength, to optically release, *d*, the charge from these deep states, either simultaneously with transition *a* or subsequent to it. Thus the loss processes can be reduced significantly.



observation suggests that the optical stimulation is thermally assisted and this combined effect causes the lift of electrons from the OSL traps into the conduction band.

### **2.2.3 Repeated and successive OSL measurements of the same sample**

OSL offers the advantage over TL that dose dependent OSL signals can be measured several times from the same dosimeter, if the stimulation is such that it only depletes the trapped charge by a limited amount. Thus repeated OSL measurements can be carried out on the same sample (dosimeter) and successively corrected for by using a previously determined decay constant. This is not possible in TL as a representative dose dependent signal requires that the sample is heated to temperatures sufficiently high to totally erase the stable TL signal. The possibility of repeated OSL measurements on the same sample can be made use of in dosimetry where personal dose meters after first measurement can be stored for later measurement in case of a legal dose-record documentation. In dating and retrospective dosimetry, repeated measurements on the same sample is the basis of the single-aliquot additive-dose protocol (Duller, 1995; Murray et al, 1997), where all necessary measurements for estimating the dose are made on a single sub-sample (see chapter 8).

A very important feature is the possibility of using "short shine" pulsed OSL (~ 0.1 s stimulation) obtained from samples prior to the measurement of the main OSL signal for normalisation of the individual sample sensitivity. Such a brief exposure is intended to deplete the total OSL signal by a negligible amount. This optical normalisation method, in contrast to the more time consuming weight normalisation, has been shown to reduce the signal variability in many cases, from typically 8-10 % to about 1-2 % (Bøtter-Jensen et al, 1991).

### **2.2.4 TL after OSL**

Another interesting feature of the relation between TL and OSL signals is the finding that the charges responsible for the signals do not all originate from the same traps. It has been shown that in some cases even almost complete erasure of the OSL signals only has a minor effect on the TL signal (Godfrey-Smith et al, 1988; Bøtter-Jensen and Duller, 1992; Duller and Bøtter-Jensen, 1993). This allows for evaluation of doses based on the residual TL signal after OSL measurements have been carried out on the same samples; this gives an additional security and documentation. In dating routines, statistics can potentially be improved simply by performing a TL date on the same sample after it has previously been OSL dated (Bøtter-Jensen and Duller, 1992). Because the TL signal is more difficult to bleach than the OSL signal, agreement between the two methods gives increased confidence that the initial bleaching was complete. It should be noted that no OSL signal is left after heating the sample to about 500°C (i.e. after TL). Fig. 2.5a shows TL curves from a sedimentary feldspar before and after infrared stimulation. Fig. 2.5.b shows the corresponding OSL curve.

### **2.2.5 Partial stimulation of samples**

It is shown later that a major feature of OSL is that stimulation light sources (e.g. lasers) can be optically focused to stimulate extremely small areas (less than 100 microns in diameter), i.e. it is possible to only stimulate a small fraction of a sample. By scanning the stimulation beam over the surface, position resolved OSL signals can be obtained. This has been made use of in automatic

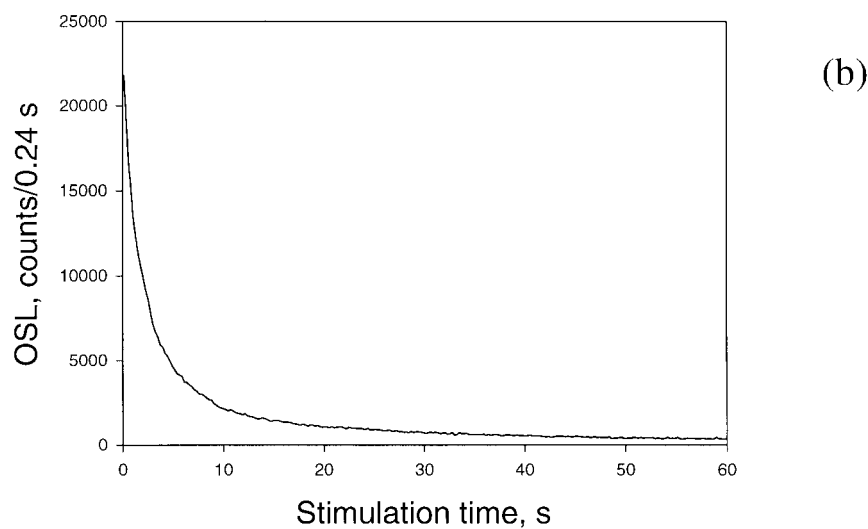
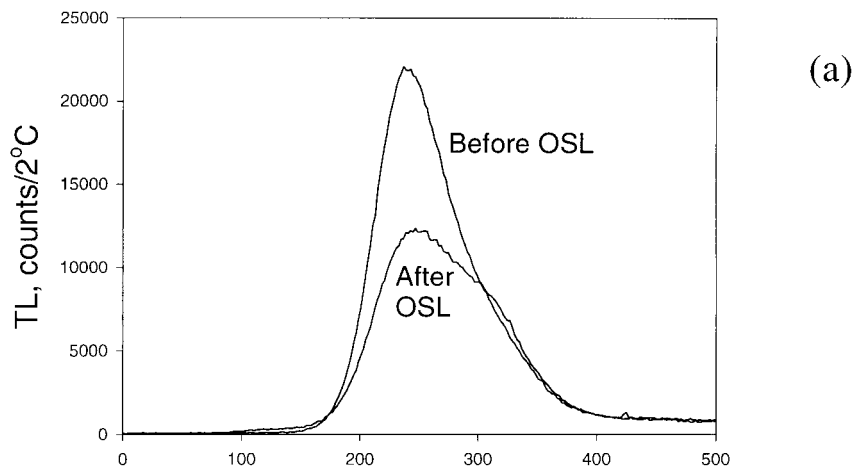


Fig. 2.5. (a) TL glow curve obtained from a sedimentary K-feldspar before stimulation with IR light and after stimulation with IR stimulation over 60 s ( $500 \text{ mW/cm}^2$ ). The effect of OSL read out is demonstrated to be minimal even using a high-power stimulation light source.

(b) The OSL (IR stimulation) decay curve obtained from the same sample as in Fig. 2.5.a.

OSL scanning devices which are described in detail later. More recently focused laser beams have been used to stimulate single sand sized grains which have enabled the analysis of the distribution of luminescence efficiency of single grains in a multi-grain sample (Duller et al, 1999a, Duller et al, 1999b). The focused laser beam stimulation technique can also be used to stimulate small regions of planar dosimeters – the basis for imaging in medical applications. In contrast, any attempt to localize the heating of a sample will cause localised conduction of heat to other parts and release TL from more or less the whole sample, although laser induced heating may be possible.

## 2.2.6 Origin of OSL traps

It should be emphasised that because OSL measures only some proportions of the trapped electron population this method can be expected to produce less alteration in the sample as a result of measurement than TL. Murray et al (1997) have pointed out that, it is likely that, before burial, wind-blown or water-lain quartz grains would have been illuminated by sunlight (bleached) many times since crystallisation, whereas such sediments will not have been heated significantly since the crystal formed. Optical stimulation measures only the component of the trapped electron population that is most sensitive to light and which will have been filled and emptied many times before final deposition. Laboratory OSL is thus repeating a treatment which has occurred many times in nature; laboratory TL heats the crystal for the first time since formation.

## 2.2.7 Dose response

To see whether OSL and TL show identical dose response, Bøtter-Jensen et al (1991) constructed complete TL and OSL growth curves by adding  $^{60}\text{Co}$  gamma doses up to 3000 Gy to the natural doses of young sediments. As an example the OSL (IRSL) growth curve from an extracted potassium feldspar is compared with the corresponding TL growth curve in Fig. 2.6. The OSL samples were preheated at  $220^\circ\text{C}$  for 10 s prior to measurement. The TL samples were preheated at  $100^\circ\text{C}$  for one hour prior to measurement and the TL signal was integrated over the region  $330\text{--}380^\circ\text{C}$ . The signals were normalised so that the two curves have similar initial slope. Exponential functions were fitted to both sets of points and the plots in Fig. 2.6 demonstrate that the OSL (IRSL) has roughly the same useful dose response range as TL with an expected physical saturation at about 5000 Gy.

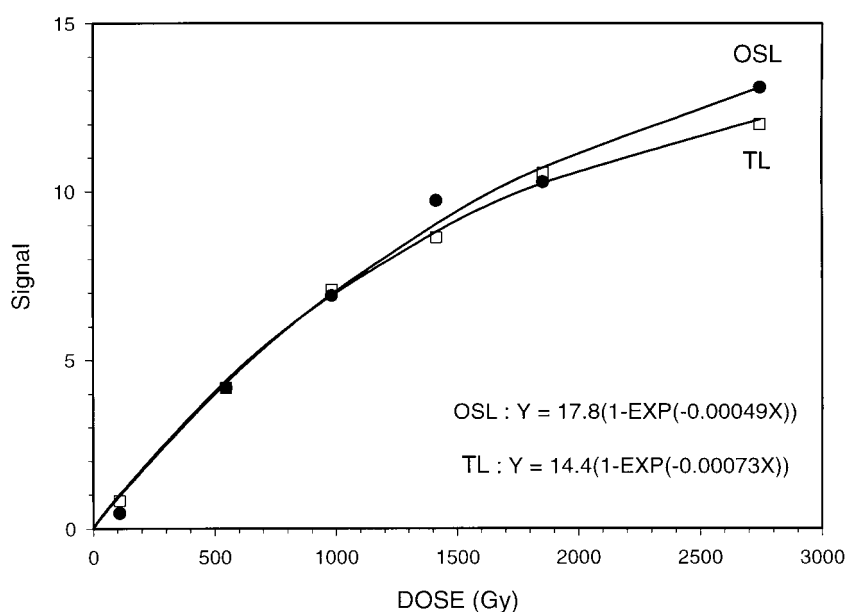


Fig. 2.6. OSL versus  $^{60}\text{Co}$  gamma dose for an extracted sediment potassium feldspar sample compared with the corresponding TL curve (from Bøtter-Jensen et al, 1991).

## 2.2.8 Summary of OSL versus TL

The main features of OSL compared to TL can be summarised as follows:

- OSL is normally measured at or near room temperature and is thus a less destructive and potentially more sensitive method than TL (because of thermal quenching).
- Parts of the OSL signal can be measured many times on same sample. TL measurements involves total erasure of the signal.
- A TL signal can usually be measured after OSL measurement on the same sample.
- Small fractions of a sample (even single grains) can be measured using OSL (e.g. using a focused laser beam).
- OSL measures the trapped electrons held in traps which are the most sensitive to light and is thus particularly important in dating geological sediment samples (zeroed in the past by sun bleaching).
- In many cases, OSL has the same dose response as TL.

## 2.3 Types of Optical Stimulation

### 2.3.1 Continuous wave stimulation

In continuous wave (CW) OSL the excitation is continuous and the emitted luminescence is detected during stimulation (illumination). This arrangement requires the use of filters to discriminate between the stimulation light and the emitted light.

In the initial studies of quartz, the use of green light (514.5 nm) from an argon laser operated in CW mode demonstrated that the energy of visible light is sufficient to empty the OSL electron traps directly in this material. Longer wavelength light is increasingly inefficient at stimulating OSL in quartz (e.g. Aitken, 1990; Bøtter-Jensen et al, 1991, Bøtter-Jensen et al, 1994b). In contrast, luminescence can be excited in feldspars with wavelengths in the near infrared, because of one or more excitation resonance features around 850 nm (1.46 eV) in this material. This has been explained in terms of a two-step thermo-optical process (Hütt et al, 1988) where charge is promoted from the ground state of the defect to a series of metastable excited states. Away from the IR resonance photons of energies exceeding about 2 eV (~ 600 nm) can raise electrons directly into the conduction band with increasingly higher efficiencies as the wavelength is decreased. The difference in stimulation characteristics between quartz and feldspar can be made use of in various ways, e.g. for testing the purity of quartz samples (feldspar contamination) and for measurements of mixed samples (e.g. Spooner and Questiaux, 1990, Bøtter-Jensen and Duller, 1992). Schematic energy diagrams for TL, infrared stimulated luminescence and green-light stimulated luminescence are shown in Fig. 2.7.

In summary the two main CW stimulation methods currently being used in routine OSL measurements are: 1) infrared stimulated luminescence (IRSL) which is useful only with feldspars and 2) visible light stimulated luminescence which works with both feldspars and quartz. Because this was first observed using green light it is sometimes referred to as GLSL. GLSL is also effective with ceramics (porcelain) and some synthetic materials such as  $\text{Al}_2\text{O}_3:\text{C}$  (see chapters 6 and 7). In both IRSL and GLSL it is vital to avoid the excitation light source affecting the PM tube. This is achieved by using a combination of suitable optical stimulation and detection filters. The relative attenuation between the stimulation light band and the PM response must be of the order of  $10^{-16}$  to

suppress sufficiently the scattered light from the excitation source. This is achieved using interference filters on the excitation side, and detection filters with a selective transmission (see chapter 3).

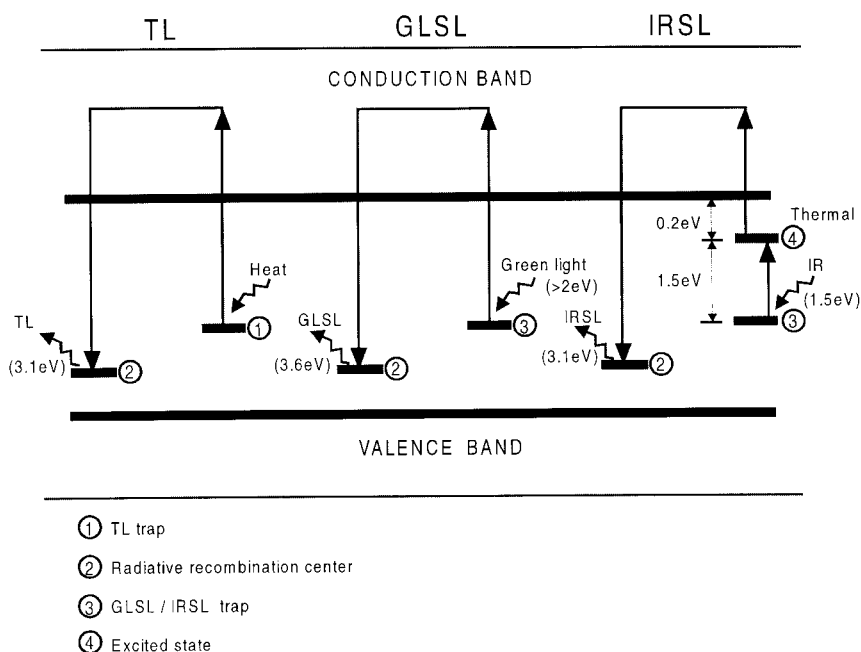


Fig. 2.7. Schematic energy diagrams for (a) TL, (b) green light stimulated luminescence and (c) infrared stimulated luminescence. The latter process is based on the Hütt et al (1988) model with the assumption that infrared photons raise electrons from the ground state into an intermediate excited state from where they are raised further by thermal effect into the conduction band i.e. by lattice vibrations.

### 2.3.2 Pulsed stimulation

In the applications of OSL discussed so far the excitation source - either laser, LED or lamp plus filter systems - is continuous and the luminescence is monitored during the period that the stimulation source is on. This arrangement requires the use of filters to discriminate between the stimulation light and the emitted light and prevents the use of stimulation wavelengths which are the same, or very close to, those observed in the emission. Recently, pulse stimulation techniques have been reported in which the stimulation source is pulsed and the OSL is monitored only after the end of the pulse - i.e. only the afterglow is measured (Markey et al, 1996; McKeever et al, 1996). Since the emission is not detected while the pulse is on, this arrangement can extend the range of stimulation wavelengths that may be used. To date, pulse widths of a few milliseconds, and powers ranging from 10 mW to 2 W, have been used successfully to measure OSL in  $\text{Al}_2\text{O}_3:\text{C}$ . Although light emitted during the pulse is not monitored, recent analysis has demonstrated that the shorter the excitation pulse, the greater is the amount of light emitted after the pulse compared with that emitted during the pulse (McKeever et al, 1996).

The use of pulsed OSL presents several opportunities in radiation dosimetry. Since millisecond pulses are all that is required to read the OSL signal a very rapid readout of radiation doses becomes possible (Akselrod et al, 1998). Also

multiple readout of one sample is feasible since the signal is not depleted in one reading at same rate as in CW mode.

## 2.4 Conclusions – TL and OSL

The principles of TL and OSL have been reviewed, and typical measurement configurations outlined. The potential advantages of OSL have also been discussed. The remaining chapters will consider the technical aspects of OSL measurements in more detail, and then consider material characterisation and dosimetry measurements undertaken using various OSL signals.

# 3 Development of OSL Measurement Technology

## 3.1 Introduction

This chapter outlines the development of the TL/OSL measurement platform at Risø. The characteristics of the various stimulation units are presented and the performance discussed. Single grain stimulation is also described. Finally, some of the OSL measurement systems for specific purposes are described.

### 3.1.1 The light detection system.

Both TL and OSL are normally detected using a photomultiplier tube which, after 40 years, still provides the most sensitive light detector for most luminescence measurement systems. The photomultiplier is a vacuum tube that includes a photosensitive cathode, a number of electron multiplying dynodes and an anode normally held at about 1000 volts. Light photons interact with the photoelectric cathode material (e.g. potassium-caesium) causing the emission of electrons that are then attracted to the positive voltage of the first dynode. Depending on the dynode material (e.g. antimony-caesium) two or three electrons are then emitted for each electron striking it. These electrons are again attracted by the next dynode and so on, resulting in several million electrons reaching the anode for each electron emitted from the cathode. Thus a light photon reaching the photocathode is converted to an electrical pulse at the anode. However, the photomultiplier is not equally sensitive to photons emitted at different wavelengths i.e. not all photons are converted to pulses. This results in a varying quantum efficiency of up to 25 % depending on the wavelength. Typically, a bialkali PM tube, such as EMI 9235, has a selective response curve with a maximum detection efficiency peaking around 400 nm which is suitable for the luminescence emission spectra from both quartz and feldspars. Other types of PM tubes, such as EMI 9658 and RCA 31034, are available with an extended sensitivity in the red region (S-20 cathode) which is particularly suitable for the investigation of the red-emission from some types of feldspar (e.g. see Visockas, 1993). S-20 cathode PM tubes normally need cooling below room temperature to reduce the dark noise. The quantum efficiency versus photon energy or wavelength is shown for bialkali and S-20 PM tubes in Fig. 3.1.a.

In principle, the PM tube can be operated in two modes. One method is based on smoothing the pulses arriving at the PM anode and thereby generating a DC

current signal that is proportional to the number of photons reaching the photo-cathode. This DC signal may be digitised using a current-to-pulse rate converter which allows a wide response range of the order of 7 decades, and the possibility of off-setting the dark current to zero (Shapiro, 1970). However, a more sensitive approach is to directly count the single pulses generated from photons interacting with the photo-cathode. A fast pulse amplifier and a pulse height discriminator are used to feed a ratemeter or scaler (e.g. Aitken et al., 1968 or Aitken, 1985). Modern alkali PM tubes, such as EMI 9235QA, are now available with a dark count-rate of less than 20 cps at room temperature. A further advantage of the single photon counting technique is that the counts accumulated during a measurement can be directly converted into absolute light intensity without knowledge of the PM amplification factor; this facilitates comparison between different systems.

### 3.1.2 Heating systems

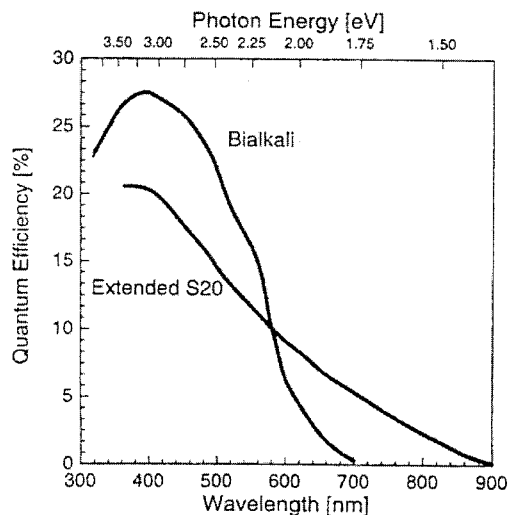
In both TL dating and in retrospective TL dosimetry using natural materials, it is important to heat samples at a constant rate to be able to get a temperature resolved glow curve for identification of peak temperatures (electron traps). It is also very important to have accurate control over the heating of samples for OSL measurements. Linear heating is normally performed using a low-mass heater strip made of high resistance alloys (eg. nickel and Kanthal) by feeding a controlled current through the heating element. A feed back control of the temperature is made using a thermocouple (eg. Cr/Al) welded to the heater strip (see Fig.2.2.a). Normally, heating is controlled by an electronic ramp that can generate various preheat functions and linear heating rates (e.g. 0.1 to 30°C/s). The maximum temperature normally used for quartz and feldspar investigations is 500°C but for special investigations of deep trap effects, temperatures up to 700°C have been employed (e.g. Valladas and Gillot, 1978).

Other heating systems are used for readout of conventional solid TL dosimeters in radiation protection. The dosimeters may be lifted into a stream of hot nitrogen (300-400°C) and the TL signal released during the resulting non-linear heating (e.g. Bøtter-Jensen, 1978). A CO<sub>2</sub> laser beam has also been used for the non-linear heating of solid TL dosimeters (Bräunlich et al, 1981).

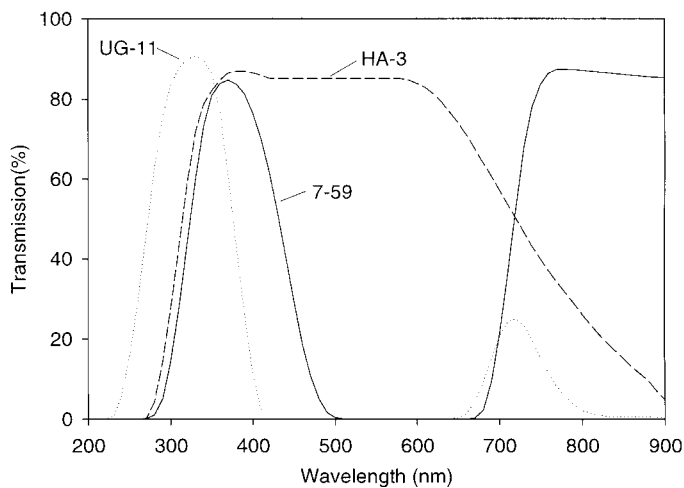
### 3.1.3 Optical filters

A limiting factor in TL measurement is the thermal background signal arising from the heating element and sample during heating to high temperatures (black-body radiation). To be able to distinguish low level TL signals it is important to use blue filters in combination with heat absorbing filters to suppress this thermal background signal. Typical blue filters used in TL measurements of quartz and feldspar are Corning 7-59 and Schott UG-11 and an efficient heat absorbing filter is Pilkington HA-3. The transmission characteristics of these filters are shown in Fig. 3.1.b.

It should be noted that the Shott UG-11 filter has a near-infrared transmission window which is the reason it cannot be used alone for either TL or infrared stimulated luminescence. An additional filter is needed with characteristics to suppress the break through e.g. Schott BG-38 or BG-39 filters.



(a)



(b)

Fig. 3.1. (a) Quantum efficiency versus photon energy or wavelength for bi-alkali and S-20 (extended red sensitivity) photomultiplier tubes (from Bøtter-jensen, 1997).

(b) Transmission characteristics of Corning 7-59, Schott UG-11 and Pilkington HA-3 filters (from Bøtter-jensen, 1997).

### 3.1.4 History of TL/OSL apparatus

The main source of inspiration for the construction of TL apparatus for research using quartz and feldspar is undoubtedly the initial Oxford design for a manual TL reader (Aitken et al, 1968). This was later adopted as a model for the design of TL readers at several dating laboratories. The first Oxford TL system consisted of a heater strip contained in a vacuum chamber, a manually removeable PM tube assembly, and electronics for converting the PM signal to glow curves on a recorder. It was discovered at an early stage that the main requirement for avoiding spurious (i.e. non-dose-dependent) signals, especially in fine grain TL measurements, included 1) evacuation of air (especially oxygen) from the sample chamber before readout, and 2) after evacuation, filling the chamber with nitrogen before heating. The Oxford concept was later taken up and modified to

meet special requirements by several research laboratories. The Oxford concept of a manual TL reader is identical to the schematic shown in Fig. 2.2.a.

In the early 1960s manually operated TL systems were designed mainly for basic studies of TL properties of synthetic dosimetric phosphors and natural materials such as quartz and feldspars. At a later stage automation was identified as a necessary tool to increase the capacity for routine measurement. When OSL techniques were introduced in the late 1980s, some laboratories took advantage of existing TL measurement platforms; this was the Risø approach.

### 3.1.5 Automated TL apparatus

In the late 1960s the demand on TL dating laboratories to carry out routinely a large number of measurements accentuated the need for equipment with automatic changing of samples. An automatic TL reader, using a planchette sample changer capable of measuring twelve samples in sequence, was first developed at Risø (Bøtter-Jensen and Bechmann, 1968). With the establishment of the Nordic Laboratory for TL Dating at Risø in 1977, microprocessor and PC controlled 24-sample automatic TL readers were developed for routine dating of a large number of samples (Bøtter-Jensen and Bundgaard, 1978; Bøtter-Jensen and Mejdahl, 1980; Bøtter-Jensen et al, 1983. Bøtter-Jensen (1988) described an automatic TL system made up of a software controlled 24-sample glow-oven/sample changer, and one or two beta irradiators, all contained in a vacuum chamber.

The fully automated Risø TL reader (model TL-DA-8) was the first of its kind in the world and became commercially available in 1983. This TL reader was controlled by a host computer (first HP 85/86 systems and later IBM personal computers) via a pre-programmed micro-processor system. Control software was developed first using a dialogue system (HP-85/86) and later a sequence editor (IBM-PC) that made it possible to create easily measurement sequences that included automatic functions such as *in situ* beta irradiation of samples, preheating and ramped linear heating. In addition the software controlled the atmosphere of the sample chamber (evacuation and nitrogen flow). A schematic diagram of the principle of the automated Risø TL reader is shown in Fig. 3.2a.

A beta irradiator containing a standard Amersham <sup>90</sup>Sr plaque source with a maximum activity of 40 mCi was directly attached to the sample changer for automatically controlled irradiations of samples. The irradiator was made of steel and covered with lead to keep the external dose rate level at a minimum. The 40 mCi Sr-90 beta source typically provides about 2 Gy/min to a mono layer of sand sized grains of quartz or feldspar.

By the mid 1980s, a heater mechanism that lifted the samples into measurement position from the rotating sample turntable was developed based on a thin low-mass Kanthal strip bent to form the heater element. The Kanthal heater strip is shaped with a depression for optimal heat conduction to the sample and to lift samples securely and reproducibly from the turntable for measurement. A low-mass (0.5 mm diameter) thermocouple is fixed to the heater using a gold rivet. This construction allows repeated heating up to 700°C, and the heater plate cools rapidly without the need for water cooling. Heating is provided by a non-switching continuous full sine wave generator at 20 kHz which is amplitude modulated by the difference signal between the thermocouple signal and the ramp generator voltage. This signal is amplified by a 100 W integrated audio frequency amplifier. The 20 kHz heater current frequency allows the use of a small size ferrite pot core transformer to transfer the required power (80 VA) to the heating element. The heating system has been thoroughly tested and has proved to be extremely reliable over many years; the design of the heater unit

has remained unchanged to the present day. A diagram of the heating system is shown in Fig. 3.2b. It should be noted that when constructing the automated luminescence reader, major effort was put into ensuring that the various moving parts did not affect the integrity of the vacuum chamber.

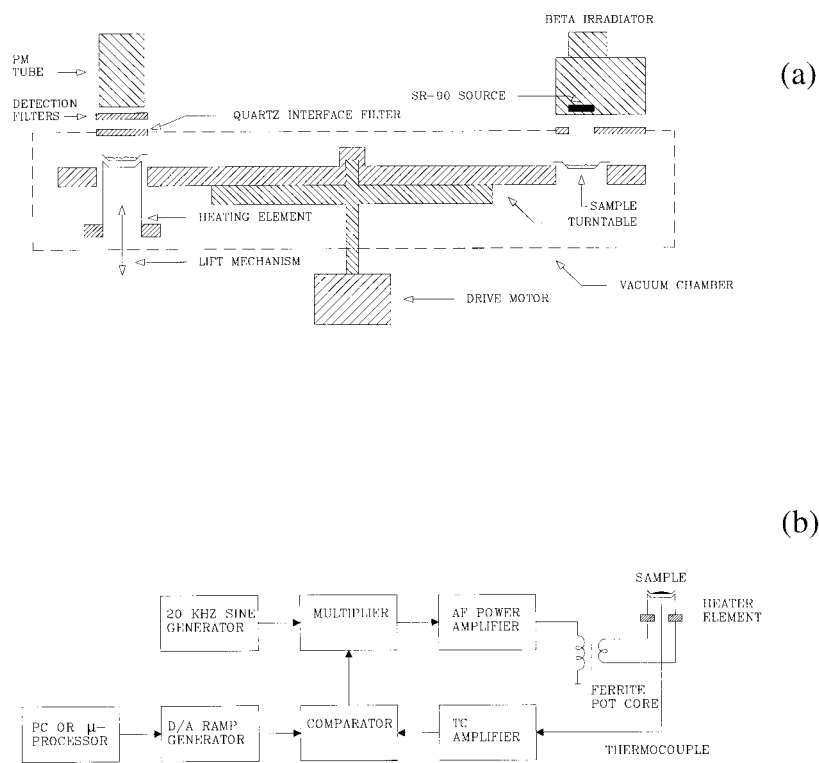


Fig. 3.2. (a) Schematic diagram of an early model of an automated Risø TL reader. The system consisted of a 24-sample turntable, heater, photomultiplier detector and an automatic beta irradiator.

(b) Block diagram of the full sine wave modulated heater system for the automated Risø TL reader.

The mechanical design of the automatic Risø TL reader, developed through the 1980s, has proved very reliable, and was chosen as the instrument platform for all later OSL developments at Risø.

## 3.2 The Recent Instrument Platform

### 3.2.1 The basic automated Risø luminescence reader

As described in the previous section the early models of automatic readers were based on a programmable host computer controlling a pre-programmed microprocessor. However in 1990 it was decided to build systems using only a programmable PC without the use of a microprocessor. This configuration used an interface card mounted directly into a free slot of the AT bus of an IBM compatible personal computer. This was intended to give greater integrated control

of measurement functions and instrument security, and greater freedom of choice in the controlling computer.

However, the limitations in programming the IBM AT bus system and the growing demand for the ability to carry out more complex luminescence measurements, e.g. for detailed physical parameter studies, lead to a complete reassessment of the design of the Risø luminescence reader which incorporates several new hardware and software features (Markey et al, 1996; Markey et al, 1997). These include a two-speed sample turntable, a detachable beta irradiator with a beryllium window vacuum interface and the incorporation of an on-board minicomputer (PC). A completely new software control system based on a WINDOWS sequence editor was developed that allows the user much wider and more flexible control of the reader. The following sections briefly describe the most recent modifications to the basic automated Risø reader. This is used as a platform for attaching different OSL systems and irradiators.

### 3.2.2 Hardware enhancements

#### *(i) On-board computer*

All direct hardware control of the new automated reader has been incorporated into a so-called "Mini-Sys" computer. The Mini-Sys unit is a 386 based PC with a 2MB flash disk and 2MB of RAM. The Mini-Sys connects to the host computer via an RS-232 serial cable thus eliminates the need for an expansion board in the host PC (see Fig. 3.3). The Mini-Sys computer is responsible for maintaining proper timing, sample positioning, data acquisition, error checking, etc. The Mini-Sys computer is also equipped with a two-line digital text display, which shows the current system status and the command which is currently being executed. This display also reports failure messages such as thermal failure, OSL lamp failure or the receipt of invalid commands.

#### *(ii) External equipment interface*

An additional expansion board may be added to the Mini-Sys, which provides access to 16 digital input channels and 8 output relays. By sending appropriate commands to the Mini-Sys it can be instructed to activate one or more relays or wait for a specific input before proceeding. This feature adds the ability to interface the reader with other laboratory equipment such as lasers and flash lamps for illumination. Also, it is possible to use external equipment to trigger the Mini-Sys to start data acquisition.

#### *(iii) Sample turntable*

A two-speed turntable was added to reduce processing time. If a sample is moved to the next position then the turntable turns at the normal speed. If, however, the turntable must advance several positions, it is accelerated to a high speed for most of the move and decelerated to slow speed before stopping. The high-speed facility may be enabled or disabled by software. The sample capacity has been increased from 24 samples to now either 36 or 48 samples. All three turntables are fully interchangeable with each other. The high capacity turntables may also be used in older systems. (Performance measurements are described in section 3.3).

#### *(iv) Detachable beta source*

A new Sr/Y-90 beta irradiator attachment has been developed in which the source is mounted in a rotating, stainless steel wheel, as shown in Fig. 3.4. This design allows the source to be positioned much closer to the sample than was

previously possible, thus increasing the dose rate by more than a factor of two. The dose received by samples under the closed irradiator has also been reduced by a factor of 4. A 0.15 mm Be window interface between the source unit and vacuum chamber has significantly improved vacuum performance and also allows the irradiator to readily be removed to allow very low light level measurements.

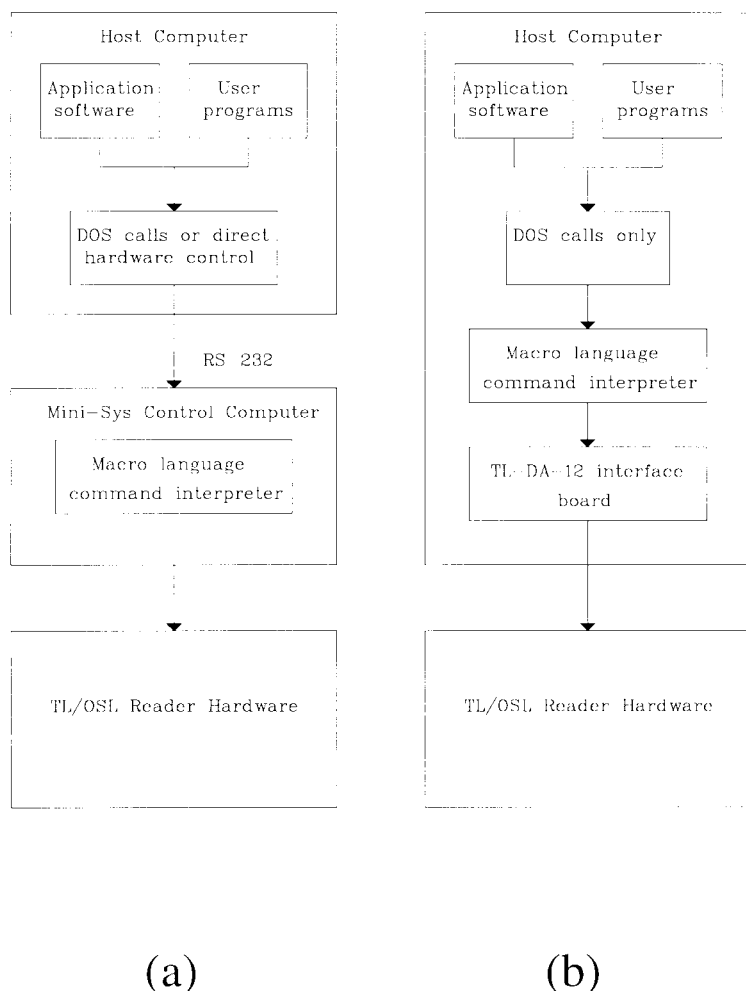


*Fig. 3.3. (a) Simplified diagram of the new Risø TL/OSL reader with the Mini-Sys control computer. The application software and other user programs communicate with the Com ports. In this new configuration the requirements of a host computer are reduced since only a simple serial connection is needed.*

*(b) For comparison, this diagram shows an older model system using a modified TL-DA-12 interface board. Also here the application software communicates with Com ports. However, the serial output is captured by the command interpreter, which controls the hardware. (From Markey et al, 1997).*

The beta source stimulates electrons within the PM tube, thus increasing the dark counts. The typical dark counts for a selected 9236QA PM tube is < 20 cps without any beta source installed into the irradiator. With the standard 40 mCi <sup>90</sup>Sr beta source installed the dark counts typically increases to about 50 cps. An

external indicator has also been added to the irradiator unit, which glows red when the irradiator is on and green when it is off, and a mechanical interlock prevents the operation of the irradiator when the system lid is open.

*(v) Beta source cross-talk*

The cross-talk, i.e. the percentage of dose given to an adjacent non-irradiated sample is, on average,  $0.266 \pm 0.007 \%$  for a 4 mg mono-layer coarse grain quartz sample using the new 48-sample carousel. The 2<sup>nd</sup> nearest sample only receives  $0.004 \pm 0.002 \%$  of the primary beta dose. For comparison the beta source cross-talk figures for the older 24-sample carousel was measured to  $0.0400 \pm 0.0001 \%$  and  $0.0020 \pm 0.0003 \%$  for the nearest and the 2<sup>nd</sup> nearest samples, respectively. However, the increased cross-talk figures for the 48-sample carousel are still encouraging small and have a negligible effect in routine measurements.

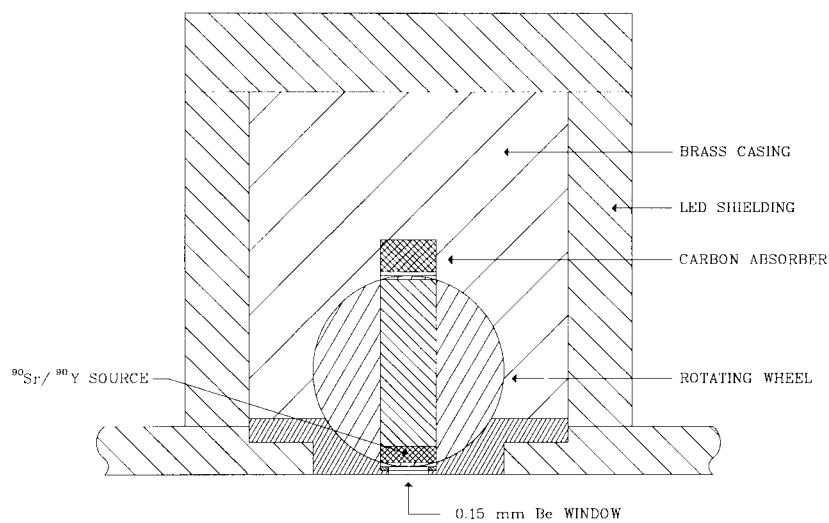


*Fig. 3.4. Cross section of the new beta irradiator design. The source is placed in a rotating stainless steel wheel as shown. When not irradiating, the wheel is rotated 180 deg. and the source is pointing upwards (from Markey et al, 1997).*

**3.2.3 Software and data**

The software to control the Mini-Sys PC is based on a Windows program for creating, editing and executing measurement sequences. The central feature of the Mini-Sys software is a high level command language interpreter. The command language consists of approximately 40 commands which allow full control of system hardware and data acquisition methods. The command language allows users to write their own control programs in PASCAL, BASIC, C, etc. and thus construct alternative measurement options to those included in the user application software.

In the past, there were procedures, which were possible with the hardware but which could not be performed due to software restrictions. The Mini-Sys control system on the other hand allows the user complete freedom to exploit all the capabilities of the Risø TL/OSL reader hardware. It is possible to choose up to 2000 data points to be recorded for each measurement. Up to 100 data points per second may be recorded if the data is to be downloaded to the control PC

while recording. If data is to be downloaded at the end of acquisition then data may be recorded at rates of up to 200 points per second.

### 3.3 Development of Optical Stimulation Sources

#### 3.3.1 IR LED stimulation

Hütt et al (1988) first showed that infrared (IR) light could stimulate luminescence from feldspars, and because it was technically easier to provide IR stimulation than green laser stimulation, several laboratories rapidly published descriptions of practical stimulation units. Poolton and Bailiff (1989), Spooner et al (1990) and Bøtter-Jensen et al (1991) described the use of infrared (IR) light emitting diodes (LEDs) for stimulation of feldspars. Bøtter-Jensen et al (1991) described an IR add-on unit that could be mounted directly between the PM tube assembly and the glow oven of the automated Risø TL apparatus. In this unit thirty two IR LEDs are arranged in two concentric rings one above the other, with each LED pointing at the sample. IR stimulated luminescence (IRSL) emitted vertically through the ring of diodes is then measured with the same PM as used for the TL measurements. A BG-39 detection filter rejects the scattered IR light. The total power delivered to the sample using GaAl/As IR LEDs (Telefunken TSHA 6503:  $875 \Delta 75$  nm) has been measured as  $40 \text{ mW/cm}^2$  at a diode current of 50 mA. A feed back servo system served to control the current through the LEDs and thereby stabilise the power. The IR stimulation unit is shown in Fig. 3.5.

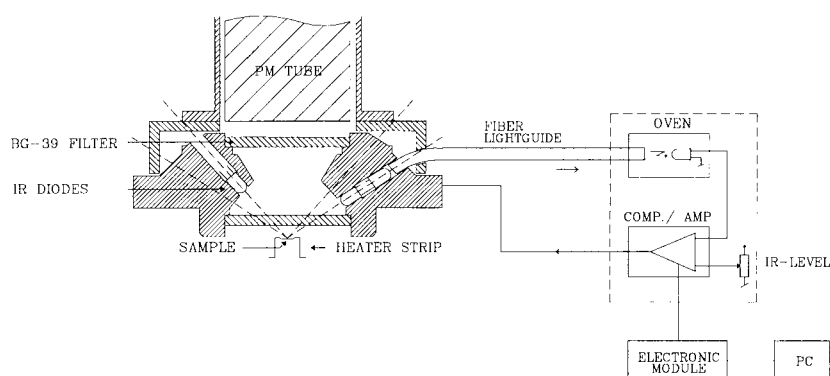


*Fig. 3.5. Schematic diagram of an IR LED stimulation unit attachable to the automatic Risø TL apparatus. Thirty-two IR LEDs are arranged in two concentric rings focusing on the sample. A feed back system for controlling the LED current is also shown (from Bøtter-Jensen et al, 1991).*

The emission spectra of the IR LEDs were measured using an Oriel Multispec 1/8 M spectrometer fitted with an IntaSpec diode array detector (1 nm resolution). The spectra were measured at LED currents of 30, 70, 90, 100 and 300 mA. For each of the LED currents, emission spectra were sampled each 10 s over 3 min illumination time starting from a condition where the LED had cooled to room temperature. For all LED currents no measurable peak shift (i.e.  $< 1$  nm) in the spectra could be detected. It is thus concluded that it is unlikely that apparent rate of decay of luminescence will be affected by changes in the

illumination wavelength, for all practical illumination powers. The published BG-39 filter and the observed IR LED characteristics are shown in Fig. 3.6.

The stimulation of adjacent samples due to cross-talk for an IR LED array, expressed as a percentage of stimulation time on the nearest adjacent sample (using 4 mg mono-layer coarse grain feldspar samples on Al discs) was measured as  $0.019 \pm 0.006 \%$  and  $0.013 \pm 0.008 \%$  for the 48-sample carousel and the 24- sample carousel, respectively. There is no significant difference in cross-talk for the two carousel configurations, and the size of the effect is negligible in routine measurements.

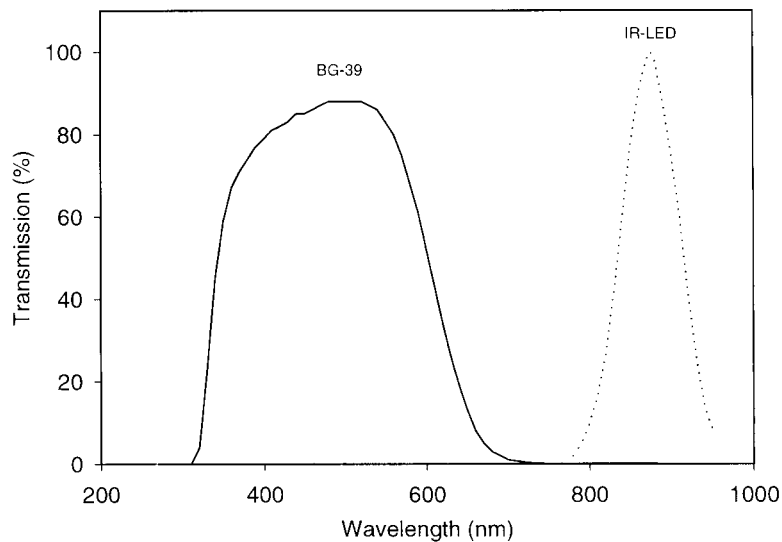


Fig. 3.6. The published BG-39 detection filter transmission and the observed IR LED emission characteristics.

### 3.3.2 IR laser diode stimulation

Normally IR LEDs peaking at 870 – 880 nm are used for stimulation of feldspars. However, Godfrey-Smith and Cada (1996) showed that the IR resonance of most feldspars is around 845-850 nm. Recently IR LEDs peaking at 840 nm have become available. An array consisting of 30-40 IR diodes close to the sample (10-20 mm), delivers typically 40-50 mW/cm<sup>2</sup> at the sample position; this provides a useful luminescence signal in most applications. However, the decay rate of the luminescence signal is slow (about 50 s to reduce the initial luminescence by about 50%). In particular in measurement protocols based on regenerating the IRSL signal, higher power is needed to be able to deplete completely the IRSL signal in a reasonable time. Rapid stimulation also increases the signal to noise ratio of the measurement system. Accordingly, the potential of solid state IR laser diodes was investigated in collaboration with Nordic Laser Systems A/S, Kvistgård, Denmark, and consequently a compact IR stimulation unit based on a 1.0 W laser diode emitting at 830 nm was developed. Using appropriate optics, such as cylindrical focal lenses, this provides a uniform illumination area of approximately 1 cm<sup>2</sup> at the sample position. The power delivered to the sample position versus laser diode current is shown in Fig. 3.7.a. The IR laser diode has been integrated with a blue LED OSL unit providing a flexible high-power combined IR/blue light OSL attachment (see section 3.3.6). Typical IRSL decay curves from a feldspar sample obtained with 1) the laser diode running at 500 mW/cm<sup>2</sup> at the sample and 2) the conventional IR LED

array ( $40 \text{ mW/cm}^2$ ) are shown in Fig. 3.7.b. The greater stimulation power provided by the laser diode is seen to give an enhanced initial light output and a steeper initial OSL decay curve; the relative depletion after 75 s is much greater.

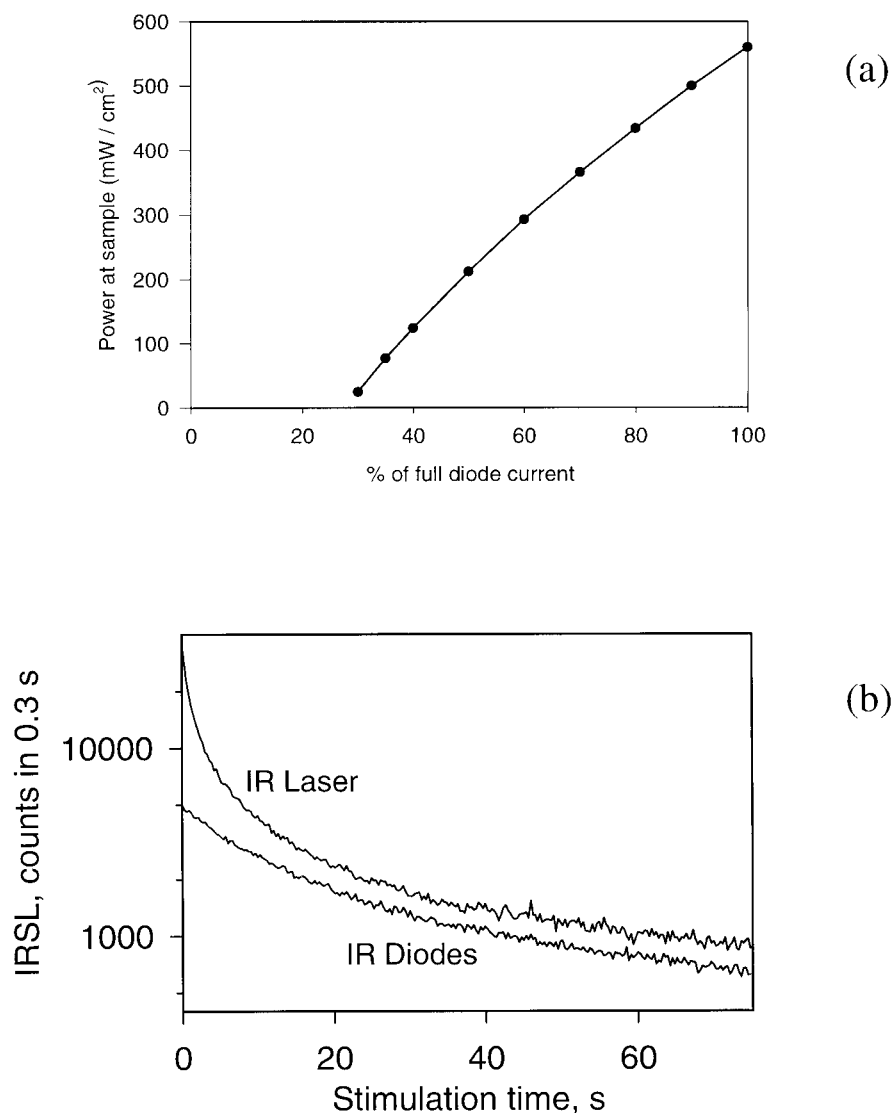


Fig. 3.7. (a) Power at sample versus IR laser diode current setting.

(b) Plots of IRSL decay curves obtained from a sedimentary feldspar using (1) a normal LED array ( $40 \text{ mW/cm}^2$ ) and (2) the new  $1\text{W}/830 \text{ nm}$  laser diode ( $500 \text{ mW/cm}^2$ ). Note the logarithmic Y-axis (from Bøtter-Jensen and Murray, 1999).

The same spectrometer set up as described in section 3.3.1 was used to obtain emission spectra from the IR laser diode at currents of 400, 880 and 1200 mA. For each laser diode current, emission spectra were sampled each 10 s over 3 min continuous illumination from a condition where the laser diode had cooled down to room temperature. The peak of the emission was seen to slightly shift towards higher wavelength with increased current and illumination time. The maximum shift of wavelength observed from cold condition to 3 min. of constant illumination was measured as 1.12, 1.24 and 3.6 nm for laser diode cur-

rents of 400, 800 and 1200 mA, respectively. Plots of wavelength versus the different diode currents are shown in Fig. 3.8a. As for the IR LEDs it is unlikely that the apparent rate of decay of luminescence would be significantly affected by these small changes of illumination wavelengths, for all practical illumination powers.

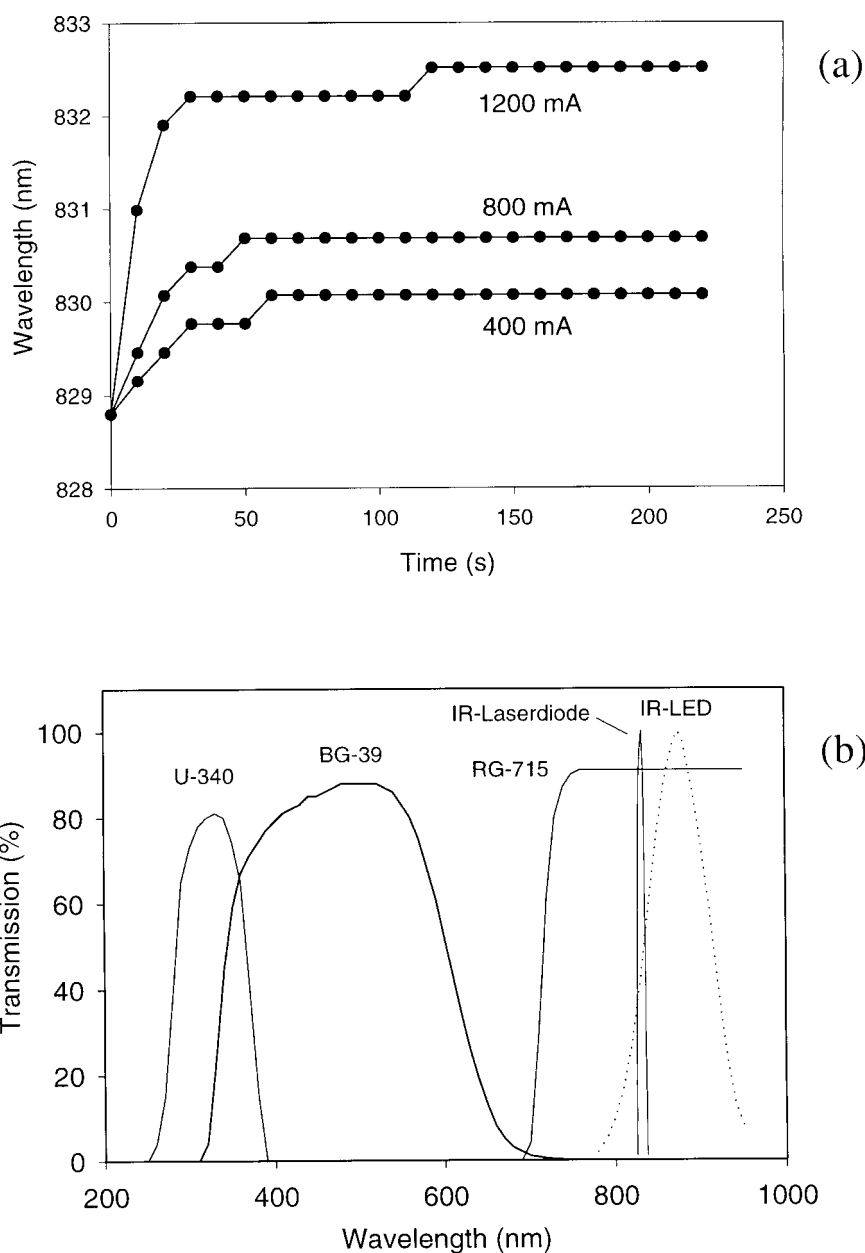


Fig. 3.8. (a) Emission peak wavelength for the IR laser diode as a function of illumination time (constant illumination power) for diode current settings of 400, 800 and 1200 mA, respectively.

(b) The observed IR laser diode and IR LED emission spectra and the published RG-715, BG-39 and U-340 filter characteristics.

The effect of full power IR stimulation on the PM background signal was also investigated. When stimulating a blank sample disc at full power using a U-340

detection filter no increase in PM background count rate was detected. However, using a BG-39 detection filter, which is often preferred in IR stimulation of feldspar (see section 3.3.1), the PM background increased from about 30 cps to about 200 cps. This increase of background is caused by a very weak blue emission from the laser diode, which appeared to be unknown to the manufacturer. The increased background can be completely removed by using a Schott RG 715 long-pass filter in front of the IR laser diode; with this in place the dark count was again reduced to about 30 cps. The observed IR emission and the published RG 715, BG-39 and U-340 filter characteristics are shown in Fig. 3.8b.

The cross-talk was measured between the adjacent samples when exposing a sample with the IR laser diode using 4 mg mono-layer coarse grain feldspar samples. The stimulation on the nearest adjacent sample on a 48-sample carousel due to cross-talk at full IR laser power was measured to  $< 0.012 \pm 0.006$  % expressed as percentage of equivalent stimulation time on the adjacent sample. A similar figure was obtained for a 24-sample carousel indicating that no measurable difference in cross-talk can be detected whether using 24 or 48 sample carousels using the IR laser diode stimulation.

### 3.3.3 GLSL apparatus

The demand for OSL dating of quartz and an inexpensive alternative to green laser stimulation lead to the development of stimulation systems based on green light wavelength bands filtered from incandescent broad band lamps. Bøtter-Jensen and Duller (1992) were the first to develop a compact green light OSL (GLSL) system based on the light emitted from a simple low-power halogen lamp. This lamp provides a broad-band light source from which a suitable stimulation spectrum can be selected using optical filters. A low-power (75 W) tungsten halogen lamp filtered to produce a stimulation wavelength band from 420-550 nm delivered a power of  $16 \text{ mW/cm}^2$  to the sample. The filtered halogen lamp was stable within 2% after an initial stabilisation period of about 2 minutes. The main feature of this construction is that the halogen lamp does not require complex cooling and the small  $2 \times 2$  mm filament can easily be imaged onto the sample, thus providing good energy transfer to the sample. The only problem encountered with this design of illumination source is that the effective lifetime of this bulb is only 30-40 hours. The GLSL unit is shown schematically in Fig. 3.9.

Huntley et al (1991) have shown that quartz OSL emission spectra are centred around a wavelength of 365 nm. Therefore, an investigation of possible filter configurations was undertaken (Bøtter-Jensen and Duller, 1992). Table 3.1 lists the results of testing six filter configurations using three different archaeological quartz samples. A variety of detection and stimulation filter characteristics were obtained using a Spectrophotometer, type Perkins Elmer Lambda 9000 (1 nm resolution) kindly made available by DELTA Light and Optics, Denmark. The observed optimal excitation wavelength band and detection filter characteristics are shown in Fig. 3.10 and Fig. 3.11 shows a typical OSL decay curve obtained from a sedimentary quartz sample using the stimulation wavelength band of 420-550 nm,  $16 \text{ mW/cm}^2$  at sample and a U-340 detection filter.

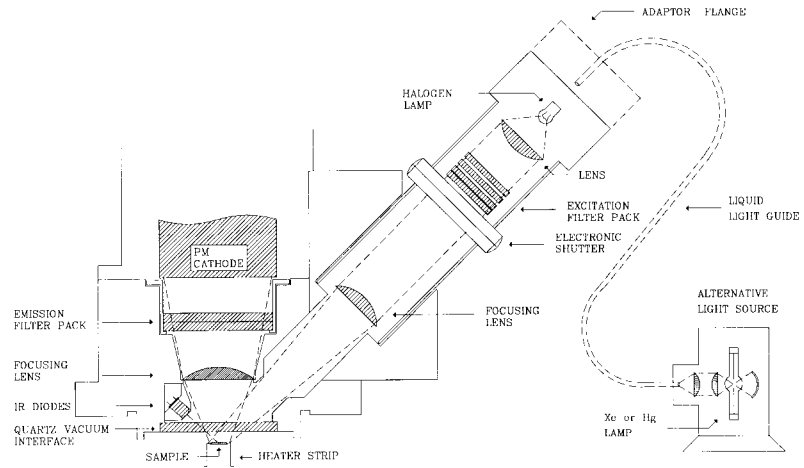


Fig. 3.9. Schematic diagram of a combined IRSL/GLSL unit attachable to the automated Risø TL apparatus. Green light stimulation is produced using filtered light from a halogen lamp and IR stimulation is produced using IR LEDs (from Bøtter-Jensen and Duller, 1992).

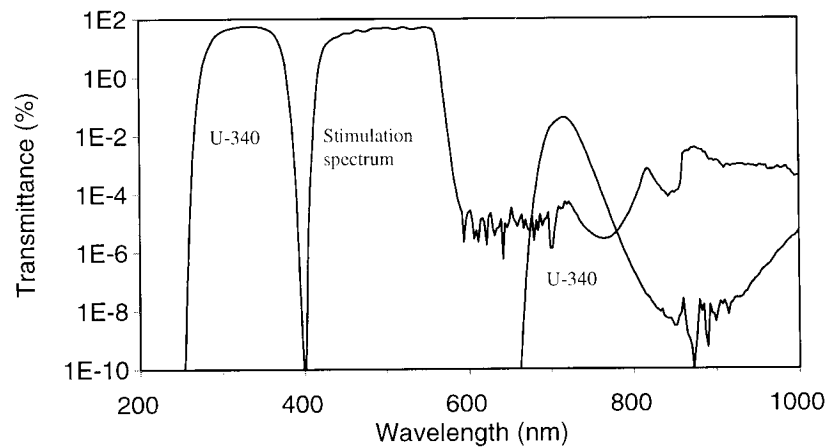


Fig. 3.10. The observed stimulation and detection characteristics of the broad-band blue/green OSL attachment (from Bøtter-Jensen and Murray, 1999).

Table 3.1. Signal-to noise ratios ( $S/N$ ) obtained as the mean values from three heated quartz samples using different filter combinations, given relative to that for the first combination. The background noise signals ( $N$ ) taken as the OSL signal from heated samples, the mean PM dark signals ( $D$ ) and the ratios ( $N/D$ ) are listed as well. (From Bøtter-Jensen and Duller, 1992).

Excitation filter	Detection filter	$S/N$ (rel.)	$N$ (cps)	$D$ (cps)	$N/D$
6 mm GG-420	5 mm U-340	1.00	68	52	1.31
6 mm GG-420	4 mm UG-11	0.39	241	58	4.16
6 mm GG-455	5 mm U-340	0.88	74	54	1.37
6 mm GG-455	4 mm UG-11	0.18	306	53	5.76
5 mm GG-455	5 mm U-360	0.48	94	55	1.71
6 mm OG-515	12 mm 7-59 + 5 mm BG-39	0.01	195	76	2.57

Cps: counts per second

Duller and Bøtter-Jensen (1996) showed that exposure of quartz to 514 nm light, such as is produced by an argon-ion laser, causes a similar loss of OSL signal as measured at stimulation wavelengths from 420 to 575 nm when detection is made with a Hoya U-340 filter and that over this range of stimulation wavelengths, the OSL signals produced behave in a similar manner (see section 4.7). The OSL signals obtained from quartz were observed to decay at the same rate as that observed using an argon laser (514 nm) delivering 50 mW/cm<sup>2</sup> at the sample, presumably because of the higher energies present in the broadband from the filtered halogen lamp. Murray and Wintle (1998) concluded that, on the basis of their measurement of the thermal assistance energy for quartz OSL, the effective stimulating wavelength of this broad-band wavelength range (420-550 nm) is about 470 nm.

The stimulation unit also incorporates a ring of IR LEDs at a short distance from the sample. This IRSL facility was foreseen to be necessary for screening the purity of quartz samples (detecting feldspar contamination) but also as a built-in IRSL facility for measuring feldspar samples. The GLSL/IRSL unit was designed to be mounted onto the automated Risø TL apparatus thus providing flexible combined IRSL/GLSL/TL features.

### 3.3.4 Optimisation of OSL stimulation and detection

A single luminescent grain emits light in all directions, i.e. in  $4\pi$  geometry. If the sample is heated or illuminated on a metal support, the maximum light signal is then reduced to about 50% (to  $2\pi$  geometry), unless the support for the sample is polished and the sample transparent etc. Sample-to-PM tube distance is thus very important, since only a small increase will lead to loss of light collected. If a greater sample-to-PM tube distance is needed, suitable optics are required to retain the sensitivity of the design. Markey et al (1996) designed and tested OSL attachments to the automated Risø system based on reflecting the luminescence from ellipsoidal mirrors; these provide the greatest flexibility for the incorporation of different excitation sources. By lifting the samples into the focal point of the ellipsoidal mirror, a gain in sensitivity of 3 to 4 was achieved compared to the standard Risø TL/OSL system whether thermally or optically

stimulated. Readout systems based on metallic mirrors are dependent on a stable reflectivity and thus the choice of a pure metal surface such as nickel electroplated with rhodium is of great importance. In the full-reflector system developed at Risø and reported by Markey et al (1997) excitation illumination is introduced by up to four optional light guides. A schematic of the full reflector system is shown in Fig. 3.12.

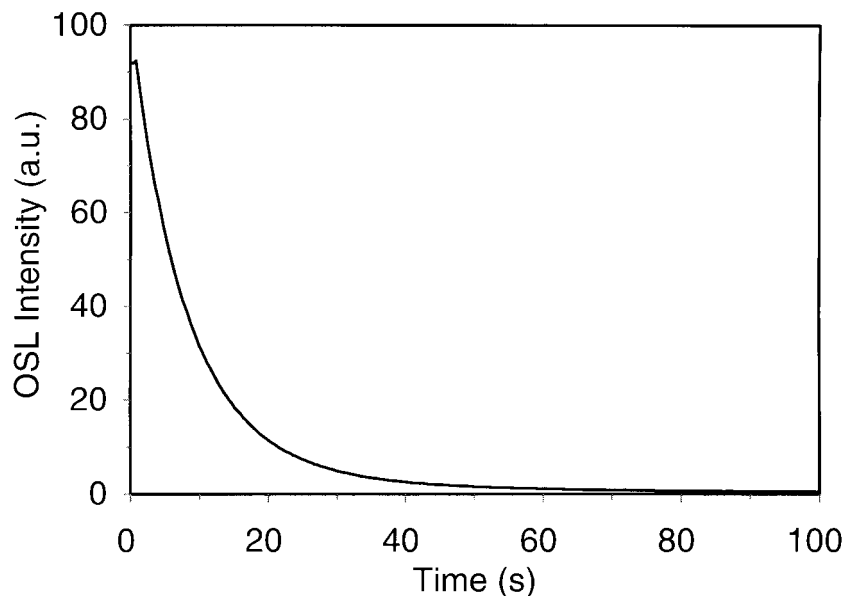


Fig. 3.11. Typical OSL decay curve from a sedimentary quartz sample given a beta dose of 2 Gy obtained using a blue-green wavelength band of 420-550 nm producing  $16 \text{ mW/cm}^2$  at the sample position.

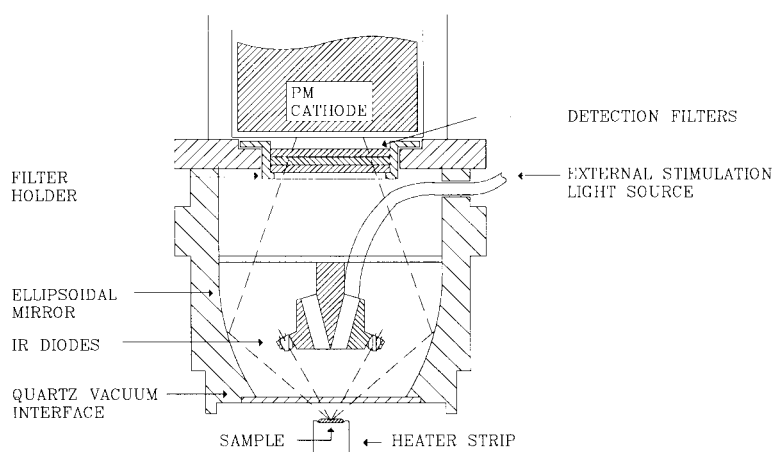
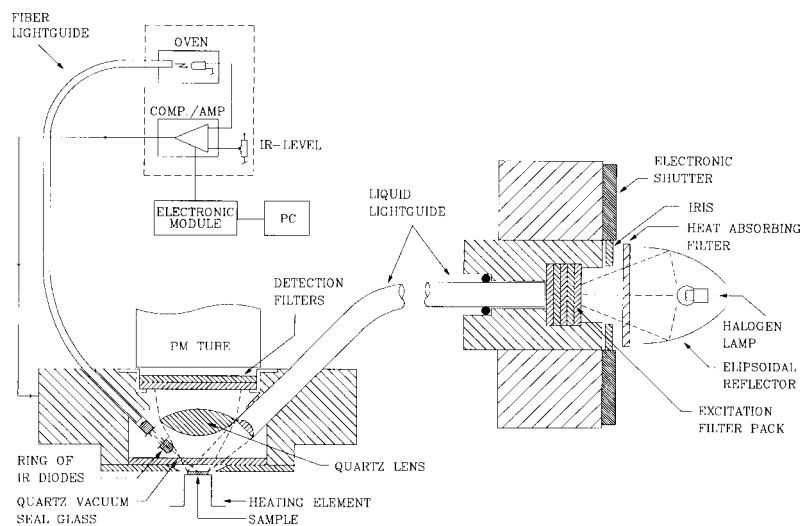


Fig. 3.12. Schematic diagram of the Risø full reflector OSL system (from Markey et al, 1996).

### 3.3.5 New broad band stimulation unit

As a cheaper alternative to the ellipsoidal mirror system a more compact combined IRSL/GLSL unit with an improved sample-to-PM tube distance was developed. A significantly enhanced power delivery is achieved by using an eight mm diameter liquid light-guide system (transmission of 98% in the range 380-550 nm) for illumination of the sample. Filtered wavelength bands are provided using either a 150 W tungsten halogen lamp or a 150 W xenon lamp mounted in a remote lamp house equipped with electronic shutter and exchangeable excitation filter pack. An important feature is that the halogen lamp used in this construction has a much improved lifetime (approximately 2000 hours). The liquid light guide terminates in a quartz lens to defocus the stimulation light and thus ensure that it falls uniformly on the sample. A schematic diagram of the broad-band stimulation unit is shown in Fig. 3.13. The signal-to-noise ratio was further improved by using multi-layer metal oxide coated ( $ZrO_2/SiO_2$ ) Hoya U-340 detection filters (DELTA Light and Optics, Denmark) which attenuates any light passed through a transmission window found in the red region of a normal U-340 filter. The detection filter characteristics were obtained using the Perkin Elmer Spectrophotometer mentioned in section 3.3.3. The observed characteristics of the coated U-340 filter are compared with those of a normal U-340 filter in Fig. 3.14. Fig. 3.15 shows a photograph of a recent automated Risø luminescence reader equipped with the broad-band OSL unit.



*Fig. 3.13. Schematic diagram of the new compact Risø liquid lightguide-based combined IRSL/GLSL stimulation unit attachable to the automatic Risø TL reader (from Bøtter-Jensen and Murray, 1999).*

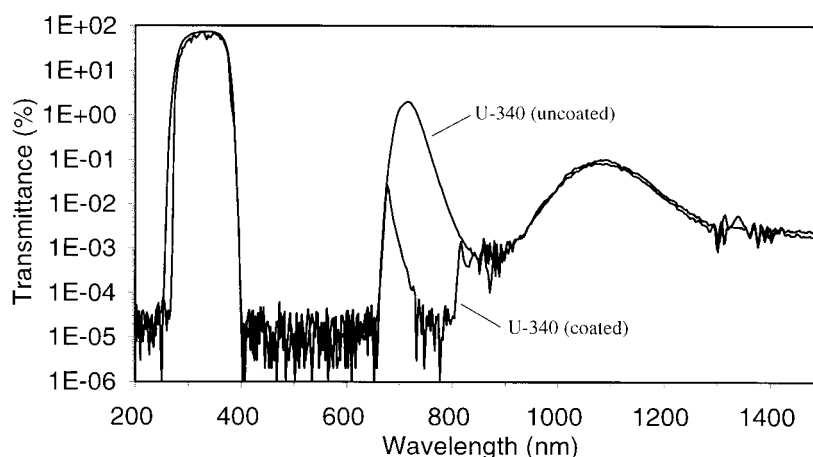


Fig. 3.14. The observed transmission characteristics of a normal Hoya U-340 detection filter overlain with that of a metal oxide coated U-340 filter. The effect of suppressing the transmission window at 700 nm is clearly seen (from Bøtter-Jensen and Murray, 1999).

### 3.3.6 Blue LED stimulation

#### (i) Introduction

Galloway (1993, 1994) described initial investigations into the use of green LEDs for stimulation of quartz and feldspars. The relatively low power that could be delivered to the sample at that time and the heavy filtering of the photomultiplier cathode necessary to avoid stray light from the LED emission band resulted in slowly decaying OSL curves that required readout times in the order of 2000 s to give useful signals for dose assessment. However, these initial investigations of green LEDs for OSL dosimetry provided a good basis for later investigations of more powerful green and blue LEDs.

Shorter wavelength light will stimulate luminescence with greater efficiency because of the exponential increase of stimulation with decreasing wavelength (Bøtter-Jensen et al, 1994b, Spooner, 1994). Because of this, considerable benefits were expected from using the blue light from LEDs (Bøtter-Jensen, 1997; Bøtter-Jensen et al, 1999a; Bøtter-Jensen et al, 1999b). It was found that for similar power densities, the higher energy light provided by the blue LEDs (470 nm) gives an order of magnitude greater rate of stimulation in quartz than that from conventional blue-green light filtered from a halogen lamp.

Based on the experience gained with infrared diodes, it was expected that visible LEDs would offer several advantages over existing laser or broad-band stimulation sources. They are inexpensive and compact, and heat dissipation is negligible. Switch-on and -off times are much shorter than can be obtained with the electromechanical shutters used with halogen lamps, and with optical feedback no warm up period is necessary. From an experimental point of view, the illumination power density can be controlled electronically. This offers the possibility of software control during experimental sequences, e.g. to provide reduced power during the brief illuminations used in normalisation, or to provide a time-varying stimulation power (Bøtter-Jensen et al, 1999b).

Galloway et al (1997) have also reported the testing of more recently developed green LEDs. The increase in illumination power improved the overall sensitivity by a factor 1000 compared with their previous green LED system (Galloway, 1994). However, the effective excitation power achieved using green LEDs is still much below that obtained with blue LEDs or filtered lamp sources.

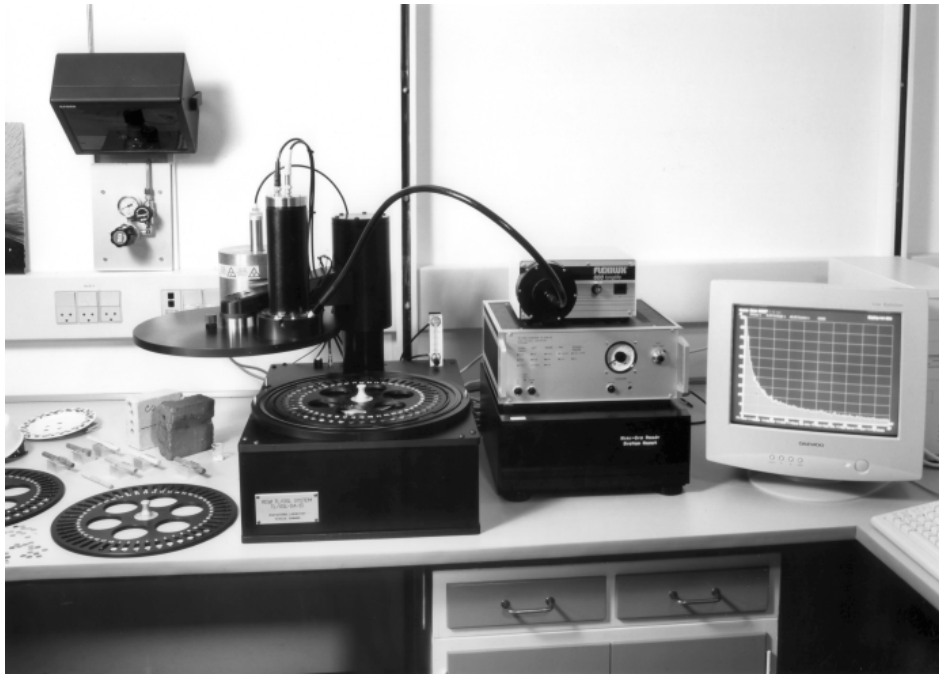


*Fig. 3.15. Photograph showing a recent model of the automated Risø luminescence reader system equipped with a blue-green broad-band OSL unit.*

*(ii) Blue LED configurations*

The blue LEDs were supplied by NISHIA (type NSPB-500S) The manufacturer describes these devices as having a peak emission of 470 nm (half width 20 nm), an emission angle of 15 degrees and a power output of about 2 cd at 20 mA current; the luminance of individual diodes from a batch (for a given current) may vary by up to a factor 2. In a batch of 100 diodes it was found that 25% of the total delivered more than  $2.5 \text{ mW cm}^{-2}$  at a distance of 2 cm, compared with the average of  $1.9 \text{ mW cm}^{-2}$ . It is clear that individual selection of diodes can easily provide a 50% increase in power over that of a random choice.

The testing of different blue LED configurations (Bøtter-Jensen et al, 1999a; Bøtter-Jensen et al, 1999b) resulted in the design of a compact OSL attachment to the automated Risø TL reader. This unit is built up of clusters of blue LEDs contained in interchangeable tubes arranged in a ring between the sample heater plate and the PM tube. Each cluster consists of six blue LEDs placed in a holder machined so that all individual diodes are directed and focused at the sample. The ring-shaped holder can contain up to seven clusters making a total of 42 diodes illuminating the sample at a distance of about 30 mm. However, normally one position is occupied by the focused IR laser diode described in section 3.5. A schematic diagram of the combined blue LED cluster and IR laser diode OSL unit is shown in Fig. 3.16a. A green long-pass GG-420 filter is fitted in front of each blue LED cluster to minimise the directly scattered blue light able to reach the PM cathode (see next section). The total power (seven clusters) delivered to the sample position was measured as  $24 \text{ mW cm}^{-2}$ . Detection is through two 3 mm Hoya U-340 filters, one of which is coated with metal oxide (see section 3.3.5). The power at sample versus current setting for the blue LED cluster unit is plotted in Fig. 3.16b.

To ensure stability of the output power, the blue diode array is equipped with an optical feedback servo-system similar to that described by Bøtter-Jensen et al (1991) and Bøtter-Jensen (1997) for infra-red LEDs. An extra diode connected in the current chain of the LED array is arranged to face an optical fibre light-

guide which in turn is connected to a phototransistor. The phototransistor output regulates the feedback comparator/amplifier that controls the LED current (see section 3.1).

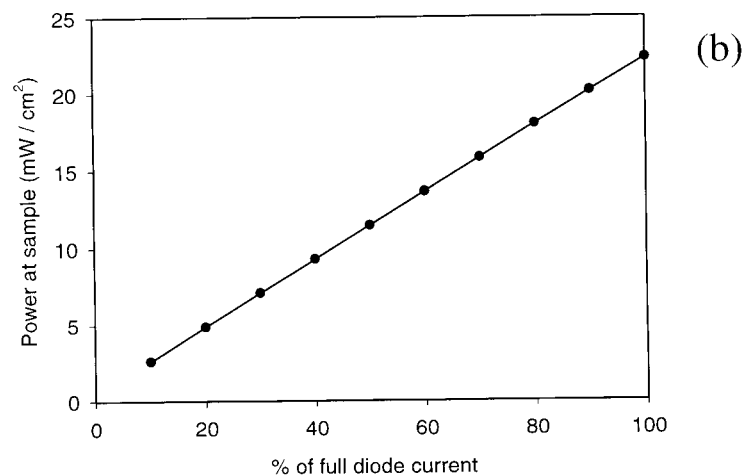
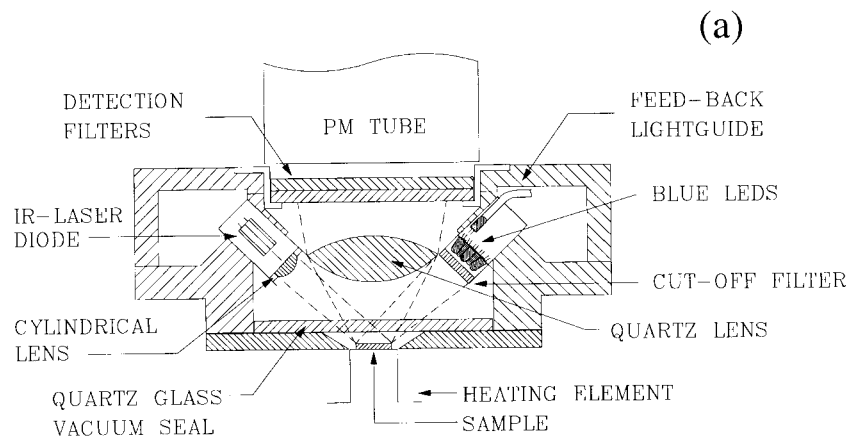


Fig. 3.16. (a) Schematic diagram of the new combined blue LED and IR laser diode OSL unit. 36 blue LEDs (in 6 clusters) emitting at 470 nm deliver max 20 mW/cm<sup>2</sup> at the sample and the IR laser diode emitting at 830 nm delivers max 550 mW/cm<sup>2</sup> at the sample (from Bøtter-Jensen and Murray, 1999).

(b) Power at sample versus current setting for the 6-cluster blue LED OSL unit.

(iii) Cross-talk characteristics

The cross-talk characteristics, i.e. the effect on the adjacent samples during stimulation, were measured for the new blue LED cluster OSL unit. Four mg mono-layer coarse grain quartz samples mounted on Al discs were used in the investigation. The stimulation of the adjacent samples due to cross-talk is expressed as percentage of the equivalent stimulation time on the adjacent sample. The effect of stimulation, i.e. loss of signal, was determined individually for each sample using the single aliquot regeneration (SAR) protocol (described in chapter 8). The cross-talk measured for the adjacent sample was  $< 0.00599 \pm$

0.00007 % and  $< 0.012 \pm 0.006$  % for the 48-sample carousel and the older 24-sample carousel, respectively. Surprisingly, an improvement of the cross-talk characteristics of a factor two for the 48-sample carousel was found when compared with the older 24-sample carousel. This is caused by an improved measurement geometry achieved using a new flange system on top of the heater lift mechanism in the new reader design.

*(iv) Blue LED and cut-off filter characteristics*

The emission spectra of five blue LEDs were measured using the Oriel MultiSpec 1/8M spectrometer fitted with an IntaSpec diode array detector (1 nm resolution), as was used to measure the emission characteristics of the IR LED and IR laser diode (see sections 3.3.1 and 3.3.2). The spectra were measured at LED currents of 2 mA and 20 mA (recommended maximum current); a maximum peak emission shift of 1.7 nm towards shorter wavelengths was detected with the increased current. The effect of short and prolonged switch-on times on the LED emission spectrum was determined by first setting the spectrometer to sample emission spectra every 0.1 s over the initial 2 s after switching on the cold diodes at a current of 20 mA. Secondly, spectra were sampled each second over the first 2 minutes after switching on the cold diodes. In both cases no measurable (i.e.  $< 1$  nm) peak shifts in the spectra could be detected. It is concluded that it is unlikely that the apparent rate of decay of luminescence will be significantly affected by changes in illumination wavelength, for all practical illumination powers.

The incorporation of a green long-pass filter has a very significant effect on background luminescence count rate (Bøtter-Jensen et al, 1999b). Fig. 3.17 shows the observed LED emission spectrum overlain with the published transmission curve of the green long-pass filter GG-420 and the U-340 detection filter. There is a significant tail in the diode emission, extending to shorter wavelengths, but this is attenuated effectively by the GG-420 filter, at the cost of about a 5% attenuation in the peak emission wavelength. There is also a long wavelength tail in the blue diode emission spectrum which extends above 600 nm (Fig. 3.17); because of the red transmission window in the U-340 response, this could contribute to the scattered light reaching the PM tube. This problem is solved by using metal oxide coated U-340 filters as described in section 3.4.

*(v) Illumination response time*

One of the advantages of OSL over TL is the possibility of using signals from brief illuminations of the samples obtained prior to the measurement of the full decay curves as a tool for normalisation of the individual sample sensitivity. In order not to deplete the OSL signal it is essential that (i) very brief illumination pulses can be delivered and (ii) the illumination power can be reduced, preferably under automatic control. When using broad band stimulation from a halogen lamp a major constraint is the shutter speed. This prevents the use of very short exposures ( $< 0.1$  s) and introduces some uncertainty in the actual exposure time because of scatter in the shutter opening and closing times. In order to test the response times and analyse the shape of the light exposure pulses from both broad-band and blue LED systems, experiments were carried out using a blue-green (420-550 nm) halogen lamp system with an electromechanical shutter (Melles Griot type 04 IES 001) and a blue LED system containing three clusters, each of 6 diodes. In both cases scattered light from the stimulation light source was measured directly by the PM tube via 5 mm of U-340 detection filter. Fig. 3.18 shows examples of 100 ms duration illumination pulses observed with a collection resolution of 1 ms. The delay in the shutter response in the broad band system is clearly seen. The delay reduces the light collected by the data collection system, which starts collection when the “shutter open” com-

mand is given (dashed vertical lines at 20 ms in Figures 3.18a,b). The lost signal during a 0.1 s pulse was calculated to be 10% and <0.5% for the broad band/shutter system and the blue LED system, respectively. It is concluded that the shutter should not be used for illumination pulses shorter than 100 ms whereas the blue LED can deliver reproducible pulses as brief as 5 ms.

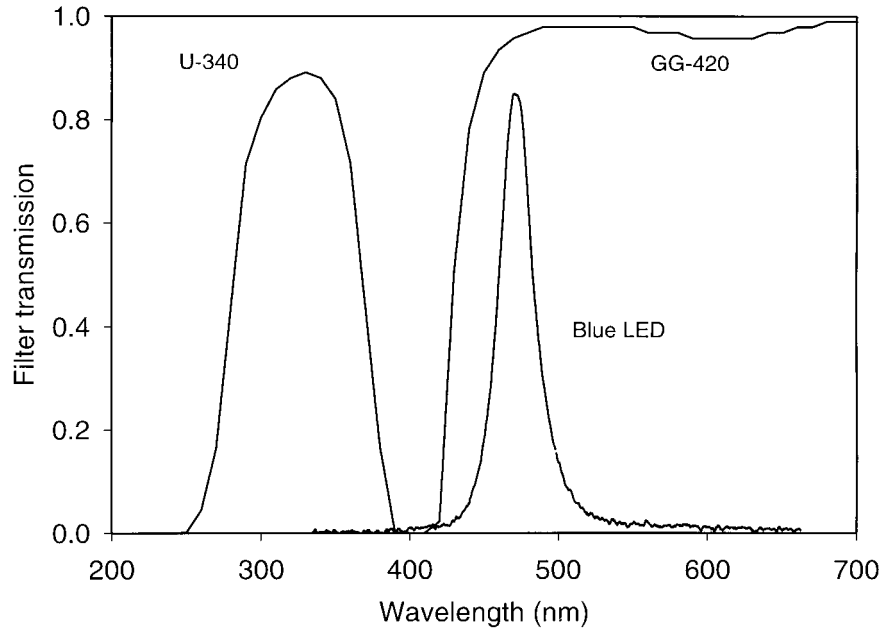


Fig. 3.17. The measured blue LED emission spectrum overlain with the transmission curves for the GG-420 green long-pass filter and the detection filter Hoya U-340 (from Bøtter-Jensen et al, 1999b).

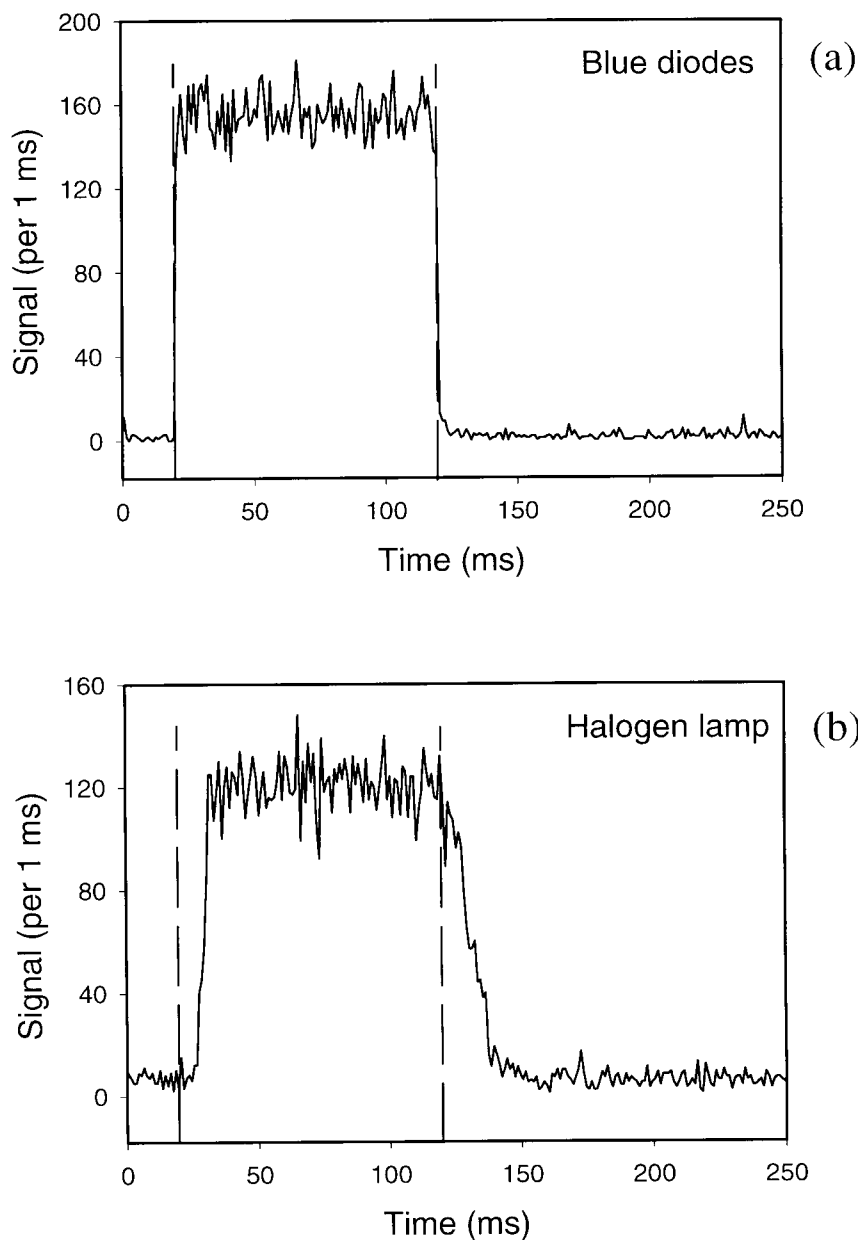


Fig. 3.18. 100 ms duration pulses observed with a collection resolution of 1 ms. For (a) the blue LED array and (b) the broad band halogen lamp system. The dashed vertical lines indicate the time at which the on/off command was issued (from Bøtter-Jensen et al, 1999b).

(vi) Comparison of stimulation light sources

The quartz stimulation efficiency of two different stimulation light sources were compared: (a) the standard broad-band blue/green (420-550 nm) attachment, delivering  $30 \text{ mW cm}^{-2}$  and (b) a blue LED stimulation unit consisting of 6 clusters of 6 LEDs delivering  $18 \text{ mW cm}^{-2}$ . All stimulations were at  $125^\circ\text{C}$ . Detection filters were two U-340 (one coated with metal oxide) in both cases.

Fig. 3.19 shows the comparison of decay curves obtained from aliquots of a natural sedimentary quartz using the two units. Note the logarithmic OSL scale. The ratio of the last 0.2 s OSL to the first in the blue data set is 0.14%; the ratio for the broad band data set is 0.13%. This observation is important because it

suggests that the blue LED system is stimulating the same set of traps in this sample as the broad-band source. In particular, it does not give any support to the suggestion that the blue LEDs ( $470 \pm 20$  nm) stimulates charge from deep traps with greater relative efficiency than the broad-band source (420 – 550 nm), when compared to the main OSL trap. This conclusion was further investigated as described in the next section.

To demonstrate further that the slope differences in Figure 3.19 are not the result of stimulation wavelength differences, the experiment was repeated using the broad-band source at full power and at approximately half power. The two curves are shown inset to Figure 3.19, and the relative differences are very similar to those of the main figure.

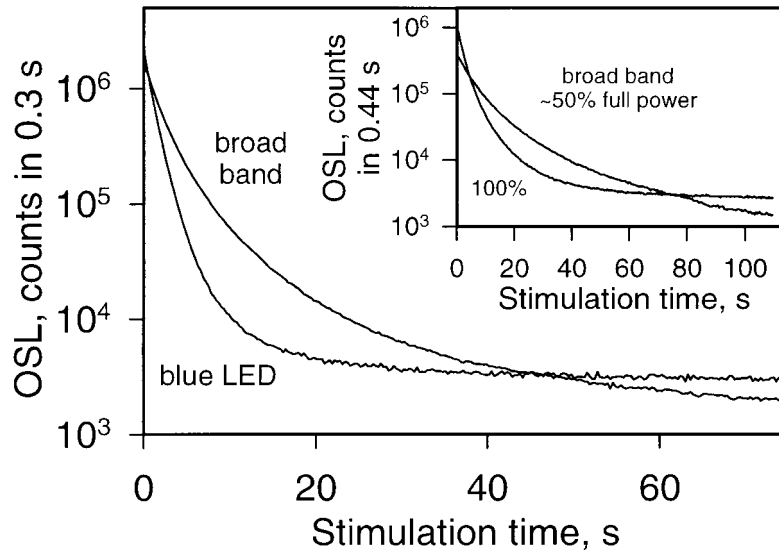


Fig. 3.19. Plots of decay curves obtained from a natural sedimentary quartz using (a) the blue LED OSL unit ( $15 \text{ mW/cm}^2$ ), and (b) the broad-band ( $28 \text{ mW/cm}^2$ ). Note the logarithmic Y-axis. A higher sensitivity and initial depletion rate seen using the blue LEDs is a result of the higher average energy of the stimulation light. For comparison the inset shows decay curves obtained with the same sample using the broad-band source at full power and at half power. (From Bøtter-Jensen et al, 1999b).

(vii) Source of blue light stimulated OSL

To confirm that stimulation with 470 nm LED light does not stimulate a different set of OSL traps in quartz to those stimulated by the broad-band source, blue LED stimulated OSL was measured as function of preheat temperature. This measurement was based on the experiment described by Wintle and Murray (1997), who used the same sample (WIDG8) and the broad-band source (the two experiments are thus directly comparable.) One natural aliquot ( $D_e=51$  Gy), was given a test dose of 0.2 Gy to populate the  $110^\circ\text{C}$  TL trap, stimulated at  $125^\circ\text{C}$  for 0.1 s, and then preheated at  $160^\circ\text{C}$  for 10s. This dose/OSL/preheat sequence was repeated for different preheat temperatures, increasing in  $20^\circ\text{C}$  steps up to  $500^\circ\text{C}$ . A further natural aliquot was exposed to full power blue light for 200 s at  $125^\circ\text{C}$ , then given a regeneration dose of 51 Gy. The preheat experiment described above was then repeated. During the repeated stimulations, the blue LED array was run at low power, such that stimulation at  $125^\circ\text{C}$  reduced the OSL by  $\sim 0.6\%$  per 0.1s illumination. Thus correction for the decay in OSL signal resulting from repeat measurement is negligible. The OSL data were

then corrected for luminescence sensitivity changes by dividing by the area of the 110°C TL peak (resulting from the 0.2 Gy test dose), which was observed immediately after each OSL measurement. This correction is discussed in detail by Wintle and Murray (1997).

The resulting curves of OSL signal against preheat temperature are shown in Fig. 3.20a. For comparison, the corresponding curves for the broad-band source (Wintle and Murray, 1997), are shown in Fig. 3.20b. From the similarity of the two sets of curves, we again deduce that there is no evidence that the blue stimulated OSL is derived from a different set of traps than that from the broad-band source.

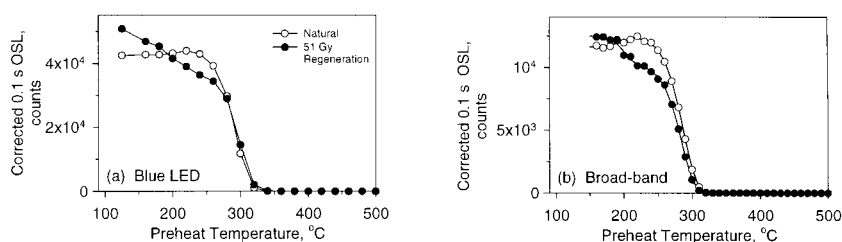


Fig. 3.20. (a) Blue LED stimulated luminescence as a function of preheat temperature from a well bleached quartz for (i) a natural aliquot ( $ED \sim 51$  Gy) and (ii) a fully bleached natural sample given a regeneration dose of 51 Gy.

(b) As in (A) but using the broad-band halogen light source (from Bøtter-Jensen et al, 1999b).

#### (viii) Ramping the stimulation light density

To illustrate the new facilities available with the blue LED array, preliminary experiments were performed to investigate the OSL response of quartz to a linearly increasing stimulation power density. Such experiments had earlier been performed using IR diodes with feldspars by Bulur (1996). Fig. 3.21 shows, as an example, the result of exposing a heated and dosed quartz sample to linearly increasing stimulation power from 0 to 15 mW/cm<sup>2</sup> over 800 s. The OSL trap distribution is clearly seen. A more detailed examination of the OSL response of quartz and feldspar to ramped stimulation power is described in chapter 4.

#### (ix) Summary – blue Leds

The investigations of the suitability of blue LEDs as a stimulation light source for quartz can be summarised as follows: 1) blue LEDs can be used to stimulate quartz more rapidly than conventional light sources, 2) switch-on/-off times allow illumination pulses of as short as 1 ms, 3) electronic control allows software to set power level and 4) ramping of power is readily achieved.

### 3.3.7 Conclusions – OSL light sources

A variety of stimulation sources for OSL measurements developed at Risø in the last few years have been outlined. Both visible-light and infrared-light stimulation sources have been improved according to the growing demand for measuring low doses, i.e. OSL signals from young samples. Important features that should be taken into account when designing OSL stimulation units are: 1) small sample-to-detector distance to improve light collection, 2) reducing the cross-talk affecting the nearest adjacent sample in the sample turntable and 3)

maximising the power delivered to the sample. Table 3.2 lists the different OSL configurations developed in recent years and gives their capabilities in terms of stimulation wavelength, whether power stabilisation is provided, power delivered to the sample and the cross-talk affecting the nearest adjacent sample.

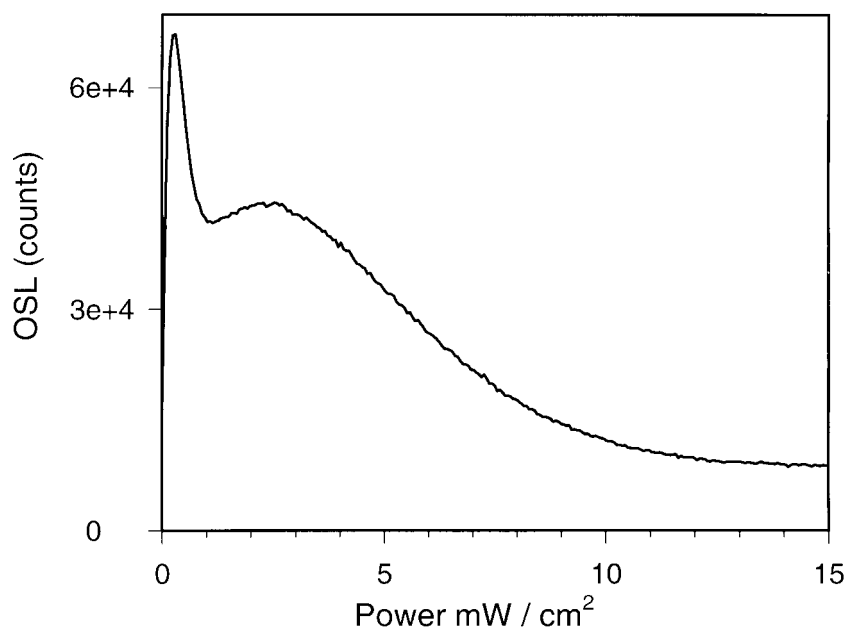


Fig. 3.21. An example of OSL versus linearly increasing stimulation light intensity obtained for a heated quartz sample using the ramp facility of the new blue LED OSL unit (from Bøtter-Jensen et al, 1999b).

Table 3.2. Data for the stimulation light sources developed at Risø in the last few years.

Stimulation light source	Wavelength (nm)	Power stabilisation (feed-back)	Power at sample (mW/cm <sup>2</sup> )	Cross-talk (%) (nearest adj. Sample)
75 W Halogen	420-550	No (burn-in: 2 min)	16	
150 W Halogen	420-550	No (burn-in: 2 min)	30	0.0058 ± 0.0013
Blue LEDs	470	Yes	24	0.00599 ± 0.00007
IR LEDs	875	Yes	40	0.019 ± 0.006
IR laser diode	830	Yes	500	0.12 ± 0.006

## 3.4 Monochromators and Spectrometry

### 3.4.1 Introduction

The use of OSL in dating and retrospective dosimetry applications is now well established, and a number of different light stimulation sources are now commonly used. Ideally, however, the spectral emission and excitation characteristics of quartz, feldspar and porcelain materials prepared for dosimetric evaluation would be routinely scanned. As well as giving valuable information about

the physical processes involved, it would also allow the possibility of choosing the most suitable energy windows in which to carry out the measurements.

*(i) Emission spectrometry*

A simple TL glow curve (TL versus temperature) does not always yield unambiguous information, for instance, when the emission spectrum changes with temperature during a TL measurement. This may be due to the radiative recombination of the released charge occurring at more than one defect site within the crystal. For this reason it is important to be able to obtain 3-D glow curves i.e. emission spectra in which the intensity is displayed as a function of both temperature and wavelength. 3-D glow curves thus give information both about the trap distribution (TL versus temperature) and the charge recombination centres (TL versus wavelength). Several instruments based on different optical principles have been developed and described in the literature. Dispersive rapid scanning systems based on a diffraction grating were described in the early 1970s by Harris and Jackson (1970) and Mattern et al (1971). Methods using optical filters have also been employed: Bailiff et al (1977) reported a rapid scanning TL spectrometer based on successive narrow band interference filters of 20 nm bandwidth fixed on a common turntable; Huntley et al (1988) built a spectrometer based on a custom-made concave holographic grating in connection with a micro-channel plate PM tube and image converter to obtain wavelength resolved spectra of a variety of mineral samples. A sensitive spectrometer based on Fourier transform spectroscopy which offers high aperture for light collection and continuous detection at all wavelengths in the range 350-600 nm was developed by Prescott et al (1988). Luff and Townsend (1993) reported a highly sensitive TL spectrometer for producing 3-D isometric plots of TL intensity against wavelength and temperature. This spectrometer uses two multi channel detectors that can measure spectra in the wavelength range 200-800 nm. Martini et al (1996) developed a high-sensitivity spectrometer for 3-D TL analysis based on wide-angle mirror optics, a flat-field holographic grating and a two-stage micro-channel plate detector followed by a 512-photodiode array. Recent developments in charge coupled device (CCD) camera techniques have led to the development of emission spectrometers with high resolution. Rieser et al (1994) reported a high sensitivity TL/OSL spectrometer based on a liquid nitrogen cooled CCD camera, with simultaneous detection over the range 200-800 nm. In this instrument thermal stimulation can be performed up to 700°C and optical stimulation from UV to IR with monochromatic light from a 200 W mercury lamp. Krause et al (1997) studied the OSL emission spectra from feldspars obtained by the CCD based spectrometer and found four wavelength maxima at 280, 330, 410 and 560 nm, respectively.

*(ii) Stimulation spectrometry*

Hütt et al. (1988) demonstrated the importance of analysing the optical stimulation spectra (i.e. OSL versus stimulation wavelength) of feldspars and Poolton et al. (1996) showed that stimulation spectra of natural samples provided some information about the mineralogy. As the OSL signal decays under constant illumination, consideration of procedures for correcting the stimulation spectra produced must be considered. Bailiff (1993) and Bailiff and Barnett (1994) used a titanium-sapphire laser, tuneable between 700 and 1000 nm, to analyse the time decaying OSL stimulation spectra from feldspars, both at room temperature and at low temperatures. Ditlevsen and Huntley (1994) used argon krypton, He-Ne, and argon-pumped dye lasers operated in CW mode to study optical excitation characteristics of quartz and feldspars. One problem using high power tuneable lasers is that the OSL obtained at each wavelength has to be normalised and corrected for the beam power and instrument response. Bailiff

and Barnett (1994) observed that the infrared resonance peak position of different feldspars shifted to higher photon energies at lower temperatures and the full-width half-maximum of the peak reduced with decreasing temperature. Clark and Sanderson (1994) performed OSL excitation spectroscopy using filtered light from a 300 W xenon lamp coupled to a computer controlled, stepper motor driven f 3.4 monochromator.

Bøtter-Jensen et al (1994a) designed a compact scanning monochromator based on variable interference filters covering the wavelength band 380-1020 nm. When mounted onto the automatic Risø TL/OSL reader, this enables high quality excitation and emission spectra to be obtained by rapid optical scanning of a variety of feldspar and quartz samples (Bøtter-Jensen et al, 1994b). A detailed description of the Risø monochromator design and features is given in the following sections.

### 3.4.2 Construction and design of the Risø monochromator

By using a variable interference filter as the wavelength dispersive element, very compact monochromator systems can be designed having reasonably good light throughputs and at the same time enabling very rapid spectral scanning. The Risø design is based around the use of two filters covering the spectral range of interest (the first usable in the range 380 to 750 nm and the second from 740 to 1040 nm). For UV/visible measurements, the Schott filter VERIL S-60 was used which gives spectral resolution of 10 nm across the entire range, transmission factors of around 35% and blocking to better than 0.01%. (The full characteristics are discussed in more detail below). The infrared filter was specially designed and built for the Risø monochromator by Barr Associates, USA, and has a similarly high performance (spectral resolution of 9 nm, transmission 60%).

Fig. 3.22a provides a detailed cross section of the construction of the Risø monochromator, and Fig. 3.22b illustrates the attachment to the automated Risø reader; it adds only 4 cm to the overall optical path length of the system, since all the focusing and collimating optics are placed in spaces already present. In the excitation mode collimated light from the 75 W tungsten halogen lamp (or other external source) is focused onto a slit, behind which the filter is scanned; the emerging monochromatic beam is then re-collimated, and finally focused onto the sample. The construction allows the slit width to be continuously adjusted from 0 to 10 mm, allowing flexibility in choice of spectral resolution down to 20 nm; with slit widths less than 1mm, no increase in resolution is achieved, since the limiting factor then becomes the filter bandwidth (in this case around 10 nm). The filter is mounted on a linear rail and is moved by means of a small stepper motor: this configuration allows for accurate positioning. The travel speed is restricted to between 0 and 30 nm/s (at 0.14 nm per step) for the visible system, or 50 nm/s (at 0.23 nm per step) with the infra-red filter, giving in each case minimum scan times of around 15 seconds for the entire spectral range.

Fig. 3.23a shows the transmitted spectrum from a high pressure mercury arc source, a HeNe laser and the output of a calibrated high resolution spectrometer set at 880 nm. This diagram highlights a number of points. Firstly, since the variation away from linearity of wavelength vs position along the filters is very small (certainly within the spectral band width), the wavelength setting can be directly measured by counting the number of steps advanced by the stepper motor (each step representing around 0.1 nm). Secondly, it will be noted that the spectral band width (at 10 nm) is nearly constant along both the filters. Thirdly, the laser line can be used to determine the stray light levels of the system. We

have determined that at 450 nm, transmission of the 633 nm laser line is lower than 0.005%, although this increases to around 0.05% at 580 nm: similar figures are measured for stray light throughputs of the infra-red filter.

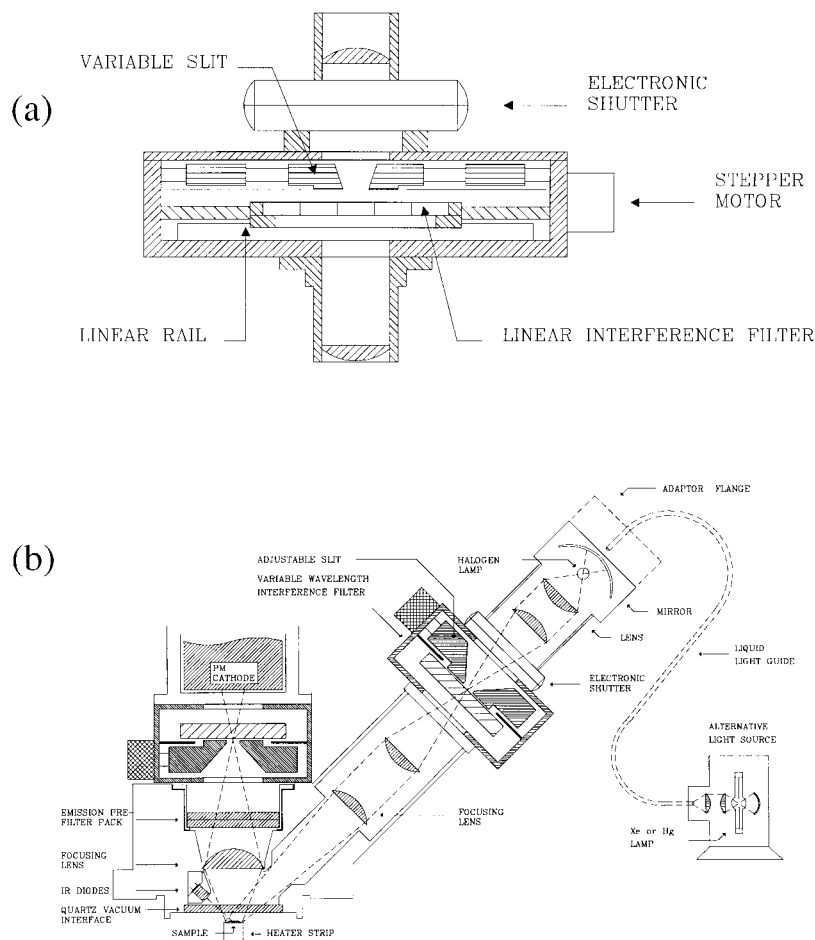


Fig. 3.22. (a) Detailed cross-section of the Risø monochromator.

(b) Schematic diagram showing monochromators mounted in both excitation and detection positions of the Risø broad-band OSL unit for obtaining stimulation spectra and emission spectra, respectively. (From Bøtter-Jensen et al, 1994a).

The transmission characteristics for the filters are shown in Fig. 3.23b. Note that these are relatively flat (unlike, for example, diffraction gratings), which makes correction to spectra for instrumental response straight forward. For the “visible” filter, transmission changes from 31 to 38% between 400 and 700 nm respectively, and for the infra red system, from 50 to 60% in the range 750 to 980 nm. These figures were measured using f2 optics with two monochromators working in tandem, the first acting as an absorption spectrometer and the second as the “sample” (Bøtter-Jensen et al, 1994a). Using a similar configuration, Fig. 3.23c shows the transmission characteristics of the two broad-band interference filters commonly used in OSL experiments.

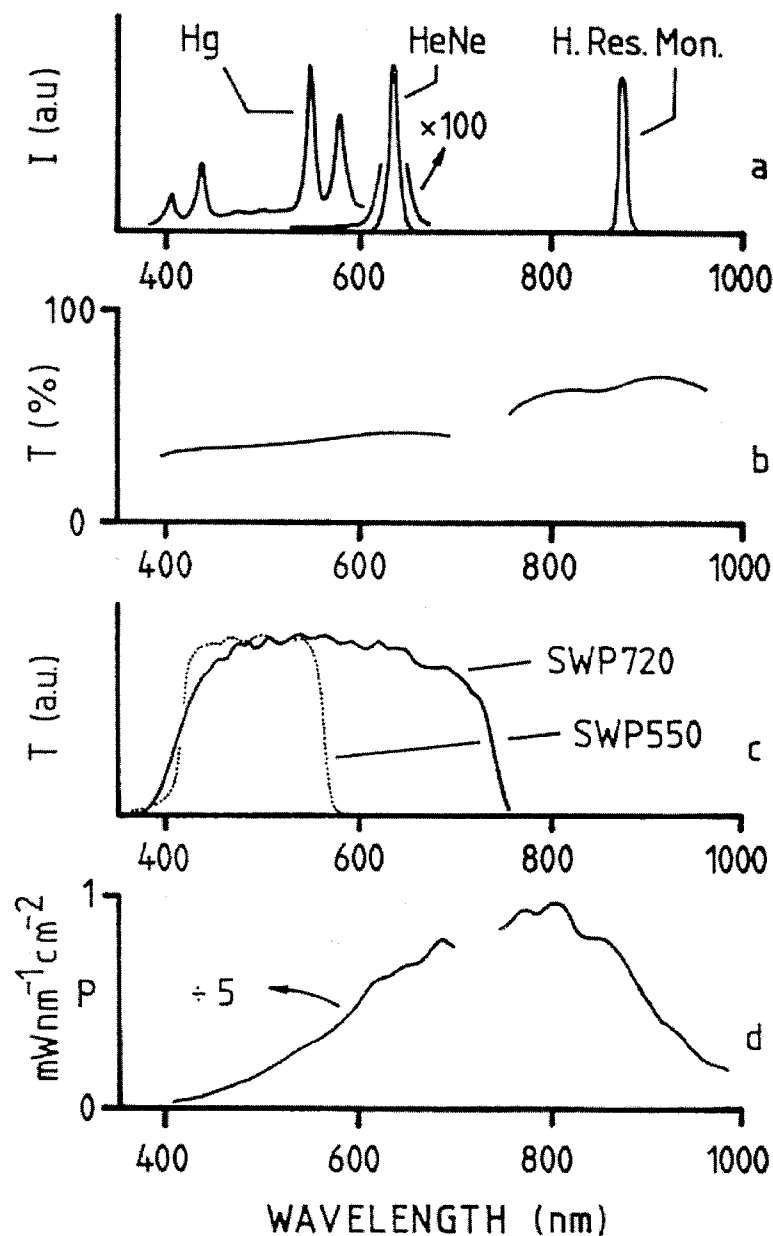


Fig. 3.23. Technical aspects of the monochromator:  
 (a) resolution, linearity and stray light rejection using a number of sources;  
 (b) transmission factors of the linear filters;  
 (c) demonstrating their use as an absorption spectrometer;  
 (d) the power throughput of the system when coupled to a 75 W tungsten-halogen light source  
 (from Bøtter-Jensen et al, 1994a).

Finally, in Fig. 3.23d, the power throughput of the system is shown, when linked to the 75 W quartz-tungsten-halogen lamp normally used for “broad band” excitation of OSL. A rear reflecting mirror was installed behind the lamp, thereby increasing the illumination intensity by around 90%, and giving better filling of the monochromator slit. The power ranges from 0.01 to 1.1 mW/cm<sup>2</sup>/nm in the range 400 to 1000 nm, following quite closely the black body curve for an emitter at 3400K: the power transmittance is not entirely

smooth due to the use of interference filters for heat rejection. Measurements were made with a calibrated pyrometer. Whilst the power throughput may appear low, it was never found that there is a shortage of excitation intensity, and the fall off in power below 500 nm is in fact a great advantage, since the efficiency of exciting trapped charge increases very rapidly at the shorter wavelengths; the two effects therefore partly compensate, making repeated scans possible whilst only marginally effecting the trapped charge population. This effect is described in more detail in section 4.2.

It was found that one advantage of splitting the spectral range is that UV/visible emission spectra can be recorded at the same time as producing variable wavelength, monochromatic excitation, thus giving a complete luminescence excitation/emission spectrometer that plugs straight onto the automated Risø reader. A demonstration of the capabilities is given in section 3.4.3.

### 3.4.3 Experimental capabilities – emission spectra

#### (i) Thermoluminescence emission spectra

As mentioned in section 3.4.2, the particular construction of the Risø monochromator means that the spectral range 380-700 nm can be scanned in around 15 seconds, taking a further 25 seconds to reset. This consequently limits the heating rates usable if the TL emission spectra are to be continuously recorded: for example, a ramp rate of 1°C/s would give a temperature resolution of 15°C to the spectra, with a repetition measurement every 40°C. Naturally, better resolution etc can be achieved either by slowing the ramp rate further, or employing a faster motor. However, analysis of the TL emission spectra previously published (Luff and Townsend, 1992) shows that in general (at least for silicate type minerals), there are not usually rapid changes of spectrum in the high temperature regions. Examples of TL emission spectra obtained from feldspars are presented in chapter 5, section 5.3.

#### (ii) Photoluminescence emission spectra

*-Time decaying OSL.* Comparison of the TL and OSL emission spectra can be very important if comparison in the dosimetric information coming from the two techniques is to be made. Since the OSL is obviously time dependant, the problems of scan rate and repetition cycle are essentially the same as discussed above. In this case, however, the difficulties are slightly easier to overcome, since the spectra are easily compensated if the time decay characteristics of the OSL is known. Further, the fall in intensity of the OSL signal can be partly compensated by scanning the luminescence spectrum from high to low wavelengths, thereby making use of the rise of PM tube detection efficiency as the signal decays. Examples of OSL emission spectra obtained from feldspars are given in chapter 6, section 5.3.

*-Time stable photoluminescence.* By illuminating many feldspar samples with deep-UV light, time-stable photoluminescence (PL) can be stimulated. The simplest method of exciting this type of signal is to use the 75 W quartz tungsten halogen lamp in conjunction with U-340 filters. Although the UV output is very low, the luminescence efficiency is often orders of magnitude higher than the OSL signal. Examples of PL emission spectra obtained from porcelain are given in Chapter 7.

### 3.4.4 Experimental capabilities - stimulation spectra

#### *(i) Time decaying OSL*

The original work of Hütt et al (1988) demonstrated the importance of analysis of the photo-excitation spectra of feldspar, and work carried out at Risø shows that detailed knowledge of the excitation spectra of natural samples provides essential information on the mineralogy (Poolton et al, 1996). The monochromator described here is ideally suited for producing such spectra.

As the OSL signal decays under constant illumination, consideration of procedures for correcting the excitation spectra produced must necessarily be made. This is a major problem if high power excitation sources are used (e.g. tunable laser systems) especially in multi-mineral samples, since the bleaching efficiency as a function of intensity and wavelength is complex. In the Risø system these problems have been minimised by using a broad band low power (75 W) tungsten halogen lamp as the excitation source. Firstly the output power is low and the intensity falls off rapidly over the same range as the photon capture cross section for the trapped charge is rising rapidly. As a consequence, during a typical wavelength resolved OSL excitation scan, only around 10% of the trapped charge is evicted. Because of this, only the intensity spectrum of the exciting lamp is required to produce a stimulation spectrum of the sample, and not a running analysis of how much charge is lost. A routine check of the validity of this method can be made by repeatedly scanning the stimulation spectrum; the method is valid as long as the excitation spectra remain the same from one cycle to the next. Examples of stimulation spectra obtained from quartz, feldspar, porcelain and  $\text{Al}_2\text{O}_3:\text{C}$  samples are presented in chapters 4, 5, 6 and 7, respectively.

#### *(ii) Time stable PL*

Whilst the energy resolved stimulation spectrum of the time decaying OSL emission of the sample probes the energy levels of the "donor" type defect (within a donor-conduction band-acceptor recombination cycle), the energy levels of the acceptor type defect can be probed by scanning the stimulating wavelengths of the time stable, Stokes shifted photoluminescence. Whilst such measurements are possible with the Risø monochromator, it usually requires highly photosensitive material.

### 3.4.5 Summary - monochromators

The main concern in dosimetry is that the most suitable choice of stimulation wavelength is made in the OSL measurement. The monochromator described above allows the entire stimulation spectrum to be scanned with very little loss of charge, so that dose-dependent growth curves can be easily measured for all stimulating wavelengths (400-1100 nm). The Risø monochromators have been used to obtain a variety of both stimulation and emission spectra from quartz, feldspar,  $\text{Al}_2\text{O}_3:\text{C}$  and porcelain. These are presented in the following chapters 4, 5, 6 and 7.

## 3.5 Development of Single Grain OSL Attachment Systems

### 3.5.1 Introduction

Recent work has shown that the natural bleaching of quartz and feldspar grains is not homogeneous, as had been previously assumed, but markedly heterogeneous (Li, 1994; Rhodes and Pownall, 1994; Murray et al., 1995; Olley et al., 1998). The effects of this heterogeneity become more pronounced as the number of grains in an aliquot is reduced, and there have been a few studies which have looked at individual grains of feldspar (Lamothe et al., 1994) and quartz (Murray and Roberts, 1997; Roberts et al., 1997). It is clear from these studies that there are considerable benefits in examining the dose distributions on a grain by grain basis, and particularly in identifying those grains which have been most completely bleached prior to deposition. This has not been practical in the past because of the time required to prepare many hundreds of grains for measurement using a conventional reader.

### 3.5.2 A CCD luminescence imaging system

#### *(i) Introduction*

The ability to image the luminescence signal from a sample, and isolate the signal from a specific part of the sample was initially achieved at Risø by using a charge coupled device (CCD) camera (Duller et al, 1997). The camera consists of the CCD chip and the associated electronics which allows the interfacing to a personal computer.

#### *(ii) The CCD device*

The CCD camera (Spectra Source Instruments) comprises the CCD itself, a thermo-electric cooling unit and the associated electronics that allow the system to be interfaced directly to a personal computer. The CCD chip is a Kodak KAF-0400 with an array of 768 x 512 pixels, with a 16 bit analogue to digital converter allowing up to 65,535 grey levels. Each pixel is 9  $\mu\text{m}$  square, giving a total active area of 6.91 x 4.61 mm. The CCD is cooled to approximately 251 K using a two stage thermo-electric cooler. An electro-mechanical shutter is placed in front of the CCD so that it is possible to control the period of time for which the CCD is exposed. Digitisation and storage of a whole image (393,216 pixels, or 768 kb of data) takes approximately 3 s, during which time the sensor is not exposed to light in order to prevent streaking across the image as the data are read from the CCD.

The system uses on-chip binning; this allows the signal, in groups of adjacent pixels, to be summed within the CCD read-out register, prior to conversion from an analogue to a digital signal and subsequent transmission to the host computer.

The camera was mounted on an automated Risø TL/OSL reader (see Fig. 3.24). The system has a maximum spatial resolution such that each pixel detects light from an area of the sample of 17 x 17  $\mu\text{m}$ . However, since this is much higher than is required when analysing coarse grained samples (typically 90 – 300  $\mu\text{m}$  in diameter), a binning procedure was used that gave a spatial resolution of 170  $\mu\text{m}$ . This increased the signal level per pixel by two orders of magnitude, and reduced the file size of an image from in excess of 750 to 11.5 kb.

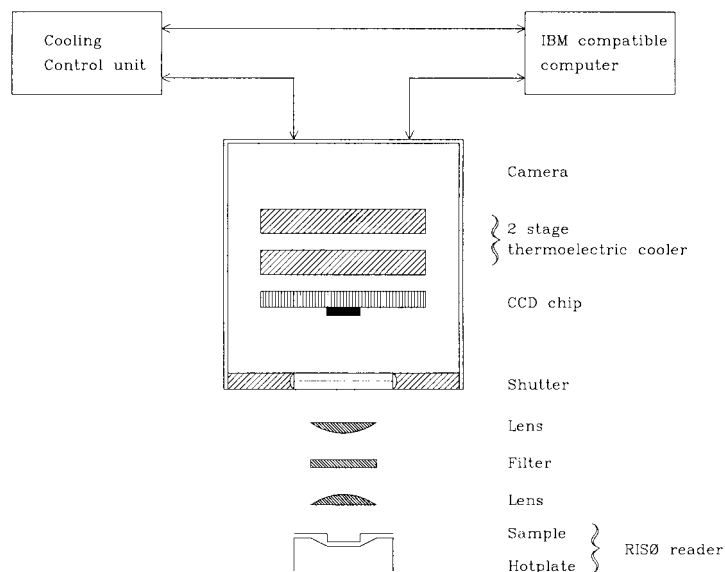


Fig. 3.24. Schematic diagram showing the components of the Risø-developed CCD system mounted on the Risø automated luminescence reader (from Duller et al, 1997).

(iii) Measurement noise

The digital signal measured for any given pixel by the host computer is affected by various sources of noise and bias within the CCD camera. These can be divided into two sources of uncertainty in the final value that is read. Under normal conditions, charge accumulates in the various pixels of the CCD during light exposure. However, electrons may also be accumulated within these pixels as a result of thermal noise, and these electrons cannot be distinguished from those generated by exposure to light. This thermal noise is the first source of uncertainty. The second source of uncertainty arises in the analogue to digital converter. The characteristics of these sources of uncertainty were measured in a series of experiments.

It was found that the bias level of the device changes with the CCD temperature. This was investigated more carefully by making measurements of the bias level as the CCD cooled from room temperature to its normal operating temperature. These are shown in Fig. 3.25a and show a substantial change in value as the device is cooled. The generation of thermal noise within the CCD was investigated by measuring the background signal for periods of time from 1 ms to 500 s without opening the shutter. Thus, any signal that was measured was due to thermal noise and was not an optically generated signal. Fig. 3.25b shows the data obtained when making these measurements both at room temperature and at the normal operating temperature of the device. Regression lines fitted through these two data sets show that the rate of generation of thermal electrons is  $31.9 \pm 0.2$  counts per pixel per s at room temperature, but that when cooled the rate is indistinguishable from zero.

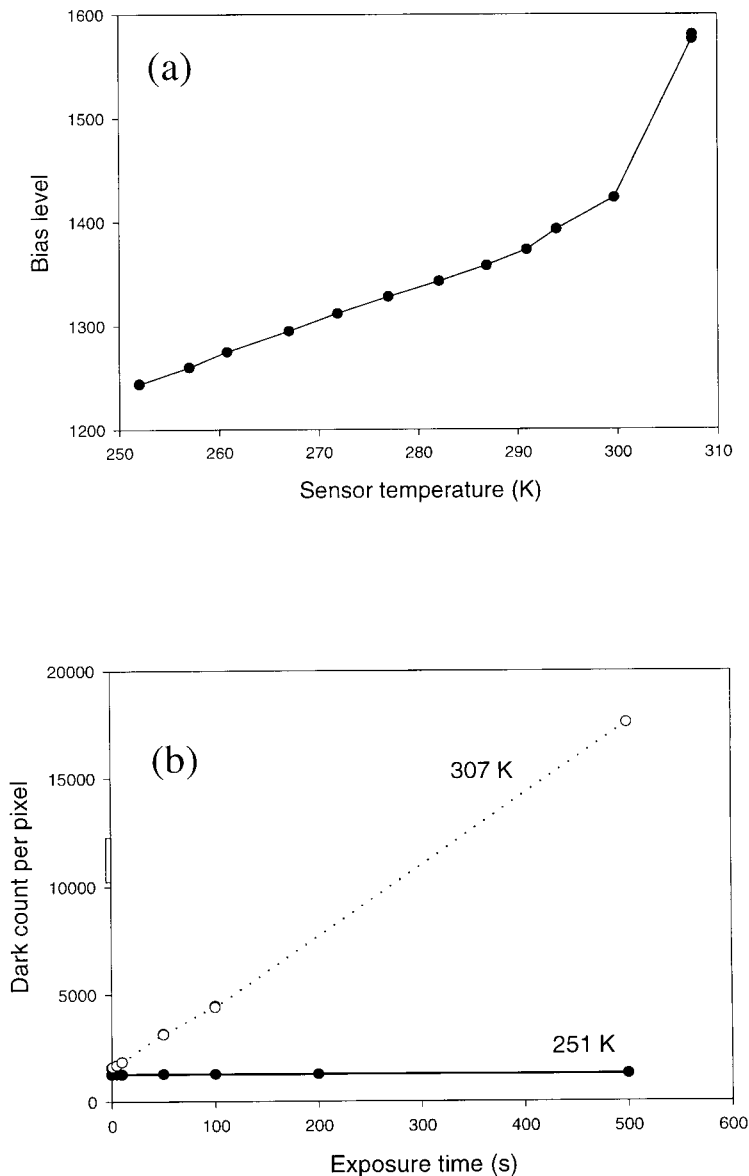


Fig. 3.25. (a) Variation in the bias level per pixel as the CCD is cooled from room temperature to its standard operating temperature (251 K).

(b) The change in the signal level per pixel after integrations, varying from 1 ms to 500 s, when the shutter is not opened. Hence, any signal that is observed is due to read noise or thermal noise. Measurements were made both at room temperature and at the standard operating temperature. (From Duller et al, 1997).

(iv) Detection efficiency

The wavelength dependence of the detection efficiency of the CCD is very different to that of a photomultiplier tube (PMT). The quantum efficiency of the type of CCD used (Spectra Source HPC-1S) is highest between 600 and 800 nm. The active surface of the CCD is shielded by silicon substrate upon which the device is fabricated and this silicon absorbs wavelengths shorter than approximately 500 nm, causing the sensitivity of the device to drop rapidly below this point. Because of this the CCD was coated with a Lumigen phosphor which absorbs photons with a wavelength shorter than 460 nm and then emits at 520

and 560 nm (Cowens et al, 1980). As seen in Fig. 3.26 this extends the spectral response of the CCD, although at a reduced sensitivity, to wavelengths as short as 200 nm (Duller et al, 1997).

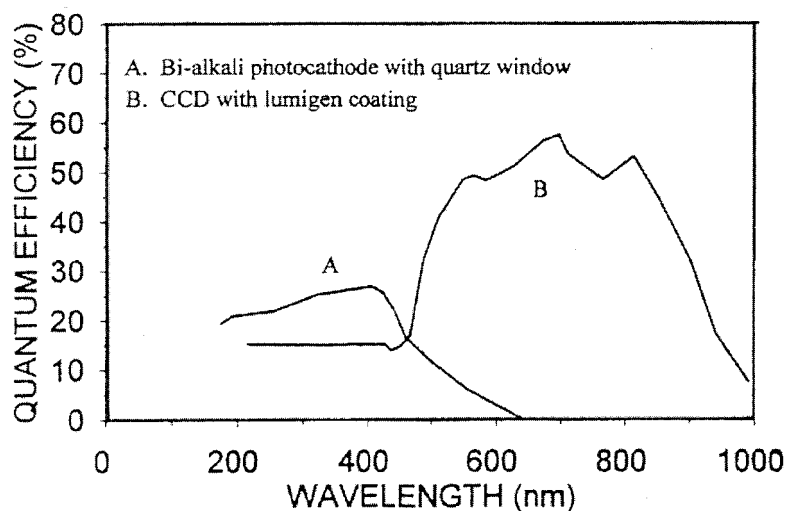


Fig. 3.26. Comparison of the quantum efficiency of a photomultiplier tube with a bi-alkali photocathode and the KAF-0400 CCD. The CCD response shown is for a device that has been coated with Lumigen to extend its detection efficiency into the blue and u.v. Without this coating, the CCD detection efficiency continues to drop rapidly below 500 nm, reaching zero at 450 nm. All data are from the manufacturers.

#### (v) Applications

Various experiments were performed with the camera mounted on an automated Risø TL/OSL reader, using two lenses to focus an image of the sample onto the CCD (see Fig. 3.23). One experiment used a 5 mg sedimentary potassium feldspar sample (180-211  $\mu\text{m}$ ) that retained its natural luminescence signal; this was placed in a sample cup in the reader. The sample was exposed to infrared stimulation (875  $\Delta$  80 nm at a power of 16 mW/cm<sup>2</sup>) and a CCD image was recorded every second for 25 s. A 1 mm thick BG-39 filter was placed in front of the CCD in order to shield it from the IR stimulation. This gave a detection window from approximately 300-600 nm. On-chip binning of 10 x 10 pixels was used for the measurements giving a spatial resolution of 170 x 170  $\mu\text{m}$ . Fig. 3.27 plots the total signal detected by the CCD during each integration. The expected decay of luminescence with stimulation was seen. The inset to Fig. 3.27 shows decay curves from five individual pixels (170 x 170  $\mu\text{m}$ ) chosen at random from the centre of the images obtained, and two other pixels from the edge of the image which show the background signal.

#### (vi) Summary

Charge coupled devices have very different characteristics from a PMT, and these differences need to be taken into account when optimising the use of the system. Firstly, the CCD has an extremely broad spectral response and so is capable of making measurements at far longer wavelengths than are possible using bi-alkali PMTs. The comparisons we have made between the detection efficiency of the CCD and the PMT demonstrate very clearly the superior perform-

ance of the CCD at longer wavelengths. Secondly, one automatically obtains time resolved data when using a PMT, whereas a CCD is an integrating device and a series of discrete images need to be taken in order to observe signal variation through time. Hence the CCD is not suitable for measurements that require high temporal resolution ( $< 0.1$  s), but is well suited to longer exposure times.

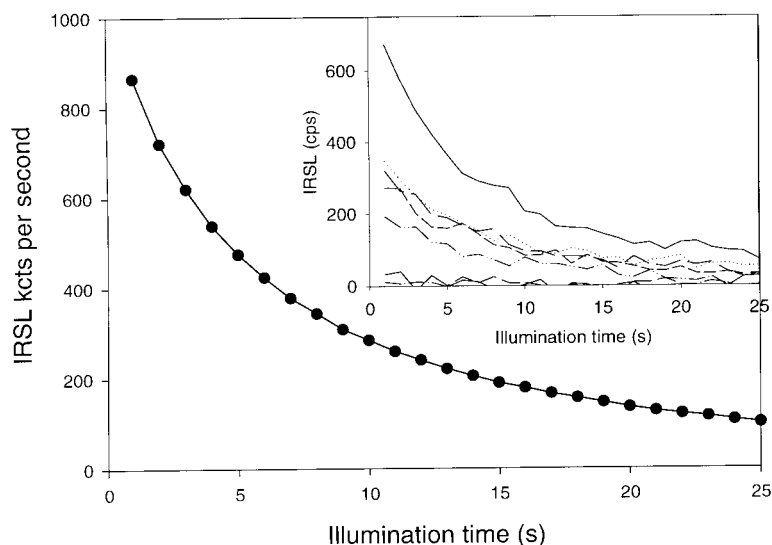


Fig. 3.27. IR-stimulated luminescence decay curves obtained from a feldspar sample using the CCD camera. CCD images were integrated for 1 s and 10 x 10 pixel binning was used, giving spatial resolution of 170 x 170  $\mu\text{m}$ . The main curve is the signal from the entire CCD, while the insert shows the signal from single pixels (from Duller et al, 1997).

A variety of quartz and feldspar coarse grain samples had both their TL and OSL signals monitored using the CCD system described above. It was concluded that the use of CCD techniques was limited to bright samples when detection is made in the visible (blue-green) range. However, it is confidently expected that CCD cameras are a strong alternative to using PM tubes for monitoring the red emission from mineral samples, whether thermally or optically stimulated, due to the significantly higher quantum efficiency obtained with CCD cameras in the wavelength range 420 – 850 nm. So far it has been beyond the scope of our experimental work to investigate the red emission from quartz and feldspars. Instead the possibilities of using scanning focused laser beams to separately measure single sand sized grains have been investigated. These experiments are described in the following section.

### 3.5.3 An automated single grain laser luminescence (SGLL) system

#### (i) Introduction

So far, OSL measurements have normally been made on groups of grains extracted from the sample that is being studied; these grains (typically quartz and feldspar) are normally separated on the basis of grain diameter and bulk density. Typically, when using coarse grain samples, between 1000 and 7000 grains in the size from 90 to 300  $\mu\text{m}$  are mounted on a single 9.7 mm diameter metal disc, and the luminescence emitted from all the grains is thus measured simultaneously.

It has been known for some years that the individual grains of a multi-grain sample mounted on a single disc may have very different luminescence properties from one to another because of the variability in chemical composition and mineralogical structure that is likely in natural materials. Therefore, a considerable potential advantage in being able to make measurements of the luminescence properties of single grains has long been foreseen. To date this has only been demonstrated by two methods, each with severe disadvantages. The first approach is to pick individual grains by hand and to mount each grain on a separate sample disc (e.g. Murray and Roberts, 1997; Roberts et al, 1997). These can then be analysed using conventional luminescence instrumentation. However, this procedure is very time-consuming, both in sample preparation and in terms of instrument time. A second approach has been to use an ultra-sensitive imaging system such as an imaging photon detector (IPD, e.g. McFee and Tite, 1994) or a CCD camera as described in the previous section. These systems have the ability to spatially resolve the luminescence signal from a sample.

In recent years a number of methods have been developed that allow dose assessment to be performed by measuring only a single aliquot of a sample (Duller, 1995). However, these procedures require that repeat measurements be made on each aliquot. In the case of using imaging systems, such as the CCD, this requires repeat measurements of the luminescence signal coming from the same area of a sample after several measurements cycles; these may include physical movement of the sample detector. This is difficult at the scale of tens of microns as required for routine single grain measurements.

A prototype of a system which enables routine measurements of the OSL signal from single grains of quartz or feldspar in the size range from 100 to 300  $\mu\text{m}$  was developed at Risø (Duller et al, 1999a; Duller et al, 1999b). This system has since been improved and the next sections describe the modified single grain OSL system and address the need to make repeat measurements of the same grain. This is the first instrument that allows measurements of many grains to be made in a routine manner without individual selection.

#### *(ii) System description*

In view of the demand for full automatic processing the single grain OSL unit was designed to fit onto the existing automatic Risø luminescence reader. The basic requirement is that each 9.7 mm diameter sample disc should be able to hold as many grains as possible to feature the ability of being able to irradiate or heat the whole multi-grain sample in operation, but that the OSL signal from each grain must be measured individually without influence from neighbouring grains.

The system employs a 10 mW Nd:YVO<sub>4</sub> solid state diode pumped laser emitting at 532 nm, and producing a spot approximately 120  $\mu\text{m}$  in diameter at the surface of the sample disc. An electro-mechanical shutter controls the entry of the beam into the measurement chamber. Individual grains are located in 300  $\mu\text{m}$  wide and 300  $\mu\text{m}$  deep holes drilled as an 8 x 8 hole grid pattern on the surface of a 9.7 mm diameter, 0.5 mm thick aluminium disc, giving a total of 64 grain positions on each sample disc. The location of the laser spot on the sample disc is controlled by two mirrors which are mounted orthogonally, making it possible to illuminate only one single grain and thus measure the OSL signal it produces. A schematic diagram of the single grain OSL unit is shown in Fig. 3.28a.

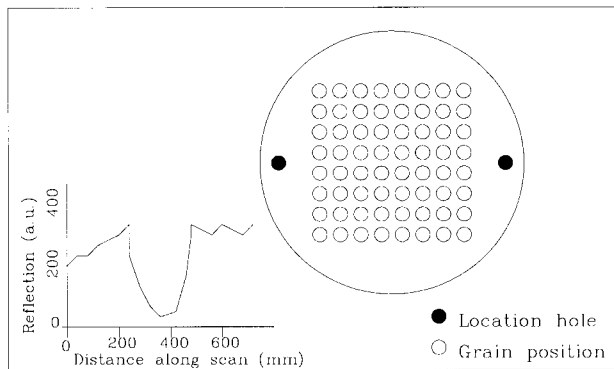
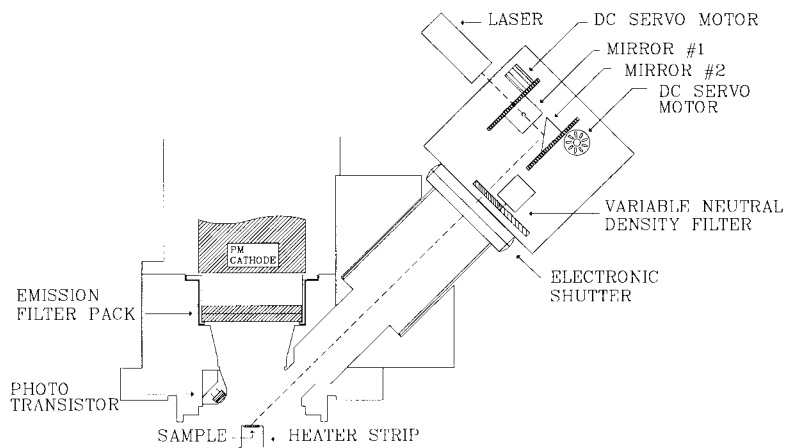


Fig. 3.28. (a) Schematic diagram showing the automated OSL X-Y laser scanning system developed at Risø.

(b) Schematic of the specially designed sample disc which can accommodate 64 single grains in a grid of 300  $\mu\text{m}$  diameter holes (from Duller et al, 1999a).

### (iii) Sample disc

An essential prerequisite of this approach is that the grains placed on each sample disc are located at precisely defined locations relative to one another. This has the obvious advantage that it enables the laser beam to be moved so that it is accurately centred on only one grain before the shutter is opened.

At this stage of development a grid size containing 64 samples holes was chosen as a compromise between a high grain capacity per disc and at the same time keeping the cross talk at a minimum. These holes were drilled into aluminium discs of 9.7 mm diameter using a computer controlled machine tool. At the same time that this grid of 64 sample holes is being drilled, two further holes for position identification are drilled at the periphery of the disc; these are 400  $\mu\text{m}$  in diameter and pass through the disc. The location of the grid holes and the position holes relative to each other is well defined and forms the basis for the

software controlled location of the grains (see next section). The sample disc is shown schematically in Fig. 3.28b

*(iv) Laser beam*

The laser beam is focused using a simple set of three lenses to give an approximately gaussian beam with 90% of the power contained within a spot of 120  $\mu\text{m}$  in diameter at the sample. The movement of the spot in two dimensions across the surface of the disc is achieved by movement of the two mirrors. Each mirror is set at  $45^\circ$  to the line of the beam and can be moved so that it causes the position of the spot on the sample disc to move along one axis. They are driven using two stepper motors attached to gear trains so that a single  $1.8^\circ$  step of the motor results in a 2  $\mu\text{m}$  movement of the mirror. The maximum scan speed of the two mirrors is 2.000  $\mu\text{m}$  per second, and the maximum travel distance is 20.000  $\mu\text{m}$ .

The single grain OSL attachment (Fig. 3.28a), consisting of the laser, the two mirrors and two stepper motors, is mounted in a plane at  $45^\circ$  to the sample disc. This is a compromise between the need to direct the beam onto the sample at a high angle to reduce cross-talk between grains, and the need to position the photomultiplier cathode close to the sample for optimal detection geometry.

*(v) Locating the grains*

As described in section 3.2 the automatic sample changer of the automated Risø luminescence reader consists of a carousel on which the sample discs are placed, and a heater strip that lifts the sample above the plane for OSL measurement. This introduces some uncertainty in the position of the sample disc relative to the laser system. Even when great care is taken in loading discs into the carousel, it is not possible to precisely locate the samples on the scale of a single grain (100-300  $\mu\text{m}$ ), and a small net rotation of the aluminium sample disc may occur during repeated carousel and sample movements. In order to correct for these small changes the approach is to use an attenuated laser beam (using a neutral density filter) to locate the positions of the two holes at the periphery of the sample disc (see Fig. 3.28b). A phototransistor is built into the measurement chamber, mounted so it is struck by the laser beam if reflected from the sample disc surface. The variation in the intensity of the reflected beam can be measured while scanning the laser beam across the sample disc and the results define the disc edges and centre points of the holes in the sample disc.

In normal procedure this is repeated on both the X and Y axes in order to define the centre positions of both of the locating holes. In this way the position of the sample disc is defined in terms of the co-ordinate system of the laser and its associated optics. From this information the control software calculates the centre of the sample disc, and its angle of rotation relative to the laser system. By combining this information with a detailed description of the positions of the various holes drilled into the sample disc, the laser spot can be moved to any of the holes containing sample grains. During the location measurements, the laser beam is attenuated by a factor of 30 using neutral density filters to reduce possible cross-talk between samples. Only the edges of the disc are scanned, to eliminate any possibility that the laser beam will intercept a sample hole.

This search routine is the starting point for each measurement of a sample disc since it defines the position and angle of rotation of the disc. The laser is then moved to the calculated position of grain number one and an OSL measurement is made using full laser power. Once a measurement of the first grain is completed the attenuator for the laser beam is inserted again and the position of the first grain hole is checked using the pattern of reflectivity. This estimate for the position of grain number one is then used to update the calculation for the posi-

tion of grain number two. Grain two is then measured at full laser power, its position checked, and the new estimate used to calculate the position of grain number three. This process continues across the whole disc, with the laser positioning constantly being updated based on the position of the last grain that was measured. In this way, any positioning errors are constantly corrected. The average standard deviation in positioning were found to be about 25  $\mu\text{m}$  on the X-axis and 30  $\mu\text{m}$  on the Y-axis; these approach the minimum step size for the laser movement (10  $\mu\text{m}$ ), and are much smaller than a grain hole (300  $\mu\text{m}$ ).

*(vi) Performance testing*

A key capability of a single grain system is that it should be able to make repeat measurements on a single grain so that single aliquot dose evaluation procedures (Duller, 1995; Murray and Wintle, 1999) can be applied. To test this a disc was prepared that contained a single 90-105  $\mu\text{m}$  grain of an  $\text{Al}_2\text{O}_3\text{:C}$  single crystal fixed in each sample hole using a liquid resin.  $\text{Al}_2\text{O}_3\text{:C}$  was chosen because of its high OSL sensitivity (Bøtter-Jensen et al, 1997; Bøtter-Jensen et al, 1999c).

The disc filled with  $\text{Al}_2\text{O}_3\text{:C}$  grains was given a beta dose in the Risø reader of approximately 8 Gy, and then the OSL signal from each grain was measured over 20 s. All measurements were made at room temperature with constant time interval between irradiation and measurement (no preheating due to the resin). This measurement cycle was repeated 11 times. For each grain, the OSL signal was integrated over 20 s of the measurement. Most grains showed systematic variations in OSL response as the sequence of measurement progressed. This was foreseen since no thermal annealing was undertaken between each measurement cycle. In order to calculate the reproducibility of the single grain reader, the set of 11 repeat OSL measurements for each grain were plotted as a function of measurement number, fitted by linear regression, and the standard deviation of the residuals from this regression analysis calculated as a percentage of the average OSL signal from the grain. Analysis of the data from all of the grains gave an average reproducibility of 3%, an order of magnitude better than was possible using the CCD system described earlier.

As an additional test, the same disc of  $\text{Al}_2\text{O}_3\text{:C}$  was given a beta dose of 100 s ( $\sim 1$  Gy) and the disc was then analysed using a modified form of the single aliquot regeneration (SAR) procedure (Murray and Wintle, 1999) to see whether this dose could be accurately recovered. The mean of the resulting dose estimates was 100 s with a standard deviation of 6.7 s, and a standard error of 0.9 s (see Fig. 3.29).

The performance of the single grain laser OSL system was further tested at Risø using a set of 320 quartz grains mounted on 5 sample discs (Duller et al, 1999a). The quartz grains were extracted from an Australian dune sand and had a natural dose of approximately 0.05 Gy. The grains were then exposed to further beta dose of 17.6 Gy. The single aliquot regeneration (SAR) method (described in chapter 8) was then used to attempt to measure this known dose. Fig.3.30a plots the normalised OSL signal as function of laboratory dose for a single grain (see Murray and Mejdahl, 1998). The signal from the 17.6 Gy dose given to the sample prior to this test is plotted on the left most axis as a filled square. Subsequent measurements were made of the OSL signal after exposure to the radiation source for different periods of time, and these were used to construct the dose response for this grain. A typical decay curve from a single quartz grain is shown inset to Fig. 3.30a. Fig. 3.30.b shows the distribution of equivalent dose for 80 grains from which relatively bright signals could be obtained. The distribution is approximately normal with a mean value of 17.8 Gy and a standard deviation of 2.2. Gy.

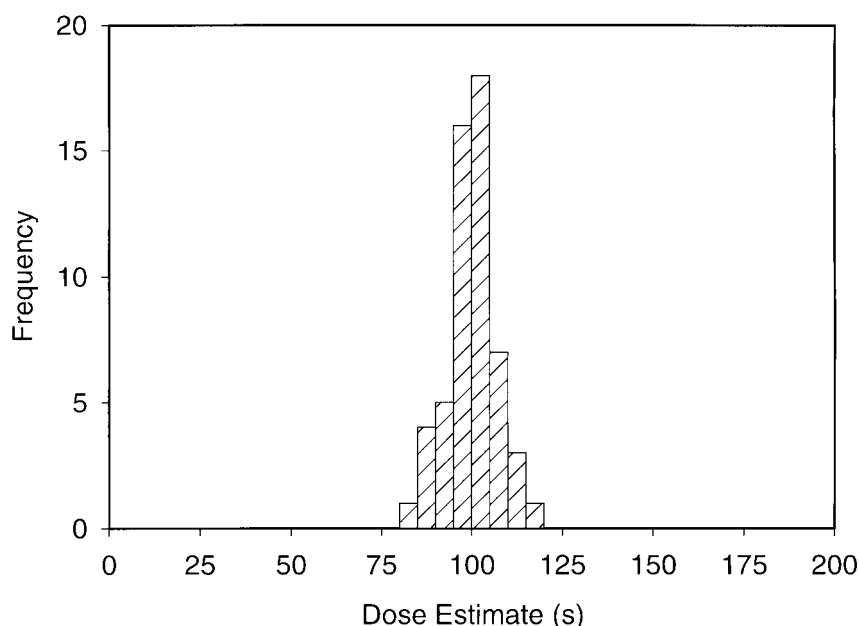


Fig. 3.29. The distribution of the apparent dose in 56 grains of  $Al_2O_3:C$  that had previously been given a beta dose of 100 s using the beta source in the automated Risø reader. The mean of the distribution is 100 s, with a standard deviation of 6.7 s. (From Duller et al, 1999b).

(vii) Summary

A system has been constructed at Risø that makes it feasible to measure the luminescence behaviour of a large number of single grains for the first time. The initial results obtained show that it is capable of locating each grain accurately, and that it is possible to make repeat measurements on a grain with a precision of 3%. Preliminary evaluations of the absorbed doses using a single grain regeneration protocol showed that a reproducibility with a standard deviation of approximately 6 % can be obtained. It has been shown that the single grain OSL system described above is capable of measuring OSL from a significant number of grains even with relatively low doses, and that a measurement procedure is available that allows a rapid evaluation of doses to which single grains have been exposed previously.

### 3.5.4 Conclusion – single grain systems

In an attempt to carry out OSL measurements on single grains two systems have recently been developed and tested. One is based on a CCD technique where the luminescence signal from a multiple grain sample is imaged and subsequently, by software, divided into signals originating from the individual grains. The CCD system was found to have limitations when emission occurs in the blue-green wavelength range. However, it is foreseen that CCD systems will be more attractive when detecting the red emission bands from both quartz and feldspar because of the significantly enhanced detection efficiency of the CCD camera in this wavelength range. The other system is a laser based single grain OSL attachment which has shown extremely high sensitivity in the blue-green emission wavelength range and is, therefore, more useful for the analysis of luminescence in the visible wavelength range emitted from single grains.

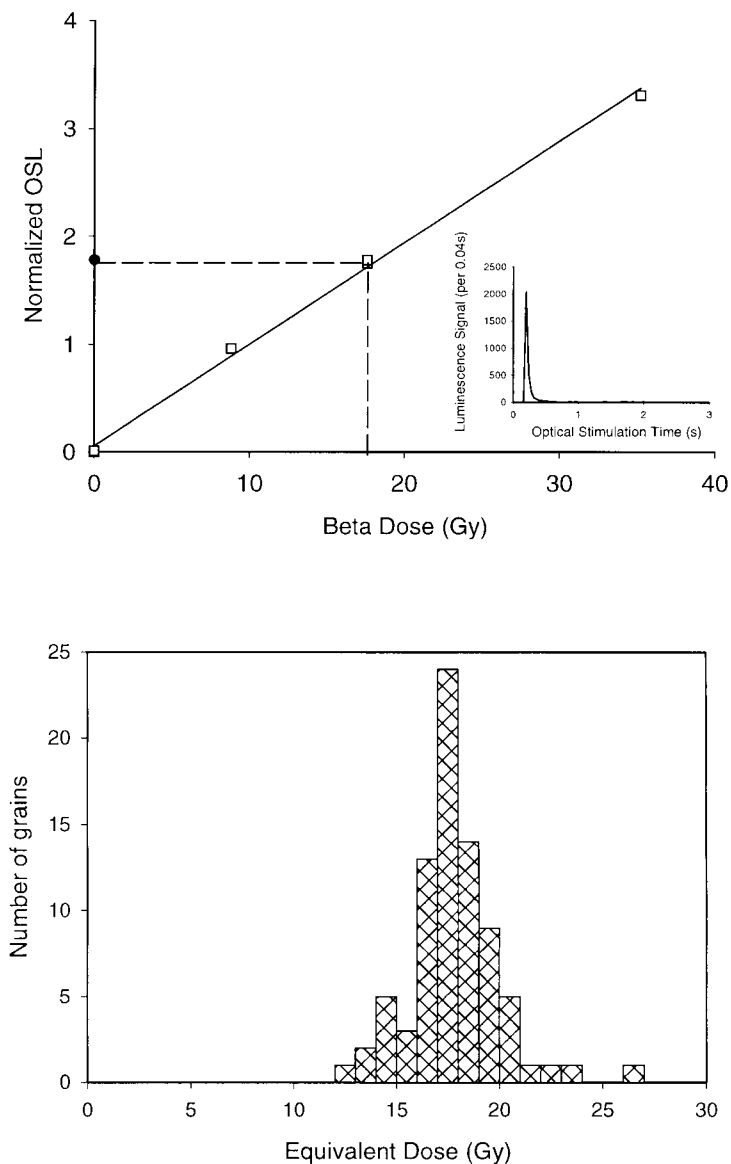


Fig. 3.30. (a) The OSL response from a single grain of quartz to laboratory irradiation. The inset shows the OSL signal for a single grain during 2 s of laser stimulation.

(b) The distribution of apparent dose in 80 quartz grains given a test dose of 17.6 Gy. The mean value of the distribution is 17.8 Gy, with a standard deviation of 2.2 Gy, and a standard error of 0.25 Gy (1.4 %). (From Duller *et al.*, 1999a).

There have been only a few studies which have looked at individual grains of feldspar and quartz. It is clear from the studies carried out at Risø that there are considerable benefits in examining the dose distributions on a grain by grain basis, and particularly in identifying those grains which exhibit bright luminescence signals. This has now become possible on a routine basis for the first time using the new automated Risø single grain OSL system described above.

## 3.6 Other OSL Measurement Systems

### 3.6.1 Automatic OSL scanner

The ability to focus stimulation light sources to illuminate only a fraction of the sample surface lends itself to the possibility of analysing position-resolved luminescence at other scales besides single grains. An integral optical sensor system was developed for rapid analysis of split sediment cores in geological applications. When several tens of metres of sediment core are available for study, it is often difficult to decide exactly where to select material for detailed analysis and age determination. The primary aim of the system was to obtain information based on OSL techniques; these provide a record of the accrued radiation dose of material since deposition. Particularly after suitable normalisation, the luminescence signal recorded along the length of the core will provide information on the relative age of the sediment. The basis for the design is a core logger system with a conveyor belt allowing optical sensors to be moved along the length of split sediment cores up to a length of 1.7 m. The optical sensor consists of a photo-excitation and detection module together with lamps for bleaching and regenerating the OSL. Both IR and blue-green stimulation is provided and these probe the feldspar, and combined feldspar and quartz components of the sediment, respectively. The ratio of the two signals can thus provide rapid information on the silicate mineralogy.

The sensor head maintains a constant height above the core surface by means of a motor and cam mechanism (with height measured using a linear displacement voltage transducer). A schematic diagram of the apparatus is shown in Fig. 3.31, along with details of the sensor head design.

Luminescence is detected using a 30 mm diameter selected bialkali photomultiplier tube (type EMI 9924) in photon counting mode, with emission passing through 6 mm of standard Hoya U-340 filter (transmitting between 280 nm and 370 nm, with a peak at 340 nm). These filters were used in detection when exciting either with green or with infrared light. Their advantage is that, since of necessity the detector is open and exposed, measurements can proceed under the normal ambient lighting levels typically used in luminescence dating laboratories (i.e. similar to that in a photographic dark room) since the detector is rendered effectively blind to red/orange light.

Measurements in the field require an excitation source to normalise the signals from the individual samples. As it is difficult, and against security regulations, to handle stronger radioactive sources in the field, UV lamps were instead tested for this purpose. However, the exact regeneration mechanism for UV excitation is not well understood, but is likely to be related to phototransfer of charge from deep traps to shallow traps. The luminescence regeneration lamp that was built into the equipment is a cold-running 20 W low pressure Hg gas discharge tube (Osram HNS-20UOZ) that yields an output of 5.5 W at 254 nm (4.9 eV) and 0.8 W at 185 nm (6.7 eV). A similar lamp has been shown to be effective as an alternative to radiation sources for OSL normalisation of siliceous sediments. Poolton et al (1996) describe the performance of the core scanner in detail and present results from measurements of Danish sediment cores.

The OSL core scanner has also been used to measure depth dose profiles on small cores drilled out of bricks for retrospective dose determination after nuclear accidents (see chapter 8, section 8.4).

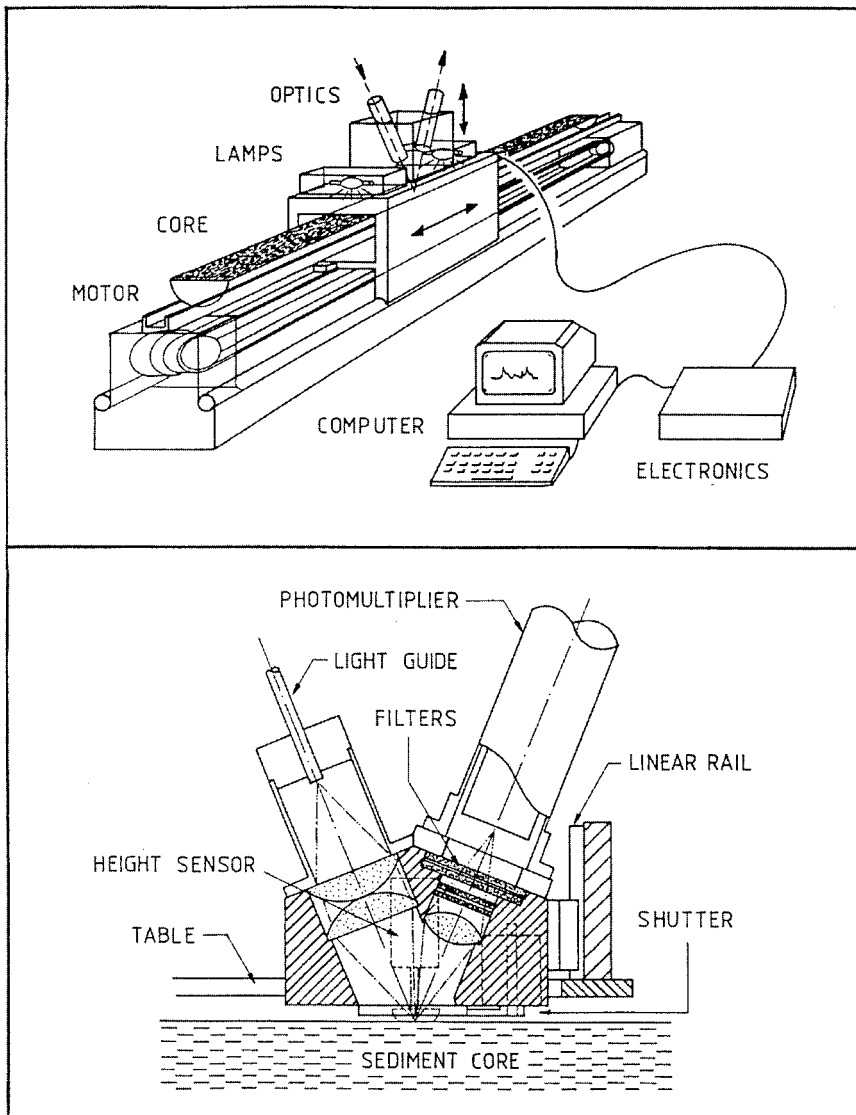


Fig. 3.31. Schematic diagram (above) of the Risø-developed OSL core scanner system and (below) detail of the luminescence excitation/detection head. The use of a light guide allows the luminescence excitation source to be physically removed from the main light collection optics. Sediment cores up to 1.7 m in length can be analysed in the system (from Poolton et al, 1996).

### 3.6.2 A portable system for OSL measurements in the field

When dating thick sediment deposits it is often difficult to decide in the field how many samples should be taken for preparation. Sampling is normally based on the visible features of the material. However, subtle changes in the sedimentological features relating to breaks in the deposition history are often not obvious to the naked eye, but will show up as discontinuities in the luminescence determination of the  $D_e$  as a result either of the age, or of different bleaching histories. As a consequence, it is desirable to be able to rapidly assess the luminescence properties of the sediment at regular intervals down a section, preferably on site.

The advent of optical stimulation methods allows the dating of mineral grains at ambient temperatures, thus making portable equipment practical. Although for precise dates this material must be prepared under laboratory conditions,

field measurement of untreated sediment may provide sufficient information to provide a sampling guide. Because of this, a compact and lightweight computer controlled system was developed that allows for the measurement of IR stimulated luminescence of samples in the field, whether in the form of loose grains or compressed pellets. The unit uses infrared diodes for excitation, with bleaching and OSL regeneration provided by cold-running gas discharge lamps (Poolton et al, 1994).

A schematic diagram showing the features of the portable OSL system is shown in Fig. 3.32. The flexibility of the field instrument means that it can be simplified to a basic unit, or extended to become a full luminescence spectrometer. Briefly, in the standard system, luminescence excitation is provided by an array of infrared LEDs. The excitation/detection unit is of similar design to that described by Bøtter-Jensen et al (1991). The luminescence is detected via a 4 mm Schott BG-39 filter by a 30 mm blue-sensitive PM tube (EMI 9924B) with the emission intensity measured using conventional photon counting. Sample bleaching is provided by a blue fluorescent lamp, and re-excitation of the OSL (for normalisation) is via a low pressure Hg discharge tube. The bleaching and re-excitation lamps were chosen to give the maximum efficiency of bleaching and regeneration of OSL in feldspars, since these are the principal minerals being measured. By using U-shaped tubes, all samples can be uniformly illuminated simultaneously, thereby saving considerable processing time (see Poltoon et al, 1994).

Up to 12 samples in the form of compressed pellets or loose grains on discs or cups are mounted onto an interchangeable cartridge, which is then loaded into the machine. The entire unit is enclosed in a light-tight box, and the samples move from one operational position to another on a trolley, driven by a motor/spindle mechanism; all this is controlled automatically by a microprocessor unit, with overall coordination and data logging made using the RS232 interface of a portable computer. A typical complete measurement cycle for 12 samples takes 30 min. The entire system fits into a small case and weighs only 5 kg; since all components run at 12 volts, either portable or car batteries can be used as power sources.

A detailed description of the portable OSL system and test results obtained from measurements of a variety of Danish sediments are given in Poolton et al (1994).

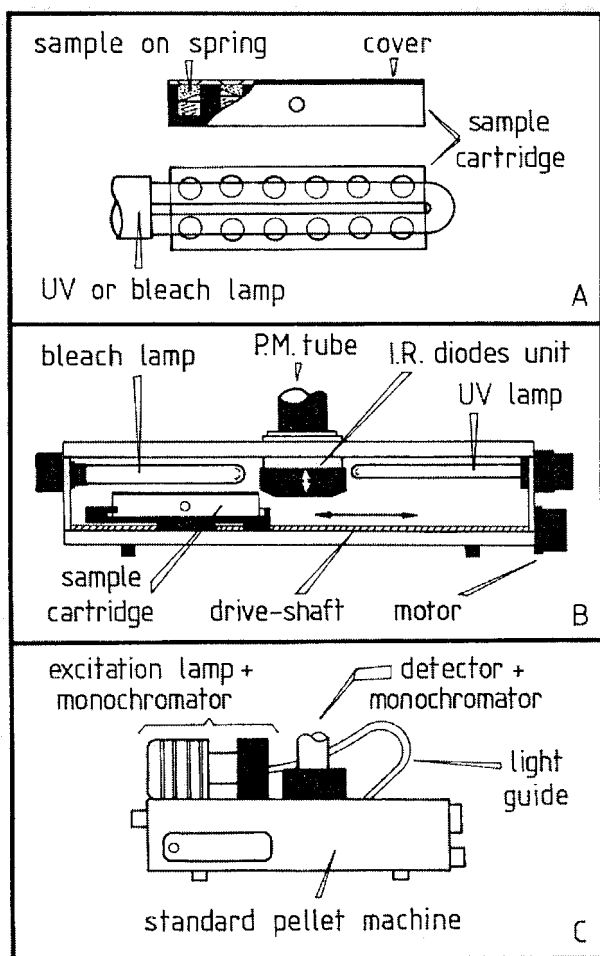


Fig. 3.32. The portable OSL system.

(a). 12 samples can be spring-loaded into the sample cartridge, which ensures that the top surface of each is always at the same elevation. The geometry of the holder is such as to allow even illumination of all samples from the U-shaped bleaching and signal regeneration lamps.

(b). Scale drawing of the complete portable system (with front panel removed). The sample holder is moved from one operational position to the next by means of a motor (drive shaft). The IR diodes excitation unit moves vertically to ensure a light-tight contact with the sample holder.

(c). The system can be extended into a complete luminescence excitation/detection spectrometer by replacing the IR excitation diodes with a halogen lamp and compact monochromator, and installing a second monochromator between the sample and PM tube. (From Poolton et al, 1994).

## 3.7 Conclusions - Instrumentation

TL and OSL techniques and methods developed at Risø over the last few years for dating and dosimetry have been reviewed and an attempt has been made to describe the state of the art in instrument development.

There is one problem which remains to be addressed in the development of combined TL/OSL instrumentation using different stimulation light spectra. This is concerned with the design of a flexible optical detection filter changing system to allow for rapid (automatic) selection of the optimal detection window whether using infrared or visible light stimulation. Changing of excitation or detection filters may, if not properly protected either by hardware or software, cause serious damage to the PM tube because of insufficient suppression of stray light from the stimulation light source.

The growing industrial interest in bright LEDs as light indicators (e.g. from automobile manufacturers) has made visible LEDs commercially available with substantially higher emission power than was available less than two years ago. These LEDs provide sufficient power to be considered a real alternative to laser and incandescent lamp stimulation light sources in OSL. The immediate advantages of using LEDs over filtered broad band lamps are: 1) reduced heat dissipation, with less effect on the stimulation optics and 2) no need for mechanical shutters to control stimulation exposure.

In the future, a major effort will no doubt be put into the further development of sensitive systems capable of measuring luminescence from single grains. The immediate advantages of this are that the accrued dose can be determined from only one grain and that variations in dose from grain to grain can be studied in detail. The latter feature will be especially valuable in dating incompletely bleached materials and in the identification of sediment disturbance in natural deposits. Such improvements will continue to require increases in detection sensitivity.

Further developments and investigations of luminescence imaging systems for obtaining spatially resolved TL and OSL signals from multi-mineral samples are also foreseen. These systems give rapid and valuable information about the mineralogy of the sample and enable individual analysis of luminescence signals from single grains of a sample. This has the potential to avoid the cumbersome mechanical and chemical separation processes presently required.

# 4 OSL Characteristics of Quartz

## 4.1 Introduction

Next to feldspars, quartz is the most abundant material in the Earth's crust (12.6 % by weight). The composition of quartz is normally very close to 100 % SiO<sub>2</sub>. Quartz is a common constituent in many igneous rocks, and also occurs as secondary material in sediments. Because of its chemical and physical resistance to corrosion, quartz is an abundant mineral and becomes concentrated during sedimentary processes to give rise to sands and sand stones of various types. The most common form is the low-temperature trigonal alpha-quartz which transforms at 575°C under normal pressure into hexagonal high-temperature quartz (beta-quartz) (see Deer et al, 1992).

Since the beginning of 1970s quartz has been used intensively in thermoluminescence (TL) dating (Aitken, 1985). Huntley et al (1985) showed that a luminescence signal could be obtained from quartz using optical rather than thermal

stimulation. They used the 514.5 nm single green line from an argon ion laser to stimulate quartz with the aim of using this technique in sediment dating. Since then, quartz optically stimulated luminescence (OSL) has been used in a number of applications that previously used TL because of the comparative ease of measurement and because in geological dating it is the light sensitive signal that is the most important. Subsequent research has attempted to clarify the nature of the OSL signal from quartz, both empirically (e.g. Spooner, 1994) and theoretically (e.g. McKeever and Morris, 1994; Bøtter-Jensen and McKeever, 1996).

In quartz, the OSL signal arises from charge related to the 325°C TL peak (Smith et al, 1986). Bøtter-Jensen et al (1994b) and Spooner (1994) showed that there is an exponential relationship between OSL and the energy of the stimulation light. Quartz OSL emission spectra obtained by Huntley et al (1991) were centred around a wavelength of 365 nm and thus luminescence detection is most efficiently made using narrow UV transmission filters.

The following sections describe research into the OSL properties of quartz carried out at Risø in recent years. Firstly features of the OSL decay curve and the optical stimulation characteristics of quartz when using different stimulation wavelengths are discussed. Then the relation between the TL and the OSL signals and the effect on the OSL sensitivity when quartz is annealed at different temperatures are outlined. Finally practical applications using quartz for low-dose measurements are discussed with a view to using this material as a sensitive OSL dosimeter in retrospective accident dosimetry.

## 4.2 The Quartz OSL Decay Curve

Bøtter-Jensen and Duller (1992) and Bøtter-Jensen et al (1993) were the first to demonstrate that the OSL signal from quartz could be stimulated using a broad-band light source providing a blue-green light spectrum (420-550 nm). Representative OSL decay curves from an archaeological (fired) quartz sample with a  $D_e$  of 1 Gy were obtained using the broad-band stimulation system described in section 3.3.3. These are shown both as a function of time (Fig. 4.1a) and integrated stimulation energy (Fig. 4.1b). The excitation system delivered a power of 16 mW/cm<sup>2</sup> to the sample, and bleached the OSL signal very rapidly, with a half-value reached after an exposure of about 25 mJ/cm<sup>2</sup>, i.e. in about 1.6 s. This is one fifth of the power required by a 514.5 nm argon laser (Smith et al, 1990), and is caused by the higher energy light present in the broad-band stimulation spectrum.

Murray and Wintle (1998) have investigated the factors controlling the shape of the OSL decay curve in quartz. They studied the effects of stimulation temperature on the shape of the quartz OSL curve, using the same green light stimulation source as Bøtter-Jensen and Duller (1992) used for an Australian quartz sample. They obtained the relationship between the initial OSL, the OSL at the end of stimulation and the full integral and deduced that a single trap/luminescence centre combination is responsible for the majority of the OSL signal at stimulation temperatures between 150 and 275°C. Thus traps giving rise to TL peaks in this temperature range cannot contribute significantly to the OSL signal, either directly or indirectly. Higher temperature traps, above the main OSL trap at 325°C, have also been shown to contribute very little, and the absence of a non-thermally-quenched component further indicates that the 375°C TL trap does not give a detectable OSL signal. However, shallow traps, especially those giving rise to the 110°C TL peak, do play a role in charge cycling. It appears that there are advantages in performing routine OSL at temperatures, which keep the 110°C TL trap empty (e.g. 125°C). Such elevated temperature stimulation gives a faster response, a smaller long time-constant

component within the OSL decay curve (Murray and Wintle, 1998) and an improvement in measurement sensitivity.

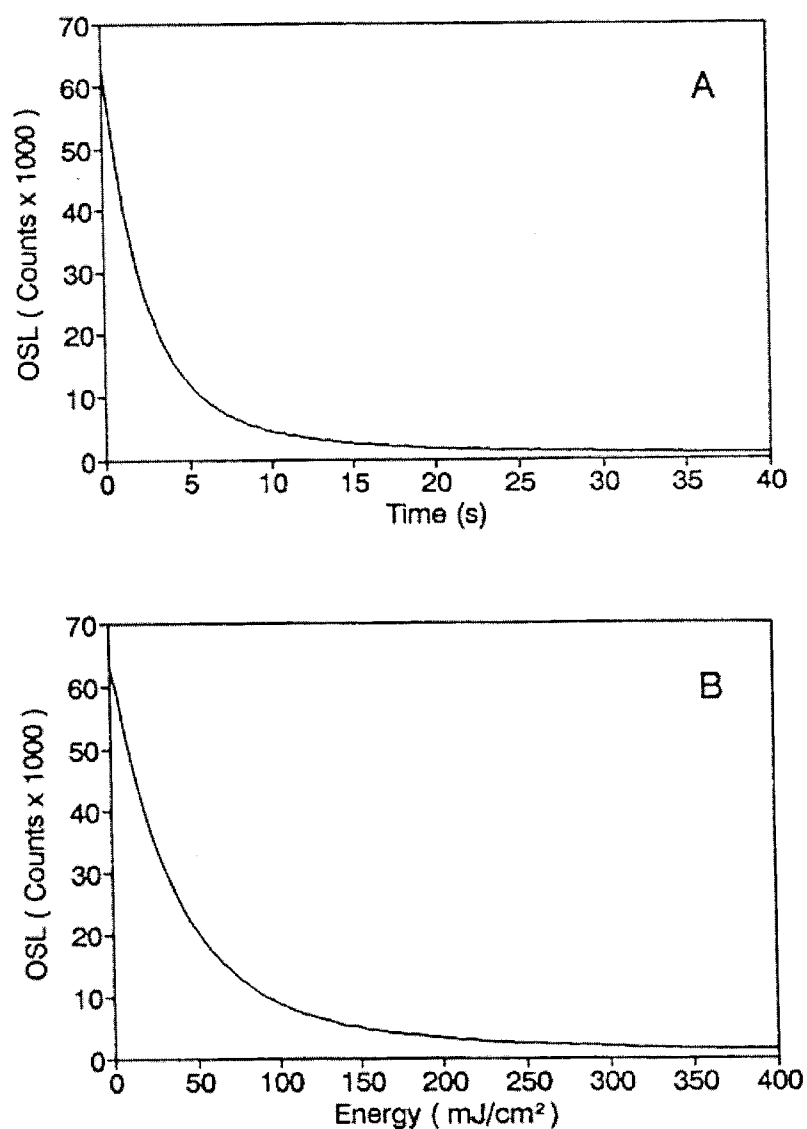


Fig. 4.1. Typical OSL decay curves obtained from a natural archaeological quartz sample ( $D_e \sim 1$  Gy) using broad-band stimulation (420-550 nm) delivering  $16 \text{ mw/cm}^2$  to the sample. (A) OSL intensity versus time. (B) OSL intensity versus energy. The half value is reached after 2 s and an exposure of about  $25 \text{ mJ/cm}^2$ . Excitation filters: 6 mm GG-420 + interference filter; detection filter: 5 mm U-340 (from Bøtter-Jensen and Duller, 1992).

Smith and Rhodes (1994) showed that the quartz OSL decay curve is not a simple decay, but can be described by the sum of three exponential functions. They further showed that there was a significant re-trapping of charge in traps responsible for the OSL in quartz. Such re-trapping will only produce a non-exponential decay if the type of recombination changes during OSL measurement. Bailey et al (1997) isolated the three exponential components by measuring quartz OSL at elevated temperatures. These components displayed differen-

tial bleaching and growth characteristics. It appears that the fast and medium components are associated with the 325°C TL peak whereas the slow component remains stable until at least 650°C.

Spooner (1994) and McKeever et al (1997) observed that the integrated quartz OSL decreased with stimulation temperature in terms of thermal quenching (Wintle, 1974), in which a recombination centre can absorb energy from the lattice vibration and return to the stable state without emission of a photon.

The OSL decay curves from quartz as function of stimulation power and stimulation wavelength were further investigated using the Risø monochromators (Duller and Bøtter-Jensen, 1996). OSL from the same quartz sample was measured using the broad-band light source (420-560 nm) for stimulation. OSL decay curves were measured using different stimulation powers. The power delivered to the sample was altered by the use of metal-coated neutral density filters, and measured quantitatively using a Newport 840-c optical power meter. Illumination times were altered such that the energy absorbed by the sample per data channel and during each measurement was kept constant. Fig. 4.2 plots the OSL data as a function of energy, and shows that over the power range tested (0.11 to 12.00 mW/cm<sup>2</sup>) the decay curves show similar form. Also the OSL light sums are the same indicating that there is no evidence for a 2-photon excitation process or other rate dependent processes.

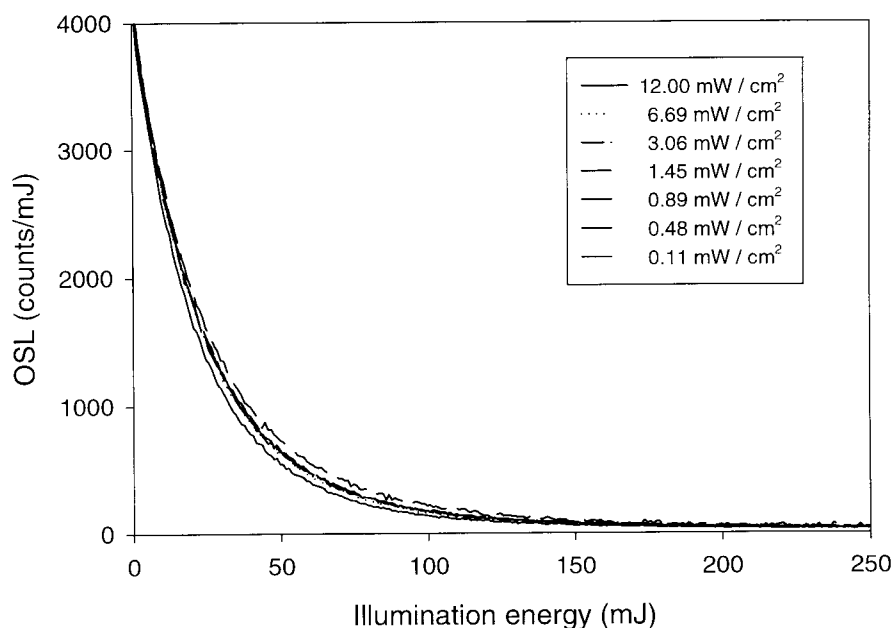


Fig. 4.2. OSL decay curves obtained using broad-band stimulation (420-550 nm) at powers varying from 0.11 to 12.00 mW/cm<sup>2</sup>. Note that the OSL axis is expressed as counts per unit energy. Measurement times were selected such that the energy absorbed per channel and during each measurement was kept constant (from Duller and Bøtter-Jensen, 1996).

## 4.3 OSL Signals from Quartz using Different Stimulation Wavelengths

### 4.3.1 Optical stimulation spectra of quartz

The difference in stimulation power required from an argon-ion laser at 514 nm and the broad-band source to generate a given OSL signal led to a study of the stimulation efficiency of quartz at different wavelengths. This investigation also used the monochromator described in section 3.4 to provide stimulation spectra (Bøtter-Jensen et al, 1994a). The monochromator was set in front of the halogen light source and during illumination it continuously scanned across the wavelength range 400 to 700 nm (1.2 to 3.1 eV), with detection using U-340 filters (peak emission 340 nm). Bøtter-Jensen et al (1994a) and Bøtter-Jensen et al (1994b) were the first to publish optical stimulation spectra from quartz obtained using an automatic continuously scanning method. An example of a stimulation spectrum obtained for a sedimentary quartz annealed at 850°C and given a beta dose of 8 Gy is shown in Fig. 4.3. There is a linear relationship between log of intensity and the stimulating photon energy within the range 1.9 eV to 2.5 eV; this is consistent with the work of Spooner et al (1988) who demonstrated an exponential relationship between the bleaching of the 325°C TL peak and the illumination wavelength. It is suggested that the slight deviation in the curve of Fig. 4.3 for photon energies above 2.5 eV is due to an absorption band in this region. Essentially the same relationship of intensity and illumination energy is found for both annealed and unannealed quartz, and the trap depth of the OSL defect was determined to be  $2.0 \pm 0.1$  eV, which compares favourably with various determinations made using isothermal decay experiments, of 1.2 (Smith et al, 1988) and 1.7 (Murray and Wintle, 1999).

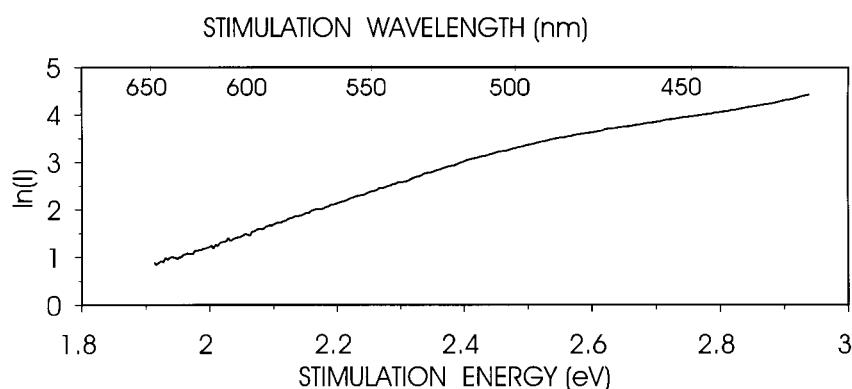


Fig. 4.3. Optical stimulation spectrum ( $\ln(I)$  vs stimulation energy) for a sedimentary quartz annealed at 850°C. Detection filter: U-340. Beta dose: 8 Gy. The spectrum is plotted, corrected for unit incident energy at the sample (from Bøtter-Jensen et al, 1994b).

A simple relationship between OSL intensity and energy suggests that the OSL signal is derived mainly from one trap. It is important to know if more than one trap is stimulated by different wavelengths, to ensure that the wavelength chosen preferentially stimulates a trap with the most desirable dosimetric characteristics.

### 4.3.2 Comparing 514 nm and broad-band stimulation of quartz

Initial visible light OSL research used monochromatic laser light such as that from a 514.5 nm argon ion laser for stimulation. With the development of alternative light sources based on the use of filters with broad band lamps (e.g. Bøtter-Jensen and Duller, 1992; Clark and Sanderson, 1994; Pierson et al, 1994; Rieser et al, 1994), a study of the relative stimulation effects of these different wavelengths was initiated.

In collaboration with Duller, an experiment was designed to measure the extent to which the OSL signal, as measured using a variety of stimulation wavelengths, is bleached using light at  $514 \pm 25$  nm (Duller and Bøtter-Jensen, 1996). This bleaching wavelength was chosen to match that from an argon laser, and the experiment aimed to see whether the rate at which the luminescence signal fell as a result of bleaching varied as a function of the stimulation wavelength.

Quartz separated from a Tasmanian dune sand (grain size 90-150 $\mu$ m) was used. After heating to 450°C, irradiating with a beta dose of 10.8 Gy and pre-heating at 220°C for 300 s, the quartz sample was exposed to  $514 \pm 25$  nm stimulation light for periods of time varying from 0 to 3200 s (power at the sample was 0.4 mW/cm<sup>2</sup>). Stimulation spectra from 400 to 650 nm were then measured (Fig. 4.4a), using the visible monochromator described in chapter 3. The same sample aliquot was used for all measurements, and the signal level measured from the aliquot when it had not been irradiated was subtracted from all measurements. It should be noted that the stimulation spectra in Fig 4.4a have not been corrected for the variation in stimulation power with wavelength since the aim of the measurements was to compare the percentage loss of signal at various wavelengths. Fig. 4.4b plots the data from Fig. 4.4a as bleaching curves, at wavelength intervals of 25 nm. This shows that the OSL signal from this quartz sample is equally reduced by exposure to 514 nm light over the stimulation range from 450 to approximately 600 nm. The similarity in these bleaching decay curves suggests that over the range from 450 to 600 nm the OSL measurements must be probing a similar group of traps. The change in behaviour seen at shorter wavelengths (<450 nm) is thought to be due to some degree of cross talk between the stimulation and detection wavelengths. This effect becomes more apparent at low signal intensities. At wavelengths longer than 600 nm the OSL signal intensity is extremely low, and this makes the subtraction of the correct background critical to determining the behaviour of the bleaching curve after long exposures to the 514 nm light source.

The monochromator system was also used to provide optical bleaching at various wavelengths from 425 to 575 nm (bandwidth: 25 nm). OSL decay curves were produced for the quartz sample for every 25 nm interval. The length of time for which each measurement was made was adjusted so that a similar loss of OSL signal occurred during the measurement at each stimulation wavelength. Fig. 4.5a shows the OSL decay curves as a function of the illumination energy to which the samples were exposed. Fig. 4.5b plots the energy required at various stimulation wavelengths to reduce the OSL signal from the quartz by 50%. It is immediately apparent that at longer stimulation wavelengths a larger energy is required to reduce the OSL signal by a given proportion. This matches very well with theory and the experimentally obtained stimulation spectra we obtained (see previous section). It is therefore suggested that, over the range from 425 to 575 nm, a similar set of traps and charge transport pathways are being used to produce OSL. It is concluded that similar phenomena should be observed whether one uses a single line argon-ion laser or a broad band light source from 420-560 nm for stimulation of quartz when detection is

made in the near UV, as achieved using the Hoya U-340 filter in front of the PM tube.

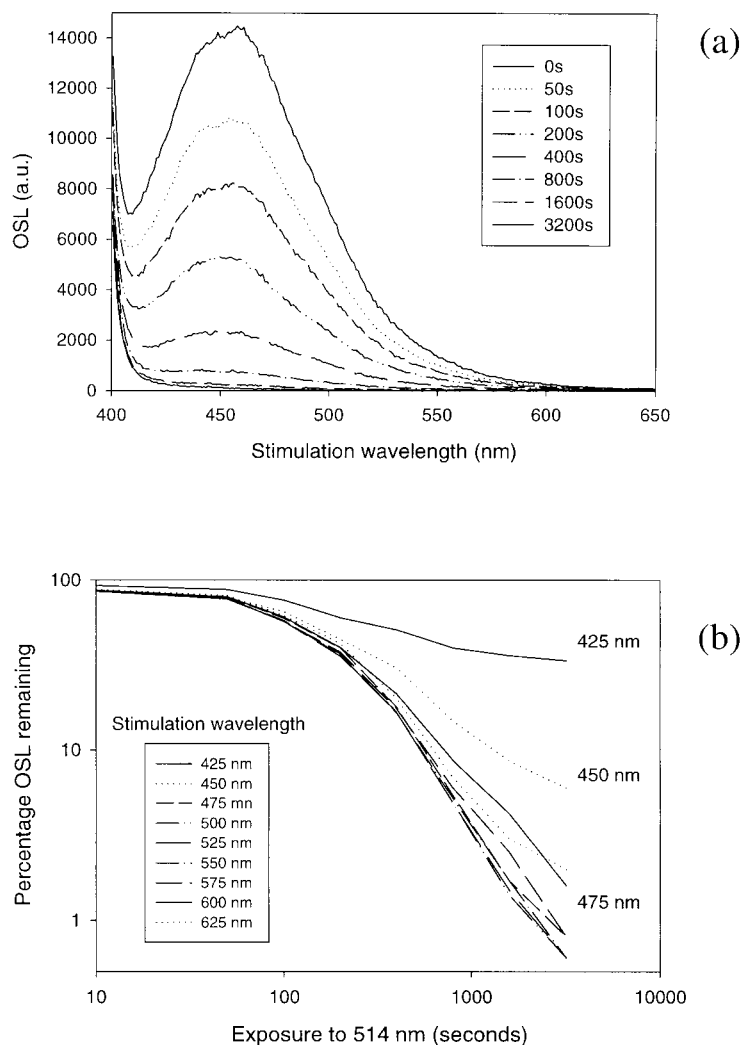


Fig. 4.4. (a) Stimulation spectra from the quartz sample after exposure to 514 nm light for periods ranging from 0 to 3200 s. The power at the sample was  $0.4 \text{ mW/cm}^2$ . Spectra were obtained using a scan speed of  $2.5 \text{ nm/s}$ , making measurements from 400 to 650 nm. The spectra have not been corrected for variations in stimulation power as a function of wavelength.

(b) Bleaching curves for the OSL signals measured in Fig. 4.4a integrated over various wavelengths (from Duller and Bøtter-Jensen, 1996).

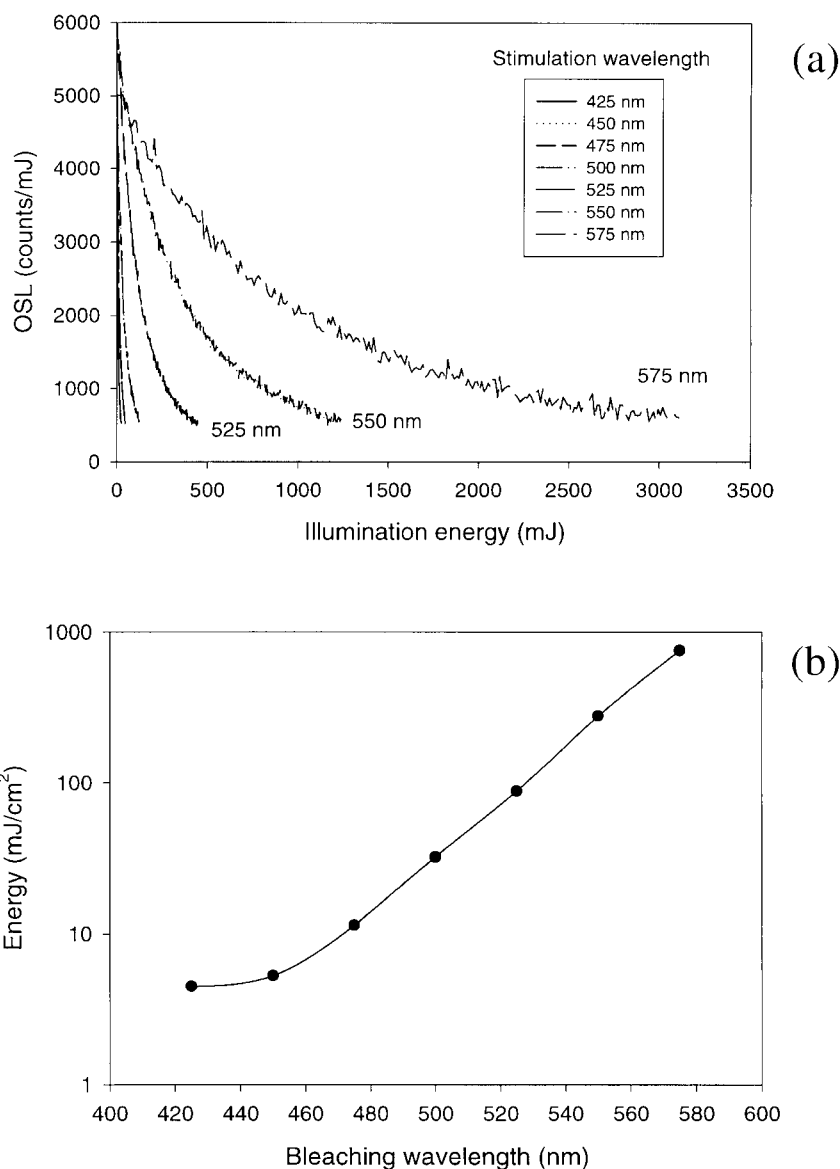


Fig. 4.5. (a) OSL decay curves obtained using various narrow stimulation bands (bandwidth 25 nm). Note that the OSL axis is expressed as counts per unit energy. Measurement times were selected such that a similar loss of OSL signal was observed in each measurement.

(b) Energy required at various stimulation wavelengths to reduce the OSL signal from the quartz by 50 %. (From Duller and Bøtter-Jensen, 1996).

### 4.3.3 IR stimulation of quartz

According to the stimulation spectra obtained by Bøtter-Jensen et al (1994b), a very weak or virtually no OSL is expected from quartz when stimulated with infrared light (see chapter 2 and section 4.3.1). Unlike feldspars (see chapter 5), there are no resonance features in the infrared range and thus IR stimulation has often been used to screen quartz samples for feldspar contamination (e.g. Spooner and Questiaux, 1989). However, Godfrey-Smith and Cada (1996) ob-

tained quartz stimulation spectra obtained at room temperature showing a weak resonance around 845 nm.

As mentioned in section 4.2, the rate of charge de-trapping in quartz increases with sample temperature dependent on the optical stimulation source. This phenomenon is termed “thermal assistance” and has been documented in a number of studies (e.g. Spooner, 1994; Huntley et al, 1996; Bailey et al, 1997; Bailey, 1998). The consequence of this effect is that low photon energies can stimulate luminescence when the sample temperature is sufficiently high.

To demonstrate the complexity of OSL at elevated temperature, the effect of IR stimulation at elevated temperature on the blue light OSL luminescence signal from three different quartz samples was investigated. Fig. 4.6 (from Banerjee et al, 1999c) shows the effect of IR-laser stimulation (830nm; 500mW/cm<sup>2</sup>) at 200°C on the blue LED (470 nm; 20 mW/cm<sup>2</sup>) stimulated signal averaged over the three quartz samples (after correction for thermal decay; see Banerjee et al, 1999c). The curve can be fitted well with the sum of two decaying exponentials; the lifetimes were calculated to about 126 ± 10s and 3900 ± 1500 s and the relative exponential amplitudes were 98 % and 1.6 %, respectively. The blue LED stimulated luminescence signal was reduced to around 1-2 % of its initial intensity after 3600 s of IR stimulation at 200°C. This depletion is explained as being associated with thermal activation and quenching (Bailey, 1998).

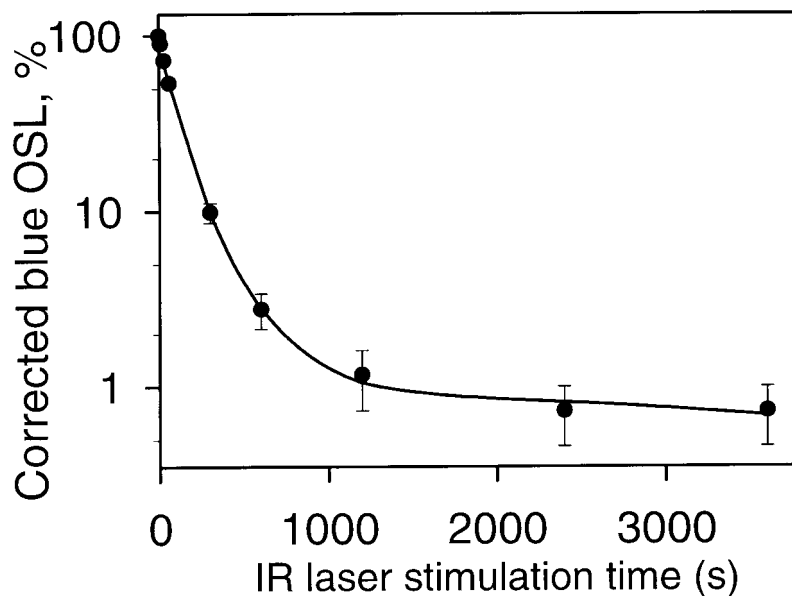


Fig. 4.6. The effect of infrared stimulation at 200°C on the blue light stimulated luminescence from a fired quartz. The symbols represent the average of three different quartz samples which are fitted with an exponential decay of the form:  $Y = A^{e^{-bX}} + C^{e^{-dX}} + E^{e^{-fX}}$  (shown as a solid line).

#### 4.4 The Quartz OSL Response to Linearly Increasing Stimulation Power

As an alternative method of investigating the origins of the quartz OSL signals, some preliminary experiments were conducted to investigate the OSL response of quartz to a linearly increasing stimulation power density (Bøtter-Jensen et al, 1999b). Related measurements have also been undertaken using IR diodes with

feldspars by Bulur (1996). The experiments used 6 clusters of blue diodes, and an aeolian quartz sample from Denmark (laboratory code 974607). A 7 mg aliquot (90-300  $\mu\text{m}$  grain size), mounted on a stainless steel disc, was heated to 500°C, and then given a regeneration dose of 10 Gy. The sample was immediately stimulated at 25°C, with a total linear ramp time (0 to 15  $\text{mW}/\text{cm}^2$ ) of 800 s. The aliquot was heated again, given a further 10 Gy dose, and then stimulated at 25°C at full power for 5 s, before being exposed to ramped stimulation light as before. This cycle was repeated 3 more times on the same aliquot, with full power exposures of 10, 20 and 40 s prior to ramping. The resulting luminescence curves are shown in Fig. 4.7a. The first part of this experiment (0 s prior exposure) was repeated on a further aliquot which was bleached at full power (100 s at 125°C) before being given the 10 Gy dose (rather than heated to 500°C). This curve is shown inset to Fig. 4.7a.

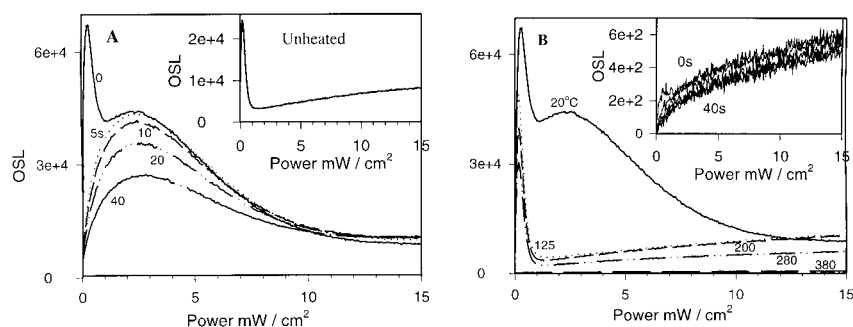


Fig. 4.7. (a) A natural quartz aliquot was heated to 500°C and given a 10 Gy beta dose (this treatment was repeated on the same aliquot before each of the curves shown here). Room temperature OSL was then observed as the diode power was linearly increased (ramped) from 0 to 15  $\text{mW}/\text{cm}^2$  over 800 s (top solid curve). After regeneration, the aliquot was exposed to 5 s of full power illumination before a further ramped OSL curve was obtained (top dashed curve, data collected in bins 3.2 s wide). This was repeated using prior 10, 20 and 40 s full power illuminations. Shown inset is the ramped OSL from another natural aliquot which was bleached at full power (100 s at 125°C) before a 10 Gy regeneration dose (i.e. this sample was not heated before dosing).

(b) The same aliquot as was used in (a) was again heated to 500°C and regenerated with a 10 Gy dose before each ramped OSL measurement at 125°C (top dashed curve, data collected in bins 3.2 s wide). After regeneration, it was then heated to 200, 280 and 380°C and the ramp measurement repeated each time (dashed/dotted curves). The top solid curve is the same as that in (A), with stimulation at room temperature. Shown inset is the effect of 0, 5, 10, 20, 40 s prior full power stimulation after a preheat to 380°C (stimulation at 125°C). (From Bøtter-Jensen et al, 1999b).

The initial easily stimulated luminescence (maximum at about 3% of full power, reached after 24 s) is the rapidly bleaching signal in quartz (see Fig. 4.7a), closely identified with the 325°C TL peak. It is completely removed by 5 s illumination at full power. The broad peak (maximum at about 20% of full power, reached after 160 s) is also light sensitive, but much less so - even a prior illumination of 40 s at full power only reduces it by about 40%. This component is absent in the unheated sample (Figure 4.7a inset). The least sensitive

component (observed at high power and long stimulation time) is negligibly affected by a prior 40 s of full power illumination.

A further sequence, using the same heated aliquot, was undertaken in which the sample was heated to different temperatures (i.e. preheated, at 125, 200, 280 and 380°C, each for 10 s) immediately after receiving the 10 Gy dose but before OSL measurement. In this case all ramped stimulation was at 125°C, to eliminate any phototransfer from the rapidly bleaching peak into the 110°C TL peak (Wintle and Murray, 1997). These curves are shown in Fig. 4.7b, together with the first curve from Fig. 4.7a (no prior full power illumination, ramp stimulation at 25°C).

From a comparison of the top two curves, it can be seen that the second, less readily bleachable, peak is completely removed by heating to 125°C and above. The same peak was not detectable in our unheated aliquot of this material. These observations, and the limited sensitivity to illumination, almost certainly identify it with the 110°C TL peak, which is known to bleach about 10 times more slowly than the fast OSL component (Wintle and Murray, 1997). The initial component is only slightly affected by low temperature preheating (the apparent decrease is mainly because of the complete loss of the underlying slow component), but it is significantly reduced by the 280°C preheat, and completely removed by the 380°C preheat. This is consistent with it being derived from the 325°C TL trap. The slowest component is also affected by the high temperature preheating, being halved by the 280°C preheat, and reduced by > 90% by a 380°C preheat. This implies that the majority of this peak originates with traps thermally emptied in this temperature range.

Shown inset in Figure 4.7b are the results of a third experimental sequence in which the same aliquot was heated at 380°C for 10 s after the 10 Gy dose, and then given various exposures to full power blue light (5, 10, 20 and 40 s at 125°C) before ramped stimulation, also at 125°C. Only the slowest component remains, and that has been reduced to < 10% of its original value (cf. 200 and 280°C curves in Fig. 4.7b).

It is concluded that ramped stimulation of quartz is a powerful new method of deconvolving the various contributions to the OSL signal; these have been studied previously using conventional full power stimulation curves (see section 4.2), and quantitative analysis has relied on the fitting of multiple exponential to deconvolve the various components (Bailey et al, 1997). The ramping method makes no assumptions about the decay function, and provides data in a more suitable form for model fitting.

## 4.5 Relation between TL and OSL Signals from Quartz

The origins of the quartz OSL signal are of interest both from a fundamental perspective, and because such knowledge has important implications for the stability of the signal and the behaviour of any sensitivity changes. One of the puzzling problems in luminescence studies is the relation between TL and OSL signals, in particular whether the charges responsible for the signal originate from the same traps. It has been found that in some cases even almost complete erasure of the OSL signals has only minor effect on the TL signals (Bøtter-Jensen and Duller, 1992; Bøtter-Jensen et al, 1993; Spooner, 1994). The relation between OSL and TL signals using the broad-band stimulation source was studied by gradually releasing the trapped electrons by preheating samples of quartz to successively higher temperatures and recording the effect on the TL and OSL signals. Such preheat experiments are explained below.

The quartz sample used for the experiment was an archaeological (fired) quartz (R-902024), of grain size 100-300  $\mu\text{m}$ . The preheat experiments were made with natural samples to which a beta dose (10 Gy) was added immediately before the measurements in order to generate the TL peak at 110°C (not present in the natural signals because of its thermal instability). Aliquots were heated for 10 s at a range of temperatures up to 450°C and the OSL signals were then measured using an exposure time of 3 s with the blue-green broad band stimulation source.

The resulting plot of the OSL signal as a function of preheat temperature is shown in Fig. 4.8a. From the plot it is clear that the 110°C TL peak (shallow trap) does not contribute significantly to the OSL signal. However, the large increase in OSL beginning at 200°C has been taken as evidence of charge transfer to deeper traps (Rhodes, 1990; Godfrey-Smith, 1991). Similar preheat experiments have been carried out with unheated quartz by Wintle and Murray (1997) with the aim of investigating the effect of prior heating at varying temperatures on the shape of the OSL decay curve at an elevated temperature of 125°C. They showed that there is a linear relationship between the initial and the fully integrated OSL signal for preheats up to 340°C, suggesting that a single trap/luminescence centre combination is responsible for 99% of the OSL signal. Unheated quartz preheats up to 270°C produced no significant change in the natural OSL signal, but between 270 and 340°C the signal rapidly decreased to a low level. A similar relationship was found for a regenerated (bleach + dose equal to  $D_e$ ) OSL signal although in that case the signal increased by about 50% when the preheat was increased from 160 to 280°C similar to the pattern seen in Fig. 4.8a.

Wintle and Murray (1998) also explained the observed increases in OSL with preheating as charge transfer from shallow to deep traps. However, Murray and Wintle (1999) and Wintle and Murray (1999) retracted this, and concluded instead that the observed increase could be better explained by changes in luminescence recombination probability resulting from the preheating. This argument is strongly supported by the constant values of equivalent dose observed as a function of preheat temperature in several heated and unheated quartz samples (Murray and Roberts, 1998; Murray and Mejdahl, 1999; and Murray and Wintle, 1999). These preheat plateaus are only observed when the equivalent dose is measured using the single-aliquot regenerative-dose protocol, which corrects for sensitivity changes (see chapter 8).

To demonstrate the effect of green light exposure on the TL signal, corresponding glow curves obtained before and after illumination with green light for 300 s prior to TL measurement are shown in Fig 4.8b (from Bøtter-Jensen et al, 1993). The main effect of green light exposure is the creation of a distinct 110°C TL peak and a reduction of the 325°C TL peak. The photo stimulated transfer of charge from deeper traps to shallow traps is called photo transferred TL (PTTL). These observations agree well with the suggestion, first proposed by Smith et al (1986), that the OSL signal for quartz is strongly associated with the 325°C TL peak. This association, and the involvement of the 110°C TL peak suggest that sensitivity changes will be frequently observed. This, and the practical implications for dose measurement, led to a detailed study of sensitivity changes in the OSL signal (see next sections).

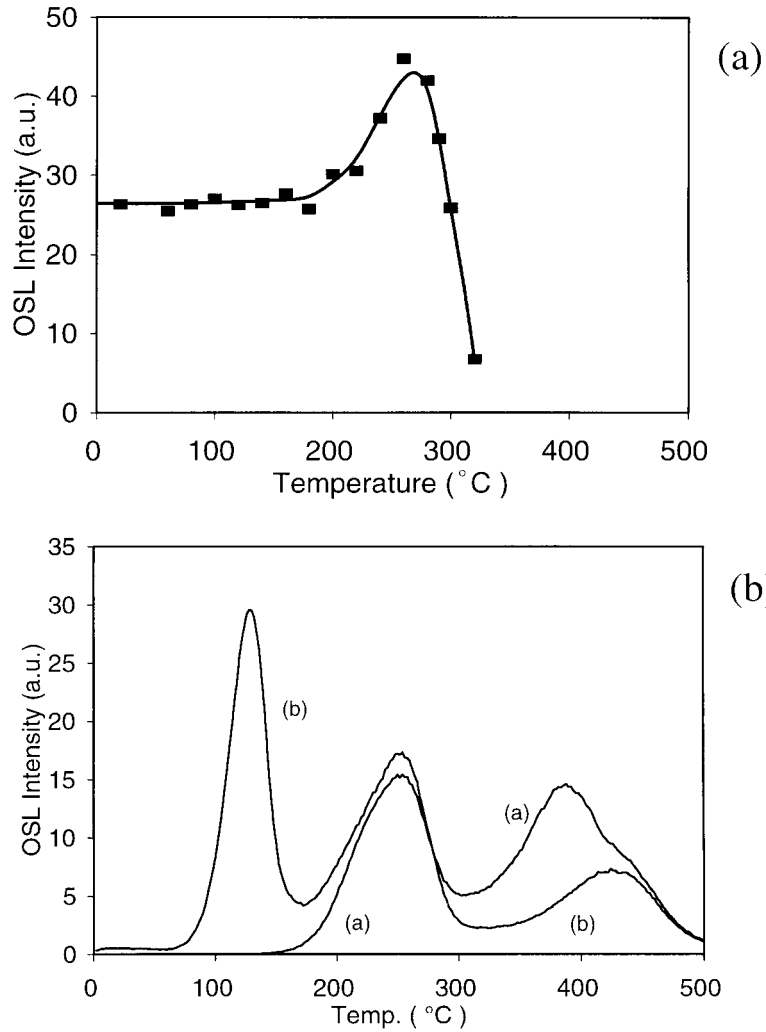


Fig. 4.8. (a) Plot of GLSL signal as a function of pre-heat temperature for a natural fired (archaeological) quartz sample to which a beta dose of 10 Gy was added to create the 110°C TL peak.

(b) TL signals from the same quartz sample. Glow curve A was obtained after preheat at 150°C for 10 s. Glow curve B was obtained after exposure to broadband (420-550 nm) light for 300 s prior to the TL measurement. Heating rate 8°C/s. Detection filter: U-340. The effect of optically stimulation is clearly demonstrated by the loss of the 325°C TL peak and the creation of the 110°C PTTL signal (from Bøtter-Jensen et al, 1993).

## 4.6 Luminescence Sensitivity Changes in Quartz as a Result of Annealing

### 4.6.1 Introduction

Dosimetry using OSL on quartz extracted from ceramic materials takes advantage of the strong OSL sensitivity changes which depend on the previous thermal treatment of the sample. It is well known that quartz heated to 500°C prior

to exposure to ionising radiation exhibits a much brighter OSL signal than quartz from sediments that were bleached by sunlight prior to irradiation (e.g. Aitken and Smith, 1988). These temperature-induced sensitivity changes seem to be connected with thermal transformation from so-called alpha quartz to beta quartz but this phenomenon is not well understood. Even in ancient sedimentary deposits the OSL signal from the natural sample has been shown in some cases to be orders of magnitude smaller than that obtained from archaeological specimens (Bøtter-Jensen and Duller, 1992).

More recently the use of OSL on quartz from house bricks for retrospective dosimetry has been reported (see chapter 8) and these studies confirm that OSL can be usefully employed as a low-dose dosimetric tool (e.g.: Bøtter-Jensen, 1995; Bøtter-Jensen, 1996; Bøtter-Jensen and Jungner, 1999; Bøtter-Jensen and Murray, 1999). In the most sensitive samples examined so far, radiation doses as low as 1 mGy have been measured (see section 4.8), which is comparable with the annual dose from the natural background radiation. However, most natural materials are not this sensitive. If these techniques are to be used to their maximum potential, it is necessary to gain knowledge of why and how sensitivity variations and changes occur from sample to sample. When retrospective dosimetry covering a wide geographical area is to be carried out, different materials must necessarily be used as the local dosimeter. Even if house bricks are to be chosen for this purpose these will often show variations (from one site to another) in the clays and firing temperatures used during manufacture, and the length of time in the kiln.

Previous studies of high temperature annealing effects in quartz have concentrated on TL enhancement following high temperature treatment. McKeever *et al.* (1983) noted sensitivity enhancement effects in both the TL and radioluminescence (RL) of quartz following annealing at high temperatures. A key feature was their conclusion that the enhancement effects were related to alterations in the recombination centers, since both RL and TL were affected in similar ways. Rendell *et al.* (1994) noted spectral changes in the TL of annealed quartz (1000°C/15 hours) as a function of cooling rate. Changes to the TL emission spectra were also observed by Hashimoto *et al.* (1994) in a study of the TL color images from hydrothermal Madagascar quartz annealed at 1000°C for 100 hours. Particularly obvious in the measurements by these authors was the enhancement (by orders of magnitude) of red emission from the materials following the annealing treatment. This again suggests a mechanism of sensitivity enhancement related to alterations in the recombination sites though this is also puzzling since most TL measurements are made in the blue part of the spectrum and not the red.

Chen *et al.* (1988) observed a large sensitivity enhancement of the 110°C TL peak in synthetic quartz following high temperature annealing (up to 900°C). These observations were examined further by these authors in later studies (Yang and McKeever, 1990; Chen and Fogel, 1993; Chen *et al.*, 1994). Yang and McKeever (1990) noted in particular the effects such annealing had upon the "predose effect", i.e. the dependence of prior dose in the material, for the 110°C TL peak.

At Risø the effect of high temperature annealing on the OSL and phototransferred TL (PTTL) signals from natural sedimentary quartz, and from synthetic quartz has been studied (Bøtter-Jensen *et al.*, 1995a). Sedimentary quartz was chosen for the study since it is thought unlikely to have undergone any high temperature annealing in nature. Likewise, synthetic quartz was examined since it is known not to have been subjected to any earlier dose, or high temperature treatment, prior to this study. The studies firstly involved experiments where the OSL and PTTL signals from both sedimentary quartz and synthetic quartz samples were obtained as a function of annealing temperature. Secondly dose

reponse curves were obtained from both annealed and unannealed quartz samples to investigate the growth characteristics whether linear or supralinear and whether these response curves go through origin.

#### 4.6.2 Samples and experimental details

The OSL and PTTL measurements were carried out using an automated Risø TL reader with a combined green light and infrared OSL attachment (Bøtter-Jensen, 1997; Bøtter-Jensen and Murray, 1999). Emission spectra were obtained using the monochromator described in chapter 3 and by Bøtter-Jensen et al. (1994a).

Three sediment samples were used for the annealing experiment, one from Denmark (lab. no. R-914804Q), one from Sweden (lab. no. R-912402Q) and one from Norway (lab. no. R-933801Q). The quartz was separated from the sediments by means of the heavy liquid technique (Mejdahl and Christiansen, 1994). The samples were treated with concentrated HF for one hour and rinsed with 10% HCl, water and alcohol. The purity of the quartz was tested by carrying out an OSL measurement using infrared light for stimulation: pure quartz does not give a measurable OSL signal when stimulating with IR at room temperature, whilst any feldspar impurities would yield a strong signal. The grain sizes for all three samples were between 90 and 212  $\mu\text{m}$ , and the paleodoses were: 50 Gy (R-914804Q), 170 Gy (R-912402Q) and 39 Gy (R-933801Q).

The sedimentary quartz samples were bleached using a fluorescent lamp (320-440 nm, Philips TL05) for 100 hours to erase any natural luminescence signal. After bleaching the samples were divided into subsamples to be annealed at different temperatures. Annealing of subsamples was made using a ceramic oven with an upper limit temperature of 1200°C. The samples were annealed at 50°C intervals for one hour in the range 20-1200°C. All temperatures were controlled by a thermocouple placed near the samples during annealing. After the annealing all sub samples were given a test dose of 3 Gy  $^{60}\text{Co}$  gamma radiation.

The synthetic quartz samples used in this study were Premium Q single crystals, described in earlier publications (*e.g.* Yang and McKeever, 1990). The crystals were crushed and washed in 1M HF for one hour, followed by 1M HCl for one hour in order to remove damaged surface layers (although TL analysis detected no discernible differences between etched and unetched grains). The original single crystal slices were y-cut plates and material from both the x- and the z-growth regions were mixed and homogenised when making the powder. Grain diameters of  $\leq 90 \mu\text{m}$  were used in the measurements. Because OSL sensitivity changes were investigated it was not possible to normalise using a normalisation radiation dose. All data in this study were mass normalised only and averaged over three sub-samples.

#### 4.6.3 Results of OSL and PTTL versus annealing temperature

The intensities of OSL and PTTL (110°C TL peak phototransferred during broad-band light illumination) are plotted as a function of pre-irradiation annealing temperature for a typical sedimentary quartz sample (R-912402Q) in Fig. 4.9a. OSL was integrated over 60 s. PTTL was measured as the integral of the 110°C TL peak (80-140°C). Nearly identical curves were obtained for the two other sedimentary quartz samples. To see the time dependence of annealing some samples were annealed at both 500°C and 800°C for 10 min, 60 min, and 12 hours. The samples annealed for 12 hours displayed an enhanced OSL sensitivity compared to that found for shorter times, typically by a factor of 2-3. This indicated a time dependency which was not further considered.

As can be seen, the OSL and PTTL signals show nearly identical curves and it is noted that two distinct maxima of the OSL and PTTL sensitivities appear in temperature ranges which are coincident with the known phase changes of SiO<sub>2</sub>, namely the  $\alpha$ - $\beta$  quartz transition at 573°C and the  $\beta$  quartz- $\beta_2$  tridymite transition at 870°C. The next major transition ( $\beta_2$  tridymite to cristobalite; see Deer et al, 1992) occurs at 1470°C but was beyond the range of these experiments.

#### 4.6.4 The effect of prior dose

To see whether the enhanced OSL sensitivity observed in Fig. 4.9a is an effect of the previous irradiation (pre dose) to which the sedimentary samples had been subjected in nature (Stoneham and Stokes, 1991), the synthetic quartz described above was used. Synthetic quartz was chosen for two reasons. Firstly, it has a high crystalline quality and is of high purity; it offers one of the simplest cases for study. Secondly, its irradiation and thermal histories are known - in particular it is known not to have received any significant prior dose. One part of a synthetic quartz sample was given a laboratory pre dose of 50 Gy <sup>60</sup>Co gamma radiation, while the other part was used without any predose. The irradiated sample was then bleached for 100 hours using the fluorescent lamp (i.e. the same bleaching procedure that was given to the natural samples). Each of the two samples was then divided into six subsamples which were individually annealed for one hour at 300, 500, 600, 800 and 1000°C, respectively, in addition to one held at room temperature. The OSL intensities versus annealing temperature for the pre-irradiated and the non-irradiated synthetic quartz samples are plotted in Fig. 4.9b. The two curves show an enhanced sensitivity at high temperatures similar to that for the sedimentary quartz - even for the sample which has received no prior dose. This observation, together with the fact that both curves in Fig. 4.9b are almost identical, suggests that the effect from the prior dose, if present at all, is minor; heating is the main cause of the large sensitivity enhancements observed in all these quartz samples.

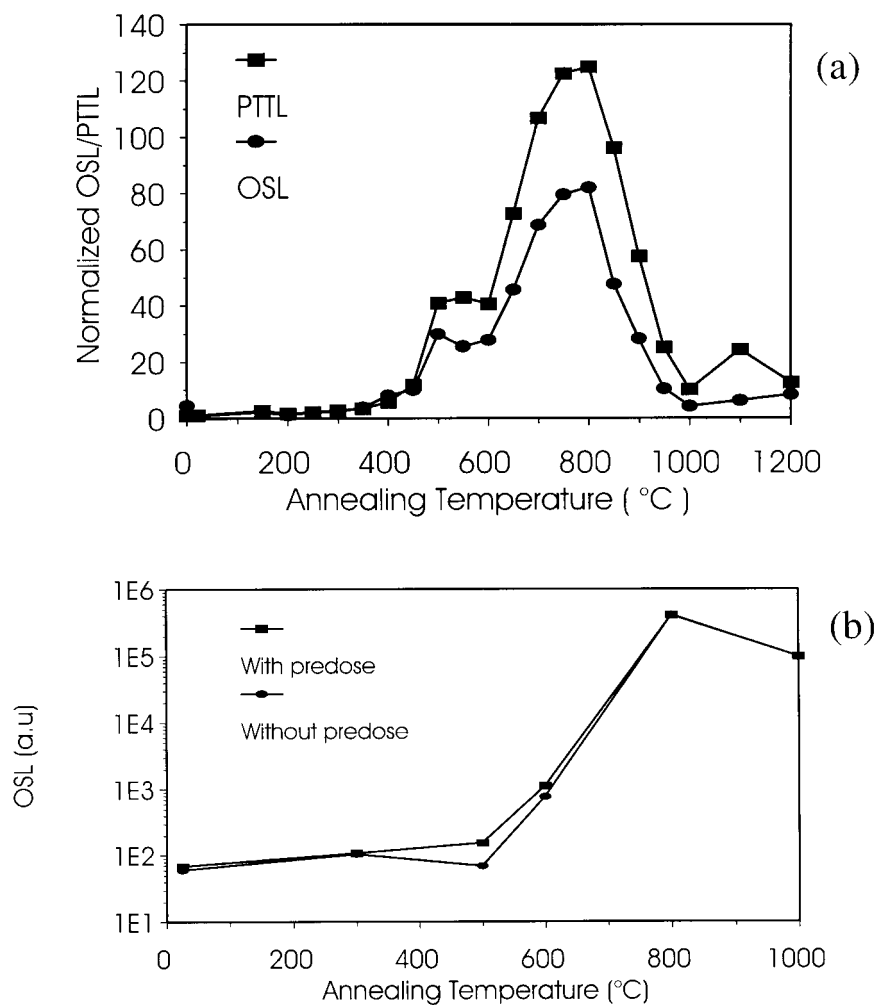


Fig. 4.9. (a) OSL and PTTL sensitivity as a function of annealing temperature for a sedimentary quartz sample. The test dose used in these measurements was 3 Gy. The OSL was integrated over the first 60 s. The PTTL was measured as the integral of the 110°C TL peak (80-140°C) created after green light exposure. A heating rate of 8°C/s was used in the PTTL measurements (from Bøtter-Jensen et al, 1995).

(b) OSL versus annealing temperature for synthetic quartz. Two data sets are shown: one for samples that did not have a pre-dose, and one for samples with a pre-dose. The pre-dose was 50 Gy and the test dose was 3 Gy (from Bøtter-Jensen et al, 1995).

#### 4.6.5 Growth characteristics

Dose response curves were obtained from two sets of bleached sedimentary quartz samples before and after annealing. Both sample sets had been bleached for 100 hours using a fluorescent lamp to erase any natural luminescence signal. Figs. 4.10a and 4.10b show the growth curves for the annealed and the unannealed samples, respectively (from Bøtter-Jensen et al, 1995). One sample set was held at room temperature before obtaining the growth curve, while the other growth curve was taken on a sample set that had been annealed at 800°C for 1 hour. The data show that the growth curve for the unannealed samples is linear, but has non-zero OSL at zero dose (despite that both subsamples had

been bleached prior to analysis). The annealed specimens, however, show a slight supralinearity, especially at low doses, and clearly give zero OSL at zero dose.

TL emission spectra obtained from both the annealed and the unannealed quartz samples indicate that changes to the recombination centres have taken place during annealing (see Bøtter-Jensen et al, 1995). In this study the primary sensitivity enhancement occurred for the 380 nm UV emission band, whereas the blue emission (near 470 nm) showed a little enhancement after annealing. The experimental facilities did not cover the red emission wavelengths, however Hashimoto et al (1994) reported large enhancements of the red emission from the high temperature range of the TL glow curve following the high temperature annealing, and moderate enhancement of the blue emission.

The interesting observation from the present work is that the OSL versus dose curve is slightly supralinear for the annealed specimens, but linear for the unannealed samples (see Figs. 4.10a and 4.10b). It is also important to observe that the dose response of the unannealed sample does not give zero OSL at zero added dose, in contrast to the annealed specimens. All of these features need to be accounted for in any model intending to explain a sensitisation effect. The observation of supralinearity in the sensitised samples is particularly interesting as this supports the expectation that enhanced sensitivity and a growth curve non-linearity will occur together. Recent theoretical exercises explaining supralinearity and sensitisation in some common TLD materials have emphasised this point (Sunta et al, 1994a; Sunta et al, 1994b).

Bøtter-Jensen et al (1995a) have attempted to explain these observations using a simple model for the OSL and TL processes. The model invokes enhanced recombination at luminescence centres along with emptying of deep traps, and is able to describe all of the qualitative features observed in practice. It is not possible to distinguish between a model that calls for the creation of luminescence centres, or one that calls for the removal of non-luminescence centres due to annealing. Each would result in increased luminescence emission and an enhanced sensitivity. Further analysis of studies of the effect on the OSL and PTTL signals from quartz as a function of annealing temperature performed at Risø are described by Agersnap Larsen (1999).

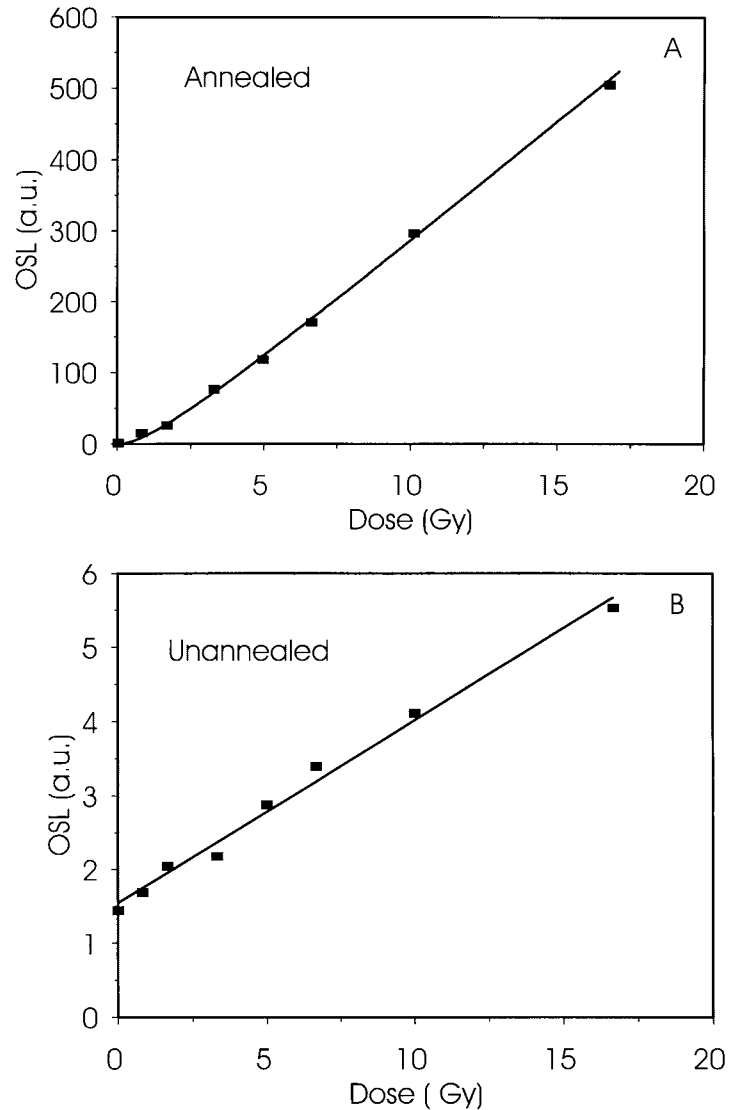


Fig. 4.10. OSL versus dose for two sets of sedimentary quartz samples. One sample set (a) had been annealed at 800°C for one hour prior to irradiation. The other (b) had not been annealed. The two curves, a and b, are plotted using the same (arbitrary) units. The system background was subtracted from both curves (from Bøtter-Jensen et al, 1995).

#### 4.6.7 Conclusions

These data show a clear enhancement of OSL and PTTL sensitivity after high temperature annealing before irradiation. These findings support similar observations made earlier concerning TL emission from similar materials (Chen et al, 1988; Yang and McKeever, 1990; Chen and Fogel, 1993; Chen et al, 1994). In addition to the enhanced sensitivity, supralinearity in the OSL versus dose curves was observed after annealing. These observations compare well with simple modelling made elsewhere (Bøtter-Jensen et al, 1995a). The conclusion is that at this stage it is still not possible to say whether the characteristics observed for the annealed quartz is due to creation of luminescence centres or re-

removal of non-luminescence centres caused by the annealing. Each would result in increased luminescence emission and an enhanced sensitivity.

The significantly enhanced OSL sensitivity observed after heating quartz at high temperatures suggests that natural quartz samples that are known to have been heated in the temperature interval 500 to 800°C in the past will be much more sensitive than unheated quartz. This has application in the field of retrospective dosimetry, where selection amongst ceramic materials is possible and in the dating of heated stones, where selection of well heated samples ensures adequate zeroing and high sensitivity.

## 4.7 Low-Dose OSL Properties of Quartz Extracted from Fired Materials

### 4.7.1 Introduction

In an effort to identify the most OSL sensitive quartz materials when collecting samples for retrospective dosimetry (see chapter 8), an examination of the OSL dosimetric properties of some natural quartz grain samples extracted from fired materials was undertaken (Bluszcz and Bøtter-Jensen, 1995). Samples of different origin were tested for their broad-band OSL sensitivities at low doses. The work aimed at establishing the dosimetric properties of natural quartz in the mGy range, and was particularly focused on high sensitivity quartz samples extracted from burnt or fired materials. Quartz grains extracted from five such samples provided by the Nordic Laboratory for Luminescence Dating at Risø were used. All samples were screened for feldspar contamination by illuminating with IR light prior to broad-band OSL measurements. The measurements were carried out using the automated Risø reader equipped with the halogen green light OSL attachment described in chapter 3.

### 4.7.2 Calibrations and beta irradiations

The samples used in the experiments are listed in Table 4.1. The irradiations of samples to produce the growth curves used for determining the absorbed doses were carried out using both the built in beta irradiator of the Risø reader and a separate calibration facility providing calibrated <sup>60</sup>Co gamma fields.

*Table 4.1. Fired quartz samples used in the low-dose experiments.*

Sample No.	Risø NLLD Lab. No.	Grain size (µm)	Type of material
1	871301	100 - 300	Fired brick
2	924447	100 - 300	Burnt stone
3	923922	100 - 300	Burnt clay
4	902023	100 - 300	Burnt stone
5	950501	100 - 300	Burnt clay

The standard 40 mCi <sup>90</sup>Sr beta source used in the irradiator was replaced with a weaker 5 mCi source to match the dose range needed for the experiments. This source was calibrated against the <sup>60</sup>Co gamma radiation and provides a

beta dose rate of  $4.1 \pm 0.2$  mGy/s according to the procedure outlined by Bluszcz and Bøtter-Jensen (1993). However, a further reduction of the dose rate was required to be able to properly reproduce irradiation of calibration doses lower than 10 mGy, and so a 2 mm thick aluminium disc was placed in front of the beta source. This thickness of aluminium almost completely absorbed the beta particles; seven holes (0.5 mm diameter), were then drilled out in a regular pattern across the disc to allow a small fraction of the beta particles to pass through. Finally, to homogenise the beta flux, a 2mm perspex disc was placed between the aluminium disc and the sample. The attenuated beta flux at the sample position was calibrated against the  $^{60}\text{Co}$  gamma source using quartz grains from sample no. 3 (burnt clay). One subsample was gamma irradiated with 4.33 mGy and three others with different beta doses. Tests were carried out to ensure that heating up to  $500^\circ\text{C}$  did not leave any measurable OSL signal. The broad-band OSL growth calibration curve is presented in Fig 4.11 together with the measurement protocol. The interpolated equivalent gamma dose rate derived using the attenuated  $^{90}\text{Sr}$  beta source was calculated to be  $110 \pm 5$   $\mu\text{Gy/s}$ .

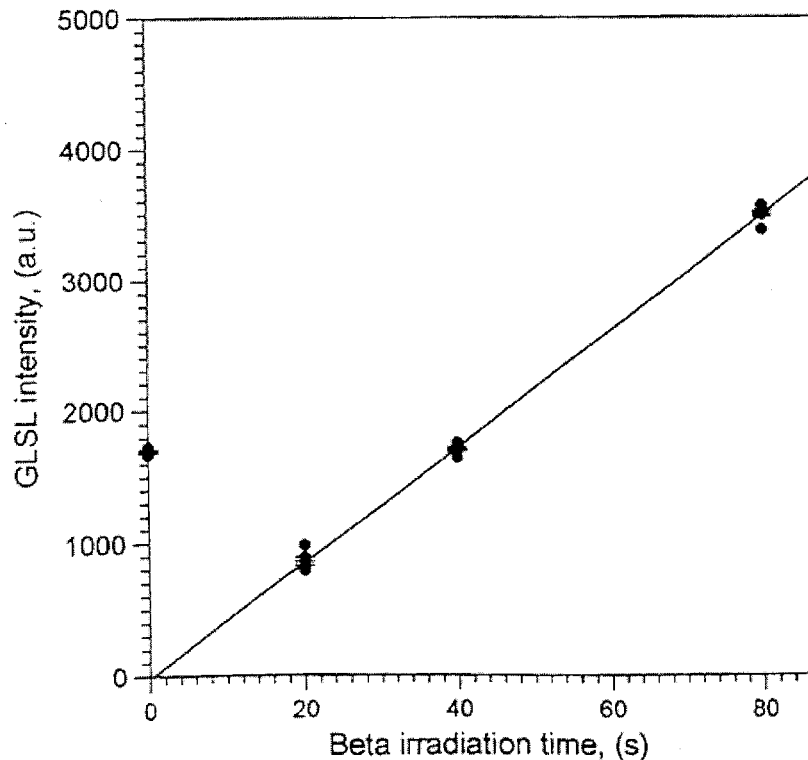


Fig. 4.11. Growth curve obtained to calibrate the attenuated 5 mCi  $^{90}\text{Sr}$  beta source. 6 mg aliquots of quartz grains from sample 3 (burnt clay) were used. The broad-band OSL measurements used the following protocol: Irradiation of samples: Groups of 6 samples were each irradiated to 20s, 40 s and 80 s beta radiation, respectively. Another group of 6 samples were irradiated to a 4.33 mGy  $^{60}\text{Co}$  gamma calibration dose. OSL measurements were made using 1) preheat at  $200^\circ\text{C}$  for 30 s, 2) OSL for 50 s, 3) heating to  $500^\circ\text{C}$  in 60 s and 4) background OSL for 50 s. The signal from the gamma dosed samples fits the line better than 5%. The beta dose rate from the source was calculated by interpolation to  $110 \pm 10$   $\mu\text{Gy/s}$ . (From Bluszcz and Bøtter-Jensen, 1995).

### 4.7.3 Dose response of high sensitivity fired quartz

This section describes the generation of low dose response curves for heated quartz. The doses used in the experiments needed to be very small, and thus the measured luminescence intensities were also small. These signals were normalised by giving normalisation doses to the same samples immediately after the first readout; in order to improve the precision the normalisation doses were approximately one order of magnitude higher than the doses given to produce the low-dose growth curves. They were, however, still in the mGy range and similar to the doses applied in the sensitivity change tests described below. The broad-band OSL measurements showed that the background signals varied from sample disc to sample disc and therefore the individual background was measured each time and subtracted from the first readings.

Two different measurement protocols were used: (i) a multiple aliquot technique and (ii) a single aliquot technique. Both of these techniques are described in detail in chapter 8.

#### *OSL response to gamma radiation using the multiple aliquot technique*

Portions of the grains, extracted from sample no. 3, were annealed at 500°C to remove their natural signal and then placed in a double quartz and aluminium container to ensure secondary electron equilibrium. Containers were placed successively in a calibrated  $^{60}\text{Co}$  gamma beam and exposed to a variety of calibration doses in the range 100  $\mu\text{Gy}$  to 4 mGy. OSL signals from irradiated 10 mg aliquots were recorded as described above. A typical dose response curve for sample no. 3 is shown in Fig. 4.12. The effect of normalising the results with OSL signals obtained from the samples that were given equal normalisation doses just after the first readout is clearly demonstrated.

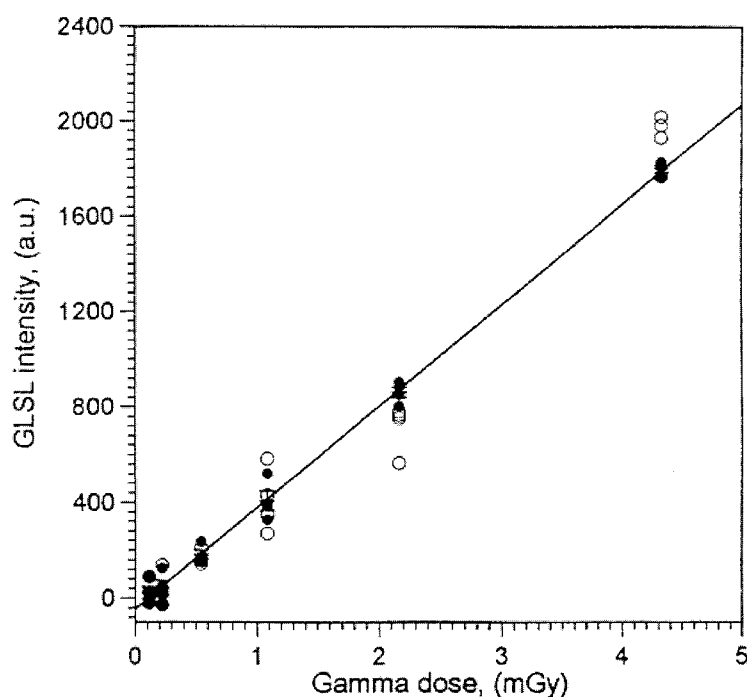


Fig. 4.12. Broad-band OSL dose response curve for sample 3. A normal multiple aliquot procedure was used. Groups of samples were irradiated to  $^{60}\text{Co}$  gamma doses in the range 100  $\mu\text{Gy}$  to 4 mGy. Filled circles represent normalised data with error bars indicating 1 SD. Empty circles represent the signals before normalisation (see text). (From Bluszcz and Bøtter-Jensen, 1995).

### *OSL response to beta radiation using a single aliquot technique*

Prior to measurement quartz grains extracted from the samples were tested for sensitivity changes caused by subsequent cycles of irradiation and thermal annealing. In the samples tested no significant sensitivity changes were found using the single aliquot measurement protocol. Beta irradiation was carried out using the built in beta irradiator containing the attenuated 5 mCi  $^{90}\text{Sr}$  source described in section 4.5.2. The single aliquot protocol was as follows: 1) beta irradiation, 2) preheat at 200°C for 30 s, 3) OSL for 50 s, 4) heating to 500°C in 60 s and 5) background OSL for 50 s.

Fig. 4.13 presents examples of broad-band OSL single aliquot regeneration growth curves obtained for samples 1, 2 and 3, respectively. Each curve represents OSL regeneration measurements of one single 10 mg aliquot.

Using the single aliquot regeneration dose method, it is estimated that for some fired quartz samples a dose of 1 mGy can be measured with a precision of 5%. The lowest detectable dose is < 0.5 mGy.

It should be noted here that a more generalised version of a single-aliquot regenerative-dose measurement protocol is applied to retrospectively determining accrued accident doses from extracted brick quartz in chapter 8.

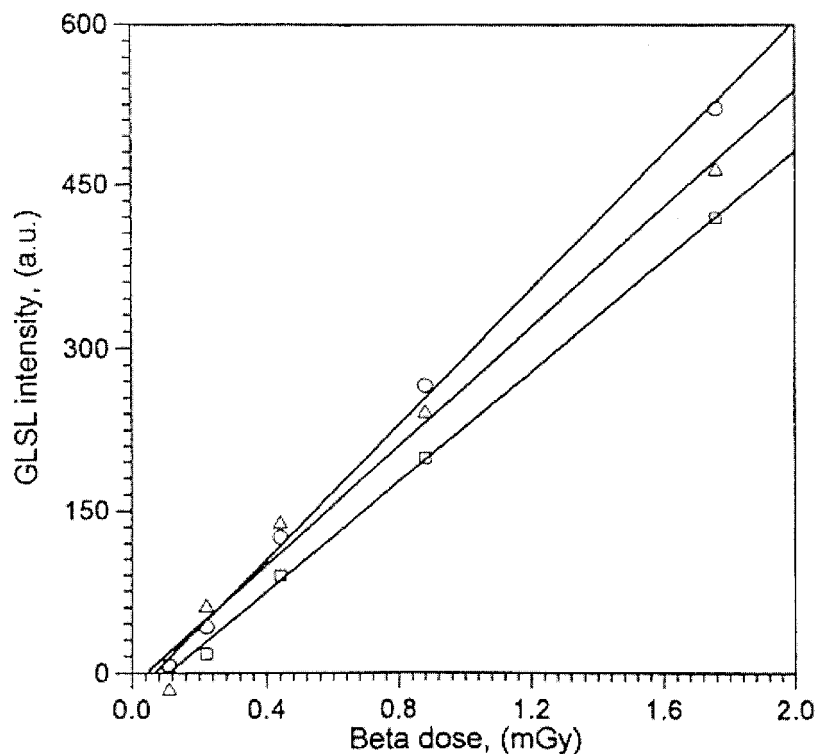


*Fig. 4.13. Single aliquot OSL growth curves obtained from extracted quartz samples nos. 1, 2 and 3. The following single aliquot measurement protocol was used: 1) beta irradiation, 2) preheat at 200°C for 30 s, 3) OSL for 50 s, 4) heating to 500°C in 60 s and 5) background OSL for 50s. Each plot is made using only one 10 mg aliquot. (From Bluszcz and Bøtter-Jensen, 1995).*

#### **4.7.4 OSL sensitivity changes in quartz due to repeated measurements**

A difficulty encountered with repeated OSL measurements of quartz has been the evident sensitivity changes associated with multiple re-use of the samples, especially in the regeneration technique (see chapter 8). Several authors work-

ing with feldspars have attempted to explain this type of sensitivity changes on the basis of the existence of different types of trap within the specimen – i.e. traps that are easy to bleach during natural or laboratory exposure to light, and those that are difficult to bleach (e.g. Duller, 1991; Richardson, 1994; Li and Wintle, 1992; Mejdahl and Bøtter-Jensen, 1994). The essential element is that there is a population of trapped charges which remains in the sample after bleaching. This population of trapped charge affects the next measurement of the OSL sensitivity. However, it is not obvious whether the sensitivity will increase, or decrease with repeated irradiation/readout cycles since the precise effect will depend upon the level of filling the unbleached centres, which in turn will depend upon both the dose history and the bleaching history. Hence, either sensitivity increases or decreases may be observed.

Collaborative work between Oklahoma State University and Risø (McKever et al, 1996; McKever et al, 1997) that included combined experimental work and computer simulations concluded that sensitivity changes in quartz during repeated OSL measurements of quartz can be explained by changing populations of trapped charges (electrons and holes) in the various levels taking part in the OSL process. The sensitivity is dictated by the concentrations and distributions of the trapped charges at the time of OSL measurement. It is important to emphasise that all energy levels present in the material take part in the OSL process – either directly or indirectly. Both shallow trap and deep trap competition may contribute to the results that were observed. Shallow traps may be important due to (1) recuperation effects – e.g. charge removed from the OSL traps during bleaching is retrapped by the shallow traps; preheating then transfers a portion of this charge back into the OSL traps before the next OSL measurement; (2) competition effects – e.g. because of dose rate differences, shallow traps do not compete effectively for trapped charge during natural irradiation but do so strongly during laboratory irradiation. If the contents of shallow traps are lost by thermal decay at ambient temperature over the period of irradiation in nature, but not in the laboratory, then the competition can be very different on the two occasions. Even if the sample is preheated after laboratory irradiation in order to remove charge from shallow traps, the competition dynamics governing the final charge distribution will not be the same as if the shallow traps had not filled in the first place (Jungner and Bøtter-jensen, 1994). As a result, irradiation in nature may not produce the same trapped charge populations as laboratory irradiation, for the same absorbed dose.

Some of the effects noted here will cause sensitivity increases with re-use, while others will cause sensitivity decreases. For a particular sample the behaviour will depend upon many factors for example preheat temperature, natural dose, bleaching history, and thermal history. However, new single aliquot protocols that have been developed and tested at Risø now effectively compensate for sensitivity changes in quartz (Murray et al 1997; Banerjee et al, 1999b). These protocols are described in more detail in chapter 8.

## 4.8 Conclusions - Quartz

This chapter has described experimental work carried out at Risø aimed at investigating some OSL characteristics of quartz. One obvious conclusion is that, since visible light is required for the stimulation, carefully selected stimulation and detection filters should be used in order to avoid stray light from the stimulation light source affecting the photomultiplier tube background. By improving the signal to noise ratio, new stimulation light sources, including blue LED OSL configurations, have significantly increased the sensitivity of quartz OSL techniques in general especially in the low-dose region (< 500 mGy). However, de-

spite the considerable number of quartz luminescence studies undertaken by different laboratories, the physical properties are still not very well understood. For example, there is still no clear correlation between the luminescence emission bands and the type of lattice defects responsible for the luminescence. Therefore, there is still considerable need for further investigations of the luminescence characteristics of quartz.

## 5 OSL Characteristics of Feldspars

### 5.1 Introduction

The different types of feldspar minerals are the most abundant constituents of igneous rocks on Earth. The ubiquity of the feldspars together with their wide range in composition has led to their use as the primary tool in the classification of igneous rocks. Most feldspars are classified chemically in three groups; Na-feldspars (albite), K-feldspars (orthoclase) and Ca-feldspars (anorthite) (see Deer et al, 1992).

Luminescence from feldspars has only been used in dating for a short period compared to that of quartz. Wintle (1973; 1974) studied the use of feldspars for dating but found that problems of anomalous fading prevented their use. However, although fading existed in some samples, Mejdahl (1983; 1985; 1986) pioneered the study of feldspar TL properties and used this material in luminescence dating. The main advantages of feldspars in luminescence applications are (i) feldspars typically have a higher intrinsic luminescence brightness than unheated quartz and can thus potentially be used to measure smaller doses, (ii) certain feldspars have a high content of radioactive potassium ( $^{40}\text{K}$ ); this contributes a large percentage of the dose to the sample. This "internal" component is unaffected by variations in the external environment, and so the uncertainty of the background dose rate is reduced, (iii) it is possible to use technically simple IR light sources to optically stimulate feldspars and (iv) feldspars have a much wider dose range than that of quartz.

The following sections review the investigations of some feldspar OSL characteristics performed at Risø in recent years. These include first OSL stimulation and emission characteristics of various feldspars. Then the relation between the TL and OSL signals is analysed. Special effort was laid in the investigation of thermo-optical characteristics of feldspars and the evaluation of thermal activation energy values at different stimulation wavelengths. Finally experiments using different dopants with feldspars with the aim of enhancing the IRSL sensitivity for environmental dosimetry is described.

### 5.2 OSL Stimulation Characteristics of Feldspars

As with quartz (chapter 4) it is important to be aware of the relative efficiency of different wavelengths for stimulating luminescence in feldspars. The monochromator (chapter 3) was used to study the stimulation spectra of various feldspar samples; this was the first time such high resolution stimulation spectra had been obtained using a rapid continuous scanning method (Bøtter-Jensen et al, 1994a; 1994b). In contrast to the rather simple stimulation spectra obtained for quartz (see section 4.3), the excitation spectra for feldspars are much more complex. Fig. 5.1a shows the optical stimulation spectra obtained from museum specimens of Amelia albite (Na-feldspar) and anorthite (Ca-feldspar). The

monochromator mounted on the halogen stimulation light source used first the Schott VERIL S-60 visible variable interference filter (380-750 nm) and then the infrared variable interference filter (700-1100 nm) produced by Barr Associates (see section 3.4.2). Detection was made in the UV using 5 mm Hoya U-340 filter. The appearance of an infrared resonance around 850 nm measured for the albite agrees well with the characteristics reported by Hütt et al (1988), Bailiff and Poolton (1991), Bailiff (1993) and Bøtter-Jensen et al (1994b).

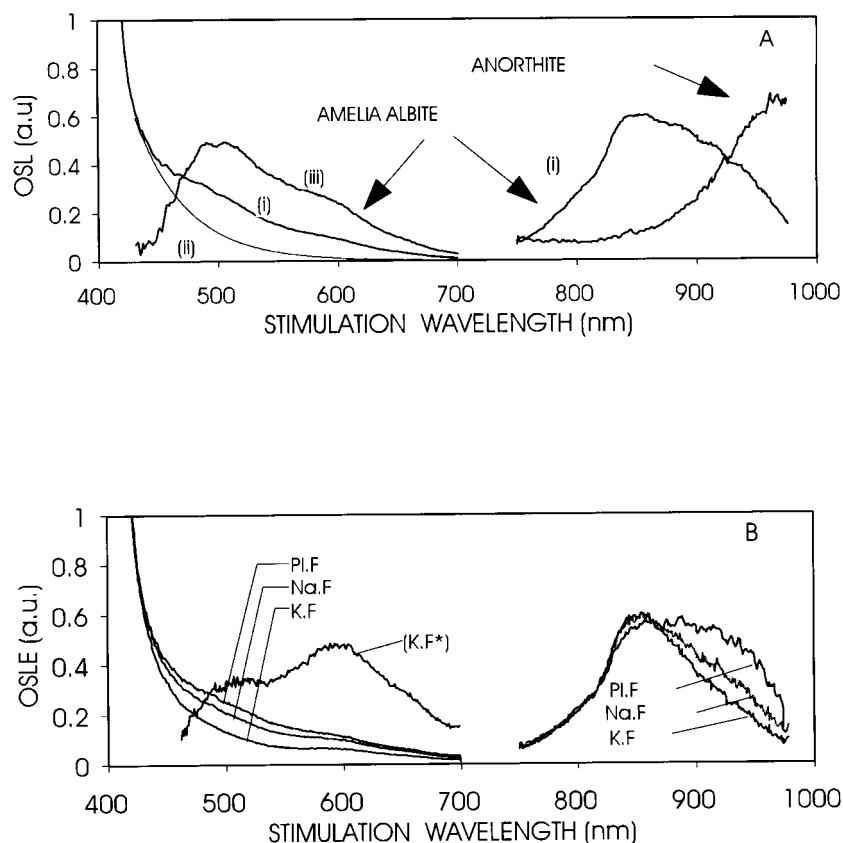


Fig. 5.1. (a) Optical stimulation spectrum (OSL vs stimulation wavelength) for a pure Amelia albite sample (curves i, ii and iii) and an anorthite sample. Detection filter: U-340. Beta dose: 60 Gy. The two resonances of the albite at 500 and 600 nm are seen more clearly in curve (iii), which is the difference between the observed stimulation spectrum (curve (i)) and an approximation to the rising continuum (curve (ii)).

(b) Optical stimulation spectra (OSL vs stimulation wavelength) for sedimentary plagioclase (all mixed with quartz), sodium-rich and potassium-rich feldspars with EDs of about 80, 90 and 100 Gy, respectively. Detection filter: U-340. The resonances at 500 and 600 nm for the potassium-rich feldspar (curve K.F\*) are highlighted in the same way as described for (a). All spectra are corrected for unit power at the sample. (From Bøtter-Jensen et al, 1994b).

In contrast, the infrared transition in anorthite shows a resonance shifted to higher wavelengths with an apparent peak at 970 nm (1.28 eV). This shift is likely to be due to higher relative permittivity in the plagioclase feldspars (Poolton et al, 1994). As the relative permittivities of albite and anorthite are 2.33 and

2.51, respectively, the infrared resonance in anorthite is expected to be, to the first-order approximation, at 1.26 eV (984 nm), as the shift away from the Na-feldspar (albite) resonance is in proportion to  $1/\epsilon^2$  (Landolt-Bornstein, 1982). This is broadly in accordance with the experimental data presented above.

At shorter stimulation wavelengths the spectrum for the albite feldspar is dominated by a steeply rising continuum similar in form to that observed for quartz (see Fig. 4.1). The resonances in this part of the spectrum can be seen more clearly by plotting the difference between the observed stimulation spectrum (marked (i) on Fig. 5.1a) and an approximation to the continuum (marked (ii)). This subtracted signal (marked (iii) on Fig. 5.1a) shows a strong peak at 500 nm (2.5 eV) and a smaller peak at 600 nm (2.1 eV).

Stimulation spectra were also obtained from sedimentary feldspars. Fig. 5.1b shows the stimulation spectra obtained for plagioclase, Na-rich and K-rich feldspars (all mixed with quartz), separated from a Danish sand deposit using heavy liquids. The resulting fraction densities were  $> 2.62$ ,  $2.62 - 2.58$ , and  $< 2.58$  with equivalent doses ( $D_e$ ) of about 80, 90 and 100 Gy, respectively. As in Fig. 5.1a the difference between the measured stimulation spectrum and an approximation to the steeply rising continuum at shorter wavelengths is shown for the K-rich sample, to highlight the resonances present in this particular sample. Unlike albite, the derived spectrum for potassium-rich feldspars is dominated by a peak at 600 nm; the residual peak at 500 nm is likely to be due to contamination from sodium feldspars, also observable in the luminescence emission spectrum (see section 5.3.2). The resonance in the infrared range for plagioclase feldspar is much broader than that for the potassium-rich component. This is interpreted as being due to the superposition of two (unresolved) peaks at 850 and 920 nm. In view of the results for anorthite (see Fig. 5.1a), the 920 nm component is expected to arise from the plagioclase (with density of 2.62) whereas the peak at 850 nm probably represents potassium feldspar contamination; the same conclusion can be drawn from the emission spectra (section 5.3.2).

The differences in the stimulation spectra of the albite (Na-feldspar), anorthite (Ca-feldspar) and K-feldspars clearly show a mineral dependence. It is therefore likely that stimulation spectra from feldspars will be sample dependent, and so it may be possible to use stimulation spectrometry on feldspars to indicate mineralogy; Clarke and Sanderson (1994) drew similar conclusions from their work. Poolton et al (1996) subsequently measured luminescence excitation spectra from a suite of 35 samples of alkali and plagioclase feldspars and correlated these to mineralogy.

## 5.3 Emission Characteristics

The emission characteristics of feldspar must also be considered, to allow the appropriate selection of filters, and to distinguish regions of the emission band likely to be derived from different types of recombination centres. TL and IRSL emission spectra were obtained from various feldspars using the Risø monochromator equipped with the Schott VERIL S-60 variable interference filter (380-750 nm).

### 5.3.1 Luminescence emission spectra from an Amelia albite

An isothermal TL emission spectrum was obtained from a sample of Amelia albite that had been given a beta dose of 60 Gy (Fig. 5.2a). The sample was held at 180°C during measurement. The IRSL (880 nm) emission spectrum of a similarly treated sample is also shown in Fig. 5.2a. The TL and IRSL emission spectra are very similar, implying that the same recombination centres are being

used by the two processes, as previously suggested by Huntley et al (1991). The spectra shown here are dominated by the well known  $Mn^{3+}$  emission at 550 nm (Tepler and Walker, 1975), with a weaker band at 400 nm. The luminescence spectra obtained compare very well with the TL emission spectrum for the Amelia albite reported by Prescott et al (1990).

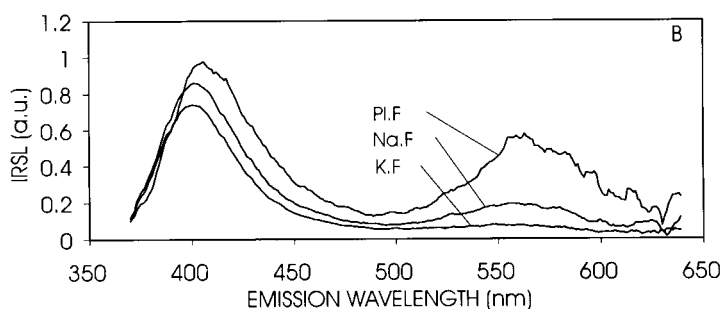
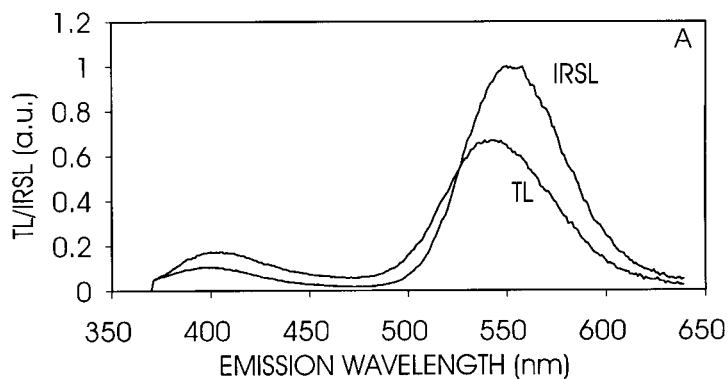


Fig. 5.2. (a) TL and IRSL emission spectra for an Amelia albite sample (TL: constant heating at 180°C. IRSL: excitation at 880 nm).

(b) IRSL emission spectra for sedimentary plagioclase (mixed with quartz), sodium-rich and potassium-rich feldspars with EDs of about 80, 90 and 100 Gy, respectively. All the emission spectra are corrected, as per unit emitted wavelength. Further explanation is given in the text. (From Bøtter-Jensen et al, 1994b).

### 5.3.2 IR stimulated emission spectra from sedimentary feldspars

The wavelength resolved IR stimulated (880 nm) emission spectra obtained for sedimentary plagioclase, sodium-rich and potassium-rich feldspars are presented in Fig. 5.2b (fraction densities: > 2.62, 2.62-2.58 and < 2.58, respectively). The emission spectra are thought to relate entirely to the feldspathic components of the samples since luminescence was stimulated using infrared (880 nm) wavelengths. Previous studies (Huntley et al, 1991, Prescott et al, 1990 and Bailiff and Poolton, 1991) have suggested that the emission spectra of potassium-rich feldspars are predominantly in the blue (approximately at 400

nm), while sodium-rich feldspars emit more strongly in the green/yellow (approximately 560 nm). This is certainly the case for the albite shown in Fig. 5.2a, but not for any of the sedimentary feldspar fractions in Fig. 5.2b, which are all dominated by the blue emission.

### **5.3.3 OSL emission spectra from feldspars as a function of sample temperature**

An OSL signal can be obtained from many feldspars when they are stimulated using wavelengths from 800 to 1000 nm. The intensity of this emission generally increases with temperature over the interval from 50 to 200°C, and measurements of this phenomenon have been used to characterise the degree of thermal activation involved in the production of the OSL signal (e.g. Hütt et al, 1988; Bailiff and Poolton, 1991; Bøtter-Jensen et al, 1994b). Such measurements would be compromised if the emission spectra altered with temperature. In collaboration with Duller it was tested whether this is a significant problem; we measured the OSL emission spectra of a number of feldspar samples at various sample temperatures. The emission spectra from a potassium feldspar obtained at different temperatures are shown in Fig. 5.3a (from Duller and Bøtter-Jensen, 1997). A small but consistent shift of the peak emission wavelength to shorter wavelengths at higher temperatures was observed. However, the magnitude of this shift is sufficiently small that it will not affect measurements of the thermal activation energy. The variation in the peak OSL emission energy with sample temperature measured on the same potassium feldspar sample under IR stimulation, and the width of the emission peak at half maximum are plotted in Fig. 5.3b.

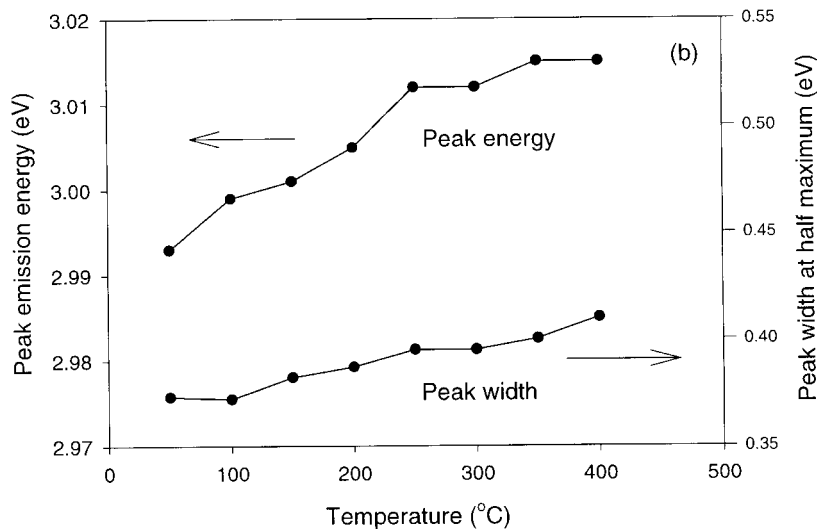
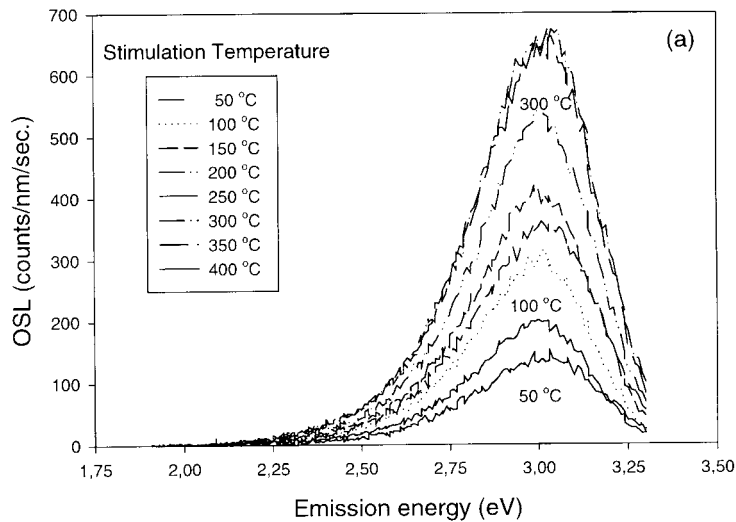


Fig. 5.3. (a) Emission spectra measured from a potassium-rich feldspar at temperatures from 50 to 400°C.

(b) Variation in the peak OSL emission energy from the same feldspar sample under IR stimulation, and the width of the emission peak at half maximum. (From Duller and Bøtter-Jensen, 1997).

## 5.4 Relation between TL and OSL Signals from Feldspars

### 5.4.1 The effect of preheat on the IRSL and GLSL feldspar signals

A knowledge of the relationship between TL and OSL provides important information on the likely thermal stability of the OSL signal, as well as being of fundamental interest.

The relationship between TL and OSL signals from feldspars was studied by performing preheat experiments i.e. gradually releasing the trapped electrons by heating samples of feldspars to successively higher temperatures and recording the effect on both the TL and OSL signals (Bøtter-Jensen et al, 1993). The sample used for these experiments was a potassium feldspar separated from a sediment (100-300  $\mu\text{m}$ ). The preheat experiment was performed with natural samples ( $D_e \sim 100$  Gy) to which a small beta dose (10 Gy) was added immediately before the measurements in order to create the TL peak at 150°C which is not present in the natural feldspar signal. Aliquots were heated for 10 s at a range of temperatures up to 450°C, cooled down to room temperature, and the OSL signals were then measured using an illumination time of 3 s of IR (LED) light, followed by 3 s of green (broad band) light stimulation. Detection filter was 5 mm U-340.

Plots of the IR and green broad-band OSL signals as functions of preheat temperature are shown in Fig. 5.4a. The two curves are very similar and suggest that the 150°C shallow trap does not contribute directly to the OSL signal whereas the main contribution comes from the 270°C peak. To demonstrate the effect of visible broad-band light exposure on the TL signal, corresponding glow curves obtained before and after illumination with green light for 300 s prior to TL measurement are shown in Fig. 5.4b (U-340 detection filters were used for both OSL and TL measurements). There is a significant reduction of the signals from the 150 and 270°C peaks and, to a lesser degree, the 330°C TL peak.

#### **5.4.2 The effect of IR and green light exposure on the IRSL, GLSL and TL signals**

The effects of IR and broad band exposure on the IRSL, GLSL and TL signals, respectively, were studied further in collaboration with Duller (Duller and Bøtter-Jensen, 1993). Twenty-four feldspar samples were prepared and normalised using a short illumination (0.1 s) to measure the individual natural IRSL and GLSL signals. The samples were divided into six groups and each group exposed to IR for different periods of time (0, 10, 50, 100, 1000, and 6000 s). The IRSL and GLSL signals remaining in each disc were measured and normalised using the initial 0.1 s values measured before any treatment. Finally, each disc had its TL measured, and these results were normalised by re-measuring the TL signal after administering a dose of 9 Gy.

The IRSL, GLSL and TL (at 270 and 330°C) signals remaining are plotted as a function of IR exposure time in Fig. 5.5a. The loss of IRSL observed is similar to that seen when measuring IRSL continuously over a long period of time. The GLSL signal falls less rapidly than the IRSL, and a larger fraction of the initial signal remains at the end of the experiment. The two TL peaks at 270 and 330°C fall to 90% of their initial value after 10 s of exposure to IR, and do not change within errors over the next 5990 s. A significant PTTL peak at 150°C was observed after 50 s exposure to IR light. After 6000 s exposure the IRSL signal has fallen to 0.3 % of its initial level, the GLSL to 13 % and the TL to 90 % at 270 and 89 % at 330°C.

An identical experiment was carried out, but samples were exposed to broad-band (420-550 nm) light instead of IR. The remaining IRSL, GLSL and TL (at 270 and 330°C) signals are plotted as function of exposure time in Fig. 5.5b. Initially the GLSL signal may decay the most rapidly of the three, but with exposures over 1000s the IRSL signal decay is indistinguishable from the GLSL. The two TL peaks present in the natural signal are both more sensitive to the blue-green light than to IR; the 270°C peak falls to 49% after 6000 s, and the

330°C peak to 64 %. A much smaller PTTL peak at 150°C than resulting from IR exposure was observed.

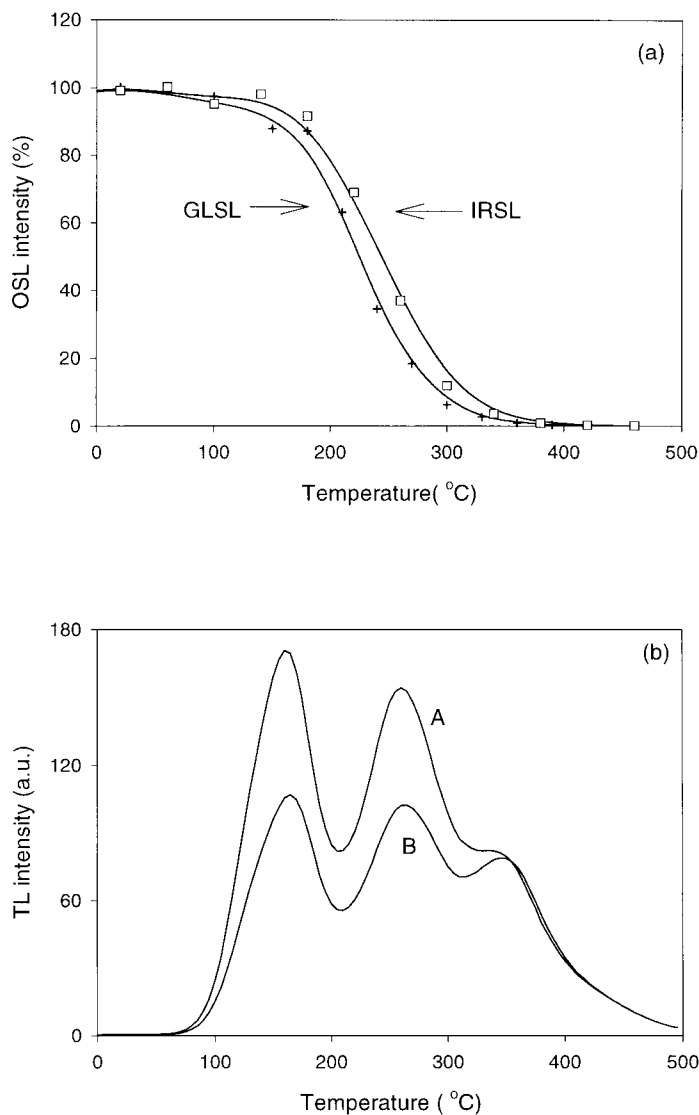


Fig. 5.4. (a) Plots of green broad-band and IR stimulated signals as a function of preheat temperature for a natural geological feldspar sample to which a beta dose of 10 Gy was added to produce the 150°C TL peak.

(b) TL signals from the same feldspar sample. Glow curve A is the natural signal (plus 10 Gy beta). Glow curve B was obtained after exposure to green light for 300 s prior to the TL measurement. Heating rate 8°C/s. Detection filter U-340. (From Bøtter-Jensen et al, 1993).

There is strong evidence that the TL and the two OSL signals observed from the potassium feldspars used in these experiments originate from at least two types of trapped charge populations, both of which give TL, but only one of which is readily optically stimulated. The IR and green OSL signals appear to share traps, but their relative sensitivities to the two wavelength bands appears to

vary, with some traps being equally sensitive to IR and green light, and others being much more sensitive to visible light.

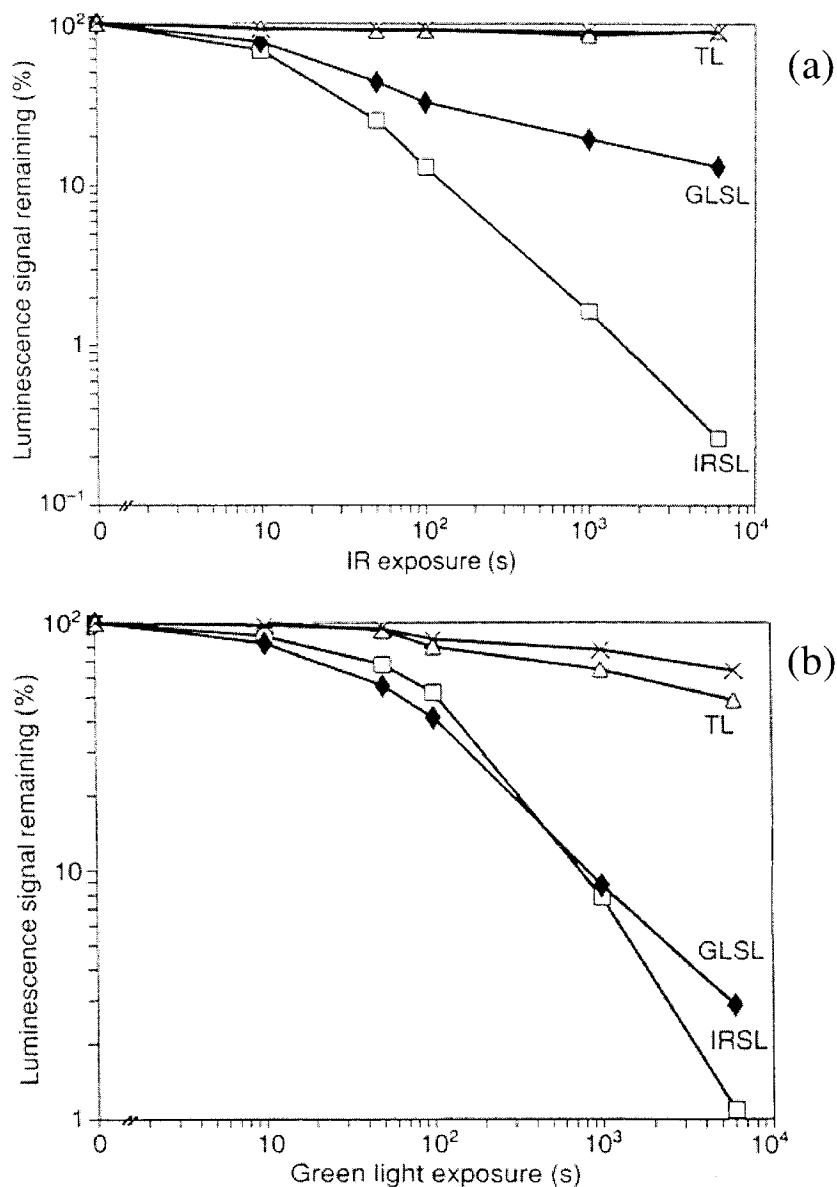


Fig. 5.5. (a) The effect of IR exposure upon IRSL ( $\square$ ), GLSL ( $\times$ ) and TL signals: ( $\Delta$ ) 270°C peak, ( $\times$ ) 330°C peak. IR power at the sample is 42 mW/cm<sup>2</sup>. Signals are plotted as a percentage of the signal for those samples not exposed to IR.

(b) The effect of exposure with a green light waveband (515-560 nm) upon IRSL ( $\square$ ), GLSL ( $\times$ ) and TL signals: ( $\Delta$ ) 270°C peak, ( $\times$ ) 330°C peak. Power at the sample is 6.5 mW/cm<sup>2</sup>. Signals are plotted as a percentage of the signal for those samples not exposed to green light. (From Duller and Bøtter-Jensen, 1993).

## 5.5 Thermo-Optical Characteristics of Feldspars

### 5.5.1 Introduction

Another way of investigating the source and stability of the feldspar OSL signal is by examining the dependence of the OSL signal on stimulation temperature. This relationship has been widely studied because of the potential information that can be obtained on the OSL mechanism and the relation between OSL and TL trapping centres. Such work also has relevance to dosimetry applications because it gives insight into the effects of the thermal treatment used to isolate the thermally stable OSL signals.

In collaboration with Duller and McKeever the factors which affect the shape of OSL decay curves from feldspars stimulated with both IR and green light were examined at Risø. Both experimental and theoretical aspects were analysed in an effort to understand and describe the behaviour of OSL as function of temperature (Duller and Bøtter-Jensen, 1993; McKeever et al, 1997).

The normal procedure for recording OSL in dosimetry applications is to record the luminescence as a function of illumination time at room temperature (see chapter 2). During illumination with IR light the feldspar OSL signal is seen to decay to a low level as a function of time, firstly with a rapid decay and then more slowly as the measurement proceeds. In general, the shape of the OSL decay curve does not lend itself to analysis using simple descriptions. The decay is usually non-exponential, typically exhibiting a long “tail” to the decay at long illumination times. In some circumstances, and for some samples, the OSL may even display an initial slow increase after the illumination is applied, followed by the more usual decrease at longer times. Overall, the decay shape is dependent upon sample, the absorbed dose, the illumination intensity and the temperature.

### 5.5.2 Thermal quenching

Trapped charge liberated by thermal or optical stimulation recombines at specific recombination centres. The energy liberated during this process may be released either in the form of a photon or a phonon. The efficiency with which charge is converted to luminescence is known to vary with temperature in certain materials, and assuming a simple one-phonon-assisted non-radiative decay for the process, it can be fitted using an equation in the form:

$$\eta(T) = 1 / [1 + C \exp(E/kT)]$$

where the luminescence efficiency  $\eta$  at temperature  $T$  (degree Kelvin) can be related to the constant  $C$  and a thermal quenching energy  $E$  ( $k$  is the Boltzmann constant).

A variety of studies have been undertaken to look at the extent to which various recombination centres in feldspars are affected by thermal quenching. For instance White et al (1986) measured the variation in the 480 nm time-stable photo luminescence (Stokes-shifted) emission of an orthoclase feldspar over the range from 77 to 300 K. This work was undertaken on the  $\text{Fe}^{3+}$  red emission centred at 700 nm and gave an activation energy for the quenching process of only 0.056 eV over that temperature range which, according to the authors, lies in the region of strong lattice vibrations for feldspars. A similar approach to that of White et al (1986) was used at Risø, but above room temperature and with a broad-band stimulation at 340 nm generating time-stable photoluminescence

spectra. Poolton et al, (1995a) obtained PL emission spectra from a plagioclase feldspar using the Risø monochromator at wavelengths from 400 to 750 nm over a temperature range from 300 to 500 K (see Fig. 5.6). The  $\text{Fe}^{3+}$  emission at 710 nm from a high-potassium feldspar was calculated using the equation above to quench with an energy of 0.34 eV over this temperature range. As seen from Fig. 5.6 the  $\text{Mn}^{3+}$  emission at 570 nm showed little change over the same range of temperatures. Poolton et al (1995a) concluded that the value of 0.34 eV is likely to be representative of internal vibrational modes of the  $\text{Fe}^{3+}$  ion and that it is reasonable that both types of vibrational energy contribute to the quenching effect. However, since OSL measurements are normally isothermal, the effects of thermal quenching will not play any serious role in dose assessment.

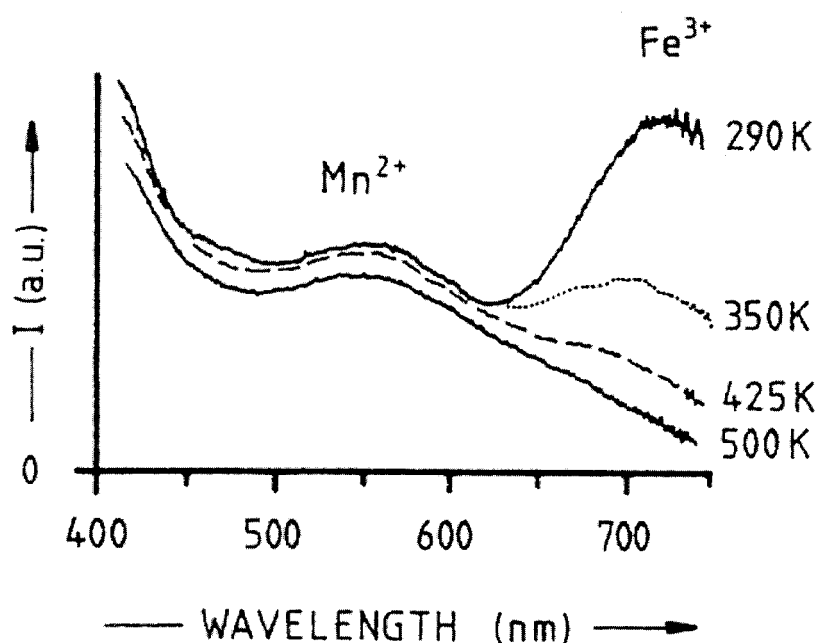


Fig. 5.6. Photoluminescence emission spectra obtained from a plagioclase feldspar sample under 340 nm excitation at a variety of temperatures. Thermal quenching of the red emission (710 nm) is evident, while very little change is seen at wavelengths shorter than 600 nm. (From Poolton et al, 1995).

### 5.5.3 Temperature dependence of feldspar OSL signals

In general the temperature dependence of OSL is complicated by the presence of shallow traps. For example, when the OSL stimulation is performed near room temperature a long tail to the OSL curve is often observed. Some of this can be attributed to the effect of shallow traps which re-trap charge released during illumination and slowly releases it again at a rate determined by the trap depth, sample temperature and optical sensitivity. The result is a slow, optically and/or thermally stimulated component to the OSL decay. In this way shallow traps may slow down the OSL decay process. This can give rise to a temperature dependent OSL component since at higher temperatures shallow traps become less effective at re-trapping charge.

Fig. 5.7a shows a set of normalised IR-stimulated OSL curves obtained at Risø for a feldspar sample (Risø FK951205) illuminated at temperatures from

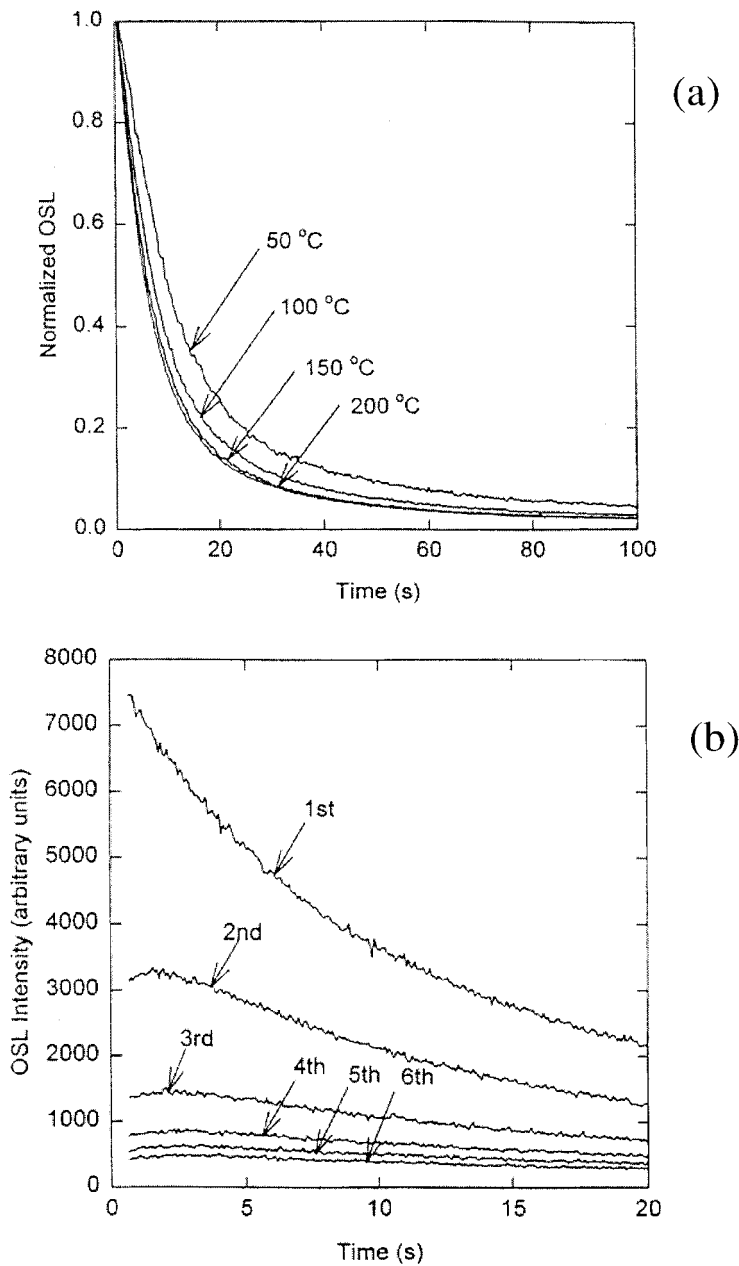


Fig. 5.7. (a) IR stimulated OSL decay curves from a potassium feldspar sample at the temperatures indicated. The sample was annealed at  $600^{\circ}\text{C}$  for 20 s, irradiated with a beta dose of 83.3 Gy, preheated at  $220^{\circ}\text{C}$  for 10 s, then stimulated with IR (880 nm).

(b) “Interrupted” IR stimulated OSL from the same feldspar sample. The sample was annealed, irradiated preheated and IR stimulated as in (a). The OSL decay curve was interrupted after 20 s, the sample pre-heated again at  $200^{\circ}\text{C}$  for 5 s, and illuminated again for 20 s to record the OSL. This was repeated several times. (From McKeever et al, 1997).

50 to 200°C. The increased rate of decay as the temperature increases is clear, in agreement with earlier similar measurements (Duller and Wintle, 1991). These observations are consistent with the expected effects of a thermally assisted process (Poolton et al, 1995b), although, no exact explanation of this phenomena can be given at the moment. Poolton et al (1995b) argued in favour of a direct donor-acceptor pair recombination process (where the thermal activation would be zero) based on the observation that if the IRSL decay is interrupted and then restarted, the decay curve does not pick up where it left off, but rather a slow increase, then decrease, is likely to be observed. This is illustrated in Fig. 5.7b where the IRSL decay was interrupted after 20 s; the sample was then pre-heated (200°C for 5 s) and the IRSL measured for another 20 s. This was repeated 5 times. A peak in the IRSL curve is clearly observed in the repeated measurement, as predicted by Poolton et al (1995b) for a direct donor-acceptor pair recombination process.

Duller and Bøtter-Jensen (1993) and McKeever et al (1997) showed that when stimulating feldspars with green light a smaller increase of the decay rate with increasing temperature was found suggesting that a thermally activated process is not occurring. These data may therefore be interpreted as being due to direct stimulation of the electrons into the conduction band followed by re-trapping at shallow traps. This is supported by the observation made by McKeever et al (1997) that the interrupted green-light stimulated OSL decay curves maintain the same basic shape and do not exhibit a peak in the initial decay curve, as was observed for the interrupted IR-stimulated OSL curves (Fig. 5.7.b). This supports the contention that green light can stimulate electrons directly into the conduction band and also implies the possibility of a direct donor-acceptor pair recombination for the IR-stimulated OSL from feldspars.

#### 5.5.4 Thermo-optical stimulation (TOL) experiments

The effect of sample temperature upon the OSL signals was also investigated by obtaining thermo-optical stimulated luminescence (TOL) signals using both IR and green light stimulation of a potassium feldspar (Duller and Bøtter-Jensen, 1993). Figs. 5.8 and 5.9 show the luminescence signals obtained from the feldspar sample when linearly raising the sample temperature from 50 to 500°C and momentarily stimulating with IR and green light, respectively. The samples were heated at 10°C/s and all luminescence signals were measured for 0.1 s every 10°C, both without any optical stimulation (to give the TL signal) and with one of the two light sources (to give the total luminescence signal). The OSL signal at any temperature was calculated by finding the difference between the TL and the total luminescence signal (Duller and Wintle, 1991). These measurements are analogues to the thermo-optical bleaching curves reported by Hütt et al (1988).

For natural samples (i.e. given no laboratory irradiation, Figs.5.8a and 5.9a) there is a linear increase in IRSL and GLSL with temperature from 50 to 250°C, the IRSL apparently increasing by a greater portion than the GLSL. The natural IRSL and GLSL signals are plotted against each other over the temperature range from 50 to 250°C in Fig 5.10. As seen the two signals increase proportionally between 50 and 200°C and a linear fit in this temperature range apparently passes through the origin demonstrating that at least parts of the IRSL and GLSL signals originate from the same traps. Above 280°C both the IRSL and GLSL signals decrease. This decrease is presumably due to thermal de-trapping of the charge, giving rise to the IRSL and GLSL signals. For the irradiated samples the IRSL (Fig 5.8b) also shows a linear increase in signal with temperature (from 50 to 250°C) in spite of the presence of the large TL peak at 150°C. How-

ever, the GLSL signal starts at a relatively high value and increases only slightly (Fig. 5.9b) in contrast to the behaviour of the natural sample as also discussed in section 5.5.3.

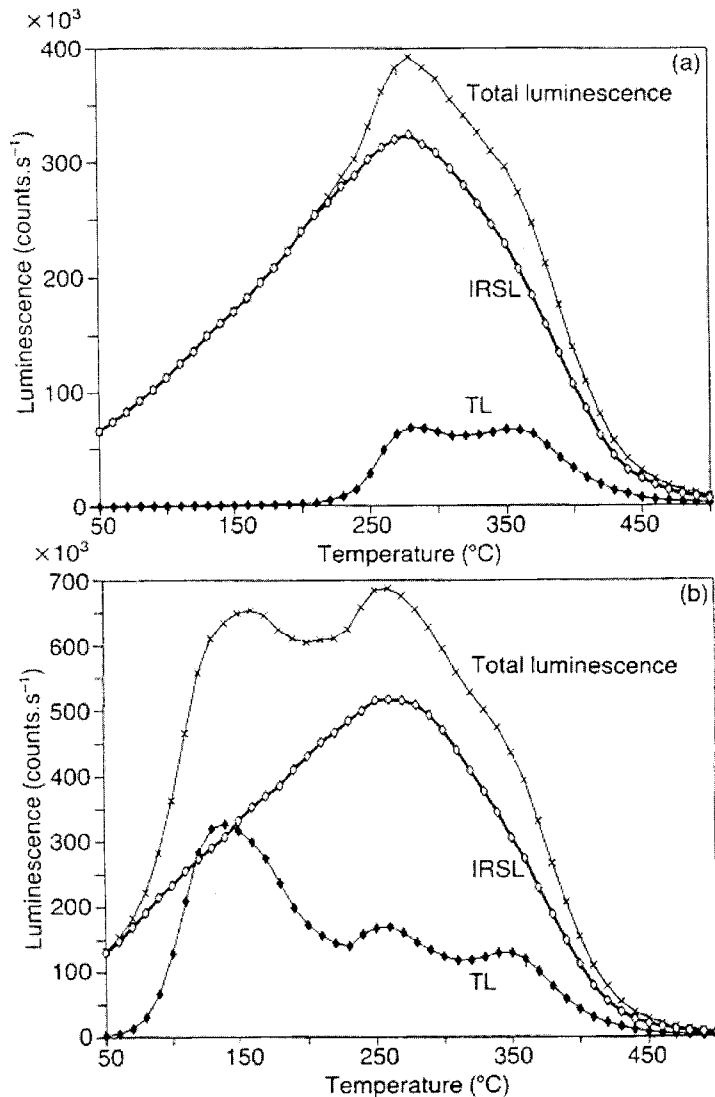


Fig. 5.8. (a) Simultaneous measurement of TL and IRSL as function of temperature for a natural sedimentary potassium feldspar. Luminescence was measured for 0.1 s every 10°C, heating at 10°C/s.

(b) The same as in (a) but the sample had added a beta dose of 18 Gy to the natural dose. See text for details. (From Duller and Bøtter-Jensen, 1993).

It is clear that the presence or absence of charge in low temperature traps has little effect on the IRSL signal (compare Figs. 5.8a and 5.8b). In contrast, when the low temperature traps are filled, the GLSL signal is affected significantly (Figs 5.9a and 5.9b). It is concluded that this technique offers the possibility of a simple method for explicitly determining the minimum preheat necessary to ensure that the natural and regenerated OSL signals originate from the same traps.

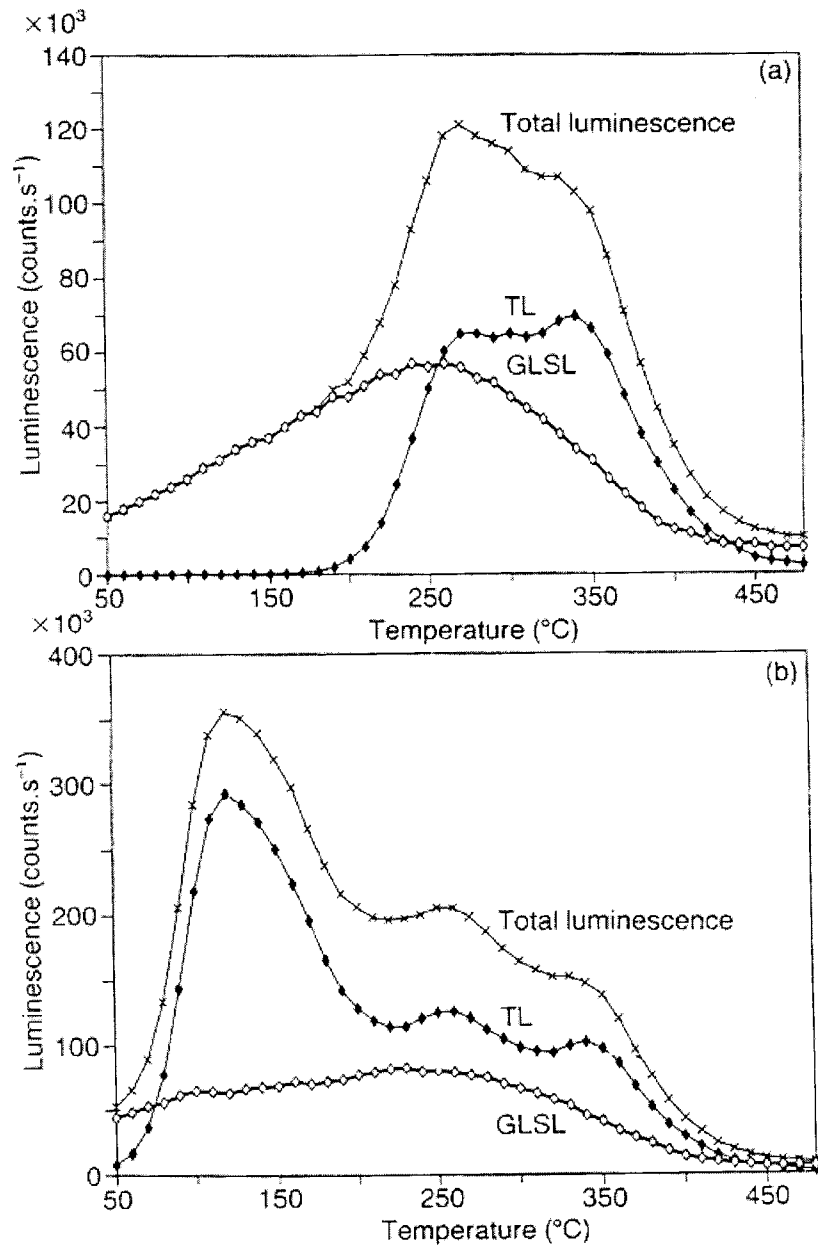


Fig. 5.9. (a) Simultaneous measurement of TL and green broad-band stimulated (420-550 nm) signals as function of temperature for a natural sedimentary potassium feldspar. Luminescence was measured for 0.1 s every 10°C, heating rate at 10°C/s.

(b) The same as in (a) but the sample had added a beta dose of 18 Gy to the natural dose. See text for details. (From Duller and Bøtter-Jensen, 1993).

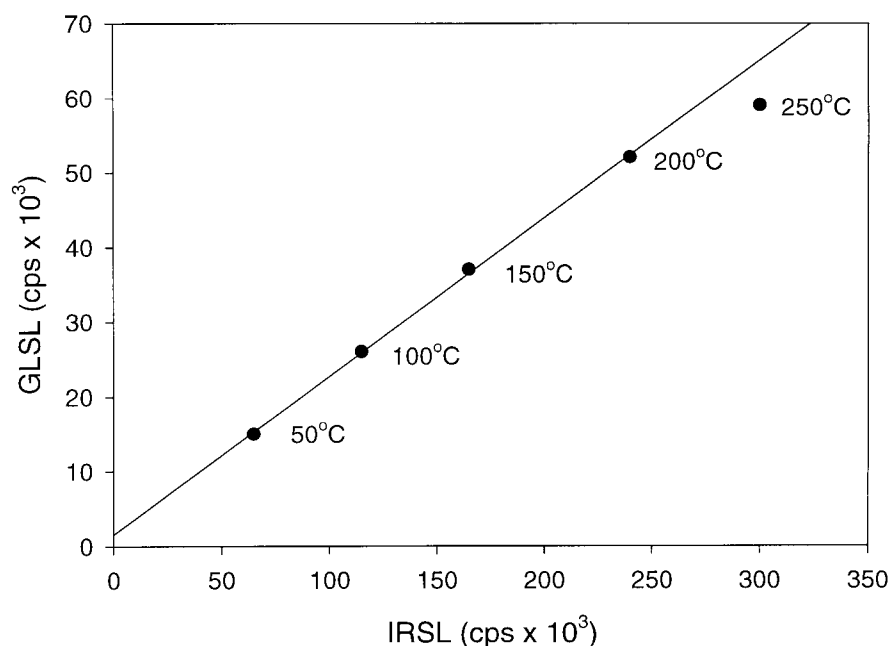


Fig. 5.10. IRSL versus GLSL signals from feldspar during linear heating from 50 to 250°C.

### 5.5.5 The effect of IR stimulation at elevated temperature on the blue light stimulated feldspar signal

The effect of IR laser stimulation (830 nm; 500 mW/cm<sup>2</sup>) at elevated temperature on the blue LED (470 nm; 22 mW/cm<sup>2</sup>) stimulated luminescence signal from two feldspar samples was investigated (Banerjee et al, 1999c). Fig. 5.11 shows the effect of IR stimulation at 200°C on the blue LED stimulated signal averaged over the two feldspar samples (after correction for thermal decay; see Banerjee et al, 1999c). The residual blue stimulated signal versus IR stimulation can be resolved with three exponentially decaying components with lifetimes of  $4.2 \pm 0.3$  s,  $150 \pm 40$  s and  $8000 \pm 4000$  s; their respective amplitudes are about 89, 9.5 and 1.3 %. This is similar to what was observed earlier on the effect of IR stimulation on the broad-band stimulated feldspar signal at room temperature (see Fig. 5.5).

### 5.5.6 Thermo-optical activation characteristics

If it is assumed that the cause of change in feldspar OSL intensity as a function of sample temperature is primarily related to the efficiency with which charge is thermally transferred from a shallow trap to the conduction band (after initial optical stimulation from the deeper OSL trap to the shallow trap) then the thermal activation energy (TAE) of this trap can be determined using an Arrhenius plot of the variation in OSL using the TOL technique described in a previous section (5.5.4). Typically a plot of the natural logarithm of the intensity versus the inverse of the sample temperature is used (e.g. see Duller, 1997).

The thermal activation energy (TAE) for IRSL has previously been measured for feldspars to be around 0.1 eV (Bailiff and Poolton, 1991) when stimulating with monochromatic light of 1.33 eV (930 nm). At Risø we were the first to use

a continuous monochromator system to determine if and how the thermal activation characteristics change over the entire stimulation wavelength range 400 to 1000 nm (Bøtter-Jensen et al, 1994b). The procedure is described below.

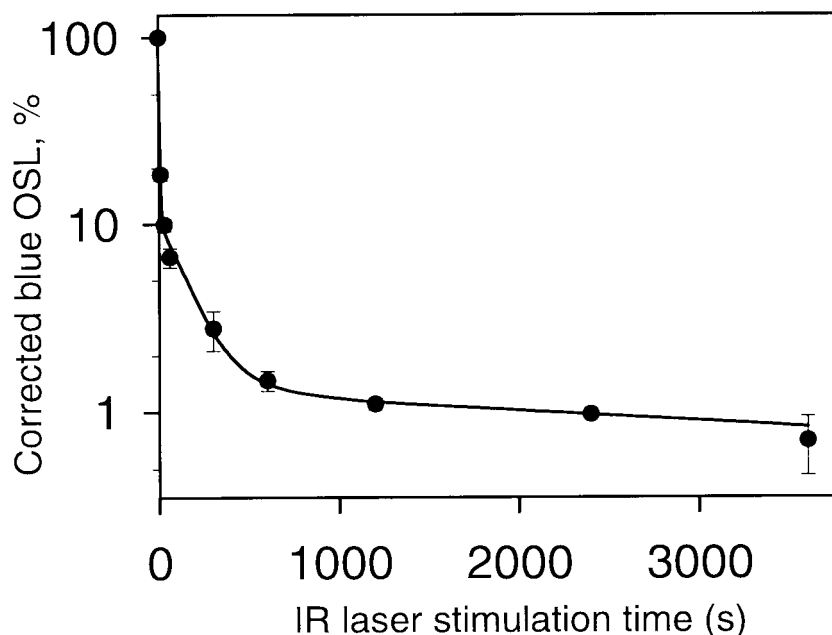


Fig. 5.11. The effect of IR stimulation at 200°C on the blue light stimulated signal averaged over two feldspar samples. The fitted line can be resolved into three exponentially decaying components (see text). (From Banerjee et al, 1999c).

A sample of Amelia albite (see section 5.1) was heated to 500°C prior to analysis to remove any trapped charge initially present, then given a beta dose of 17.8 Gy and finally preheated at 220°C for 10 minutes to remove any unstable luminescence components. The procedure for measuring the TAE was based on the TOL technique described above (Duller and Wintle, 1991; Duller and Bøtter-Jensen, 1993). The sample was heated to 500°C at a rate of 1°C/s and at every 10°C interval the OSL signal was measured using a U-340 filter by subtracting the TL signal from the total luminescence signal (see section 5.5.4). The TAE was determined by constructing a standard Arrhenius plot (natural logarithm of intensity against the inverse of sample temperature) over the temperature range 50 to 180°C. This measurement procedure was repeated at 25 nm intervals (with a 10 nm bandwidth).

As shown in Fig. 5.12 (from Bøtter-Jensen et al, 1994b), the plot of the TAE versus optical stimulation energy is complex since it is a superposition of several processes (Poolton et al, 1994b). First, for stimulation energies greater than the trap depth, the TAE represents the energy needed to allow charge to move within the conduction band tail; the TAE increases linearly with decreasing optical energy, reflecting the extra energy required to escape from such localised states. Superimposed on this simple situation is the complication caused by the optical resonance features at about 850, 600 and 500 nm (1.5, 2.1 and 2.5 eV, respectively; see Fig. 5.1a). At 850 and 400 nm, the TAE drops to a similar value, possibly because the excitation is directly into the high mobility conduc-

tion band states. The main features are that for high photon energies (2 to 3.2 eV) the TAE is lowest (at around 0.06 eV) but increases when lower photon energies are used, except for a well-defined dip at 1.5 eV.

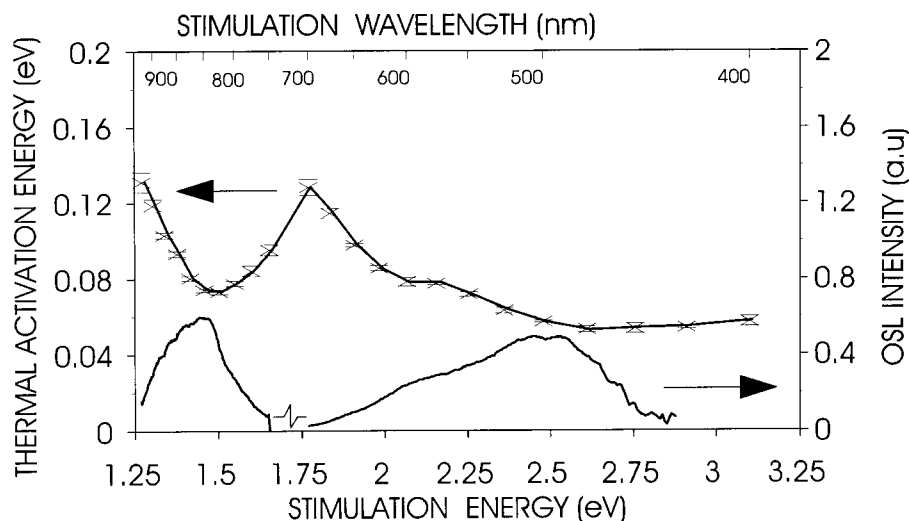


Fig. 5.12. Thermal activation energy versus optical stimulation energy for a pure *Amelia albite* sample (beta dose: 17.8 Gy). The resonance at around 1.4 eV is clearly seen. For comparison the stimulation spectrum (after subtraction of the continuum given in Fig. 5.1.a is also shown (from Bøtter-Jensen et al, 1994b).

The photo excitation spectrum from the same sample is also plotted in Fig. 5.12 (taken from Fig. 5.1a). At each energy where there is a peak in the excitation spectrum, there is also a dip in the thermal activation energy curve, namely at 1.5 eV, 2.1 eV and 2.5 eV. Similar behaviour has been observed in all samples of albite examined so far. An explanation for these features is not simple but, as suggested by Poolton et al (1994b), it reflects the complex nature of the conduction bands in feldspar minerals. Spooner (1993; 1994) produced bleaching curves which also exhibit a similar pattern. These results show that the stimulation processes in feldspar appear to be more complex than those originally proposed by Hütt et al (1988) who measured a more simple relationship between IRSL and stimulation wavelength.

This work was extended to provide thermal energy versus optical energy data for three feldspar samples; albite, orthoclase and oligoclase (Poolton et al, 1995b). Fig. 5.13 plots the thermal activation energy versus optical stimulation energy characteristics for these samples. They show broadly similar behaviour, but the absolute values of TAE are different, and the fine structure also shows significant variations.

### 5.5.7 Summary - TOL characteristics

Several processes have been seen to affect the behaviour of OSL decay curves of feldspars as a function of temperature, depending upon the precise mechanism by which the OSL is produced. Shallow traps play an important role whenever the OSL process involves stimulation into delocalised bands. The trapping of charge by the shallow traps, followed by the thermal release of this charge back into the conduction band, yields a non-exponential tail to the OSL

decay curve, reduces the initial intensity of the OSL, and can, in the right circumstances, even give rise to a peak in the OSL curve.

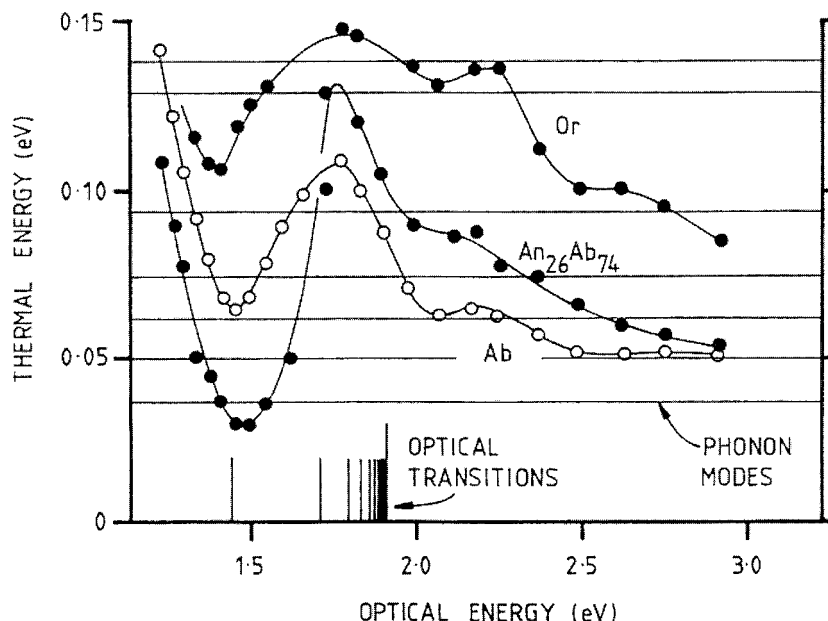


Fig. 5.13. Variation in thermal activation energy of three feldspars (*Ab* = albite; *An* = anorthite; *Or* = orthoclase) when stimulated at different wavelengths. The TAE was measured using TOL measurements. See text for details (from Poolton et al, 1995b).

## 5.6 Doped Feldspars with Enhanced IRSL Sensitivity

The spectral and radiation dose characteristics of a range of artificially doped natural silicate materials were surveyed at Risø, with the intention of searching for alternative, high sensitivity materials that could potentially be used as infrared stimulated luminescence (IRSL) dosimeters for the measurement of environmental dose rates (Poolton et al, 1997).

All samples in this study were natural feldspars, provided by the Mineral Collection of the Geological Museum, University of Copenhagen. Diffusion experiments were made at 950°C in a tubular, alumina-ceramic clad furnace, at atmospheric pressure. During the annealing, the furnace was continually swept with a purge of pure nitrogen gas. Samples were heated from, and cooled to, room temperature in approximately 100 s in nitrogen atmosphere. The choice of 950°C as the anneal temperature was dictated by the need to have a high temperature to assist the diffusion process, and at the same time remain below the temperature at which both feldspars melt (1150 and 1118°C in K and Na feldspars, respectively: Deer et al, 1992), and below the melting point of the metals used as the dopant (e.g. 1083°C in copper). The choice of such a temperature was also aimed at reducing the possibility of inducing structural change in the crystals (at 980°C in albite, for example), a problem encountered by Jaek et al (1995) in their diffusion work carried out at 1100°C.

The effect of eight dopants were investigated, and compared with the effects of simply heating in air and nitrogen. The IRSL sensitivities to a test beta dose of 2 Gy were compared before and after treatment: the results for an orthoclase sample, are given in Fig. 5.14. There are several points of significance to derive from the diagram. Firstly, heating the samples only in a pure nitrogen atmosphere gives rise to enhancement of the IRSL sensitivity, and so any further advantage caused by a particular dopant must be assessed in comparison with this. Treatment with copper, silver and gold provided significant luminescence enhancement, whilst iron and zinc reduced the luminescence efficiency. Nickel has no observable effect. Somewhat surprisingly, Dy and Eu which are frequently used dopants in artificial TL phosphors cause, if anything, a reduction of the sensitivity of the material. Jaek et al (1995) also found copper to increase sensitivity, but they also observed enhancement with Eu. The reason for this disagreements between the two studies is uncertain, but might lie in the fact that a different anneal temperature (1100°C), atmosphere (air) and pressure were used by Jaek et al.

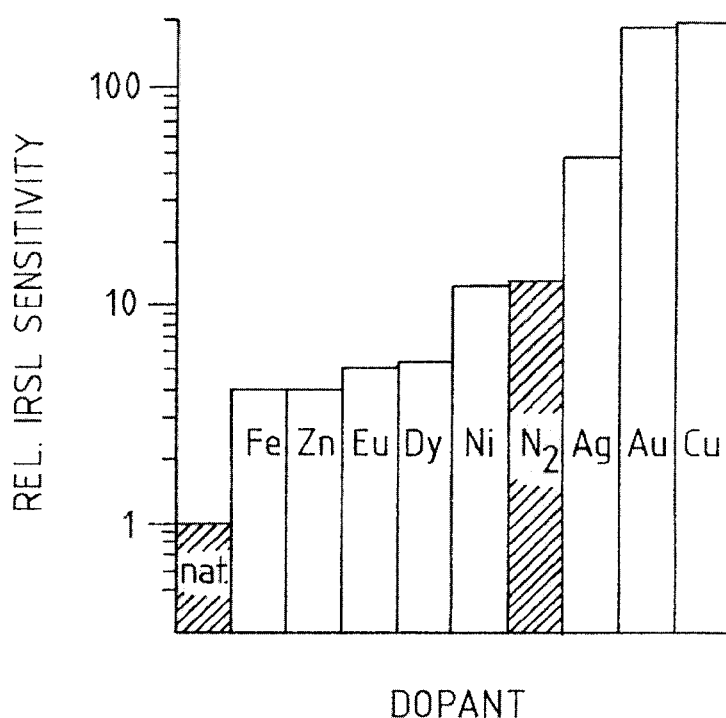


Fig. 5.14. Comparison of the change in IRSL sensitivity on heating orthoclase feldspar in the presence of nitrogen gas and the materials indicated. Annealing was made for 1 h at 950°C. Note the logarithmic scale. (From Poolton et al, 1997).

Fig. 5.15 shows the diffusion time dependence of the IRSL sensitivity for copper in the same orthoclase sample, indicating that for this particular sample, the IRSL sensitivity enhances for diffusions up to one hour, after which there is a slow decline. Similar curves were also found for all albite and orthoclase samples studied, with only small variation in the peak time.

The preliminary studies reported here show that the diffusion of Cu, Ag and Au in feldspars can enhance the IRSL sensitivity of the materials typically by two orders of magnitude.

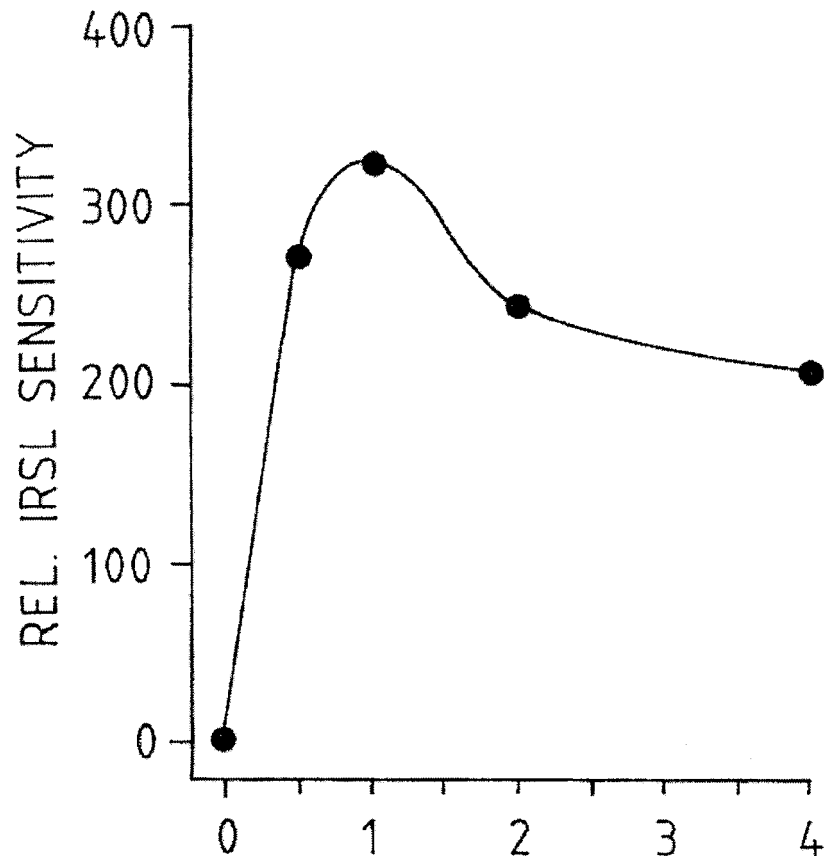


Fig. 5.15. Time dependence for the change in IRSL sensitivity of orthoclase feldspar caused by heating in the presence of nitrogen gas, and copper metal at 950°C. (From Poolton et al, 1997).

## 5.7 Conclusions - Feldspars

The chemical and structural complexities of feldspars cause them to exhibit a variety of luminescence behaviours. Many of the OSL characteristics are common to a broad range of feldspar types, and suggest that these signals may be simpler to analyse than those obtained by TL. Further work is required to fully understand the fundamental processes by which optically stimulated luminescence is produced in feldspars. However, as indicated in the sections above, it is likely that OSL measurement techniques, and in particular the analysis of stimulation spectra, can be useful in the analysis of the mineralogy of a variety of feldspar samples.

# 6 OSL Characteristics of Al<sub>2</sub>O<sub>3</sub>:C

## 6.1 Introduction

The use of anion-defect  $\alpha$ -Al<sub>2</sub>O<sub>3</sub>:C single crystals as highly sensitive TL dose-meters has been described by Akselrod et al (1990). They improved the dosimetric characteristics of Al<sub>2</sub>O<sub>3</sub> significantly by the inclusion of oxygen vacancies into its structure. This was done by annealing and melting the material un-

der strongly reducing conditions in the presence of graphite. Akselrod et al (1990) prepared the anion-defect  $\alpha$ - $\text{Al}_2\text{O}_3:\text{C}$  single crystals as 5 mm diameter rods that were cut into 1 mm thick single dosimeters. The main contribution to  $\text{Al}_2\text{O}_3:\text{C}$  luminescence is made by the F-centres (Akselrod and Kortov, 1990) with a distinct emission peak centred about 420 nm

The OSL properties of  $\text{Al}_2\text{O}_3:\text{C}$  single crystals and their use as OSL dosimeters for rapid assessment of the environmental photon dose rate have been intensively investigated at Risø (Bøtter-Jensen and McKeever, 1996; Bøtter-Jensen et al, 1997; Bøtter-Jensen et al, 1999c). It has been shown that  $\text{Al}_2\text{O}_3:\text{C}$  potentially possesses higher OSL sensitivity than TL sensitivity. In TL measurements of  $\text{Al}_2\text{O}_3:\text{C}$  thermal quenching is a major problem that crucially depends on the heating rate used. The OSL procedure has the advantage that it is not necessary to heat the material, and so quenching of the luminescence signal is avoided (Bøtter-Jensen et al, 1997). The following sections review the investigations of some OSL characteristics of  $\text{Al}_2\text{O}_3:\text{C}$  at Risø. It is demonstrated that the very high OSL sensitivity and the energy response (equal to that of quartz and feldspar) make  $\text{Al}_2\text{O}_3:\text{C}$  ideal for measuring the environmental dose rates in connection with retrospective dosimetry (and dating) using natural materials and ceramics (Bøtter-Jensen et al, 1997; Bøtter-Jensen et al, 1999c).

## 6.2 TL Versus OSL from $\text{Al}_2\text{O}_3:\text{C}$

The introduction of  $\text{Al}_2\text{O}_3:\text{C}$  as a material for TL dosimetry (Akselrod et al., 1990) has opened the possibility of several promising applications for high sensitivity measurements, particularly for short-term exposure in environmental dosimetry. Of special interest for dating applications and in retrospective dosimetry is that  $\text{Al}_2\text{O}_3:\text{C}$  possesses a photon energy response nearly identical to that of quartz and feldspar (Akselrod et al., 1990) and is, therefore, ideal for monitoring the environmental photon dose rate in connection with determining absorbed doses in natural materials and ceramics. An additional major advantage of  $\text{Al}_2\text{O}_3:\text{C}$  is that it possesses a TL sensitivity 40-60 times greater than that of LiF TLD-100 making it a strong candidate for low dose, short-exposure applications. However, thermal quenching processes in the material cause the TL sensitivity to depend strongly on the heating rate used, with less sensitivity being observed at higher heating rates (Kortov et al., 1994). This feature can be a disadvantage in routine TL dosimetry where fast heating automatic readers are often applied. Another potential limitation in the use of this material is its sensitivity to light. Light sensitivity manifests itself in this material mainly in two ways: (a) a light-induced fading of the TL signal and (b) in irradiated samples, the phototransfer of charge from deep states to shallower states giving rise to a phototransferred TL (PTTL) signal (e.g. Colyott et al., 1996). These features were reflected in a recent international intercomparison of TL materials used for environmental radiation measurements that revealed a large scatter in measurement results, and consequently a higher uncertainty from  $\text{Al}_2\text{O}_3:\text{C}$  than from all of the other TL materials employed (Bøtter-Jensen and Thompson, 1995).

However, the light-induced fading of the TL signal from  $\text{Al}_2\text{O}_3:\text{C}$  and the subsequent photo transferred TL (PTTL) into shallow traps indicated the potential of this material as a sensitive OSL dosimeter. The phenomenological model presented in chapter 2 predicts an even higher sensitivity (i.e. emitted luminescence photons per unit radiation dose) for OSL than for TL (Bøtter-Jensen and McKeever, 1996; McKeever et al., 1996). Given that  $\text{Al}_2\text{O}_3:\text{C}$  is already one of the most sensitive TL materials, the OSL sensitivity is promised to be exceptionally high.

### 6.3 OSL Stimulation Characteristics of Al<sub>2</sub>O<sub>3</sub>:C

The OSL stimulation spectrum (i.e. OSL versus stimulation wavelength of Al<sub>2</sub>O<sub>3</sub>:C) was obtained using the Risø scanning monochromator (visible range 400-750 nm) attached to a broad-band stimulation light source (Bøtter-Jensen et al., 1994a; Bøtter-Jensen et al., 1997). The detection was made in the UV via 6 mm U-340 filters. The spectrum, which is corrected for the wavelength response of the system, is shown in Fig. 6.1a. In addition to a rising continuum at lower wavelengths a smooth broad stimulation resonance was found peaking around 500 nm which is well matched to the Risø filtered halogen lamp OSL system with a standard broad stimulation wavelength band from 420-550 nm

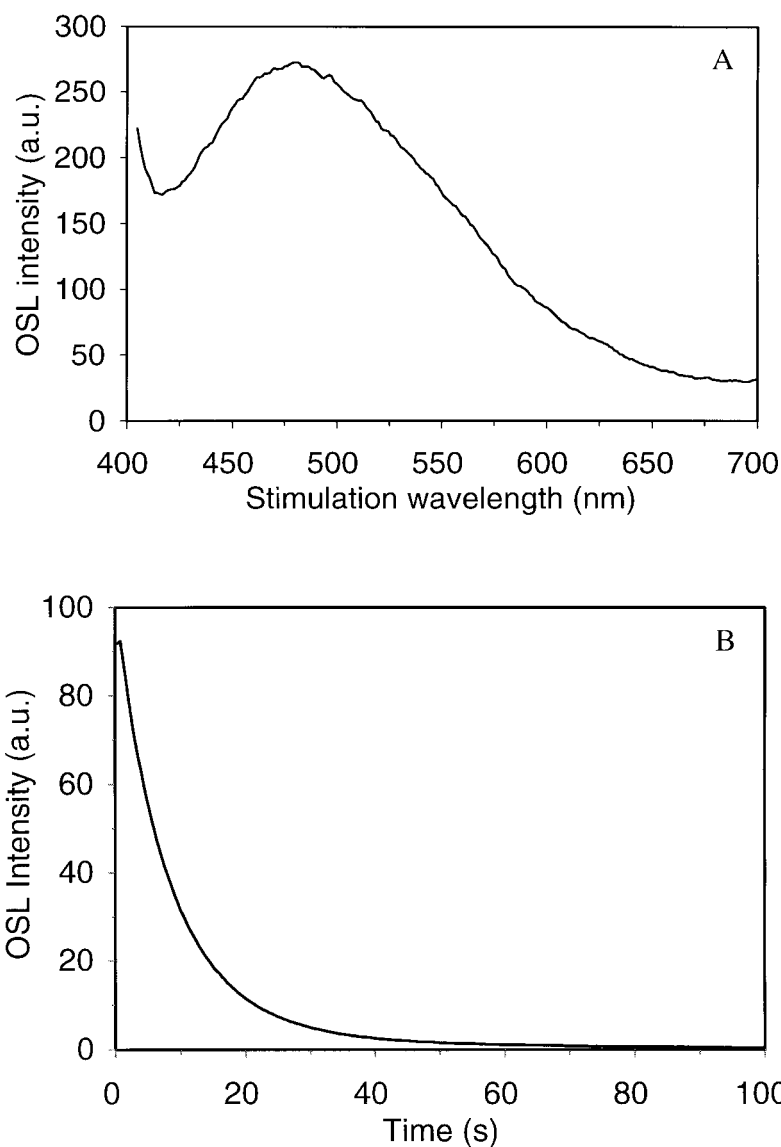


Fig. 6.1. (a) OSL stimulation spectrum (OSL versus stimulation wavelength) for Al<sub>2</sub>O<sub>3</sub>:C obtained using the Risø visible monochromator and a broad-band halogen lamp stimulation light source. Detection filter: U-340.

(b) OSL decay curve from Al<sub>2</sub>O<sub>3</sub>:C after irradiation to a <sup>90</sup>Sr beta dose of 60 mGy and stimulated with wavelength band 420-550 nm (16 mW/cm<sup>2</sup>) (from Bøtter-Jensen et al, 1997).

(Bøtter-Jensen and Duller, 1992). As a result, the OSL signal from  $\text{Al}_2\text{O}_3:\text{C}$  is a bright, rapidly decaying curve. Fig. 6.1b shows the OSL decay curve from  $\text{Al}_2\text{O}_3:\text{C}$  that had been given a dose of 60 mGy and stimulated with broad band green light ( $16 \text{ mW/cm}^2$ ).

## 6.4 The OSL and TL Responses of $\text{Al}_2\text{O}_3:\text{C}$ to Radiation Exposure

A simple regeneration approach is the obvious technique for rapid determination of the environmental dose rates using OSL with  $\text{Al}_2\text{O}_3:\text{C}$  and this also simplifies OSL measurements if made on location, e.g. using portable instrumentation (Poolton et al., 1994). A crucial point, however, is whether sensitivity changes occur during repeated use of  $\text{Al}_2\text{O}_3:\text{C}$ . Therefore, experiments were performed in the automated Risø TL/OSL reader to investigate the changes resulting from different treatments of  $\text{Al}_2\text{O}_3:\text{C}$  in repeated measurement cycles. An initial annealing at  $900^\circ\text{C}$  for 30 min. was applied to the dosimeters before use in order to remove all charge from deep traps (Akselrod et al, 1990).

### 6.4.1 Sensitivity changes of the OSL signal

Some of the OSL characteristics of  $\text{Al}_2\text{O}_3:\text{C}$  have been investigated previously (Bøtter-Jensen and McKeever, 1996; Bøtter-Jensen et al, 1997). However, when using regeneration methods it is particularly important to determine whether any changes in luminescence sensitivity occur as a result of repeated OSL readout. These characteristics were studied for  $\text{Al}_2\text{O}_3:\text{C}$  pellets at room temperature by initially bleaching them either using broad-band green light (Bøtter-Jensen et al, 1997) or 470 nm light from blue LEDs (Bøtter-Jensen et al, 1999c).

In one experiment the pellets were given a regeneration dose of 116 mGy, preheated at  $100^\circ\text{C}$  for 10 s and the blue light OSL signal measured over 50 s. This sequence was repeated 6 times and the regenerated OSL signal was seen to vary within  $< 1.7\%$ . This is well within the uncertainties arising from other sources (such as the beta source calibration) and it is concluded that a simple regeneration approach can be used for  $\text{Al}_2\text{O}_3:\text{C}$  without any sensitivity corrections. In principle, an OSL measurement of the unknown dose and a matching laboratory regeneration dose should be sufficient for a dose evaluation. However, the single aliquot regeneration dose evaluation measurements in this study were carried out using three different regeneration doses (see chapter 8). The radiation exposed dosimeters were first preheated at  $100^\circ\text{C}$  for 10 s and then had their unknown OSL signals measured using blue light stimulation at room temperature for 60 s. The pellets were then given three different consecutively higher regeneration doses (each preheated to  $100^\circ\text{C}$  for 10 s) using the procedure described above and their OSL signals were measured for 60 s after each beta dose. These results were generally used to plot growth curves from where the individual unknown doses were evaluated by interpolation.

Another experiment was designed to simulate the evaluation of short term exposure to environmental photon radiation. Repeated measurements were carried out where  $\text{Al}_2\text{O}_3:\text{C}$  dosimeters were given a dose of  $4 \mu\text{Gy}$   $^{60}\text{Co}$  radiation in the laboratory and each time measured in the OSL reader. These measurements were repeated several times using broad-band green light bleaching, with and without preheat at  $100^\circ\text{C}/30 \text{ s}$  prior to OSL readout, and the results are shown in Fig. 6.2a. As seen, when exposed to such low doses no measurable sensitivity change was observed whether a preheat was used or not. This result permits a

very simple measurement protocol to be used for measurement of low doses with  $\text{Al}_2\text{O}_3:\text{C}$ .

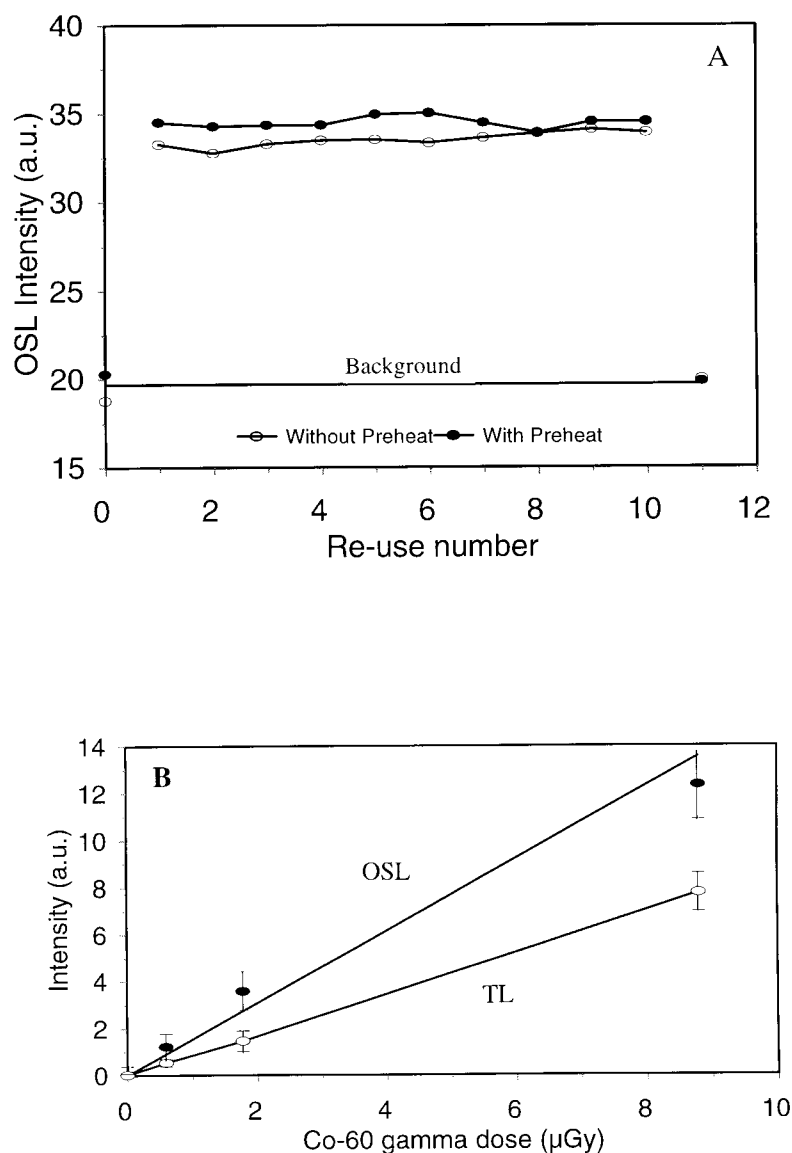


Fig. 6.2. (a) Repeated single aliquot regeneration OSL measurements of  $\text{Al}_2\text{O}_3:\text{C}$  after irradiation to a regeneration dose of  $4 \mu\text{Gy}$   $^{60}\text{Co}$  gamma radiation. The two curves represent: (i) regeneration using preheat  $100^\circ\text{C}/30 \text{ s}$  and (ii) regeneration without preheat. Note the background readings (undosed dosimeter readings) before and after the regeneration cycles.

(b) Net OSL and TL signals (background subtracted) from  $\text{Al}_2\text{O}_3:\text{C}$  versus  $^{60}\text{Co}$  gamma radiation. TL heating:  $2^\circ\text{C}/\text{s}$ . (from Bøtter-Jensen et al, 1997).

#### 6.4.2 Comparing the light sums of OSL and TL from $\text{Al}_2\text{O}_3:\text{C}$

Experimental comparisons of the total light sum for OSL with that for TL, showed that the OSL sensitivity is at least a factor of 2 times higher than the TL

sensitivity when using heating rates in the range  $1\text{-}2^{\circ}\text{C s}^{-1}$ . Dose response curves at low doses were obtained for  $\text{Al}_2\text{O}_3\text{:C}$  using both green light OSL (stimulation band 420-550 nm producing about  $16\text{ mW/cm}^2$  at the sample) and TL by heating to  $500^{\circ}\text{C}$  at a heating rate of  $2^{\circ}\text{C/s}$ . Plots of the net OSL and TL signals (background subtracted) versus  $^{60}\text{Co}$  gamma radiation are shown in Fig. 6.2b. The OSL yield is significantly higher than that of TL, and doses lower than  $0.5\text{ }\mu\text{Gy}$  (5 hours exposure to the natural background radiation) can easily be measured with good statistics using OSL. The OSL dose response has been shown to be linear up to about 50 Gy (McKeever et al., 1996).

The fading of the OSL signal from  $\text{Al}_2\text{O}_3\text{:C}$  at room temperature was tested over 85 days following  $100\text{ mGy }^{60}\text{Co}$  gamma irradiation. No fading (within 1 SD) of the initial OSL signal could be detected over that period.

## 6.5 Low-Dose Field Measurements using $\text{Al}_2\text{O}_3\text{:C}$

The capability of using OSL with  $\text{Al}_2\text{O}_3\text{:C}$  to measure the environmental photon radiation over short periods was tested at the Risø Natural Environmental Radiation Measurement Station (Bøtter-Jensen and Thompson, 1995). One experiment aimed at comparing the response of  $\text{Al}_2\text{O}_3\text{:C}$  with a high pressure ionisation chamber (Reuter Stokes RS-111) that continuously monitored the natural background radiation at the location. Two packages, each of 9  $\text{Al}_2\text{O}_3\text{:C}$  dosimeters, were placed adjacent to the ionisation chamber at the field site where they integrated the environmental dose rate over two different short integration periods of 15 and 72 hours, after which their OSL signals were immediately measured. The result of this experiment is given in Table 6.1. As seen, even at such low doses, the OSL uncertainties are small and the OSL measurements agree very well with those obtained with the ionisation chamber. To illustrate the OSL yield, the decay curves from  $\text{Al}_2\text{O}_3\text{:C}$  exposed to integrated natural environmental radiation doses of  $0.98$  and  $5.10\text{ }\mu\text{Gy}$  obtained over 15 and 72 hours, respectively, compared with that from a  $44\text{ }\mu\text{Gy }^{60}\text{Co}$  gamma calibration dose are shown in Fig. 6.3a.

*Table 6.1. Comparison between the response of high pressure ionisation chamber (HPIC) and  $\text{Al}_2\text{O}_3\text{:C}$  dosimeters after short term exposure to natural environmental photon radiation. 9 single  $\text{Al}_2\text{O}_3\text{:C}$  single chips were used for each dose evaluation.*

Exposure time (h)	HPIC ( $\mu\text{Gy}$ )	$\text{Al}_2\text{O}_3\text{:C}$ ( $\mu\text{Gy}$ )
15	$1.04 \pm 0.05$	$0.98 \pm 0.03$ (n = 9)
72	$5.13 \pm 0.01$	$5.10 \pm 0.02$ (n = 9)

Further OSL measurements were carried out over a study period of 33 days at the Risø Natural Environmental Radiation Measurement Station where  $\text{Al}_2\text{O}_3\text{:C}$  dosimeters were exposed to the natural environmental radiation for different integration times ranging from 1 to 33 days. The OSL results obtained, with and without preheat applied prior to OSL readout, are compared with data measured by the continuously monitoring Reuter Stokes high pressure ionisation chamber in Fig. 6.3b. The agreement is very good.

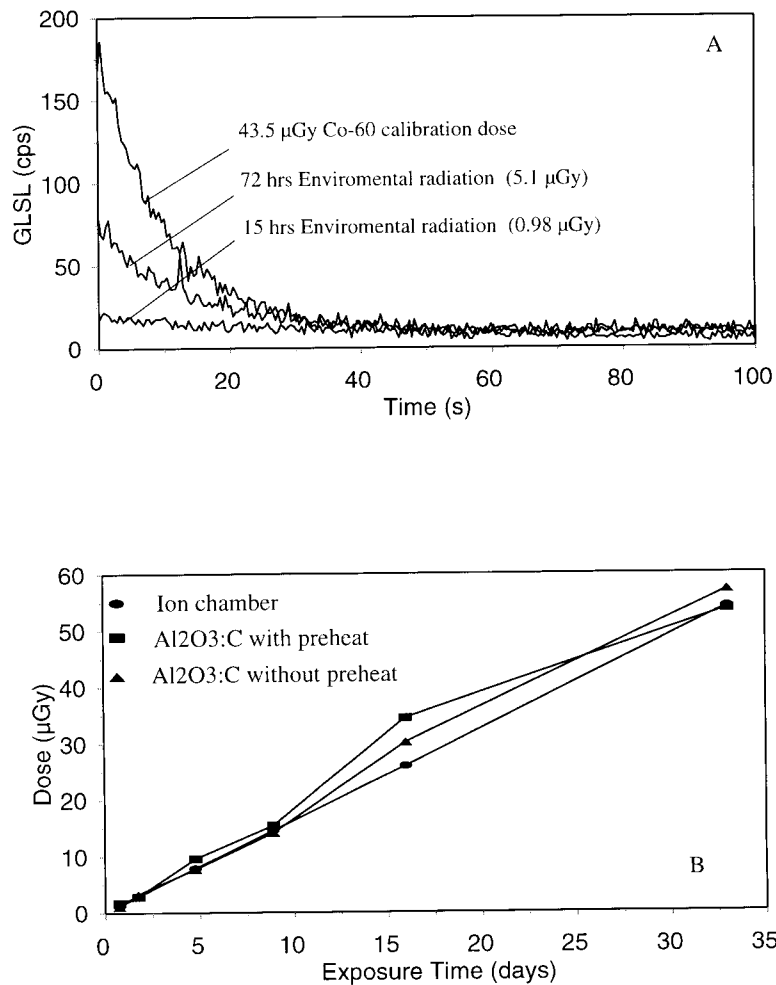


Fig. 6.3. (a) OSL decay curves from  $\text{Al}_2\text{O}_3:\text{C}$  dosimeters exposed over 15 and 72 hours to the natural environmental background radiation representing evaluated integrated doses of 0.98 and 5.10  $\mu\text{Gy}$ , respectively, compared to that from a 44  $\mu\text{Gy}$   $^{60}\text{Co}$  gamma calibration dose.

(b) Short-term OSL measurements of the natural environmental photon radiation using  $\text{Al}_2\text{O}_3:\text{C}$  (with and without preheat  $100^\circ\text{C}/30\text{ s}$  applied prior to read-out) carried out over different time periods ranging from 1 to 33 days compared with data obtained by a continuously monitoring high pressure ionisation chamber (Reuter Stokes RS-111) (from Bøtter-Jensen et al, 1997).

## 6.6 The Temperature Dependence of OSL from $\text{Al}_2\text{O}_3:\text{C}$

### 6.6.1 Thermo-optical (TOL) characteristics of $\text{Al}_2\text{O}_3:\text{C}$

If  $\text{Al}_2\text{O}_3:\text{C}$  is irradiated at  $-73^\circ\text{C}$ , the TL glow curve consists of three peaks – peak I at  $\sim 0^\circ\text{C}$ , peak II at  $\sim 70^\circ\text{C}$  and peak III at  $\sim 200^\circ\text{C}$  (when heated at  $0.4^\circ\text{C}\cdot\text{s}^{-1}$ ). Peak III is the so-called “dosimetric peak” and is the signal moni-

tored during conventional TL dosimetry using this material (Akselrod et al, 1990; Akselrod et al, 1993; Kortov et al, 1994). Measurements of the variation of the shape and position of peak III as function of dose and pre-annealing temperature indicate the presence of several overlapping components.

In order to fully develop OSL of  $\text{Al}_2\text{O}_3:\text{C}$  in dosimetry an understanding of the mechanisms of OSL production is necessary, at least at the phenomenological level. Experimental investigations of the temperature dependence of the OSL emission and also computer simulations of the possible OSL mechanisms were performed at Risø by numerically solving the rate equations describing the traffic of charge between energy levels during OSL excitation (Markey et al, 1996).

Thermo-optical (TOL) measurements on  $\text{Al}_2\text{O}_3:\text{C}$  single crystals were undertaken on the variation of the OSL signal as function of temperature using the Risø TL/OSL system equipped with U-340 detection filter (see section 5.5.4). The samples were heated at a linear rate ( $2^\circ\text{C}\cdot\text{s}^{-1}$ ) from room temperature to  $400^\circ\text{C}$ , and the OSL emission was monitored during periodic blue light (470 nm) excitation, each of 0.1 s duration. In this mode the total luminescence measured is the sum of OSL plus TL. The OSL temperature dependence is then calculated by subtracting the TL signal from the total signal according to the procedure described by Duller and Bøtter-Jensen (1993). The TOL curve is shown in Fig. 6.4a.

Fig. 6.4a demonstrates that the efficiency with which OSL is produced is temperature dependent. The OSL output increases up to  $\sim 150^\circ\text{C}$ , beyond which, a sharp decrease occurs. The decrease is interpreted as being partially due to emptying the dosimetric traps, and partially due to strong thermal quenching of F-centre emission (Akselrod et al, 1993; Kortov et al, 1994). For comparison the TL curve is also shown in Fig. 6.4a and the TL peaks II and III are clearly seen.

Previous studies of the light-induced fading of the TL from  $\text{Al}_2\text{O}_3:\text{C}$  (Akselrod et al, 1993) have indicated that illumination of an irradiated specimen with visible light will remove the main dosimetric TL peak. PTTL measurements support this observation (Akselrod et al, 1993). An obvious proposition, therefore, is that the OSL signal is induced when charges are optically released from the main dosimetric traps, recombine with carriers of the opposite polarity, and produce the observed F centre emission at  $\sim 420$  nm.

The deep traps contribute only  $\sim 2\text{-}3\%$  of the OSL signal when stimulated with 500 nm light. Decreasing the wavelength was observed to increase the contribution from these deep traps. Both of these observations are in agreement with the data from the PTTL experiments in which the wavelength dependence is investigated more thoroughly (Colyott et al, 1996). It is difficult to separate the temperature dependence of the OSL due to the deep traps from that of the OSL due to the dosimetric trap(s). For example, in separate experiments a sample was pre-irradiated with a large beta dose (1.5 Gy) and preheated to temperatures  $> 230^\circ\text{C}$ . This treatment fills the deep traps, but empties the dosimetric trap(s). An OSL temperature dependence similar to that shown in Fig. 6.4a was then observed. At first sight this appears to indicate that OSL from deep traps displays a temperature dependence similar to that observed from the dosimetry traps. However, interpretation is complicated by the phototransfer of charge from the deep traps to the dosimetry traps during OSL measurements (Colyott et al, 1996), accompanied by the simultaneous optical stimulation of charge out of the dosimetry traps. Thus, the observed temperature dependence may still be that of the OSL from the dosimetry traps, rather than from the deep traps (Markey et al, 1996). It has been suggested that stimulation using the high energy 470 nm light emitted from blue LEDs removes slightly more charge from the deep traps of  $\text{Al}_2\text{O}_3:\text{C}$  than broad-band green light (420-550 nm).

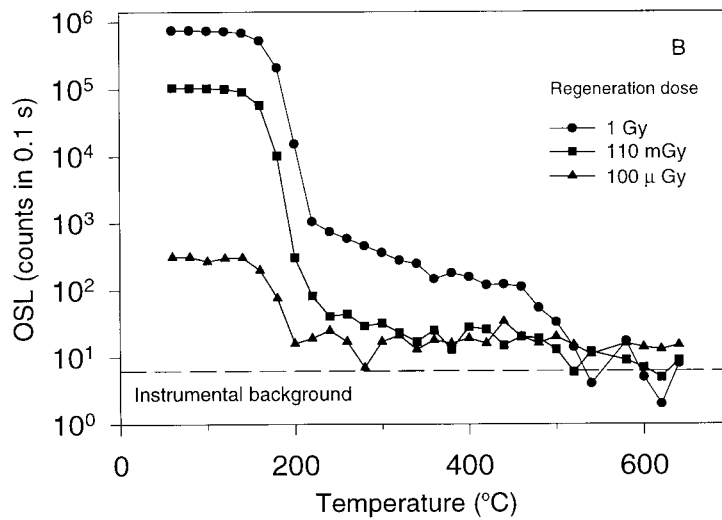
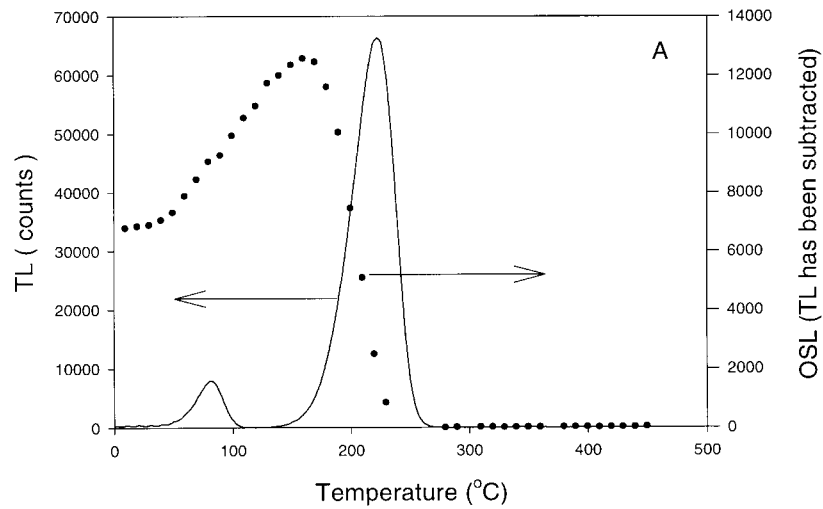


Fig. 6.4. (a) Thermo-optical luminescence (TOL) characteristics (OSL and TL plotted against temperature) of  $\text{Al}_2\text{O}_3:\text{C}$  after 1 Gy  $^{90}\text{Sr}$  beta dose delivered at room temperature and heated at 2 K/s.

(b) OSL plotted against pre-heat temperature for  $\text{Al}_2\text{O}_3:\text{C}$  chips exposed to 1 Gy, 110 mGy and 100  $\mu\text{Gy}$   $^{90}\text{Sr}$  beta radiation, respectively, at room temperature. Note the logarithmic scale (from Bøtter-Jensen et al, 1999c).

### 6.6.2 Thermal zeroing of the OSL signal from $\text{Al}_2\text{O}_3:\text{C}$

In a single aliquot regeneration measurement sequence it is necessary that the natural and regenerated luminescence signals in repeated measurements of the same aliquot are reduced to negligible fractions of the initial values by either thermal annealing or bleaching with stimulation light. Earlier studies of the OSL characteristics of  $\text{Al}_2\text{O}_3:\text{C}$  have suggested that annealing at 900°C is necessary to avoid the effect of charge in deep traps on repeated measurements if using regeneration doses higher than 1 Gy (Markey et al, 1996). Bøtter-Jensen et al (1997) showed that the deep trap effect is negligible in environmental dosimetry where smaller doses (1 mGy) are measured (this is a typical annual

gamma dose from natural radiation (terrestrial + cosmic)). The zeroing of the OSL signal in  $\text{Al}_2\text{O}_3:\text{C}$  was studied by analysing both annealing and bleaching parameters (Bøtter-Jensen et al, 1999c). Firstly the dependence of the OSL signal on preheat temperature was measured to investigate the relationship between the OSL signal and the known TL traps. The OSL signal was measured as a function of preheat over the range 60-640°C for  $\text{Al}_2\text{O}_3:\text{C}$  chips that had received three different  $^{90}\text{Sr}$  beta doses of 1 Gy, 110 mGy and 100  $\mu\text{Gy}$ , respectively. The experimental conditions were as follows:

- 1) The  $\text{Al}_2\text{O}_3:\text{C}$  pellets were bleached using 470 nm blue light (20 mW/cm<sup>2</sup>) for 75 s to deplete the OSL signal.
- 2) Three different groups of pellets were irradiated with 1 Gy, 110 mGy and 100  $\mu\text{Gy}$  beta regeneration doses, respectively.
- 3) All were preheated at 60°C for 10 s.
- 4) OSL was measured for 0.1 s at reduced illumination power.
- 5) Steps 3 and 4 (preheat, OSL) were repeated using gradually higher preheat temperatures (20°C intervals).

It should be noted that the repeated pulsed 0.1 s OSL signals (step 4) obtained after each preheat temperature from the same sample had only a negligible depletion effect on the initially induced regeneration signal. The resulting plots of the OSL as a function of preheat temperature are shown in Fig. 6.4b. The main features observed for all three doses is a flat plateau region from 60°C to 140°C which show that no OSL is coming from shallow traps; then a steep decrease over the range 150-220°C is seen suggesting that the most OSL sensitive traps may relate to the 200°C region of the TL glow peak. The remaining signal then decays slowly over the temperature range 220-500°C. These observations agree with and extend the previous work by Markey et al (1996). However, even for the dosimeter chip that had received 1 Gy beta dose, above 500°C the OSL has fallen to instrument background; this suggests that even for significant prior doses an annealing temperature of 500°C is sufficient to completely zero  $\text{Al}_2\text{O}_3:\text{C}$ .

### 6.6.3 Optical zeroing of the OSL signal from $\text{Al}_2\text{O}_3:\text{C}$

In an investigation of the effect of bleaching  $\text{Al}_2\text{O}_3:\text{C}$  with blue light (blue LEDs), two groups of dosimeters were initially annealed at 500°C and exposed to 110 mGy and 100  $\mu\text{Gy}$  beta radiation, respectively. Their OSL decay curves were then measured over 75 s at room temperature. These decay curves are shown in Fig. 6.5 (from Bøtter-Jensen et al, 1999c). The initially regenerated OSL signal is depleted to less than 1% of the initial value over 35s (note the logarithmic Y-axis). A particularly attractive feature of erasing the OSL signal by bleaching is the potential of being able to zero effectively the OSL signal by sunlight on location in the field, e.g. when  $\text{Al}_2\text{O}_3:\text{C}$  is used for environmental dosimetry. This is particularly important when carrying out environmental dosimetry over short periods (a few weeks) where the delivery dose, i.e. the dose collected by the dosimeter during the time from when it is annealed until it reaches its location in the field, becomes significant. This feature can be particularly important when dosimeters are mailed over long distances (by air, with a significant cosmic ray dose rate) to remote field sites. The effect of sunlight bleaching was tested by irradiating several  $\text{Al}_2\text{O}_3:\text{C}$  dosimeters with 100  $\mu\text{Gy}$  from  $^{60}\text{Co}$  gamma radiation and then leaving them behind a normal window glass where they were exposed to filtered daylight for 8 hours. After bleaching,

a residual OSL signal dose of  $< 0.4 \mu\text{Gy}$  was measured which is close to the instrument background and is considered negligible.

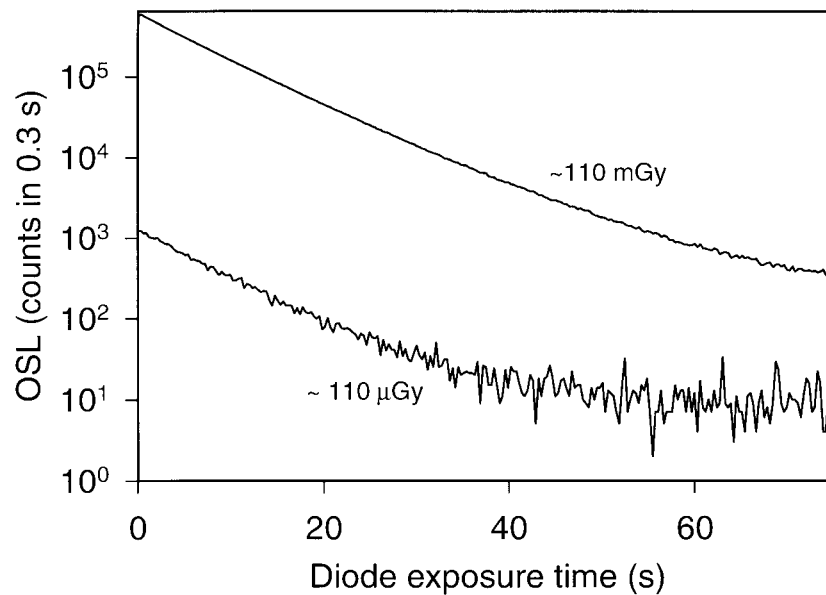


Fig. 6.5. OSL decay curve curves from  $\text{Al}_2\text{O}_3:\text{C}$  exposed to (a) 110 mGy and (b) 100  $\mu\text{Gy}$  beta radiation read at room temperature. Note the logarithmic Y-axis (from Bøtter-Jensen et al, 1999c).

## 6.7 Conclusions – $\text{Al}_2\text{O}_3:\text{C}$

The OSL of  $\text{Al}_2\text{O}_3:\text{C}$  has strong potential for use in a variety of radiation dosimetry applications. The process of optically stimulating the emission of luminescence is, in principle, intrinsically more sensitive than thermally stimulated processes. There is no need to heat the material, and this simplifies the instrumentation. The high OSL sensitivity of  $\text{Al}_2\text{O}_3:\text{C}$  has been demonstrated and its suitability for use as an alternative method for rapid assessment of the environmental photon dose rate has been outlined.

It has further been shown that  $\text{Al}_2\text{O}_3:\text{C}$  can be completely emptied of trapped charge by exposure to daylight for some hours. This observation effectively improves the minimum detection limit of the dosimeter; by zeroing the  $\text{Al}_2\text{O}_3:\text{C}$  immediately before field measurement, any dose absorbed during travel to the site is removed. Sensitivity changes during normal measurement cycles have been shown to be negligible; this allows a simple regeneration dose measurement, without the need for any special procedures to deal with sensitivity changes.

The next chapter shows that  $\text{Al}_2\text{O}_3$  is a common component in porcelain production and its responsibility for the high OSL sensitivity of many crockery porcelain wares.

# 7 OSL Characteristics of Porcelain

## 7.1 Introduction

Porcelain is potentially a very important material in accident dosimetry because it is widespread in the domestic and industrial environment. The potential of OSL for dose measurements on various porcelain ceramic materials has been investigated at Risø (Poolton *et al* 1995c; Bøtter-Jensen *et al*, 1996), and Hübner and Göksu (1997) have reported their use of the OSL pre-dose effect in porcelain from electric-power insulators to retrospectively assess accident doses. Although the principle raw materials used in the manufacture of porcelain are quartz, feldspar and china clay (kaolinite), a minor component of  $\text{Al}_2\text{O}_3$  is often added. As described in chapter 6,  $\text{Al}_2\text{O}_3:\text{C}$  has shown to be a very sensitive OSL radiation dosimeter. However, the sensitivity of any of the potentially usable dosimeters contained within porcelain ceramic is likely to depend strongly on the production conditions (firing temperature, atmosphere etc), as well as the exact composition of the starting materials.

Porcelain manufacturers tend to use different production cycles and raw ingredients, depending on the final use of the material. Products requiring high mechanical strength, and likely to undergo many heating-cooling cycles in its lifetime (oven or furnace-ware, for example) will differ considerably from sanitary wares (Baker, 1991) or wall tiles (eg. Leonard, 1992; Sainamthip and Reed, 1989) which can be made of lower quality materials and then glazed. One of the main problems in porcelain manufacture is the  $\alpha$ - $\beta$  quartz phase transition at  $573^\circ\text{C}$ , since this is associated with a very large change in the thermal expansivity of the material (Leonard, 1992; Bøtter-Jensen *et al*, 1995a), and micro-cracks in the material caused by this transition obviously lead to poorer mechanical properties. As a consequence, alternatives to the use of  $\alpha$ -quartz as a starting material are often sought. These range from the replacement by zircon (Tavcar *et al*, 1990) or alumina (Tkalec *et al*, 1984) or both (Majumdar *et al*, 1986).

In view of these comments, it is to be expected that the radiation dose sensitivity of porcelain will vary, depending on the particular product selected for measurement. This chapter examines the question of sensitivity variation, and in particular whether signatures in the luminescence spectra of a particular sample can be used to give information about the dose sensitivity. If measured in the field such characteristics could be used to ensure that, in a contaminated site, only highly OSL sensitive materials are removed for retrospective dose evaluation. The bleaching effect of sunlight on the OSL signal as a function of depth into the bulk porcelain was also examined to ensure that samples for OSL measurements be taken from a depth that has not been affected by light exposure.

## 7.2 Samples and Experimental Details

Since this work is relevant to the field of retrospective dosimetry, the materials studied were from a collection of mass-produced ceramics that was considered representative of materials commonly found in many households. Both the glazing and ceramic body of these products were analysed. Samples included toilet tanks, crockery and an electric fuse.

In all cases, the samples were drilled with a diamond-tipped tubular saw to create a short cylinder of material, diameter 8 mm, and this was subsequently cut into slices (thickness 1mm) using a diamond edged, water cooled circular saw. All luminescence and dose measurements were carried out in the auto-

mated Risø TL/OSL reader (Bøtter-Jensen, 1997), equipped with the Risø compact scanning monochromators, usable in the wavelength range 380-1100nm (see chapter 3). The spectra presented in the following sections are corrected in terms of the incident number of photons per unit energy. Both bialkali (blue sensitive: EMI 9635QB) and S-20 (red sensitive EMI 9658A) photomultiplier tubes were used in the study.

UV stimulation for photoluminescence measurements was provided by a broad-band 75W tungsten source, filtered with 6 mm standard Hoya U-340 (giving a narrow band centered at 340nm). Dose response measurements were made using the beta emission from a  $^{90}\text{Sr}/^{90}\text{Y}$  source (2Gy/minute). OSL was carried out using broad-band (420-550nm) light source delivering  $20 \text{ mWcm}^{-2}$  to the sample.

Ten different typical porcelain and ceramic samples were investigated including both the porcelain body and glaze and representing a broad selection of materials relevant to retrospective dosimetry. The samples analysed are listed in Table 7.1.

*Table 7.1. Porcelain samples used for the investigation of OSL properties*

Sample no.	Place	Item	Material
1P	Chernobyl	Toilet	Porcelain
1G	Chernobyl	Toilet	Glaze (white)
2P	Denmark	Sugar bowl	Porcelain
2G	Denmark	Sugar bowl	Glaze (white)
5P	Italy	Plate	Ironstone
6P	Denmark	Egg cup	Porcelain
6G	Denmark	Egg cup	Glaze (clear)
10P	Finland	Plate	Porcelain
13P	Denmark	Salt cup	Porcelain
20P	Estonia	Fuse	Ceramic

## 7.3 The Origin of OSL from Porcelain

In general, optical stimulation of both the main porcelain matrix and the glazing layer gives rise to two types of luminescence signals. These are time-decaying dose-dependent OSL signals, when the stimulation energy is less than the emission energy, and time-steady dose-independent photoluminescence (PL), when the stimulation energy is greater than that of emission.

### 7.3.1 Time-decaying dose-dependent OSL signals

As described in chapter 4, a strong link has been shown between the OSL and TL peak at 110°C in quartz (Stoneham and Stokes, 1991; Bøtter-Jensen and Duller, 1992; Bøtter-Jensen et al, 1995). In porcelain, an indication that at least part of the dosimetric information arises from the quartz phase of the material is provided by monitoring the TL at 110°C both before and after OSL. As shown in Fig. 7.1, illumination of the sample causes photo-transfer to this low temperature TL trap (PTTL), a process that is typically associated with OSL in quartz (Bøtter-Jensen and Duller, 1992; Bøtter-Jensen et al, 1995; Poolton et al,

1995c). However, as described below the quartz component is certainly not the only OSL active material present.

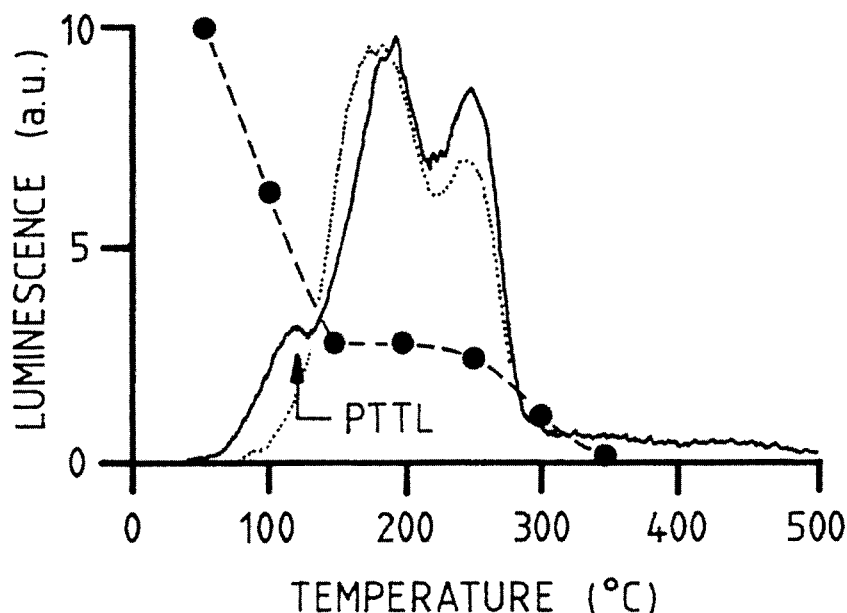


Fig. 7.1. The TL signals from a porcelain sample (1P) irradiated to 20 Gy and thermally washed at 120°C both before and after illumination with green light: the photo-transferred TL signal (PTTL) at about 110°C is typical for that of quartz. Thermal washing of the sample to successively higher temperatures (dotted line) indicates that the OSL probably originates from several of the TL traps (from Poolton et al, 1995c).

Thermal washing of fired porcelain samples to successively higher temperatures following irradiation indicates that the time decaying OSL signals are composed of at least three components. Fig. 7.1 shows the result from an experiment where a porcelain sample was given a 20 Gy dose using  $^{60}\text{Co}$  gamma radiation, and then the OSL was measured at 20°C for 0.1 s. This stimulation was not long enough to significantly deplete the OSL trap populations. Subsequently, the sample was pulse-annealed in steps of 50°C in the range 50 to 350°C for 10 s, with the OSL each time monitored for 0.1 s at room temperature. During the thermal treatment between 50 and 150°C, the OSL decreases significantly and it can be deduced that a significant fraction of the initial OSL probably arises from low temperature TL traps. The TL curve in Fig. 7.1 does not show these, since the sample here was heated to 120°C prior to measurement. For thermal washing between 150 and 250°C, no significant change in the OSL trap population was observed, but for heating beyond 250°C, the OSL decreased rapidly. This indicates that an unstable OSL signal is present in a freshly irradiated porcelain sample and a proper preheat treatment is required for obtaining a time stable OSL signal suitable for dosimetry.

As might be expected, the time decay properties of the various OSL components are not the same. Fig. 7.2 shows OSL curves recorded at 20°C under constant broad band (420-550 nm) illumination at 16 mW/cm<sup>2</sup>. The remaining OSL component after thermal washing to 350°C has a very slow decay rate and the time decay is close to exponential over the time range measured. In contrast, the OSL component stable up to 150°C decays rapidly, such that within 10 s there is

no significant signal remaining. The OSL arising from the thermally-unstable low-temperature TL traps shows highly non-exponential decay characteristics, probably indicating that a range of defects are being excited with varying depths and/or optical capture cross-sections.

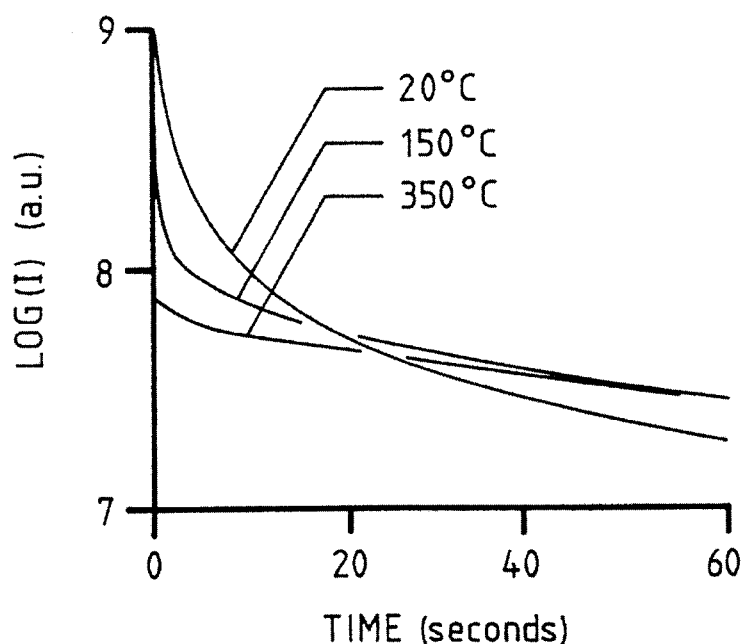


Fig. 7.2. Time decay characteristics of OSL in porcelain (sample 1P) following 5 Gy radiation dose and thermal washing at the temperatures indicated; the OSL excitation intensity was  $16 \text{ mW/cm}^2$  in a band 420-550 nm (from Poolton et al, 1995c).

To determine the relative dose sensitivities of the glazing and porcelain body a core from a toilet tank had its position resolved OSL signal measured across the entire section using the OSL scanner described in chapter 3. Fig. 7.3 shows the OSL signal observed when scanning an excitation beam through a complete cross section of the toilet tank top that had been exposed to a uniform  $^{60}\text{Co}$  gamma dose of 40 Gy (Bøtter-Jensen et al, 1995b). The cross section was 12 mm wide, and had a 0.7 mm glazing layers on each side. These layers are seen to be about eight times more sensitive than the porcelain. The OSL scanning method is further described in chapter 8.

### 7.3.2 OSL stimulation spectra from porcelain

The OSL stimulation spectra, i.e. OSL versus stimulation wavelength, for the Chernobyl toilet porcelain (sample no. 1P) and glazing (sample no. 1G) were obtained using the Risø scanning monochromator in the visible range with detection filter U-340. These spectra are shown in Fig. 7.4a. A prominent broad transition is observed peaking around 540 nm (particularly in the glazing material), together with a rising continuum at lower wavelengths. It should be noted that the occurrence of the 540 nm feature is unlikely to arise from quartz, where only structure-less excitation characteristics have been reported previously (Bøtter-Jensen et al, 1994b).

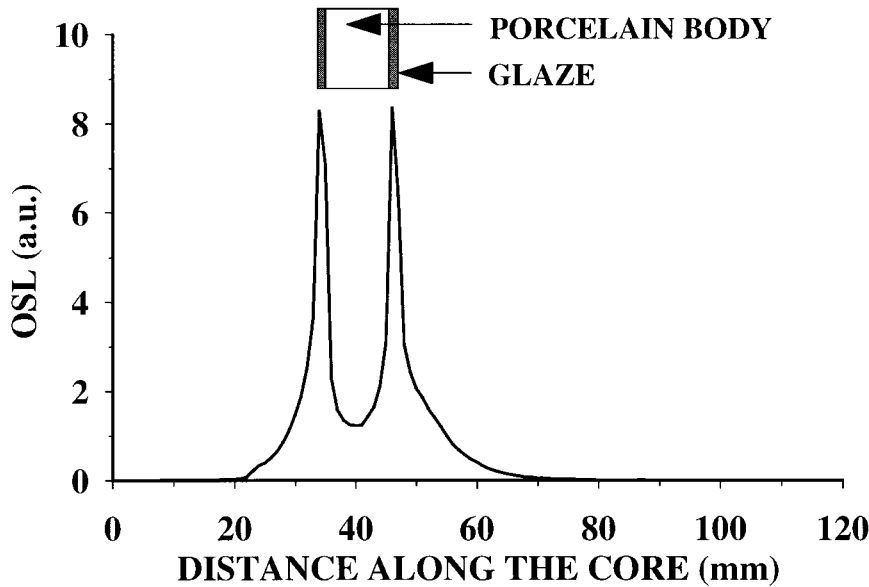


Fig. 7.3. A scanning profile (position resolved OSL signal) of the dose dependent OSL signals stimulated across a porcelain toilet tank (sample 1P). The highly dose sensitive layers on both sides are glazing (from Bøtter-Jensen et al, 1996).

An OSL excitation spectrum was also measured using another typical porcelain (sample no. 2P). This spectrum is shown in Fig. 7.4b and a similar smooth stimulation resonance was found peaking around 500 nm, well matched to the filtered halogen lamp producing a stimulation wavelength band from 420-550 nm. Similar excitation spectra were obtained from all the other porcelain samples investigated.

### 7.3.3 Time-steady PL emission spectra from porcelain

Bøtter-Jensen et al (1995) examined the emission characteristics of different porcelain samples by recording the time-steady photoluminescence (PL) emission spectra using the Risø monochromator. UV stimulation was provided by the halogen lamp, filtered with U-340 filters (peak transmission at 340 nm). Analyses of the spectral emission features of the crockery porcelain and glazes allow the possibility of identifying both the principle luminescent matrix, and the luminescent defects contained within it. The time-steady dose-independent PL emission spectra (excited by 340 nm light) were recorded for the crockery porcelain samples nos. 5P and 10P as shown in Fig. 7.5a. PL spectra were also obtained from two glazes (Fig. 7.5b) where sample 2G is a white glaze and sample 6G is a clear glaze.

To identify the structures seen in the PL spectra of porcelain TL spectra were obtained from two artificial phosphors namely calcium sulphate doped with dysprosium ( $\text{CaSO}_4:\text{Dy}$ ) and aluminium oxide doped with carbon ( $\text{Al}_2\text{O}_3:\text{C}$ ). These spectra are shown in Fig. 7.5c. The bright TL emission peak near 700 nm from  $\text{Al}_2\text{O}_3:\text{C}$  is consistent with the observations by Akselrod and Kortov (1990) and Kortov et al (1994) who identified this emission as an internal transition of  $\text{Cr}^{3+}$ , a very common impurity of this material. Typically, this gives

sition of  $\text{Cr}^{3+}$ , a very common impurity of this material. Typically, this gives rise to a main emission at 693 nm, with satellite lines at 670, 714 and 740 nm, at relative intensities depending on the dopant concentrations (Lapraz et al, 1991). The broad emission band from  $\text{Al}_2\text{O}_3:\text{C}$  peaking at 410 nm corresponds directly with the well known F-centre emission arising from the  $^3\text{P} \rightarrow ^1\text{S}$  transition (Lee and Crawford, 1979; Akselrod and Kortov, 1994). The TL spectra obtained from  $\text{CaSO}_4:\text{Dy}$  clearly shows the sharp emissions at 490 and 580 nm which represent the well known distinct blue-green and yellow emission signals caused by the  $\text{Dy}^{3+}$  dopant (e.g. McKeever et al, 1995).

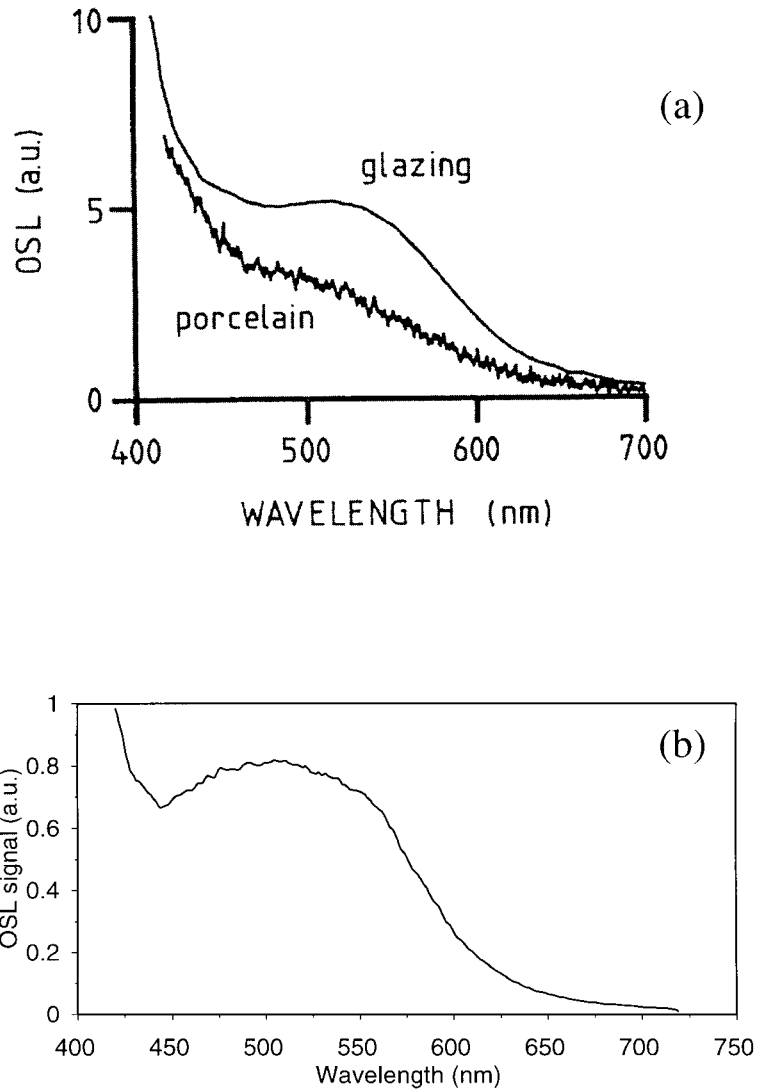


Fig. 7.4. (a) The dose dependent OSL excitation characteristics for the Chernobyl toilet tank (sample 1P).

(b) The OSL stimulation spectrum (OSL plotted against wavelength) for porcelain sample No. 2P (from Bøtter-Jensen et al, 1996)

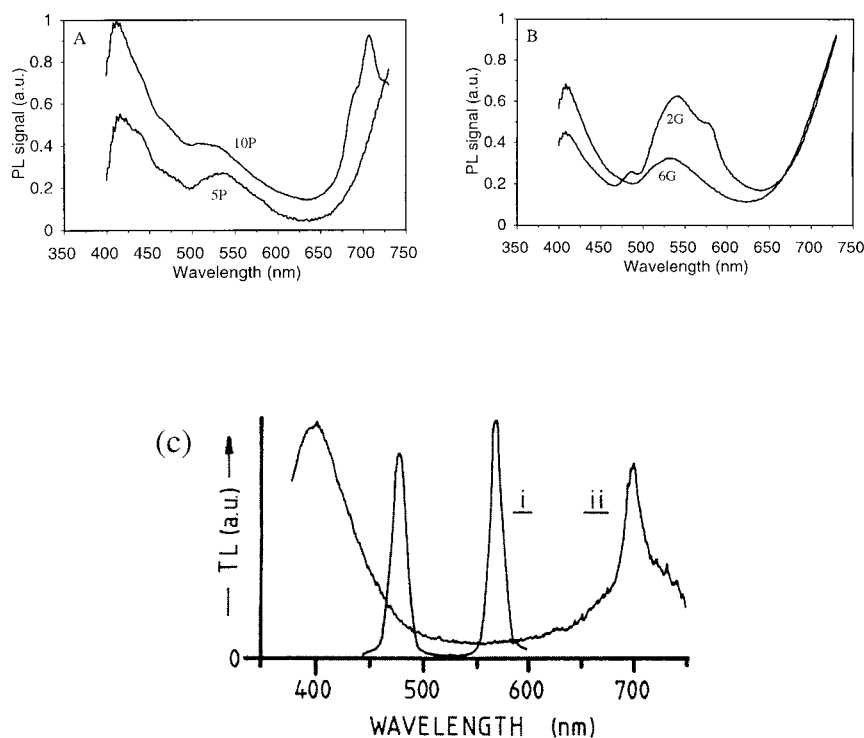


Fig. 7.5. (a) PL spectra (PL plotted against wavelength) for two bulk porcelain samples (Nos 5P, 10P). The emission from  $Al_2O_3$  is clearly demonstrated by the typical peaks at 410 and 700 nm. (From Bøtter-Jensen et al, 1996)

(b) PL spectra (PL plotted against wavelength) for two glazed samples. Sample 2G is a white glaze and clearly shows emissions from  $Al_2O_3$  and  $Dy^{3+}$ . Sample 6G is a clear glaze also showing emission from  $Al_2O_3$  (from Bøtter-Jensen et al, 1996).

(c) PL spectra from two artificial phosphors, namely (i)  $CaSO_4:Dy$  and (ii)  $Al_2O_3:C$ . The results indicate the similarity of the porcelain with that of  $Al_2O_3:C$ , with some  $Dy^{3+}$  impurities present.

From comparison with the TL spectrum of  $Al_2O_3:C$  (Fig. 7.5c) the PL spectra from the two crockery porcelain samples in Fig. 7.5a clearly show identical emissions at 410 and 700 nm and thus indicate that the principal luminescent matrix of bulk porcelain material is identified as being  $Al_2O_3$ . The PL spectra from the two glazes in Fig 7.5b clearly show peaks at 410, 490 and 580 that identify emissions from both  $Al_2O_3$  and  $Dy^{3+}$  (sample 2G) which is a white glaze and from  $Al_2O_3$  for sample 6G which is a clear glaze. Experts consulted from the Royal Danish Porcelain Company in Copenhagen confirmed that  $Al_2O_3$  is a frequently used component of bulk porcelain matrixes and both  $Al_2O_3$  and  $Dy^{3+}$  are components often included in glazes used as decorations and cover of crockery porcelain.

## 7.4 OSL Dose Response of Porcelain

Typical OSL decay curves for sample 2P that had been given  $^{60}\text{Co}$  gamma doses from 30 mGy to 2 Gy are shown in Fig. 7.6. As quartz and  $\text{Al}_2\text{O}_3$  were considered major components in the porcelain, a preheat of  $150^\circ\text{C}$  for 30 s was used to remove unstable components before any OSL readout in attempting to stabilise and reproduce the signal. The dose-response curves i.e. OSL versus  $^{60}\text{Co}$  gamma dose, are shown for three main porcelain samples (nos. 2P, 6P and 13P) in Fig. 7.7. It should be noted that the growth curves were made using the attached  $^{90}\text{Sr}$  beta source and each sample was subsequently individually calibrated against  $^{60}\text{Co}$  gamma radiation. In general, the OSL sensitivity of the glazed samples was found to be more than one order of magnitude higher than that of bulk porcelain, which is ascribed to the high content of  $\text{Al}_2\text{O}_3$  and  $\text{Dy}^{3+}$ . Unfortunately, the glazed samples will not be suitable for OSL dosimetry except in unusual circumstances, because the OSL signal from this material will, in most cases, be bleached by ambient light. This problem is investigated further in the next section. For most porcelain samples the OSL signal increases linearly from 10 mGy up to about 20 Gy and shows a further sub-linear increase up to at least 200 Gy. Green light allowed doses lower than 50 mGy to be measured with a statistical uncertainty of 10 % using the more sensitive fired porcelain samples (see Fig. 7.7b) and the lower detection level was determined to be about 10 mGy.

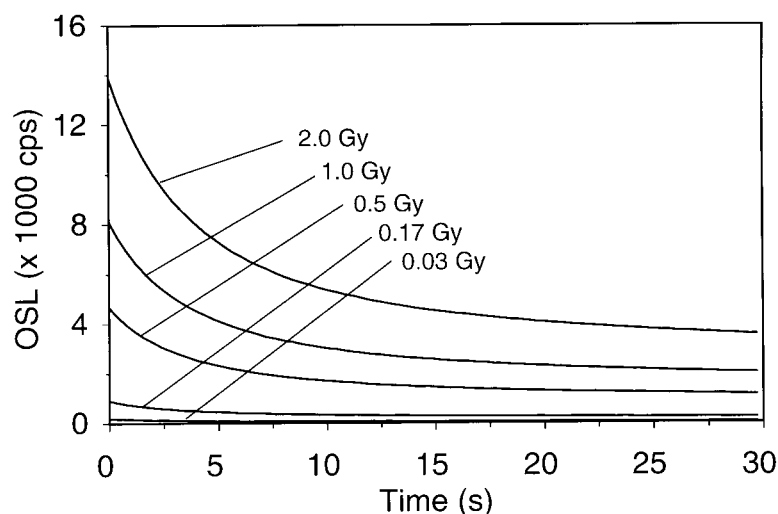


Fig. 7.6. Typical OSL decay curves for porcelain sample No 2P representing different doses from 30 mGy to 2 Gy  $^{60}\text{Co}$  radiation (from Bøtter-Jensen et al, 1996).

An important point in dosimetry is the long-term stability (fading) of the radiation induced OSL signal. The fading of a porcelain sample was examined over twenty days with successive OSL measurements of pre-irradiated samples every second day. The irradiated samples were stored at room temperature. The normalised plot of OSL against time was well represented by a horizontal line with a scatter of measurements of less than 2.5 % (1 SD). It is concluded that no fading could be detected over the storage period.

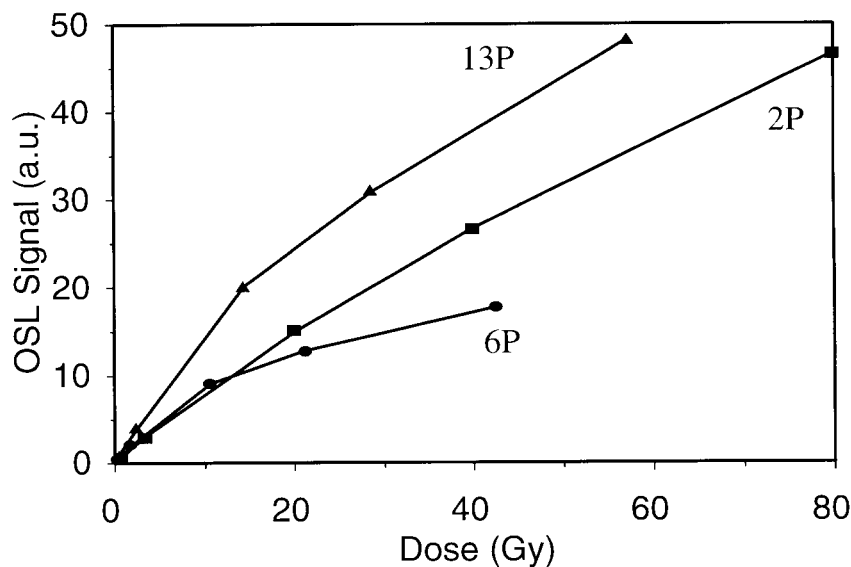
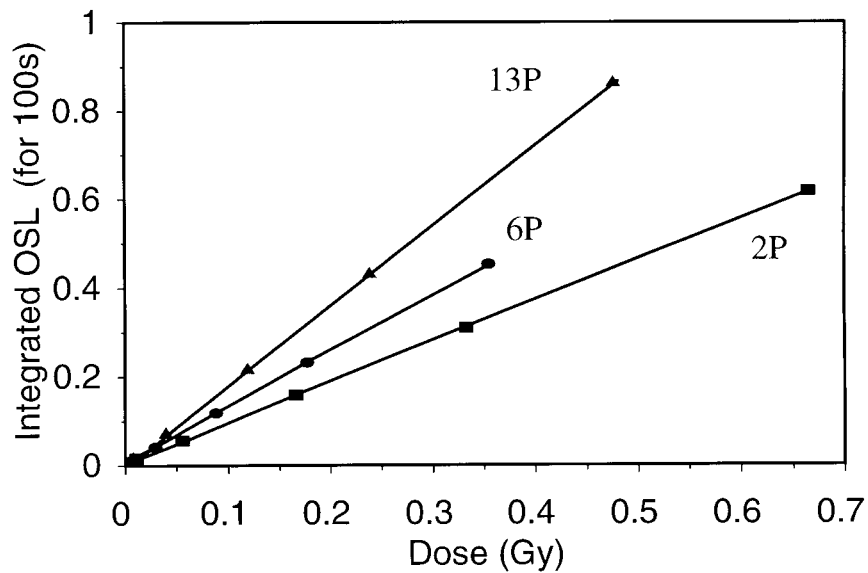


Fig. 7.7. OSL versus  $^{60}\text{Co}$  gamma dose for three different porcelain samples (Nos 2P, 6P and 13P). Note that beta dose exposures have been individually calibrated against  $^{60}\text{Co}$  gamma radiation for each sample (see text). (From Bøtter-Jensen et al, 1996).

## 7.5 Dose-Depth Profiles in Porcelain and the Effect of Transparency

A ceramic fuse (sample No 20P) collected from a nuclear accident contamination site in Russia had its “natural” OSL signals analysed to determine the depth-dose profile into the material. An 8 mm diameter and 12 mm long core was drilled across the fuse and sliced into 1 mm discs. The normalised OSL signals measured from the individual discs are shown in Fig. 7.8a. The curve shows a bleaching effect on the OSL signal in the outer layers of the material.

From approximately 2 mm depth a slightly decaying depth-dose profile can be seen indicating the incident direction of the irradiation.

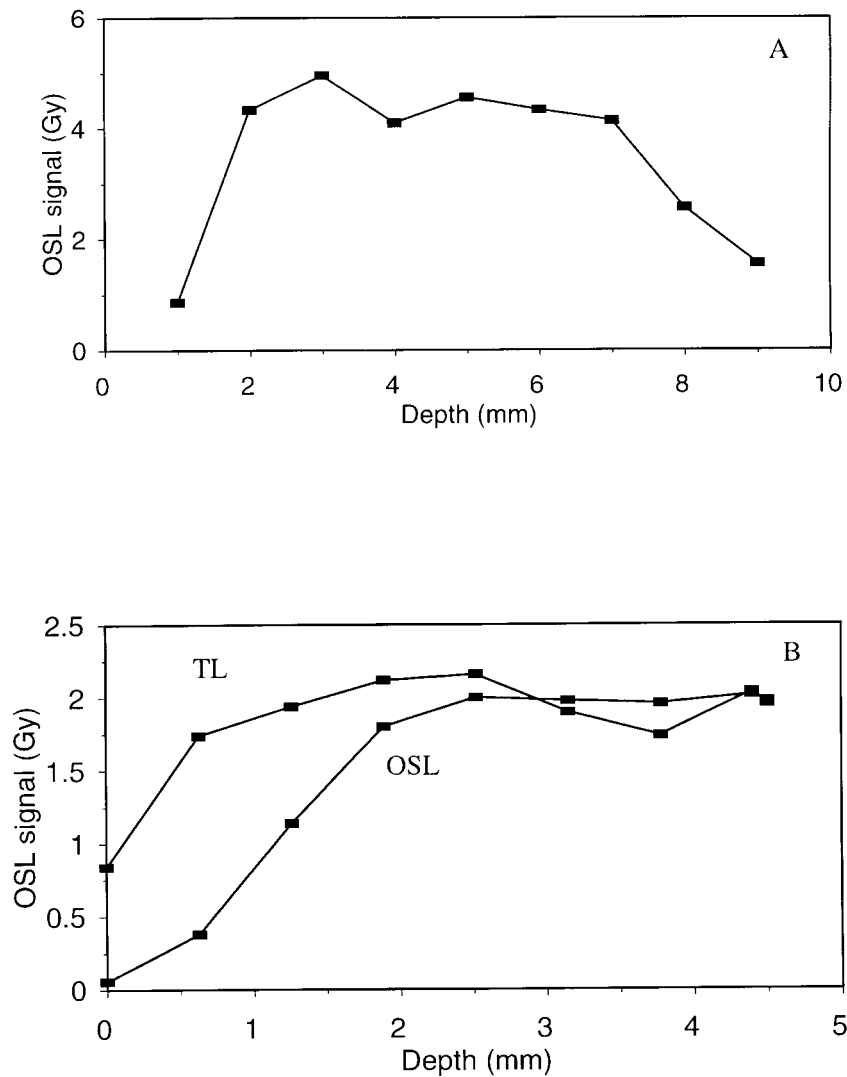


Fig. 7.8. (a) "Accident" OSL dose relative to depth into a ceramic fuse (sample No 20P). Procedure: slicing of cross section core into discs and subsequent measurement of individual OSL signals. (From Bøtter-Jensen et al, 1996).

(b) OSL and TL relative to depth into porcelain material (ceramic fuse, sample No 20P) after exposing a cross section core to 2 Gy  $^{137}\text{Cs}$  gamma radiation and subsequently placing the core in daylight for 8 hours such that only one end was illuminated (see text) (from Bøtter-Jensen et al, 1996).

In order to directly examine the transparency of porcelain and the consequent bleaching effect caused by ambient daylight, OSL measurements were made along a 12 mm long core drilled from the ceramic fuse. The core was given a uniform  $^{137}\text{Cs}$  gamma dose of 2 Gy at right angles to the long axis and subsequently placed in sunlight for 8 hours so that only one end of the core was illuminated. Discs (1 mm thick) sliced from the core had their OSL signals measured and the normalised OSL is plotted against the depth into the ceramic in

Fig. 7.8b. For comparison TL measurements were also made on the same discs and TL versus depth is plotted as well. It is clear that samples for both TL and OSL measurements must be taken at a depth of at least 2 mm in order to be unaffected by the bleaching ambient daylight. This suggests that thin porcelain items (crockery) are unsuitable in dosimetry applications, because the entire body of the material will be significantly affected by daylight exposure.

## 7.6 Conclusions - Porcelain

There is strong evidence that the most important dosimetric component of porcelain and glazing, measured using OSL techniques, is  $\text{Al}_2\text{O}_3$ . In some cases, the PL spectra suggested that the recombination centres were  $\text{Cr}^{3+}$ ,  $\text{Dy}^{3+}$  and F centres. Most of the porcelain samples included in the experiment gave rise to OSL signals that are dose dependent. Porcelain clearly has a great potential as an OSL dosimeter in retrospective dosimetry and we have demonstrated that most commonly used household porcelain ware, such as plates and cups, yield relatively high OSL signals per induced unit gamma radiation. Doses as low as 50 mGy in heated materials can be measured with good statistical uncertainty in most porcelain ceramics, provided the samples have not been exposed to light. Investigations on the light-induced bleaching caused by the transparency of the porcelain materials have shown that samples suitable for both TL and OSL measurements must be taken at a depth of at least 2 mm into the material. This precludes the use of most crockery, and it is concluded that large items such as sanitary ware and electric insulators are likely to provide the most suitable materials.

# 8 Retrospective Dosimetry

## 8.1 Introduction

In the event of a large-scale nuclear radiation accident, a quantitative assessment of the radiation dose to the general population requires the availability of suitable techniques and procedures for reconstruction of doses. Dose reconstruction can be defined as the process of estimating doses to the public from previous releases of radionuclides to the environment and dose reconstruction contributes to society in the following ways: 1) by helping to better understand the significance of past releases of contaminants to the environment, 2) when combined with epidemiology, dose reconstruction provides new information on the implications of risk associated with exposure to environmental radiation and 3) because these studies are leading the way in the designing and testing of measurement methodologies and mathematical models that predict the transport of radionuclides, these studies can thus be helpful in risk analysis and decision-making for decontamination of old sites, and evaluation of new sites.

The main purpose of dose reconstruction, or retrospective dosimetry, in relation to the local population after a nuclear accident, can be summarised as follows:

- to guide the provision of proper medical treatment and protection for people exposed to radiation,
- to provide input data for epidemiological studies,
- to provide information to the population,
- to help carry out research to improve methods and preparedness.

The methods used for dose reconstruction have been based on:

- 1) Dose modelling e.g. Monte Carlo simulations based on direct measurement results obtained from local active dose rate meters (GM counters etc.) (e.g. Meckbach and Chumak, 1996).
- 2) Application of luminescence methods with ceramics (TL and OSL) including modelling and photon transport calculations (e.g. Bailiff and Stepanenko, 1995).
- 3) Direct measurement of accumulated doses in human tissues using:
  - a) Electron Paramagnetic Resonance (EPR) on tooth enamel (e.g. Wieser et al, 1999).
  - b) Chromosome analysis of lymphocytes in blood. Fluorescence In Situ Hybridisation (FISH) painting methods (e.g. Lloyd et al, 1996).

Solid state dosimetry methods based on luminescence, including TL and OSL, and electron paramagnetic resonance (EPR) are particularly useful because they enable the integrated absorbed dose to be measured. In the case of external sources of radiation, materials found within the accident area can be used, e.g. bricks and tiles from buildings in the case of luminescence, and tooth enamel in the case of EPR. The absorbed dose may be evaluated many years after the accident. Consequently both EPR and luminescence have the potential to provide data essential for dose reconstruction in areas and locations where radiation monitoring measurements were not carried out. Haskell (1993a; 1993b) and Bailiff (1995; 1997) have recently reported the basis and operation of TL techniques and critical factors concerning their use.

In mid 1990s Risø suggested the application of OSL techniques to ceramics for the retrospective assessment of accident radiation doses. The following sections describe the development of these OSL techniques and analytical procedures at Risø, particularly for the measurement of doses from materials collected in the Chernobyl accidental area. Most work has been done on the determination of the accrued gamma doses using quartz extracts from bricks, and this is described in some detail.

## 8.2 Materials and Sampling

The types of ceramic generally found to be suitable for retrospective dosimetry include the following fired materials: brick, glazed and unglazed tiles, roof tiles, interior floor tiles, porcelain fittings (e.g. sanitary ware) and exterior fittings such as lamp holders and electrical power line insulators (see Fig. 8.1). These materials can usually be found in various locations, allowing an investigation of both nature of the external field and the degree of shielding within the interiors of buildings. Brick buildings offer the highest degree of flexibility in choice of samples because ceramic material is available at a range of depths within the wall. The composition and form of suitable material varies according to the geographical location and the nature of the building environment. Ceramic materials have so far proved to be the only candidates for measurement of doses at the 10 mGy level.

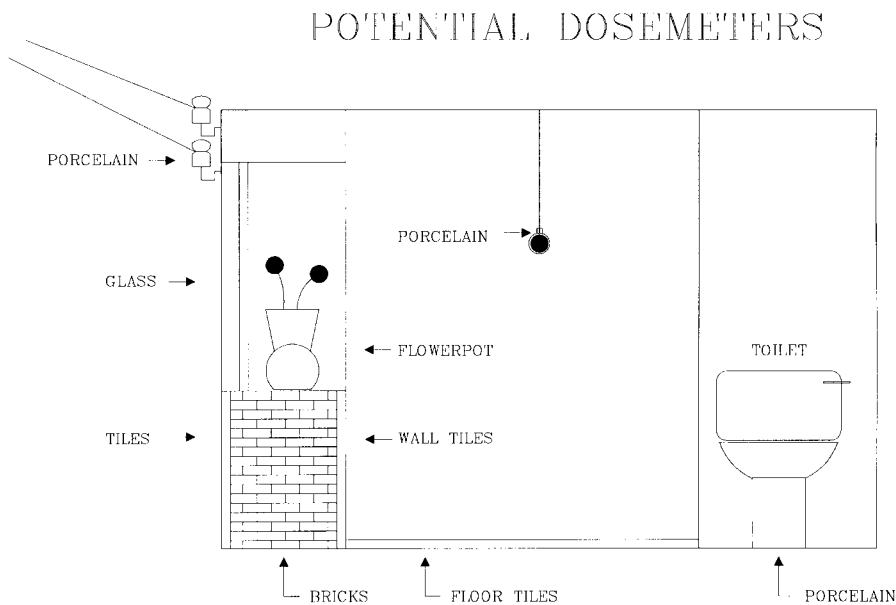


*Fig. 8.1. Schematic of a house showing ceramic materials potentially usable as doseimeters for retrospective dose evaluations.*

In most cases, bricks contain a high proportion of quartz and variable amounts of feldspar of 90-150  $\mu\text{m}$  grain diameter; the size range most suited to the use of the inclusion or coarse-grain technique. However, the quality of the bricks may vary significantly (as shown later) depending upon the manufacturing procedures used. Some manufacturers add roughly crushed quartzite to the clay and this can result in poor characteristics from point of view of dosimetry. A homogeneous distribution of quartz inclusions is essential when a depth-dose profile is to be measured (see section 8.6).

The selection of appropriate samples is one of the most important aspects of retrospective dosimetry. The interpretation and use of the results relies heavily on the assumptions made concerning the relationship between the sample and the radiation sources contributing to the transient dose. So far a comprehensive sampling methodology has yet to emerge. Wider use of the method is likely to accelerate the demand for standard procedures to be established so that the selection of appropriate samples for both accrued dose and dose rate evaluation according to the type of building and dosimetry problem can be optimised. On the basis of current developments, it is likely that computational modelling will be used to a greater extent in sample selection as a predictive tool to test consistency with calculation for given source inventories and source distributions; such an approach is being pursued in current EU sponsored Chernobyl-related studies on a building-to-building basis (e.g. Bailiff and Stepanenko, 1996).

When sampling in the field there is a need to both record and take into account the immediate environment of the ceramic selected, not only because this is a source of natural radiation contributing to the background dose, but also because it provides a potential source of back-scattered radiation, depending on the configuration and composition of the structure from which the sample has been extracted, e.g. tiles fastened to a concrete wall. A variety of ceramic sample extraction procedures are in use – most using basic hammer and chisel or drilling techniques depending on whether an electricity supply is available.

Table 8.1 summarises the basic minerals and materials suitable for OSL measurements (this summary is based on work described later). Potential OSL dosimeters collected in nuclear accident areas are preferably parts of, or items from the buildings which accommodated the local population at the time of the accident. Fixtures (brick, tiles, insulators etc.) are generally to be preferred to moveable materials (flower pots, crockery) because both their natural dose rate, and their relationship to the accident exposure and exposed inhabitants are better known.

*Table 8.1. Materials suitable for OSL measurements, and appropriate stimulation light sources*

Material	OSL Method
<u>Natural:</u>	
Extracted quartz	VLSL
Extracted feldspar	IRSL (+ VLSL)
<u>Ceramics:</u>	
Porcelain	VLSL
Raw brick material	VLSL (+ IRSL)
<u>Artificial:</u>	
Al <sub>2</sub> O <sub>3</sub> :C	VLSL

VLSL = Visible-Light (blue-green) Stimulated Luminescence  
 IRSL = Infra-Red Stimulated Luminescence

As part of the joint EU IVth framework project “Dose Reconstruction” representatives from different participating laboratories (including Risø) took part in field trips to the nuclear accident areas in Russia and Ukraine (Chernobyl) where they collected materials that could be used as potential dosimeters for reconstruction of the transient gamma doses received by the population. House bricks taken from standing buildings were the most common type of sample collected for luminescence measurements as these contain both quartz and feldspar. However, porcelain samples were also recovered.

### 8.3 Sample Preparation and Experimental Details

To estimate the dose in mineral grains a sample must be extracted without exposure to light to avoid any bleaching of the luminescence signal. In the laboratory the samples are handled in dim red or orange light (similar to that in a photographic darkroom). Any outer bulk material that may have been exposed to daylight must be removed; this may be kept as reserve for dose-rate determinations and particle size analysis. Bricks were sliced into 10 mm sections and these were crushed and sand sized grains (90-180 µm) extracted by sieving and treated with HCl. Quartz grains were then concentrated by heavy-liquid separation using sodium polytungstate (2.62-2.65 g/cm<sup>3</sup>). These were then etched in 40% HF to remove any residual feldspars. Acid-soluble fluorides were subsequently removed in 15% HCl. If only quartz is to be measured, satisfactory results can be obtained without heavy liquid separation; the selected particle size range is treated with HCl and H<sub>2</sub>O<sub>2</sub>, and then placed directly in concentrated

HF. An automated Risø TL/OSL reader, model Risø TL/OSL-DA-15, was used for the OSL measurements (see chapter 3). The extracted quartz samples were stimulated using either broad band blue-green stimulation light (420-550 nm) filtered from a halogen lamp delivering 28 mW/cm<sup>2</sup> to the sample or blue LED stimulation (470 nm) delivering 22 mW/cm<sup>2</sup> to the sample (see chapter 3). Detection filters were in all cases 6 mm Hoya U-340. The quartz extracts were irradiated using a 185 MBq <sup>90</sup>Sr source delivering a dose rate of 8.2 mGy/s to the sample. The measurement sequences were performed using the Risø MiniSys sequence editor (see chapter 3).

## 8.4 Determining the Transient Accidental Dose

### 8.4.1 Estimation of the dose rate

The dose rate absorbed by a mineral grain is a function of the radioactivity both in the grain and in the surrounding media. For quartz the internal dose rate, derived from within the grain, is usually very small (Aitken, 1985). The external dose rate depends mainly on the concentrations of <sup>40</sup>K and <sup>238</sup>U and <sup>232</sup>Th series radionuclides in the surrounding media, and a component derived from cosmic rays. The water content of the media may affect the dose derived from the natural radioactivity surrounding the grain, by absorbing some energy, and thus decreasing the dose rate to the mineral grain. Consequently, to determine the dose rate, it is necessary to measure the radionuclide concentrations in the surrounding media. These calculations are summarised by Aitken (1985; 1998).

The dose received by quartz grains from natural radionuclides within the brick material can be as much as 5 mGy/year. The background dose can thus make up a considerable part of the total dose, particularly if bricks are collected from older buildings. As the background component is a major component of error in estimating the accrued accident dose it is important that this background component be minimised, and accurately determined. The annual dose rate resulting from internal emitters can be determined in different ways e.g. by gamma spectrometry (for details see Murray et al, 1987) and beta counting (Bøtter-Jensen and Mejdahl, 1985; 1988). Sensitive artificial TL/OSL phosphors such as Al<sub>2</sub>O<sub>3</sub>:C (Akselrod et al, 1990) have also been used to perform in-situ measurements of the integrated gamma doses over short periods without the need to correct for differences in mass absorption characteristics at low photon energies (Bøtter-Jensen et al, 1997; Bøtter-Jensen et al, 1999c). The assessment of the environmental dose rate using Al<sub>2</sub>O<sub>3</sub>:C and quartz together with further experimental results are discussed in detail in section 8.6.

The cosmic-ray contribution is calculated from relationships given by Prescott and Stephan (1982), and Prescott and Hutton (1988). The thickness of overlying material, and the latitude and longitude are required for these calculations. Having measured the radionuclide concentrations in the surrounding media, and calculated the cosmic ray contribution the total dose rate is calculated using the conversion factors of Olley et al (1996). Allowance must also be made for the finite dimensions of the brick wall; this is discussed further in section 8.6.3.

### 8.4.2 Estimation of the equivalent dose

The radiation energy stored within a grain as trapped electrons is usually measured by comparison with the energy stored in the same material after it has been exposed to the calibrated beta source in the laboratory. The source is calibrated

in terms of the energy delivered to the grain per unit time and thus the dose rate is expressed as:

$$\text{Gy/s} = (\text{J/kg/s})$$

Only a very small fraction of this energy is stored in the electron traps discussed above; the rest is dissipated as heat.

If the response of the material was independent of its history, then the simplest method of determining  $D_e$  would be to measure the luminescence signal arising from the natural dose, give the sample a known dose in the laboratory, and measure the luminescence response to this dose. The natural dose would then be given by proportion. However, this is very rarely possible, and various different methods have evolved to overcome the dependence of the dose on the history of the sample.

Analytical protocols to determine  $D_e$  in the mineral grains fall into two broad categories: multiple-aliquot and single-aliquot. These protocols are discussed further in section 8.5.

#### 8.4.3 Estimation of the transient accidental dose

The total absorbed equivalent dose ( $D_e$ ) is the dose absorbed by the mineral inclusions in the ceramics (e.g. quartz and feldspar) and is built up of two components: (i) the background dose accrued since the manufacture of the ceramics (brick) due to naturally occurring radioactive isotopes in the surrounding media and (ii) the transient dose due to sources introduced to the local environment by the radiation accident. The transient dose is the difference between the total equivalent dose ( $D_e$ ) delivered to the minerals (evaluated by luminescence measurements) and the accrued natural background dose. Thus the total dose  $D_e$  is expressed as:

$$D_e = D_x + A(D_\alpha + D_\beta + D_\gamma + D_c)$$

where  $D_x$  is the cumulative transient gamma dose observed by the ceramics due to the accident,  $A$  is the time since manufacture of the sample in years;  $D_\alpha$ ,  $D_\beta$ ,  $D_\gamma$  and  $D_c$  are the effective annual alpha, beta, gamma and cosmic ray doses, respectively, due to natural sources of radioactivity. Evaluations of  $D_x$  for quartz inclusions in ceramics can be related to dose in air at an external reference location by use of conversion factors that are derived from computational modelling (Bailiff and Stepanenko, 1996).

A large part of the luminescence work performed within the IIIrd and IVth EU framework programmes has been concerned with dose evaluations in bricks. This is largely due to the predominance of that material at the sites studied so far. Further details are reviewed by Bøtter-Jensen (1995), Bøtter-Jensen (1996), Bailiff (1997) and Bøtter-Jensen and Jungner (1999).

## 8.5 Development of Analytical Protocols

### 8.5.1 Introduction

All the measurement protocols used in accident dosimetry are based on protocols developed for dating archaeological materials (pottery, heated stones etc.) and geological sediments. Until recently, evaluation of the equivalent dose ( $D_e$ )

using OSL is usually undertaken using multiple-aliquot protocols either the additive-dose or the regenerative-dose protocols developed earlier for TL (reviewed by Wintle (1997)). These methods require many tens of sub-samples for a single estimation of  $D_e$ . A single-aliquot additive-dose protocol has been developed for feldspar (Duller, 1995), and more recently regenerative-dose single-aliquot protocols have been developed for quartz (Mejdahl and Bøtter-Jensen, 1994, 1997; Murray and Mejdahl, 1999; Murray and Roberts, 1998). In the latter, the OSL is first measured, and in the process the light sensitive traps are emptied. A regeneration dose is then given, approximately equal to the natural dose, and the OSL is measured again. Unfortunately, there is usually a significant sensitivity change in such a cycle of measurements, especially if the sample is heated between dosing and measurement, and this prevented the application of this very simple approach in the past.

### 8.5.2 Multiple-aliquot protocols

One of the earliest measurement protocols to be developed was the multiple-aliquot additive-dose protocol. In its simplest form this approach requires a minimum of two (in practice more, perhaps as many as 100) sub-samples (or aliquots) of identical characteristics. One sample is given a laboratory dose in addition to the natural dose, and the luminescence signal (TL or OSL) of both is measured. The two signals are plotted against laboratory dose, and the equivalent dose determined by extrapolation.

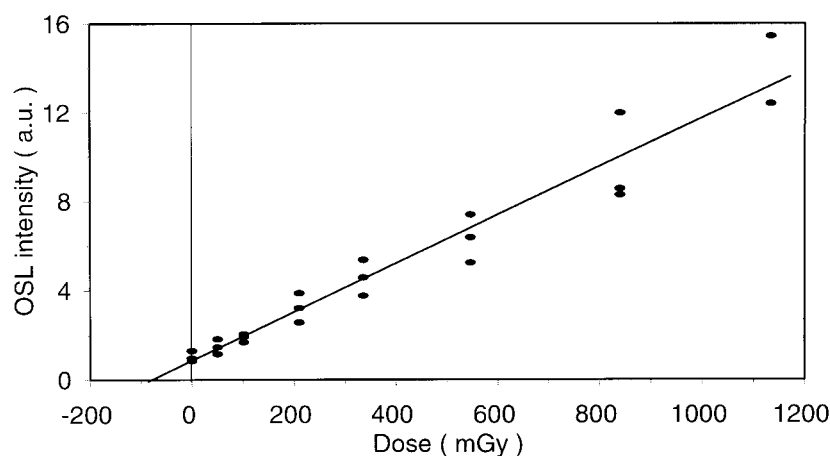


*Fig. 8.2. Typical multiple-aliquot additive-dose growth curve obtained from extracted brick quartz. Aliquots were each about 4 mg, and were normalised using the OSL signal from a brief stimulation of all aliquots, prior to addition of any laboratory doses. The solid line is best linear fit. The intercept gives the estimate of a  $D_e$  of 98 mGy.*

Fig. 8.2 illustrates this procedure with a practical example, which uses 21 aliquots of 90-125  $\mu\text{m}$  quartz grains extracted from a Chernobyl brick, and 6 different laboratory doses. Each aliquot weighed about 4 mg. Because of the extrapolation, the actual value of  $D_e$  will clearly depend on the algebraic relationship used to fit the data. In the example shown in Fig. 8.2, a linear fit was used. The OSL signals are moderately reproducible, and the predicted uncertainty on the estimated  $D_e$  is about 10 %. The multiple-aliquot additive-dose protocol gets

its name from the fact that many aliquots are needed, and because laboratory doses are added on to the natural dose, to generate that portion of the dose-response curve, or growth curve, which lies above the natural dose. Table 8.2 lists typical  $D_e$  results obtained in the dose range 65 – 160 mGy from a variety of extracted brick quartz samples using the multiple-aliquot additive-dose method. Broad band (420-550 nm) stimulation was used in all cases. The samples were taken at different depths across the brick section to be able to determine the dose-depth relationship (see section 8.6). An average precision of 5.3 % was obtained over this dose range.

*Table 8.2. Equivalent dose results obtained using the OSL multiple-aliquot additive-dose protocol on extracted brick quartz samples at the 100 mGy level. Each sample weighed approximately 4 mg and broad-band (420-550 nm) stimulation was applied. The average precision obtained is 5.3 %.*

Sample	Depth (mm)	Equivalent dose (mGy)	SE (%)
CH-1	10	158.5 ± 7.0	4.4
-	35	111.8 ± 5.7	5.1
-	65	97.7 ± 3.2	3.3
-	80	88.6 ± 4.3	4.9
-	100	65.6 ± 3.3	5.1
CH-2	10	125.7 ± 7.5	6.0
-	35	80.7 ± 4.6	5.7
-	65	77.5 ± 4.7	6.1
-	80	74.1 ± 4.3	5.8
-	100	80.8 ± 5.2	6.4

### 8.5.3 The Single Aliquot Regeneration Added Dose (SARA) protocol

The single aliquot regeneration and added dose (SARA) method introduced by Mejdahl and Bøtter-Jensen (1994; 1997) is based on repeated measurement on each aliquot and has the advantages of: (1) a small sample, (2) high precision and (3) no need for normalisation.

Duller applied single aliquot measurements with both regeneration and added dose procedures, but abandoned regeneration because of the sensitivity changes found as a result of the reuse of aliquots. Sensitivity changes associated with regeneration have been further studied in detail by Li and Wintle (1992), Jungner and Bøtter-Jensen (1993), McKeever et al (1997a) and Murray and Mejdahl, (1999).

The SARA method requires a minimum of two aliquots and thus is not a truly single aliquot method. The procedure can be summarised as follows (see Fig. 8.3a): (1) add beta doses ( $B_0, B_1, B_2, B_3$ ) to aliquots containing their natural dose; (2) carry out single aliquot regeneration measurements (exposure time 50 s) on these aliquots to obtain doses ( $D_0, D_1, D_2, D_3$ ); (3) plot these doses as a function of the known added doses ( $B_0, B_1, B_2, B_3$ ); and (4) extrapolate the regression line through the points to intercept the added dose axis to obtain the intercept I. The intercept will then represent the true equivalent dose (ED) irrespective of any sensitivity change introduced during the regeneration procedure.

There is one important restriction: the sensitivity change must be the same for the doses  $D_0$ - $D_3$  independent of the beta doses added initially. A simple procedure for testing this is as follows (see Fig. 8.3a)

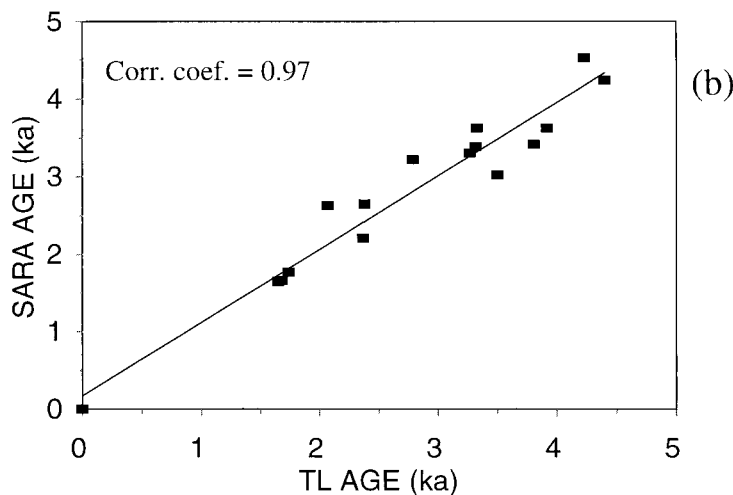
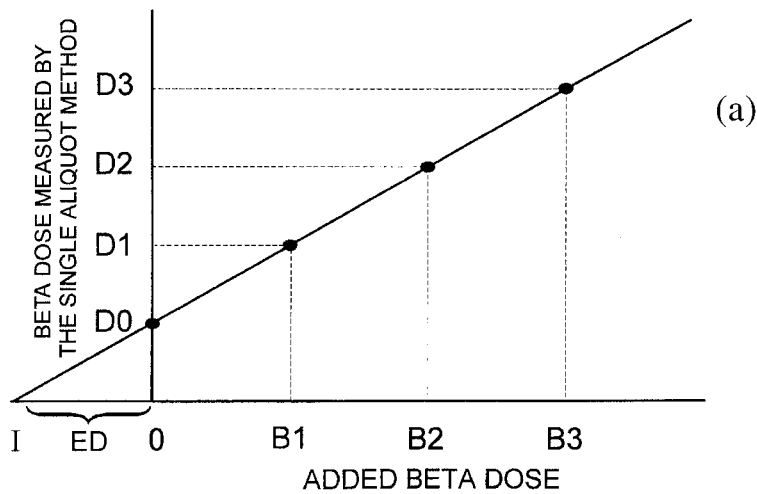


Fig. 8.3. (a) Principle of the SARA method, schematically. The figure illustrates the doses determined by regeneration versus the added doses.

(b) SARA age plotted as function of TL (added dose) ages for 14 heated quartz and K-feldspar samples extracted from ceramics and burnt stones (from Mejdahl and Bøtter-Jensen, 1997).

From the two triangles  $O_0, D_0, I$  and  $I, B_3, D_3$  one can deduce that a condition for the sensitivity change being independent of the added dose is given by the following expression:

$$D_0/ED = D_3/(ED + B_3)$$

The test can be illustrated for a representative heated K-feldspar sample where  $D_0/ED = 0.876$  and  $D_3/(ED + B_3) = 0.870$  (from Mejdahl and Bøtter-Jensen, 1997). These are almost identical, with the difference being around 1 %; the maximum added dose was 8 Gy. A further requirement is that the regression coefficient in the added dose plot should be very close to one and this is nearly always the case. For the measurement discussed above it was 0.999. This test is carried out routinely for all samples and, for the majority of measurements, the two expressions are almost identical. If the difference is larger than 3 %, the measurement is not used.

Initial measurements were carried out using IRSL (880 nm) from feldspars and broad-band (420-550 nm) OSL from both quartz and feldspars. The preheat procedures adopted for IRSL and broad-band OSL are: (1) after irradiation and prior to OSL, preheat all samples to 220°C for 40 s; (2) after cooling, carry out the OSL measurement; (3) before next irradiation, preheat all samples to 220°C for 40 s; (4) next irradiation followed by preheat, and so on.

This “dual preheat” procedure appeared to be the best treatment for obtaining optimal reproducibility (Murray, 1996). It has the effect that the charges in the low-temperature traps from charge transfer during the OSL measurement are removed so that trapping conditions during irradiation remain the same (McKeever et al, 1997a)

Three regeneration doses were usually used to determine each value of  $D_e$ ; these were adjusted so that the “natural” signal fell within the signal interval determined by the regeneration doses. This is necessary because the regeneration growth curves are not always linear. By repeating the measurements, the dose interval can be narrowed so that the interpolation errors are negligible. The SARA method has been extensively used with fired (archaeological) materials, ceramics, bricks and burnt stones which are relevant to retrospective dosimetry. For burnt stones the SARA OSL method was used almost exclusively because this method can be applied to the quartz fraction whereas it was found that TL cannot be used on quartz from burnt stones because of large uncertainties (Mejdahl, 1997). TL can be used for the feldspar fraction, but as discussed in chapter 5 feldspar often suffers from a large anomalous fading. A comprehensive intercomparison of TL and SARA OSL measurement results is shown in Fig. 8.3b for 15 heated (archaeological) quartz and feldspar samples. These were extracted from burnt stones and bricks. Taken as a whole, rather good agreement between the SARA and the TL results for these heated samples was found with a correlation coefficient of 0.97.

Mejdahl and Bøtter-Jensen (1994; 1997) applied their OSL SARA protocol to both heated and non-heated quartz and feldspar samples and Murray (1996) used it on sedimentary quartz. He showed that the growth curve ( $D$  against  $\beta$ ) will be linear, even in the presence of some non-linearity in the OSL dose response curve. Because SARA is a regeneration-based protocol, no inter-aliquot normalisation is necessary, and the precision of  $D_e$  estimates obtained using only a few aliquots (typically 9) was a significant improvement over the earlier multiple-aliquot methods. For well heated or well bleached quartz and feldspar samples the SARA method was rapidly adopted as the standard OSL protocol at the Nordic Laboratory for Luminescence Dating (Mejdahl and Bøtter-Jensen, 1997).

Much higher precision can be obtained using the SARA protocol compared with the multiple-aliquot additive-dose method. Therefore, the OSL SARA protocol was applied intensively to the measurement of equivalent doses ( $D_e$ ) from quartz extracted from Chernobyl bricks. Table 8.3 presents some typical SARA results obtained at the 100 mGy level from such brick samples. The quartz samples were taken across a brick section (No. CH-95) at 10 mm intervals. An av-

erage precision of 3.2 % was obtained using the SARA method at this dose level.

*Table 8.3. Typical  $D_e$  results measured from extracted brick quartz (sample No. CH-95) using the SARA method. The average precision obtained is 3.2 %.*

Depth (mm)	SARA $D_e$ (mGy)	SE (%)
10	123 ± 2.2	1.8
20	109 ± 3.2	2.9
40	114 ± 3.9	3.4
60	116 ± 3.8	3.3
80	113 ± 4.5	3.9
90	115 ± 4.9	4.3
100	112 ± 3.5	3.1

#### 8.5.4 Automated iterative SARA method

The initial SARA method suffered from the problem that it implicitly assumed that the operator had some prior notion of the equivalent dose ( $D_e$ ) level of the material being studied. To overcome this problem an automated version of the SARA procedure was developed in collaboration with Duller. This procedure is able to automatically adjust the radiation dose levels that are administered to the sample (Duller et al, 1999c). An initial value for the first radiation dose is entered, and then the algorithm adjusts this value within a suite of analyses until the induced OSL falls appropriately close to the initial light level.

Only one single regeneration measurement is used on each aliquot in order to eliminate the risk of non-uniform sensitivity changes during different regeneration cycles. The iterative procedure uses each measurement of the natural to regenerative luminescence signal ratio for each aliquot to make an improved estimate of  $D_e$  for the next aliquot. This improved estimate is used in turn to adjust the next regeneration dose to improve the matching of light levels.

A series of fired (archaeological) quartz samples was selected for the evaluation of the individual  $D_e$  using the automated SARA method with the threshold for matching light levels set to 5%. All the samples had their  $D_e$  measured previously using the standard SARA method. The samples were preheated at 220°C for 40 s, and had their GLSL signals measured at room temperature for 50 s. In the standard method, three regeneration cycles were performed on each aliquot in order to match the light levels and to determine a  $D_e$ . The samples were re-measured using the automated SARA protocol and the results are plotted in Fig. 8.4. Generally good agreement was obtained, with only one outlier.

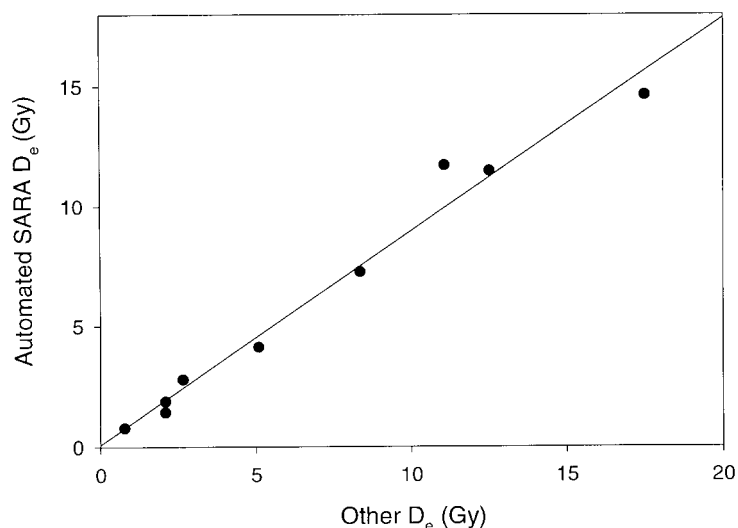


Fig. 8.4. A comparison of equivalent doses obtained using the automated SARA procedure, with those obtained previously for the same samples using other methods (from Duller et al, 1999c).

### 8.5.5 True single aliquot protocols

#### (i) Introduction

The advantages of single aliquot procedures over multiple aliquot techniques are: 1) improved precision, 2) they allow studies of the dose distribution within a sample, 3) rapid measurement, 4) no need for normalisation, 5) no correction for supra-linearity (in the case of regeneration protocols) and 6) less sample is needed.

Single-aliquot protocols allow all measurements required for the estimation of  $D_e$  to be made on one sub-sample (or aliquot). There has been rapid development in this area, with additive dose protocols receiving attention first (Duller, 1991; Galloway, 1996; Murray et al, 1997). More recently, regenerative-dose single-aliquot protocols have been developed for quartz (summarised by Murray and Wintle, 1999). These methods are conceptually the simplest - the OSL is first measured, and in the process the light sensitive traps are emptied. A regeneration dose is then given, approximately equal to the natural dose, and the OSL is measured again. If there has been no change in sensitivity, then  $D_e$  is given by the ratio of the two OSL signals, multiplied by the known laboratory dose. As was discussed above, in practice there is usually a significant sensitivity change, especially if the sample is heated between dosing and measurement. However, recent work has shown that a precise correction for sensitivity can be made, based on the OSL signal from a test dose given immediately after the natural or regenerated OSL measurement. In this case there is no heat treatment between dosing and measurement (other than a fixed heat to 160°C to empty the 110°C TL trap). It has been shown (Murray and Mejdahl, 1999; Murray and Wintle, 1999) that the OSL from the test dose provides a signal that is proportional to the luminescence sensitivity relevant to the preceding natural or laboratory induced OSL signal. Thus dividing the latter by the test dose OSL removes the effects of any changes in sensitivity.

The single-aliquot regenerative-dose (SAR) protocol was applied to estimate the equivalent dose of brick quartz extracts (Banerjee et al, 1999a; Banerjee et

al, 1999b; Bøtter-Jensen et al, 1999c). The SAR protocol was also used to evaluate the  $D_e$  for young bricks of known age ( $\ll 100$  years).

*(ii) Procedures and samples*

The samples used were taken from whole bricks collected from various buildings from the Chernobyl nuclear accident regions in the Ukraine and Russia and bricks collected from the vicinity of Roskilde, Denmark. The Danish bricks, Rosk-1 and Rosk-2, were taken from buildings known to be 37 and 72 years old, respectively. Quartz samples were extracted from all the brick samples according to the procedures described in section 8.3, and the OSL measurements were carried out using an automated Risø TL/OSL apparatus equipped with either a blue LED stimulation unit or a broad-band blue-green halogen lamp stimulation unit as described in chapter 3.

*(iii) Variation of OSL signal with preheat*

In a previous study aimed at determining the effect of preheating on the OSL signal of porcelain and brick quartz, Godfrey Smith and Haskell (1993) observed very small sensitivity changes with preheats of 180°C and 200°C. Jungner and Bøtter-Jensen (1994) found that in regeneration experiments using quartz an increase in the sensitivity was observed in the temperature interval 200 to 250°C. Above this temperature the sensitivity remained relatively constant. Keeping the quartz sample at an elevated temperature of 120°C during OSL measurements, to keep the trap associated with the 110°C TL peak empty, had no effect on the sensitivity change. Wintle and Murray (1999) found significant sensitivity changes in both the natural and regenerated OSL signals from a sedimentary quartz, after heating to various temperatures above 160°C for 10 s.

The dependence of the initial natural and regenerated OSL signal on preheat temperature was investigated for a young fired natural quartz, using sample 1/9-2 ( $D_e \sim 690$  mGy). A single aliquot was first stimulated at 125°C for 0.1 s for normalisation. A reduced stimulation power was used during all 0.1 s stimulations in this section, to ensure negligible depletion of the OSL signal by stimulation. A test dose of about 8 mGy was then given to the aliquot, followed by a preheat to 140°C and stimulation for 0.1 s at 125°C. This cycle was repeated a further 18 times, with the preheat temperature increasing by 20°C each time. During each preheat, the 110°C TL peak was measured.

A second aliquot was also stimulated at 125°C for 0.1 s for normalisation, then bleached for 360 s at 125°C and given a regeneration dose of 690 mGy ( $\sim D_e$ ). It was heated to 160°C to empty the 110°C TL trap, and then treated in the same manner as the natural aliquot. A third aliquot was also stimulated for 0.1 s at 125°C for normalisation, heated to 500°C, and given a regeneration dose of 690 mGy. It was then heated to 160°C, and subsequently treated in the same manner as the natural aliquot. Fig. 8.5a shows the variation in OSL signal with preheat temperature, and Fig. 8.5b shows the corresponding variation in the 110°C TL peak area. All data have been normalised to 1 for the initial natural OSL. Following the results of Wintle and Murray (1998) and Murray and Roberts (1998) it is assumed that the change in the 110°C TL sensitivity, as measured by the test dose response shown in Fig. 8.5b, also applies to the OSL data. This assumption is supported by the results shown in the next section.

The temperature dependence of the natural, bleached and regenerated signals are similar to each other in this sample. Thus it is deduced that it should be possible to use an additive-dose protocol with these samples, with any preheat in the range 160 to 280°C. The single aliquot regenerative dose protocol discussed in the following sections does not require such an agreement between the natural and regenerated response to preheating.

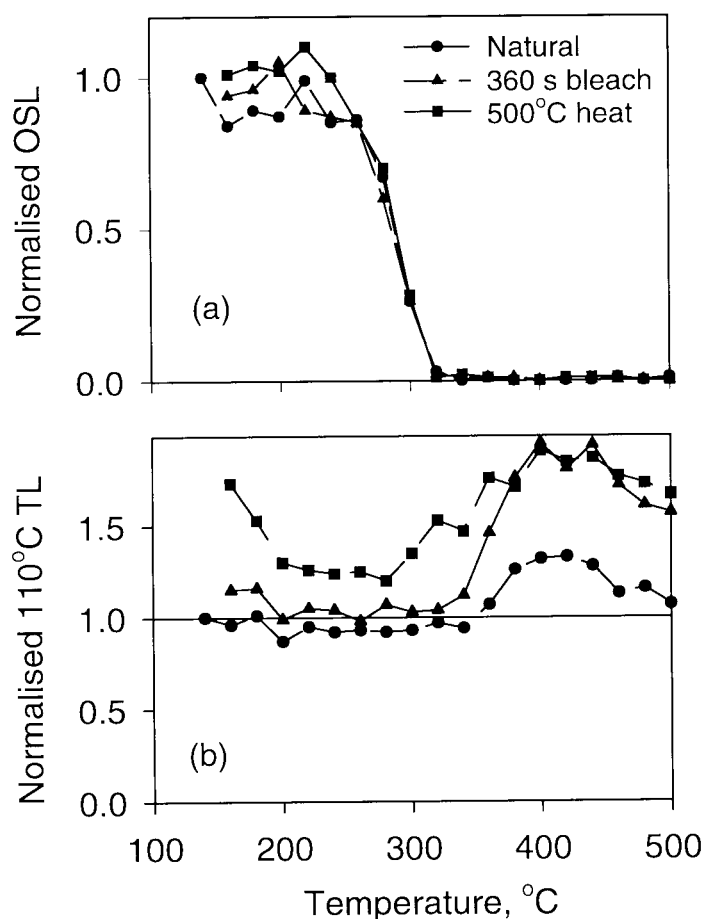


Fig. 8.5. (a) Variation of OSL with preheat temperature. The circles are derived from a natural aliquot which had been given a test dose of 8 mGy before each preheating to increasingly higher temperatures (140 to 500°C); each preheat was followed by 0.1 s stimulation at 125°C. A second aliquot was bleached for 360 s at 125°C and given a regeneration dose of 690 mGy. It was heated to 160°C to empty the 110°C TL trap and then treated as before (data shown as triangles). A third aliquot was heated to 500°C and then given a regeneration dose of 690 mGy; this aliquot was treated in the same way as the natural aliquot (data shown as squares). All three OSL data sets were normalised using the OSL signal observed from a 0.1 s stimulation (with low power) before any treatment.

(b) The 110°C TL peak area (observed during preheating) plotted against temperature for the three aliquots, using the same symbols as above. The peak areas have been normalised with respect to each other, with the TL intensity of the natural aliquot after the 140°C preheat being fixed at unity. (From Banerjee et al, 1999b).

(iv) Choice of OSL signal

Murray and Wintle (1997) discussed which part of the OSL decay curve should be used in dose estimation. Banerjee et al (1999b) were more concerned with the signal-to-noise ratio since at Risø we wish to measure precise measurements of small doses of the order of few mGy. The measurement procedure is based on the subtraction of an underlying background taken as the signal observed at

the end of the stimulation period. Banerjee et al (1999b) found that for both dim and bright signals the smallest statistical uncertainty in the net OSL signal is achieved using the first few seconds of the decay curve. Although the initial and the total OSL signal behave similarly it has nevertheless been demonstrated that there is a significant (10%) hard-to-bleach component in the total integrated signal. This contributes much less to the initial signal. It is important in a regenerative protocol using OSL that the signal used in calculations is dominated by the most rapidly decaying component of the quartz OSL signal, and so the initial signal was used after subtracting the underlying slow component measured over similar channels at the end of the signal (see Fig. 8.6a).

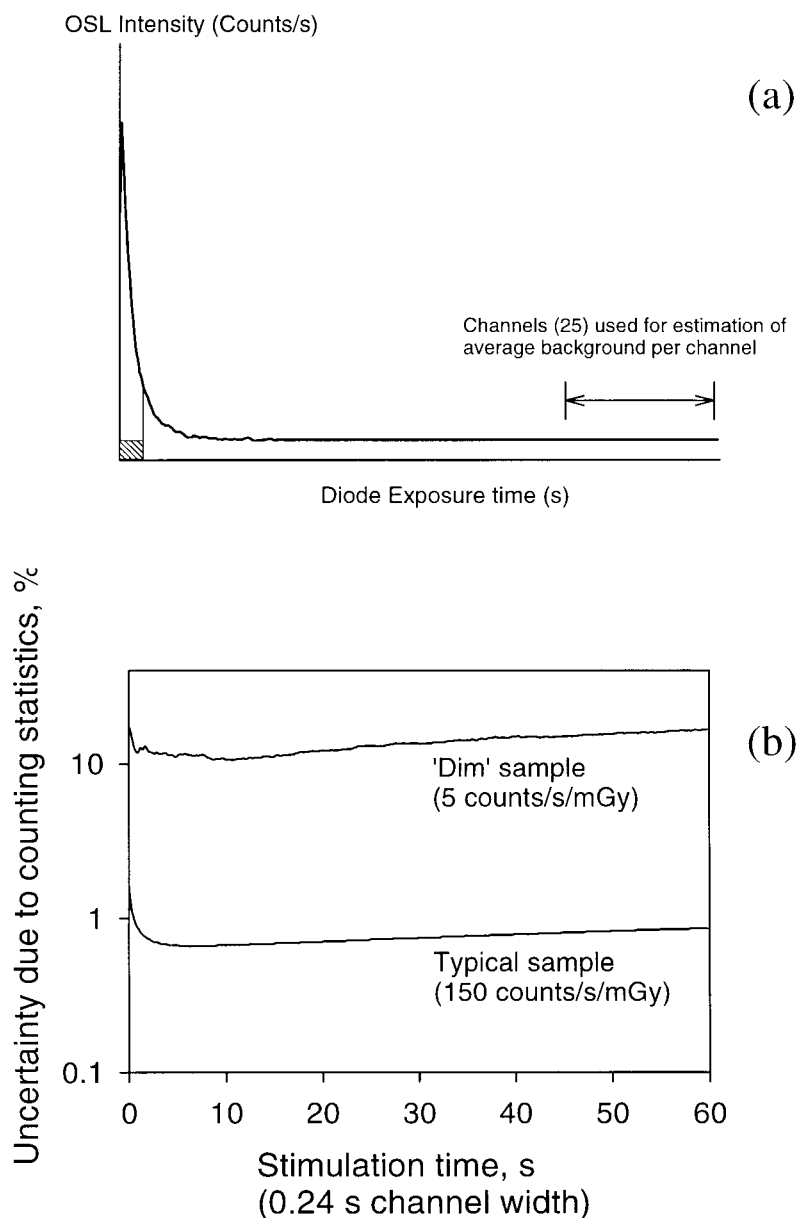


Fig. 8.6. (a) OSL decay curve indicating the initial signal and the underlying slow component.

(b) Random uncertainty in the net OSL signal plotted as function of integration time. See text for definition of the uncertainty. (From Banerjee et al, 1999b).

Fig. 8.6b (after Banerjee et al, 1999b) shows the random uncertainty arising from counting statistics as a function of total integration time, where the random uncertainty was estimated using the expression:

$$\sigma = (\sum_i S_i + 2Bn)^{1/2} / \sum_i S_i - Bn$$

$S_i$  is the signal from the  $i$ th channel ( $i = 1, 2, \dots, n$ ) and  $B$  is the average background, in this case determined over the last 6 s of a 60 s stimulation. For a typical “dim” sample (50 counts in the first 0.24 s, and containing a natural dose of 50 mGy), the uncertainty in the background corrected signal decreases from 18% (first 0.24 s only) to 12 % upon integrating the signal over the first 1.2 s. It decreases by only another 1 % using further 7.2 s. Integration of all 60 s leads to an increase in uncertainty to ~ 17 %. For a “bright” sample (4000 counts in the first 0.24 s), it makes little difference statistically if one integrates over the first 1.2 s or over the whole stimulation curve; both have an uncertainty of about 0.9 % associated with the background corrected signal. There is only a minor absolute improvement (from 1.6 % to 0.9 %) between analysis using only the first 0.24 s and the first 1.2 s.

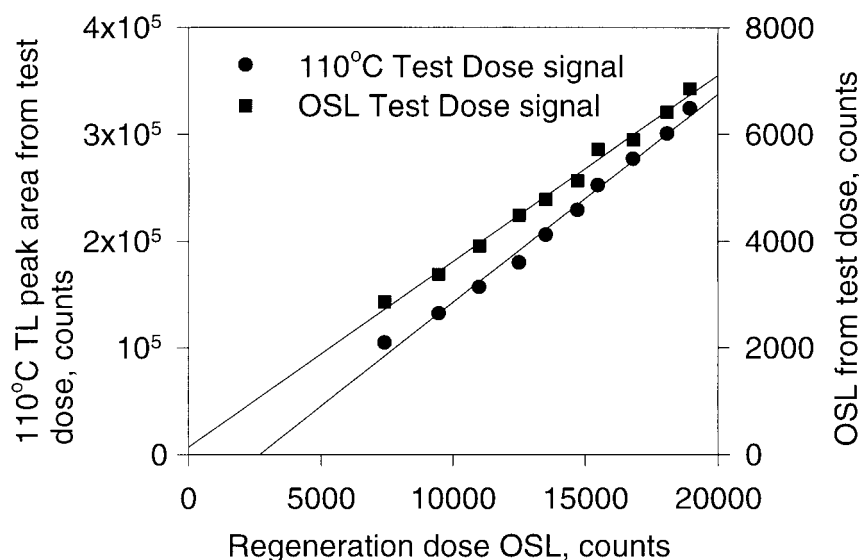


Fig. 8.7. Dependence of test dose 110°C TL peak area and test dose OSL on the regenerated OSL for brick sample Rosk-2 (from Banerjee et al, 1999a).

(v) Sensitivity changes with regeneration cycles

For the single-aliquot regenerative-dose protocol to be applicable, it must be demonstrated that luminescence sensitivity changes are negligible or that they can be corrected for by using a measurement of a proxy signal. A brick quartz extract was used to investigate the effect of repeated regeneration procedures (preheating, bleaching) on the luminescence sensitivity of the sample. An aliquot was first bleached for 60 s at 125°C before given a regeneration dose of 2.5 Gy. It was then heated to 160°C (to remove the 110°C TL peak due to regeneration dose) and given a test dose of 0.8 mGy. The 110°C TL sensitivity was re-measured again using 0.8 mGy test dose and heating to 160°C before cooling immediately. This was followed by blue stimulation at 125°C for 60 s to measure the regenerated OSL. The 110°C TL sensitivity was again estimated by

heating to 160°C after a 0.8 mGy test dose, and then the OSL signal from this test dose was measured at 125°C for 100 s. This measurement was repeated identically several times on the same aliquot. Fig. 8.7 shows the dependence of both the 110°C TL peak area and the OSL signal from the second test dose, after the measurement of the regeneration OSL for sample Rosk-2. Both the 110°C TL signal and the OSL from the test dose correlate well with the regenerated OSL ( $R^2 = 0.991$  and  $0.993$ ). A significant intercept on the horizontal axis is observed for the 110°C TL correlation; the correlation with the OSL test dose signal has a negligible intercept. Thus the results from this sample confirm the earlier observations (Murray and Mejdahl, 1999; Murray and Wintle, 1999) that a single measurement of the OSL test dose signal can be used to correct for sensitivity changes in the regenerated OSL by dividing natural and regenerated OSL signals by a subsequent test dose OSL signal.

*(vi) The single aliquot regeneration (SAR) protocol*

The SAR protocol used employs four OSL measurements. The natural sample is first preheated at an arbitrary temperature between 160°C and 300°C for 10 s. This material has already received some dose before sampling, i.e. the sum of the accident and the background dose. This natural OSL signal is measured (e.g. 100 s stimulated at 125°C) to give  $L_n$ . A test dose is applied (10-20% of the natural dose) and heated to 160°C to empty charge from the 110°C TL trap. The OSL signal is measured again, to give  $T_n$ . A regeneration dose ( $D_r$ ) is then applied, which is followed by preheating and measurement of the regenerated OSL ( $L_r$ ). The test dose is given again, heated to 160°C, and the OSL signal measured to give  $T_r$ . Using the observation that the correlation between  $L$  and  $T$  passes through origin, the natural dose  $D_e$  is given by:

$$D_e = (L_n/L_r) (T_r/T_n) D_r$$

This calculation assumes that the OSL dose response curve is linear, or that  $D_r \sim D_e$ . To avoid the need for this assumption, least three regeneration doses are normally used, chosen to encompass  $D_e$ ;  $D_e$  is then estimated by interpolation. To verify that any sensitivity changes during measurement have been adequately corrected for, the first regeneration dose is then given to the sample again and its OSL measured. A ratio of the sensitivity normalised signals of the first and the fourth regeneration measurements of close to unity confirms that sensitivity changes, if any, have been properly accounted for in the evaluation of the equivalent dose. Finally, the OSL signal is also measured without giving an additional regeneration dose before preheating and measurement. The sensitivity normalised zero signal gives an indication of the degree of thermal transfer from the hard-to-bleach traps to the OSL trap. The SAR protocol is outlined in Fig. 8.8.

*(vii) Growth curves and dependence of preheat*

To demonstrate the robustness of the SAR protocol for young brick samples, a natural aliquot of a Chernobyl sample (Chn 2-1) was heated to 220°C for 10 s and then stimulated with blue light for 60 s at 125°C. The aliquot was given a test dose of 24 mGy, heated to 160°C to empty the 110°C TL peak and stimulated as before. Next, a regeneration dose of 0.5 Gy was given followed by heating at 220°C for 10 s and optical stimulation for 60 s. This cycle was repeated 69 times, with the same test dose but different regeneration doses up to ~ 56 Gy. Fig. 8.9 (Banerjee et al, 1999b) presents the uncorrected and sensitivity corrected OSL growth curves. The main features of the sensitivity uncorrected growth curve are (i) supralinear growth up to ~ 5 Gy, (ii) linear growth between 5 and 22 Gy (iii) sub-linear growth beyond 22 Gy. The discontinuity in the un-

corrected data about 18 Gy arose because of a 24 hour pause in the measurement sequence. The main distinction between the sensitivity corrected and sensitivity uncorrected growth curves is the removal of supralinear growth in luminescence after sensitivity correction. This suggests that this non-linearity in the initial growth with dose is related to changes in the ratio of non-luminescence to luminescence centres i.e. in the probability of luminescence recombination. Finally, after 56 Gy measurement cycle, the 0.5 Gy dose was repeated. After sensitivity correction, this OSL signal lay within 10 % of the first 0.5 Gy, thus suggesting that sensitivity changes had been well accounted for throughout the 70 regeneration cycles.

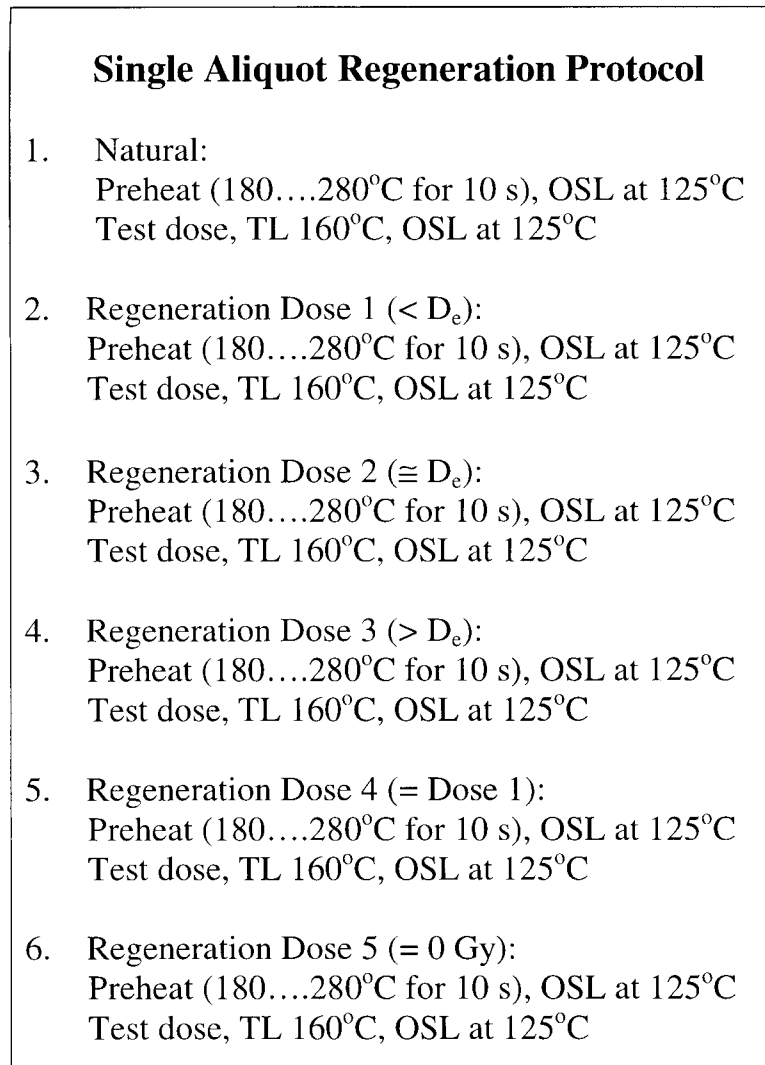


*Fig. 8.8. Routine application of the SAR protocol.*

Fig. 8.10a presents a routine application of the SAR protocol to the measurement of  $D_e$  in sample Chn 3-2 (Banerjee et al, 1999b). Three regeneration doses ( $D_{r1}$ ,  $D_{r2}$ ,  $D_{r3}$ ) are used and chosen so that  $D_{r1} < D_e$ ,  $D_{r2} \sim D_e$  and  $D_{r3} > D_{r2}$ . The equivalent dose ( $D_e$ ) is then interpolated from this limited section of the regenerated dose-response curve. A fourth regeneration dose ( $D_{r4}$ ) is administered to the same aliquot equal to the first ( $D_{r4} = D_{r1}$ ). The corrected luminescence signal ( $R_4$ ) is shown as an open triangle in Fig. 8.9a. The ratio of the fourth corrected luminescence signal to the first ( $R_4/R_1$ ) gives a measure of how accurately the

sensitivity correction has performed over the first 4 regeneration cycles (in this case  $R_4/R_1 = 0.998$ ). A fifth regeneration dose ( $D_{r5}$ ) is then given. Ideally  $R_5$  should be zero, but some recuperation may be observed. The zero-dose corrected regeneration signal ( $R_5$ ) is shown as a filled circle in Fig. 8.10a.

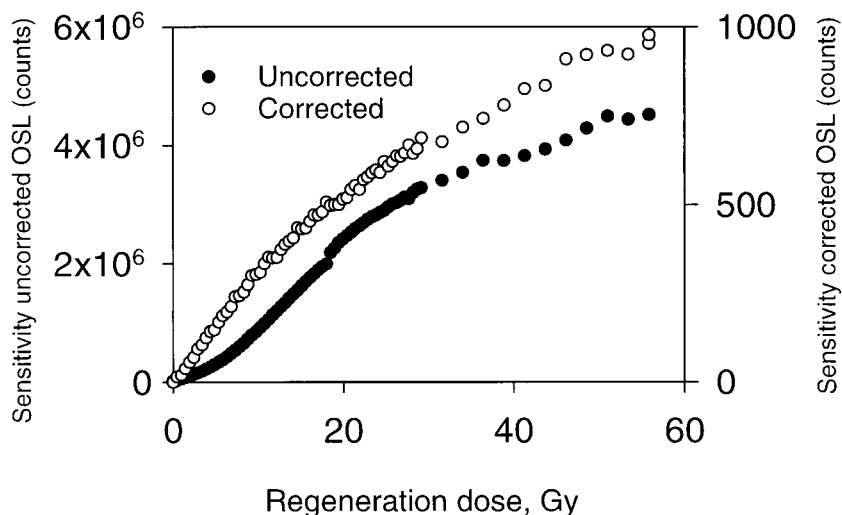


Fig. 8.9. Sensitivity corrected and uncorrected OSL growth curves for a Chernobyl quartz sample. (From Banerjee et al, 1999a).

After sensitivity correction, the fourth and fifth regeneration dose signals ( $R_4$  and  $R_5$ ) are indistinguishable signifying that sensitivity changes have been satisfactorily corrected. The sensitivity normalised zero dose signal is negligibly small. The sensitivity corrected growth curve is linear ( $R^2 = 0.998$ ) and passes through the origin in this dose range.

Fig. 8.10b presents a typical plot of the variation of  $D_e$  with 10 s preheat at temperatures between 180°C and 280°C (Banerjee et al, 1999b). These data were obtained over 12 hours. The equivalent dose is virtually independent of preheat temperature; a result consistent with earlier observations (Murray and Mejdahl, 1999; Murray and Wintle, 1999) that after sensitivity correction, there is no evidence of significant thermal transfer of charge in the natural dose. Had transfer occurred in nature, a systematic change would be observed in  $D_e$  with increasing preheat temperatures until a plateau was reached, when the preheat equalled or exceeded the natural thermal transfer. No such change in  $D_e$  is observed, and we conclude that thermal transfer of charge is minimal for these fired quartz extracts.

*(viii) Precision and accuracy of equivalent dose estimates*

The same brick quartz extract sample (CH-95) that had earlier been measured using the SARA protocol (see Table 8.3) was measured using the new SAR method. Table 8.4 presents these data together with the SARA results for comparison; the  $D_e$  values agree very well. 15 aliquots were used for the SAR measurements an average precision of 1.3 % was obtained (compared to 3.2 % obtained using the SARA method).

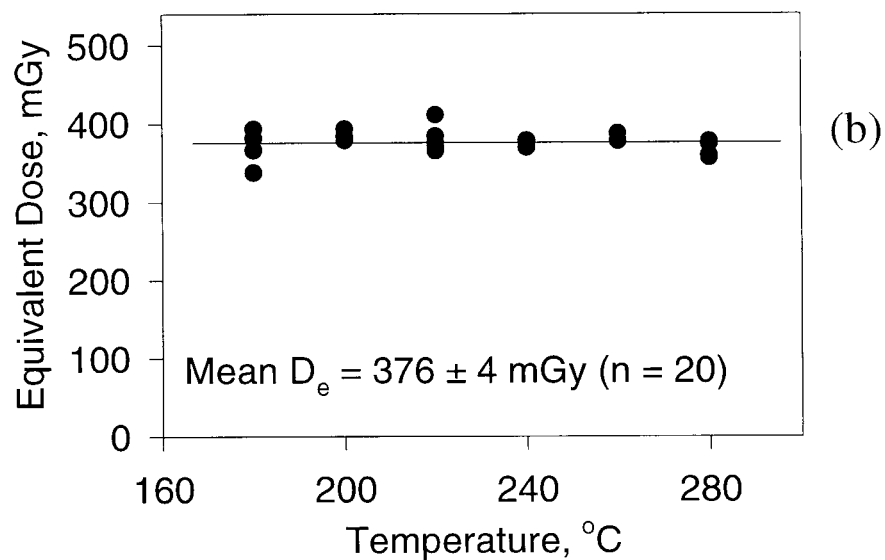
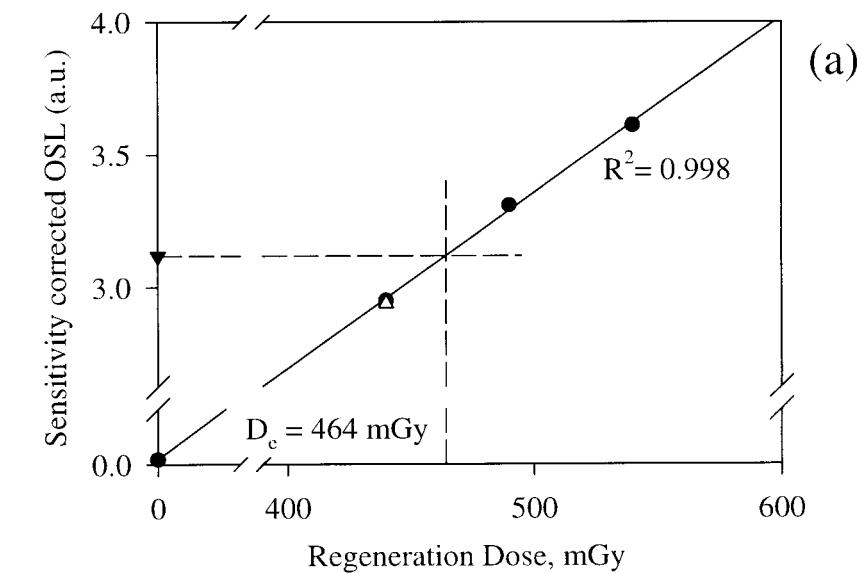


Fig. 8.10. (a) Sensitivity corrected OSL growth curve for a Chernobyl quartz sample following the sequence given in Fig. 8.8.

(b) Variation of the equivalent dose with preheat temperature for another Chernobyl quartz sample (from Banerjee et al, 1999a).

Table 8.4. Typical  $D_e$  results measured from extracted brick quartz using the SAR method. The average precision obtained is 1.3 %. For comparison the results obtained using the SARA method on the same samples (from Table 8.3) are also shown. As seen the  $D_e$  values agree very well although a substantially higher precision is obtained using the SAR method.

Depth (mm)	SAR $D_e$ (mGy)	SE (%)	SARA $D_e$ (mGy)	SE (%)
10	123 ± 0.9	0.7	123 ± 2.2	1.8
20	123 ± 1.3	1.1	109 ± 3.2	2.9
40	120 ± 1.2	1.0	114 ± 3.9	3.4
60	119 ± 2.1	1.7	116 ± 3.8	3.3
80	115 ± 1.6	1.4	113 ± 4.5	3.9
90	111 ± 2.0	1.8	115 ± 4.9	4.3
100	115 ± 1.8	1.5	112 ± 3.5	3.1

Values of  $D_e$  for various bricks from the Chernobyl area and Roskilde estimated using the SAR method are presented in Table 8.5. The standard error associated with the mean for the Chernobyl samples is ~ 1% ( $n > 14$ ). Thus, high precision estimates of the mean values of  $D_e$  are achievable with SAR procedures. The uncertainties associated with the dose estimates from the two Danish sites is slightly higher (~ 4%) because the absolute luminescence sensitivity is a factor of 100 less than that of a majority of bricks from the Chernobyl region and the doses are up to three times smaller.

Table 8.5. Summary of dose measurements made on Chernobyl and Roskilde bricks.

Sample	Sample location	SAR equivalent Dose <sup>+</sup> (mGy)	Numb. of aliquots	SE (%)	Expected dose (mGy)
Chn 1-1	Chernobyl	416 ± 5	17	1.2	Not known
Chn 2-1	Chernobyl	376 ± 4	20	1.1	Not known
Chn 3-2	Chernobyl	488 ± 3	14	0.6	Not known
Rosk-1	Roskilde, DK	131 ± 5	3	3.8	131* ± 6
Rosk-2	Roskilde, DK	262 ± 11	20	4.2	246* ± 12

\* Calculated using the known age of the brick and the estimated annual dose (see text).

+ Uncertainties are standard errors of the mean value. They do not include systematic uncertainties, estimated at ~ 3 %, in either equivalent dose or expected dose.

The absolute accuracy of the SAR protocol was tested by comparing estimates of the  $D_e$  with known doses, calculated from the two known age bricks (see Table 8.5). The SAR  $D_e$  was determined for quartz from the samples Rosk-1 and Rosk-2 as 131 ± 7 and 262 ± 14 mGy, respectively (in contrast to the results given in Table 8.5, these uncertainties given here include the systematic error of

the beta source calibration). These bricks are from buildings known to be 37 and 72 years old, respectively. To evaluate the expected  $D_e$  for these bricks, estimations of annual beta and gamma (+ cosmic) doses were carried out using gamma spectrometry and  $Al_2O_3:C$  OSL dosimeters (section 8.7). The annual doses for Rosk-1 and Rosk-2 were  $3.45 \pm 0.15$  and  $3.42 \pm 0.17$  mGy/a, respectively (these uncertainties include systematic errors in calibration of the gamma spectrometer). The expected  $D_e$  values using the known age and dose rate are  $131 \pm 6$  and  $246 \pm 12$  mGy. It is concluded that it is not possible to distinguish the measured values of  $D_e$  from the predicted values, and thus the SAR protocol is accurate within the limits of testing.

*(ix) Estimation of the precision of the fall-out dose*

The accident dose is given by  $D = D_e - B$ ; where  $D_e$  is the equivalent dose and  $B$  is the background dose. If the background constitutes the majority of the dose, or only few dose values are available, a direct estimate of the background is necessary.

As has been demonstrated, the single-aliquot regenerative-dose method can easily be used to give random uncertainties in the determination of  $D_e$  of  $< 3\%$ . Systematic sources of error (e.g. beta source calibration) then dominate, and the overall uncertainty in  $D_e$  is probably  $\sim 3\%$ . For a single total estimate, it is suggested that the background dose can be estimated at best to within 4% with present technology. Thus for a sample with  $D_e = 150 \pm 4.5$  mGy and  $B = 100 \pm 4$  mGy,  $D = 50 \pm 6$  mGy. It is concluded that it is possible to resolve at best a fall-out dose component of 18 mGy ( $3\sigma$ ) on a background dose of 100 mGy, because of uncertainties of the beta source calibration and in the estimation of background dose (e.g. analytical uncertainties in radioactivity measurements, variation of water content since the sample was fired, inhomogeneity of the radiation field and reliability of the age of the wall being dated). Furthermore, the matrix involved (a brick wall) is not an infinite matrix with respect to gamma rays and thus some modelling of the radiation environment is necessary before one can precisely assess the background dose. To significantly improve the minimum detection limit for accidental doses, new buildings should be selected for measurement, which should be performed as soon as possible after the accident. This would provide a potential minimum detection limit of  $\sim 5$  mGy. If older buildings must be used, effort needs to be directed towards high precision measurements of the natural dose-rates and modelling of the radiation fields in such environments.

### **8.5.6 Conclusions – analytical protocols**

The application of single aliquot regeneration and added dose (SARA) and the true single aliquot regeneration (SAR) OSL methods for the estimation of doses in quartz extracted from modern house bricks have been outlined. It has been argued that, from both a physical and statistical points of view, the initial OSL signal should be used for equivalent dose estimation. High precision on the mean estimate of the values of  $D_e$  ( $SE \sim 1\%$  for  $n = 20$ ) can be achieved. It is further concluded that, with present techniques, a fallout component of  $\sim 18$  mGy is resolvable on a natural background dose of  $\sim 100$  mGy. To improve this detection limit significantly, uncertainties in the estimates of natural dose rates must be reduced.

## 8.6 Retrospective Assessment of Environmental Dose Rates

### 8.6.1 Introduction

As part of the assessment of the usefulness of natural and artificial dosimeters in retrospective accident dosimetry, the natural photon dose rates within bricks have been measured using the OSL from  $\text{Al}_2\text{O}_3:\text{C}$  single crystal dosimeters (Bøtter-Jensen and McKeever, 1996; Bøtter-Jensen et al, 1997 and also chapter 6 of this thesis). Such measurements help to confirm modelled natural dose rates, and thus support the calculation of the natural background contribution to the total dose recorded after an accident (except in the case of very short lived contamination, this background cannot be measured directly after the accident).

$\text{Al}_2\text{O}_3:\text{C}$  dosimeters were placed in bricks in house walls for a period to integrate the environmental dose rates. The observed doses were compared with 1) doses derived from OSL measurements of quartz samples extracted from the same bricks and 2) dose rates determined from laboratory measurements of the natural radionuclide concentrations.

Measured natural radionuclides concentrations were first used to calculate the infinite matrix gamma ray dose rate (the infinite matrix dose rate is the dose rate at the centre of a volume of brick much larger than the range of the most energetic natural gamma-ray  $\sim 2.7$  MeV). Secondly, ways of directly measuring the field dose rate in the finite brick wall were investigated, so that an empirical ratio could be derived between the infinite-matrix gamma dose rate and that in the brick. Unfortunately quartz cannot be used directly to make these luminescence measurements, because it is insufficiently sensitive. Passive solid state detectors, such as TL phosphors based on  $\text{LiF}$ ,  $\text{CaF}_2$ , and  $\text{CaSO}_4$  have all been used in the past to determine environmental dose rates, but all these require exposure times of months to determine the dose rate precisely. Of greater concern is the different energy dependence of the photon response of these phosphors when compared with quartz. Converting the observed dose rate to a quartz dose rate introduces additional errors in the experiment.

### 8.6.2 Experimental details

The  $\text{Al}_2\text{O}_3:\text{C}$  detectors used in all experiments were single crystal chips (TLD-500), 1 mm thick and 5 mm diameter ( $375 \text{ mg/cm}^2$ ) provided by Stillwater Sciences LLC, Stillwater Oklahoma, USA (Akselrod et al, 1990). Coarse grain (90-180  $\mu\text{m}$ ) quartz grains were extracted from bricks for the OSL measurements. The bricks were first sliced into 10 mm sections. Material from each section was crushed and treated with 10%  $\text{HCl}$ , 40%  $\text{H}_2\text{O}_2$  and dry-sieved to separate the 90-180  $\mu\text{m}$  grain size fraction. This fraction was then etched in 40%  $\text{HF}$  for 45 minutes to extract the quartz. An automated Risø TL/OSL reader, model Risø TL/OSL-DA-15, was used for the OSL measurements. The  $\text{Al}_2\text{O}_3:\text{C}$  dosimeters were stimulated using 470 nm light from blue light-emitting diodes (LEDs) delivering  $20 \text{ mW/cm}^2$  to the sample (Bøtter-Jensen et al, 1999b). The extracted quartz samples were stimulated using either broad band blue-green stimulation light (420-550 nm) for the Chernobyl bricks or blue LED stimulation for the bricks from Denmark. Detection filters were in all cases 6 mm Hoya U-340. The  $\text{Al}_2\text{O}_3:\text{C}$  chips were irradiated automatically within the OSL reader using a  $150 \text{ kBq } ^{90}\text{Sr}$  source delivering a dose rate of  $0.88 \mu\text{Gy/s}$  to the sample. The quartz extracts were irradiated using a  $185 \text{ MBq } ^{90}\text{Sr}$  source delivering a dose rate of  $8.2 \text{ mGy/s}$  to the sample.

The dose evaluations using both the  $\text{Al}_2\text{O}_3\text{:C}$ : single crystals and the extracted quartz grains were based on the single aliquot regeneration protocol described by Banerjee et al (1999a). Further details of these protocols are given in section 8.5.5.

### 8.6.3 In situ dose rate measurements

The  $\text{Al}_2\text{O}_3\text{:C}$  single crystals were used to determine the environmental photon dose rates in two different brick walls prior to removing bricks for dose rate assessment of the material in the laboratory. Two sites were chosen for the experiment, one (Rosk-1) from a laboratory building at Risø with a known age of 37 years and another (Rosk-2) a house in a nearby village with a known age of 72 years. Aluminium tubes, 12 cm long, with an inner diameter of 6 mm and a wall thickness of 1 mm (to absorb beta particles) were packed with 30 freshly annealed  $\text{Al}_2\text{O}_3\text{:C}$  pellets arranged in groups of three distributed over the length of the aluminium tube using 10 mm plastic spacers; this provided 10 measurement points over the entire cross section of the brick. The aluminium tubes were then placed in drilled holes in the middle of bricks in the two walls and left there for 18 days to integrate the environmental photon dose. At the end of the exposure period the dosimeters were immediately removed from the aluminium tubes and their OSL signals measured. The bricks that held the aluminium tubes were then removed from the walls and quartz grains extracted for OSL measurements according to the experimental procedures described in section 8.3. Remaining bulk material was crushed and the natural radionuclide concentrations were determined using a high resolution gamma spectrometer (Murray et al, 1987). These results are listed in Table 8.6. The two depth dose profiles measured with  $\text{Al}_2\text{O}_3\text{:C}$  are shown in Fig. 8.11.

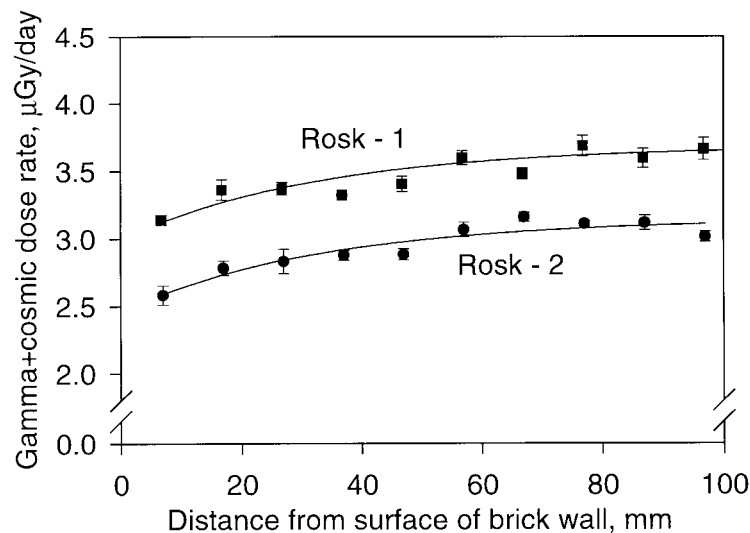


Fig. 8.11. Depth dose profiles measured with  $\text{Al}_2\text{O}_3\text{:C}$  chips across sections of bricks from (a) Risø laboratory building (37 years old) and (b) village house (72 years old) (from Bøtter-Jensen et al, 1999c).

The measured Al<sub>2</sub>O<sub>3</sub>:C dose rates were first compared with the dose rate derived from the measured quartz total dose and the known age (Table 8.7, column 1). The Al<sub>2</sub>O<sub>3</sub>:C measurement includes a cosmic ray component (Prescott and Stephan, 1982), estimated as 0.27 mGy y<sup>-1</sup>, which has been subtracted to give the observed gamma dose rate alone (column 3). The quartz dose rate includes the same cosmic component, an infinite matrix beta dose rate (derived from the measured concentrations, see Table 8.6) and an internal alpha component, estimated using 10% of the bulk concentrations, and an ‘a’ value of 0.15 (this alpha contribution amounts to approximately 5% of the total). When these contributions are subtracted from the total quartz dose rate, the values shown as “Derived  $\gamma$ ” dose rates are obtained (Table 8.7). The uncertainties on the derived dose rates are between 15 and 17%. This is because the beta, alpha and cosmic-ray dose rates together amount to 60 to 70% of the total, resulting in an inevitably large uncertainty on the residual gamma dose rate. Thus, although the ratios ‘Derived/Observed’ cannot be distinguished from unity, the uncertainties are large (~20%). Secondly, the observed Al<sub>2</sub>O<sub>3</sub>:C dose rates (after cosmic dose rate subtraction) were compared with the infinite matrix gamma dose rates (Table 8.6). These ratios (‘Observed/Infinite matrix’, Table 8.7) of  $0.67 \pm 0.05$  and  $0.79 \pm 0.05$  suggest that the field gamma dose rate is about 25% less than the infinite matrix gamma dose rate.

Table 8.6. Measured radionuclide concentrations and infinite matrix\* dose rates.

	<sup>238</sup> U (Bq/kg)	<sup>226</sup> Ra (Bq/kg)	<sup>210</sup> Pb (Bq/kg)	<sup>232</sup> Th (Bq/kg)	<sup>40</sup> K (Bq/kg)	Beta (mGy/y)	Gamma (mGy/y)
Rosk-1	43 ± 5	39.6 ± 1.0	43 ± 7	37.1 ± 0.9	615 ± 21	2.20 ± 0.10	1.32 ± 0.06
Rosk-2	43 ± 5	41.9 ± 1.0	34 ± 4	38.7 ± 0.9	564 ± 21	2.01 ± 0.09	1.22 ± 0.04

\* Derived from concentrations using data presented in Olley et al (1996).

Table 8.7. Comparison of calculated and observed gamma dose rates.

	Tot. dose rate (mGy/y)	Derived $\gamma^{(a)}$ (mGy/y)	Observed $\gamma^{(b)}$ (mGy/y)	Derived/ observed	Observed/ Infinite matrix
Rosk-1	3.54 ± 0.14	0.88 ± 0.17	0.88 ± 0.05	1.0 ± 0.2	0.67 ± 0.05
Rosk-2	3.64 ± 0.15	1.14 ± 0.19	0.95 ± 0.06	1.2 ± 0.2	0.79 ± 0.05

- (a) Derived from total dose rate by subtracting infinite matrix beta dose rate (table 8.6), and estimate of internal alpha and cosmic ray dose rate.
- (b) Derived from observed Al<sub>2</sub>O<sub>3</sub>:C dose rate by subtracting estimated cosmic ray dose rate of 0.27 mGy/y. Water content corrections < 1 %.

#### 8.6.4 Conclusion

In conclusion it is not possible to tell the difference between the gamma dose rates measured directly using Al<sub>2</sub>O<sub>3</sub>:C, and the quartz derived gamma dose rates (although the uncertainties are large). It is further concluded that radiochemical analysis of bricks probably can be used to derive the natural background dose

rate, if the infinite matrix gamma dose rate is reduced by about 25%. At this stage an uncertainty of about  $\pm 10\%$  is associated with this figure.

## 8.7 Evaluation of Dose-Depth Profiles in Bricks

### 8.7.1 Introduction

In the retrospective assessment of accident doses using luminescence methods with bricks, measurements of the dose-depth profiles into the brick material gives information about the energy of the incident photon radiation (Bøtter-Jensen et al, 1995b). For this reason it is desirable to compare such dose-depth profiles with those obtained from bricks irradiated using known gamma sources in the laboratory. Laboratory-irradiated bricks also provide a basis for comparison with modelling using Monte Carlo simulations. Such Monte Carlo simulations have been performed at Risø (Bøtter-Jensen et al, 1995b; Bøtter-Jensen et al, 1999c)) and by Meckbach (in Bailiff and Stepanenko, 1996); these simulations ultimately predict the absorbed dose in air at an external reference location for a given source energy and configuration. If assumptions on the source configuration can be made, the dose-depth profiles are expected to reflect the time-integrated energy spectrum of the external radiation field. Thus, measurements of dose-depth profiles are important because they provide support for the assumption used to convert from dose in brick to dose in air.

### 8.7.2 A continuous OSL scanning method

#### *(i) Introduction*

Whilst beta and alpha radiation are rapidly absorbed in the outer layers of brick, gamma radiation penetrates many tens of centimetres, and by monitoring the attenuation of the radiation induced luminescence, information on both the dose and energy spectrum of the gamma rays can be obtained. For TL methods, careful sample preparation is required, extracting the crystals used as dosimeter (quartz and feldspar) from matrices at set intervals. However, since OSL can be measured at room temperature, the technique naturally lends itself to the development of continuous scanning measurements of brick cross sections allowing the radiation depth dose profiles to be measured directly on the unseparated material.

A method was developed for direct measurements of depth-dose profiles in brick, tile and porcelain cores, without the need for sample separation techniques (Bøtter-Jensen et al, 1995b). Using brick cores, profiles were generated by laboratory radiation using different photon energies from  $^{137}\text{Cs}$  and  $^{60}\text{Co}$  gamma sources; the measured depth dependency was then compared with theoretical calculations derived from Monte Carlo simulations, and with experimental measurements made using more conventional optically stimulated luminescence methods of analysis.

#### *(ii) Samples and experimental details*

The brick core OSL scanning system is shown schematically in Fig. 8.12 (see also chapter 3).

Measurements were carried out on cores drilled from a variety of bricks which had been previously exposed one side to point sources of  $^{137}\text{Cs}$  and  $^{60}\text{Co}$  gamma radiation, respectively, using laboratory sources. Photo-excitation was made via a 75 W tungsten-halogen lamp, filtered to select a blue/green band 420-550nm.

The output of the lamp was passed through a circular-to-rectangular glass waveguide and on emerging, the light source was imaged 1:1 onto the brick surface. As a consequence, the brick is illuminated in the form of a slit 10 mm long by 1 mm wide, and this defines the spatial resolution of the system. The profile of the beam, taken along the scanning direction, is shown in Fig. 8.13a. The profile is approximately Gaussian in shape; the known slope allowed the data to be taken by stepping in discrete 1 mm intervals along the length of the core and measuring for only a short period (typically 1 s) at each position.

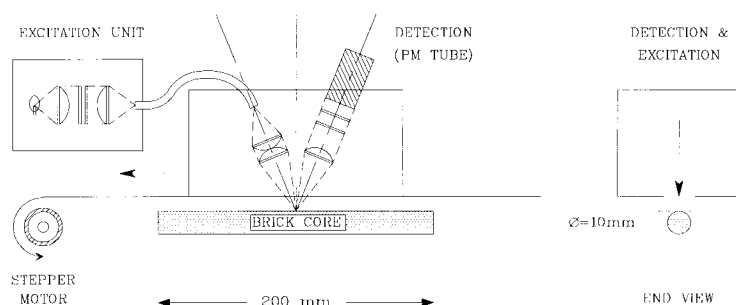


Fig. 8.12. Schematic diagram of the automatic OSL brick core scanning system; the excitation beam is 1 mm wide (from Bøtter-Jensen et al, 1995).

The beam profile also influences the form of the luminescence decay. Consider a hypothetical situation where a single section of the core (point 1 in Fig. 8.13a) decays according to:

$$I(t) = aJD \exp(-btJ)$$

where  $D$ ,  $J$  and  $t$  are the dose, excitation intensity and time, respectively;  $a$  and  $b$  are constants. As shown in Fig 8.13b, if the single point is now enlarged to cover the whole beam profile (a situation expected in a totally homogeneous brick, for example), the ensuing luminescence decay becomes non-exponential, with the extra components at longer times arising from the weakly illuminated parts of the brick. Although, the decay function is not in fact exponential even for the single point, the luminescence decay form is modified in a similar fashion to that shown in Fig. 8.13b.

All measurements using the automatic OSL core scanning system were made on material prepared in the form of cylindrical cores, extracted by means of a diamond-headed water-cooled tubular saw. The diameter of the cores was either 8 mm or 10 mm, and the maximum length was 100 mm. Material in this form could be directly measured in the scanning system, although we restricted the excitation only to a slit 4 mm long (by 1 mm wide); over this length the beam profile is reasonably uniform on the circular cross-section. Higher sensitivity (by a factor 2) could be achieved by using entire 10 mm length of the excitation beam, on split cores having a planar surface. More sensitive OSL measurements were also made on the cores using conventional methods (Bøtter-Jensen and Duller, 1992) by slicing the cores perpendicular to the core length, again using a

water cooled diamond saw. Typically, 60 slices were produced from a 100 mm core.

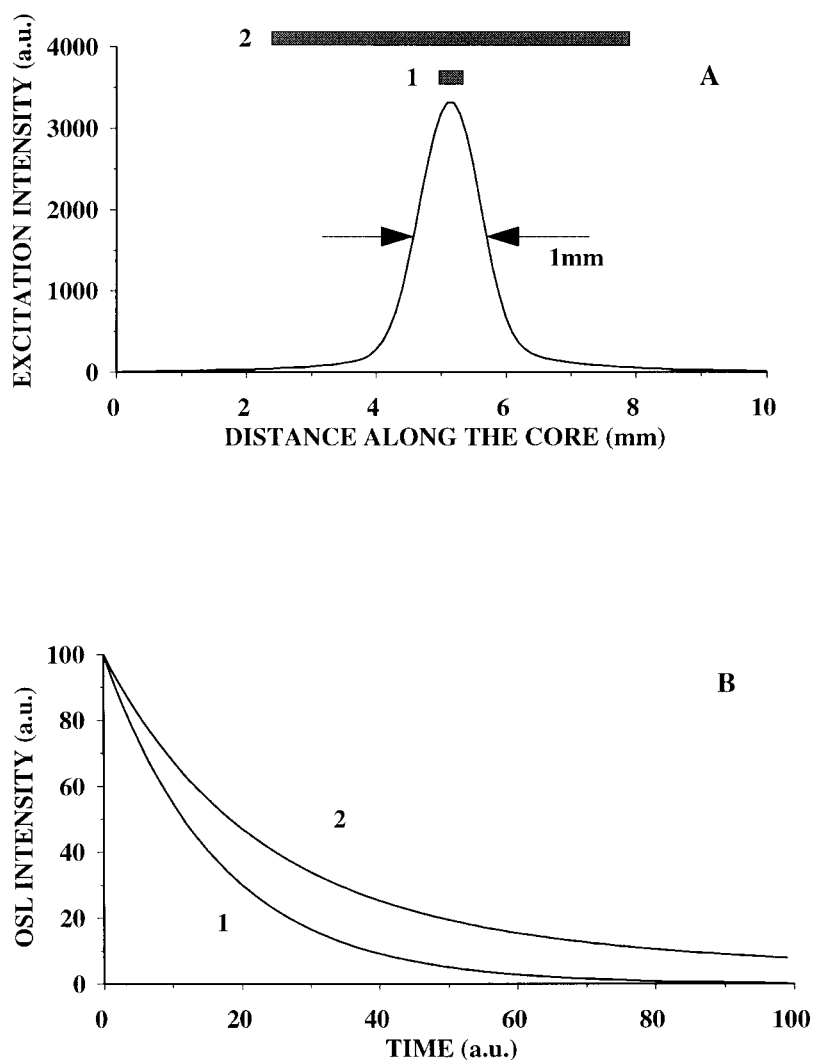


Fig. 8.13. (a) Profile of the luminescence excitation beam. The FWHM is 1 mm and within this zone, the excitation power density is measured to average  $20 \text{ mW/cm}^2$ .

(b) Demonstration of the modification to a hypothetical OSL decay curve due to the excitation beam profile. Curve 1 is a simple exponential function, relating to a single point-like sample, whereas curve 2 is that expected for an extended, uniform sample (such as a brick core with uniform sensitivity) (from Bøtter-Jensen et al, 1995).

(iii) continuous OSL scanning measurements of brick cores

A variety of cores were measured, extracted from both antique and modern house bricks. The modern house bricks were mostly uniform in nature, with no visible obvious grains of sand, whereas the old bricks were of poor quality, including many voids, coarse sands and calcareous material. The OSL sensitivity of the latter was very low and they are not considered further.

Bricks were initially heated to 500°C to remove any accrued dose in the material, and subsequently one end was irradiated in the laboratory using either  $^{137}\text{Cs}$  or  $^{60}\text{Co}$  gamma sources, and given a dose of 46 Gy at the front surface. A rest time of 24 hours at room temperature between radiation and OSL measurement was used to stabilise the OSL signal. After the OSL scanning of individual cores taken from the bricks, the cores were optically bleached and given a normalisation dose of 46 Gy from the  $^{137}\text{Cs}$  source, perpendicular to the core length (i.e. such that the dose was constant all along the core). The OSL profiles were again measured after a rest time of 24 hours at room temperature as described above; the initial dose-depth profiles were normalised by dividing by the latter profiles. The results are summarised in Fig. 8.14. Although the cores appeared to be visually uniform, the OSL is seen to be extremely variable along the core (Fig. 8.14a), with individual highly dose-sensitive quartz grains giving rise to a very well structured curve. However, Figs 8.14b and 8.14c demonstrate that normalisation effectively removes all such structure, indicating that both dull and bright portions of the OSL signal from the core are linearly related to dose.

The continuous core measurements clearly show a difference in the absorption coefficients between the  $^{137}\text{Cs}$  photons (660 keV) and the  $^{60}\text{Co}$  photons (1.25 MeV), with  $I_{1/2}$  occurring at 90 mm and 110 mm from the surface, respectively. As discussed below, these figures compare very well with those calculated using Monte Carlo simulations.

#### *(iv) Discrete measurements from core slices*

Cylindrical cores drilled from the same bricks as described above were sliced, and more accurate measurements (though considerably more labour intensive) could be made of the radiation depth-dose profiles. The 8 mm diameter x 1 mm thick slices had their OSL signals measured in the automated Risø TL/OSL reader using green light stimulation of the surface of the discs (see chapter 3). The following measurement sequence was used: (1) preheat at 140°C for 10 s; (2) OSL measured over 60 s; (3) 10 Gy beta dose to all discs for calibration and normalisation; (4) preheat at 140°C for 10 s; and (5) OSL measured over 60 s for calibration and normalisation. The measured doses, as function of depth into the brick material for the  $^{137}\text{Cs}$  and  $^{60}\text{Co}$  irradiation geometries, are shown in Figs 8.15a and 8.15b, respectively. The fitted exponential attenuation curves compare very well with those obtained with the automatic OSL core scanning system (see Figs 8.14b and 8.14c) and those calculated by a Monte Carlo code (see next section).

#### *(v) Monte Carlo calculations of depth-dose profiles*

In Monte Carlo calculations the particle/photon tracks or histories are generated by simulating the random nature of the particle/photon interaction with matter. The Monte Carlo code MCNP (Monte Carlo Neutron Photon) used in this study is a general purpose, continuous-energy, generalised-geometry, time-dependent, coupled neutron-photon Monte Carlo transport code (Briesmeister, 1986). The MCNP was used to calculate the doses absorbed in the bricks in the actual  $^{137}\text{Cs}$  and  $^{60}\text{Co}$  gamma source irradiation geometries, respectively. The  $^{137}\text{Cs}$  irradiation was made in a collimated beam, whereas the  $^{60}\text{Co}$  irradiation used an isotropic radiation field. The absorbed doses were calculated in the actual geometries for each mm depth into the brick over the entire cross-section (200 mm). The MCNP calculated depth dose profiles for the  $^{137}\text{Cs}$  and  $^{60}\text{Co}$  irradiated bricks are shown in Figs 8.16a and 8.16b, respectively, and compared with the attenuation curves obtained with the automatic OSL scanning system; the two curves are in very good agreement in each case. It should be noted that the measured curves over the total core of 200 mm are made from two separate sec-

tions, each of a core length of 100 mm. The drilling tool used only allows cores of 100 mm maximum length to be drilled from a brick.

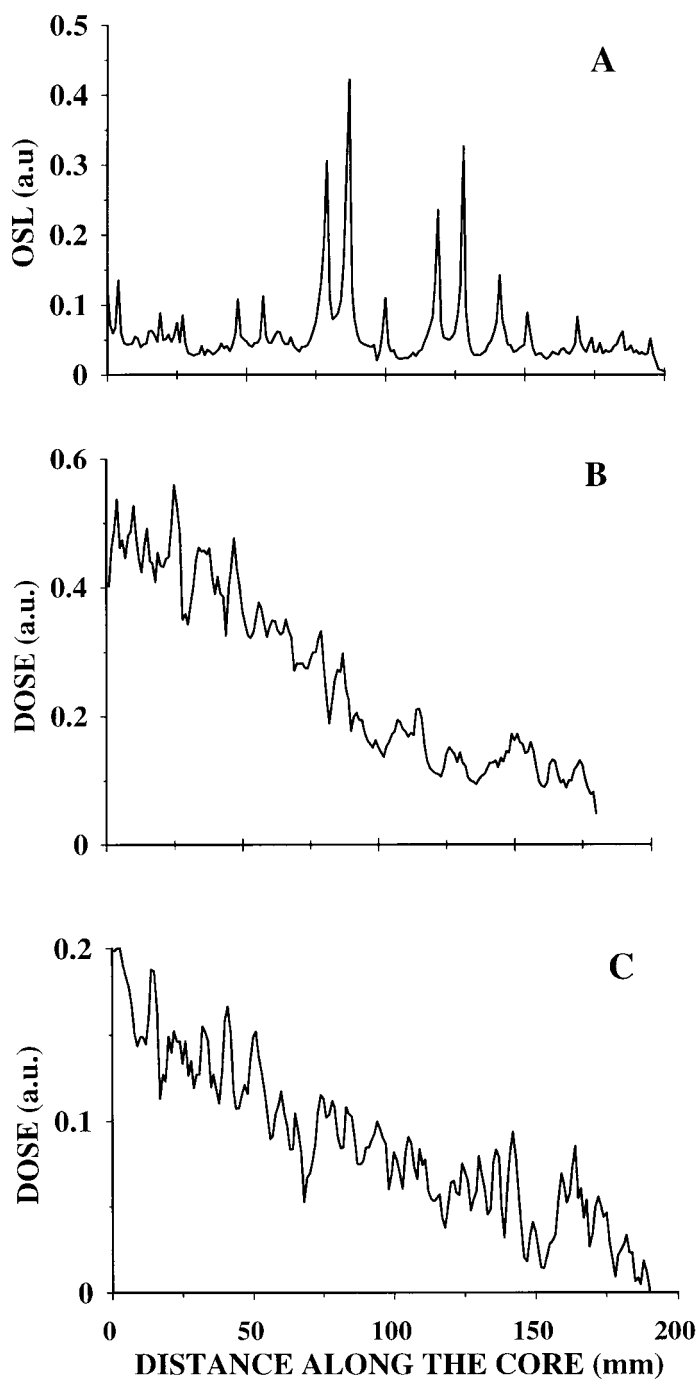


Fig. 8.14. (a) OSL sensitivity of a typical modern clay house brick. The core section has been uniformly gamma irradiated over its surface.

(b,c) Normalised relative depth-dose profiles for bricks irradiated from one side, using  $^{137}\text{Cs}$  and  $^{60}\text{Co}$  gamma radiation, respectively (from Bøtter-Jensen *et al.*, 1995).

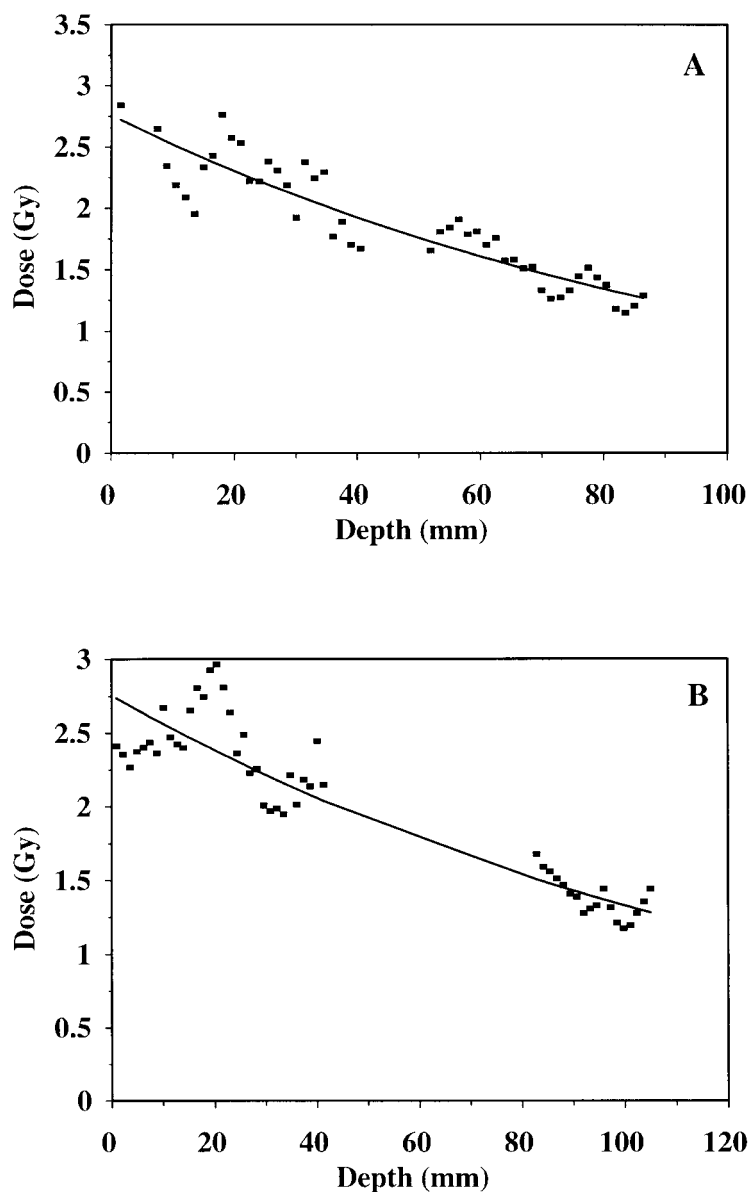


Fig. 8.15. Dose versus depth into a brick irradiated with gamma radiation from one side. Measurements were made using green light OSL on 8 mm diameter  $\times$  1 mm thick slices cut from a core through the brick: (a) profile for 5 Gy  $^{137}\text{Cs}$  gamma radiation; and (b) profile for 5 Gy  $^{60}\text{Co}$  gamma radiation (from Bøtter-Jensen et al, 1995).

(vi) Conclusions

It is concluded that continuous OSL scanning of irradiated bricks provides a very rapid method for analysing dose-depth profiles: normalisation can be made by exposing the cores to gamma radiation perpendicular to the core length. The method highlights the extreme variability in luminescence sensitivity from different portions of the unseparated brick material, although these variations are mostly removed using normalisation. A limiting factor is the general sensitivity of the system that only allows bricks with doses higher than 1 Gy to be measured. Significantly higher sensitivity can be obtained using separation tech-

niques on quartz extracted from bricks which, however, requires much more labour time.

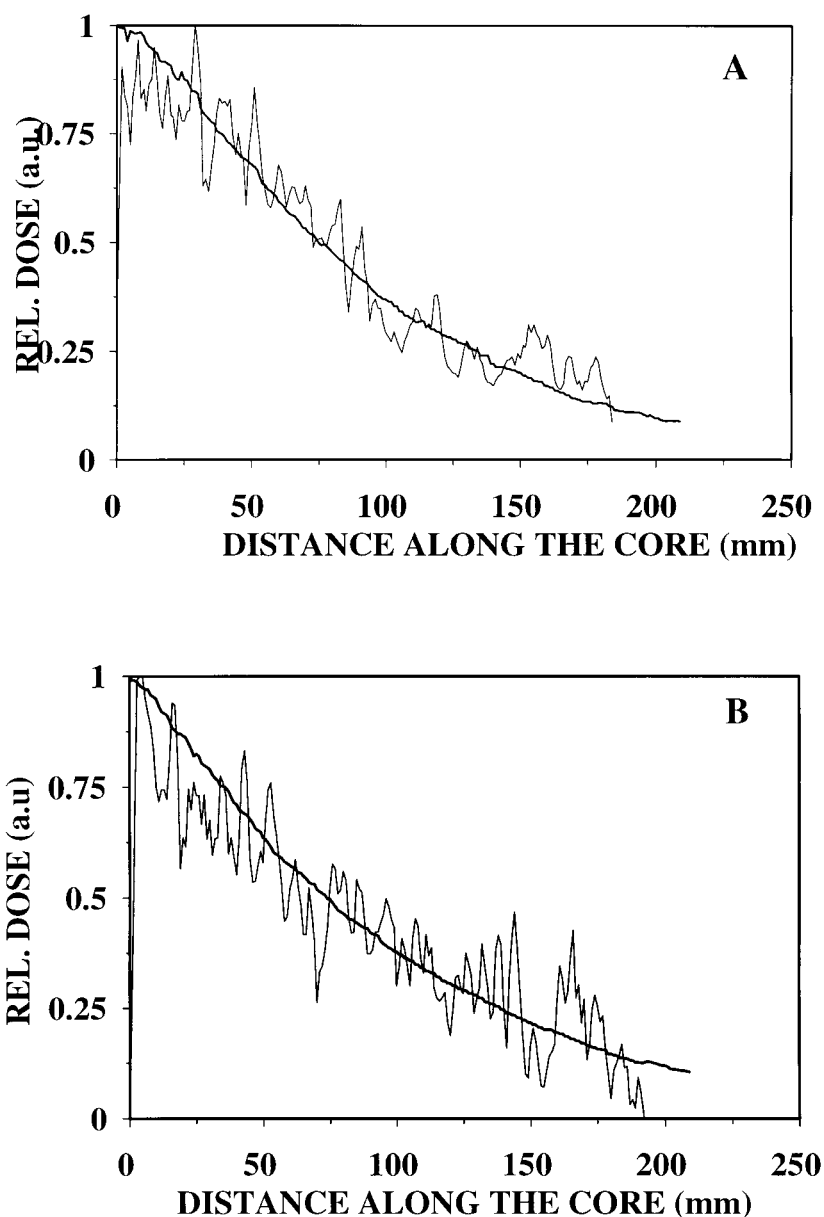


Fig. 8.16. Relative depth-dose profile into a brick from (a)  $^{137}\text{Cs}$  and (b)  $^{60}\text{Co}$  gamma radiation from one side, as calculated by the Monte Carlo code MCNP (bold lines). For comparison, the relative depth-dose profiles measured with the automatic OSL core scanner system are also shown (from Bøtter-Jensen et al, 1995).

### 8.7.3 Dose-depth profiles determined from laboratory irradiations

A section of the Risø brick described in the previous section was used to determine the dose depth profiles from 662 keV  $^{137}\text{Cs}$  gamma photons. The brick had 10 holes of 5 mm diameter drilled from the back side; these were consecutively deeper in the range 10 mm to 100 mm with intervals of 10 mm. Firstly, the brick was given 2.5 Gy  $^{137}\text{Cs}$  gamma radiation on the front face to ensure a suf-

efficient absorbed dose level for the measurement of the dose depth profile using the OSL of quartz extracts. Secondly, three annealed  $\text{Al}_2\text{O}_3:\text{C}$  single crystals were placed at the base of each of the holes in the brick drilled to different depths so they were uniformly distributed over the entire cross section of the brick. 5 mm diameter aluminium rods were placed behind the dosimeters to fill the holes and secure secondary electron equilibrium. The brick containing the dosimeters was then given an additional dose of 55 mGy of  $^{137}\text{Cs}$  radiation on the front side to populate the  $\text{Al}_2\text{O}_3:\text{C}$  traps. Immediately after the exposure the dosimeters were removed from the brick in darkness and their OSL responses measured. The brick was then sliced into 10 mm sections and coarse grain (90-180  $\mu\text{m}$ ) quartz samples were extracted from each section; these had their OSL signals measured as described above.

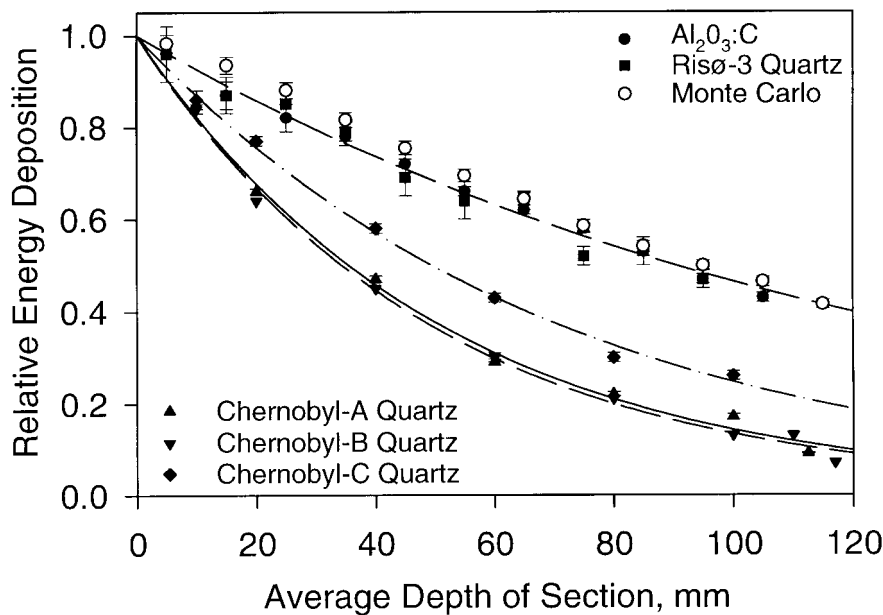


Fig. 8.17. Depth dose profiles in bricks obtained using OSL and  $\text{Al}_2\text{O}_3:\text{C}$  and extracted quartz grains; (a)  $\text{Al}_2\text{O}_3:\text{C}$  chips placed across a brick in drilled holes and irradiated to 55 mGy  $^{137}\text{Cs}$  gamma laboratory dose, (b) quartz extracted from samples taken across the same brick after an additional laboratory exposure of 2.5 Gy  $^{137}\text{Cs}$  gamma radiation and (c,d,e) quartz extracted from bricks collected in the Chernobyl area exposed to the accidental dose. Also seen (f) is the Monte Carlo calculated depth dose curve for  $^{137}\text{Cs}$  photons attenuated in the brick material. (From Bøtter-Jensen et al, 1999c).

Fig. 8.17 shows the normalised dose depth profiles for both the  $\text{Al}_2\text{O}_3:\text{C}$  chips and the quartz grains. Each  $\text{Al}_2\text{O}_3:\text{C}$  point is the average of the results from three pellets and the quartz extract data are based on single aliquot regeneration measurements (section 8.5.5). The normalised profiles for  $\text{Al}_2\text{O}_3:\text{C}$  and quartz agree well; this is not surprising since the energy responses of  $\text{Al}_2\text{O}_3:\text{C}$  and quartz are almost identical. A Monte Carlo simulated absorption curve produced using the MCNP code (Briesmeister, 1986) is also shown; these calculations agree well with observations. OSL dose depth profiles obtained from bricks collected in the Chernobyl accident area (from section 8.7.4) are also shown in the figure. The different absorption rates with depth demonstrate that the average energy of the accidental radiation was somewhat lower than that from unscat-

tered  $^{137}\text{Cs}$  gamma rays. This is consistent with the known composition of the initial accident radiation spectrum that was dominated by radiation from short-lived low-energy radionuclides, although a scattered  $^{137}\text{Cs}$  source would also tend to give a similar more rapidly attenuated absorption curve.

#### 8.7.4 Determination of depth-dose profiles from Chernobyl bricks

Optimum sensitivity will usually be obtained by using samples of pure minerals (quartz and feldspar) extracted from the bulk material. This extraction technique has been used extensively to measure dose-depth profiles in a variety of brick samples, collected from inhabited sites in the Chernobyl accident area during field trips in Russia and the Ukraine. Sub samples for measuring dose-depth profiles were prepared by slicing a cross section of the brick into 10 mm thick sub sections and coarse grain (90-150  $\mu\text{m}$ ) quartz samples were extracted from each section as described in 3.1. These sub samples (each 4 mg) had their OSL measurements measured using either broad band or blue LED stimulation sources. The thickness of each slice represents the limit on spatial resolution. Thinner slices could be used, but the cross sectional area would have to be increased in proportion.

Examples of equivalent doses measured from various bricks from three sites using the SAR protocol are summarised in Table 8.8. Standard deviations range from 2 % ( $D_e = 690$  mGy, sample 1/9-2 at 20 mm depth) to 9 % ( $D_e = 43$  mGy, sample 2/8-3, at 60 mm depth). These give rise to a range in standard errors on the mean of 0.6 % to 2.3 %, illustrating the high precision achievable when it is practical to make many measurements of  $D_e$ .

Table 8.8. Values of  $D_e$  measured using the SAR protocol in bricks accidentally exposed to ionising radiation (from Banerjee et al, 1999b).

Sample	Depth into Brick (mm)	$D_e$ (mGy)	Standard error (mGy)	n	Standard deviation (%)
Site 1/9-2	10	867	10	18	5
	20	691	4	17	2
	40	527	5	19	4
	60	403	7	17	7
	80	323	2	18	3
	100	252	3	17	5
	110	248	2	17	4
	120	218	3	18	6
Site 2/7-6	10	115	1.1	19	4
Site 2/8-3	60	43.4	0.9	16	9
Site 2/9-3	10	54.8	0.6	16	4
Site 3/1-1	10	331	3	20	4
	20	301	4	20	7
	40	244	1.9	19	3
	60	218	2	17	4
	80	188	1.8	19	4

Fig. 8.18a shows a typical OSL decay curve obtained from an extracted quartz sample having a natural background dose of approximately 100 mGy. The two depth dose profiles (1/9-2 and 3/1-1) are shown in Fig. 8.18b. Both bricks were collected in regions affected by fallout. The data have been fitted using the sum of

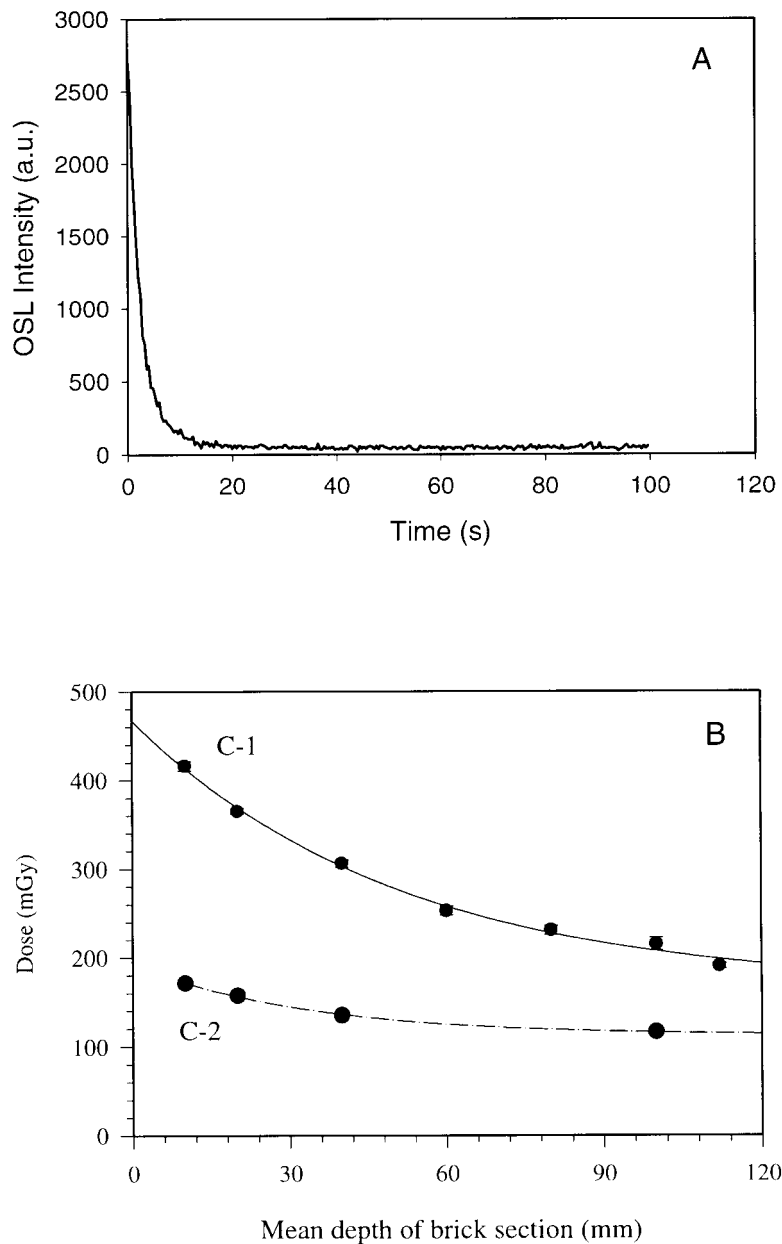
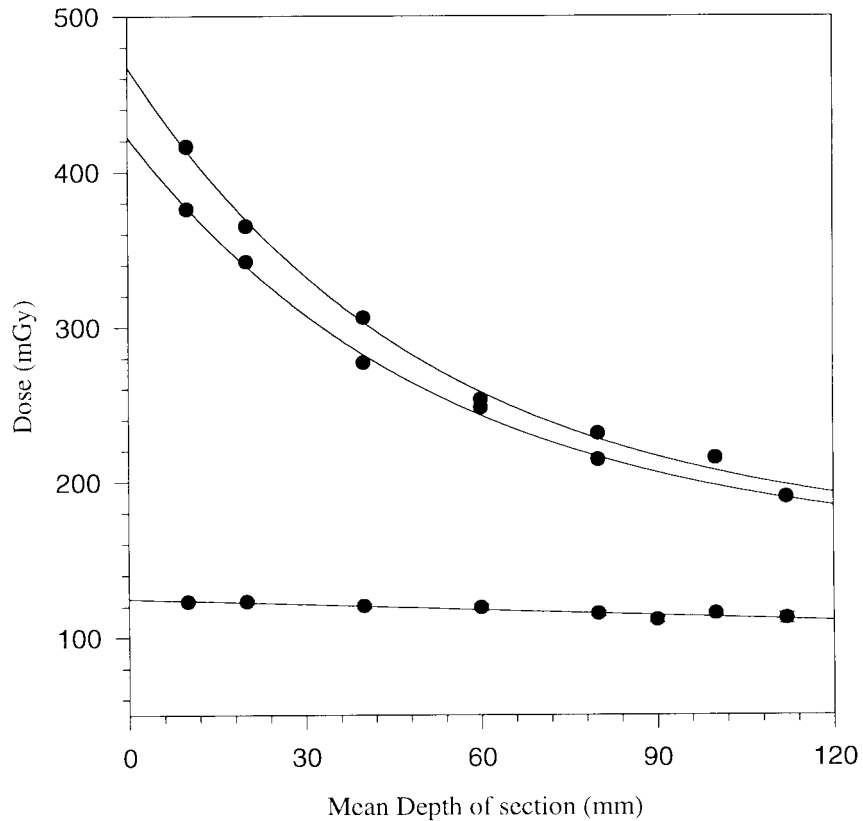


Fig. 8.18. (a) Typical OSL decay curve measured from an extracted brick quartz with a  $D_e$  of about 100 mGy.

(b) Depth dose profiles obtained from two different Chernobyl bricks. Each point represents 12 single aliquot dose determinations with an average calculated precision of 1-2%. Note that the error bars are within the symbols.

an exponential decay and a constant background. The fitted curves agree very well with the experimental data, providing further evidence that the random error estimation in the SAR protocol is reliable. Fig. 8.19 shows three further dose-depth

profiles obtained from Chernobyl bricks. The two upper curves represent the results from bricks that have been exposed from one side to external accidental photon doses and the exponential decay rates compare well with that obtained from a brick irradiated to 660 keV  $^{137}\text{Cs}$  photons in the laboratory (see section 8.7.3). The lower curve represents a brick that has not been exposed to any significant dose other than those from the internal radionuclides in the matrix and the ambient photon radiation including the cosmic radiation. Note that the error bars (precision) are within the symbols.



*Fig. 8.19. Typical dose-depth profiles measured from Chernobyl bricks using the SAR protocol. Note the error bars are within symbols.*

A large number of brick samples collected during field trips in Russia and Ukraine were measured during 1998 using blue light stimulation and the SAR protocol. Representative results from these measurements are presented in Table 8.9. In most cases dose-depth profiles were determined by measuring quartz samples that were extracted at intervals of 10 mm across the brick section.

*Table 8.9. Dose evaluation results (mGy) obtained from a variety of quartz samples extracted from bricks collected in the Chernobyl accident areas in Russia and Ukraine. The SAR protocol was used in all cases and stimulation was made using either blue LEDs (470 nm) delivering 18 mW/cm<sup>2</sup> at the sample or broad-band filtered from halogen lamp (420-550 nm) delivering 28 mW/cm<sup>2</sup>. An average of 15 aliquots were used for each dose determination.*

Depth (mm)	10	20	40	60	80	100
Loc. 1	105 ± 7.1	95 ± 5.1	97 ± 4.9	95 ± 4.7	90 ± 4.3	98 ± 6.4
Loc. 2	111 ± 0.8	111 ± 1.2	108 ± 1.1	107 ± 1.9	104 ± 1.4	104 ± 1.6
Loc. 3	331 ± 3.1	301 ± 4.5	244 ± 1.9	218 ± 2.2	188 ± 1.8	-
Loc. 4	366 ± 4.6	321 ± 2.7	269 ± 3.9	223 ± 4.4	203 ± 4.7	189 ± 6.5
Loc. 5	424 ± 10.8	353 ± 6.6	321 ± 4.3	265 ± 5.1	220 ± 4.6	204 ± 4.0
Loc. 6	152 ± 2.7	155 ± 1.4	120 ± 1.4	-	-	103 ± 1.7
Loc. 7	980 ± 18.0	745 ± 10.0	466 ± 8.0	339 ± 4.2	280 ± 5.3	213 ± 4.4
Loc. 8	525 ± 4.7	434 ± 2.8	331 ± 2.0	259 ± 2.6	235 ± 2.7	193 ± 2.2
Loc. 9	527 ± 12.0	472 ± 4.3	362 ± 4.5	283 ± 5.3	246 ± 2.8	219 ± 1.9
Loc. 10	867 ± 10.3	691 ± 4.1	527 ± 4.6	402 ± 7.2	323 ± 2.5	252 ± 3.2
Loc. 11	115 ± 1.1			89 ± 1.8		
Loc. 12	45 ± 1.1			43 ± 1.0		
Loc. 13	55 ± 0.6			60 ± 1.0		
Loc. 14	85 ± 2.8			69 ± 3.3		
Loc. 15	54 ± 3.3			35 ± 1.2		
Loc. 16	210 ± 7.0			165 ± 7.3		

### 8.7.5 Absolute errors and estimated precision of the equivalent dose

The dose received by quartz grains from internal natural radionuclides in the brick material can be as much as 5 mGy/year. The background dose can thus make up a considerable part of the of the total dose, particularly if bricks are collected from older buildings. As the background component is a major component of error in estimating the accrued accident dose it is important that this background component be minimised, and accurately determined.

The absolute accuracy of the total dose estimates obtained using the SAR protocol has been demonstrated for known age house bricks (< 100 years) and a precision of < 3% are readily achievable (see Table 8.8). The absolute uncertainties in the accident dose (i.e.  $D_e$  – natural background dose) derived from the results are probably dominated by systematic uncertainties such as those arising from the calibration of the beta source (typically ~ 3 %), and the estimation of the background dose. The overall uncertainty associated with the latter component is probably around 4 % for a known age sample, depending on the analytical method used to determine the dose rate (e.g. by some form of radio element analysis).

For a sample with  $D_e = 100 \pm 3$  mGy, and background =  $50 \pm 2$  mGy (equivalent to the natural dose in a 15-20 year old brick), the accident dose is  $50 \pm 4$  mGy. A typical minimum detection limit for a fallout dose in these circumstances would be about 12 mGy (3 standard errors). This detection limit can most easily be optimised by selecting buildings that were built immediately before the accident. Obviously, measurement should be made as soon after the

accident as possible. Close to detection limits, the largest single source of uncertainty will probably arise from the estimation of the background dose-rate, and it is in this area that effort should be concentrated to improve sensitivity

### 8.7.6 Summary

The application of the single-aliquot regenerative-dose method to the estimation of equivalent dose in quartz extracts from modern house bricks exposed during a nuclear accident has been illustrated. High precision (1 % s.e. for  $n = 15$ ) in the measurement of equivalent dose is readily achievable, and with present methods we estimate a detection limit of about 12 mGy for the accident component on a natural background of 50 mGy. To improve this detection limit significantly, uncertainties in the estimates of the natural dose-rates must be reduced.

The importance of obtaining dose-depth profiles into materials collected for dosimetry has been demonstrated especially in view of getting information about the average energy of the photon radiation present during the accident

## 8.8 Retrospective Dosimetry - Conclusions

In the Chernobyl area, locations that have remained inhabited have officially recorded contamination levels of up to 40 Ci/km<sup>2</sup> but more commonly < 20 mCi/km<sup>2</sup>. In the majority of areas that are being investigated, the main contributor to external gamma dose is <sup>137</sup>Cs (<sup>131</sup>I was the main source of internal dose, derived from ingested milk). The integrated external transient dose resulting from these levels of contamination is expected to be significantly less than 100 mGy. This is in a very demanding dose range for luminescence since the total background dose is typically 40-60 mGy for a house built in the mid-1970s. The challenge in Chernobyl and similar studies is thus to routinely evaluate transient doses of less than 100 mGy with a precision of  $\pm 10$  %.

Optically stimulated luminescence techniques with ceramic materials, as discussed in this Chapter, appear to have widespread suitability for retrospective dosimetry. Porcelain provides a widely available dosimeter material for measurements in shielded locations and its glazed surface also provides the advantage of low fall out retention when used in exterior locations. In rural areas in Russia and the Ukraine, porcelain insulators are more common than brick. The use of bricks from walls to obtain dose depth profiles provides important information concerning the nature of the time-averaged incident external photon field. Because of their speed and high precision, the new OSL measurement techniques have shown major advantages in routine dose evaluations and in the evaluation of depth-dose profiles using cut brick sections.

In the case of populated areas that have received radioactive fallout, the combined use of luminescence and computational modelling provides a means of validating calculated values of absorbed dose in air for contaminated areas and to provide dose values for subsequent modelling of dose to population groups within the area studied. The validation and use of models supported by direct measurements is crucial to epidemiological investigations and subsequently to arriving at a more accurate assessment of risk to members of the population exposed to ionising radiation.

The selection of appropriate samples is one of the most important aspects of retrospective dosimetry since the interpretation and use of the results relies heavily on assumptions made concerning the relationship between the sample and the radiation sources contributing to the transient dose. So far a comprehensive sampling methodology has yet to emerge. Wider use of the method is likely

to accelerate the demand for standard procedures to be established so that the selection of appropriate samples for both accrued dose and dose rate evaluation according to the type of building and dosimetry problem can be optimised. On the basis of current developments, it is likely that computational modelling will be used to a greater extent in sample selection as a predictive tool to test consistency with calculation for given source inventories and source distributions; such an approach is being pursued in current Chernobyl-related studies which are being published within the EU's Fourth Framework Programme.

## 9 Concluding Remarks

Summaries of the investigations presented in this thesis are provided in the closing sections of each of the respective chapters, and the reader is referred to these for specific summary statements. This final statement is to briefly reflect on the general philosophy of the specific areas described and to consider the likely direction of future studies.

Of necessity, this thesis is multidisciplinary in nature, combining aspects of measurement technique developments and aspects of applied luminescence dosimetry research. It has been shown that although we lack a full understanding of the physical processes in OSL, important information about the general OSL dosimetric features of some natural materials and artificial ceramics can be generated. This will help to improve future physical modelling and the general understanding of luminescence processes.

The present work has particularly concentrated on the development of OSL techniques and the characterisation of OSL features specific to quartz, feldspars, aluminiumoxide and porcelain for use in retrospective accident dosimetry.

Chapter 2 reviews the basic principles of TL and OSL and the potential advantages of using OSL methods over TL methods have been outlined.

Chapter 3 reviews TL and OSL apparatus, techniques and methods developed at Risø over the last few years especially for use in dating and retrospective dosimetry with ceramics. The use of recently developed bright LEDs as OSL stimulation light source has contributed significantly to enhancing sensitivity and reproducibility. The development of apparatus for analysing the OSL signals from single sand-sized grains has the potential to provide a more detailed analysis of samples prepared for luminescence measurements and a higher accuracy in dose determination. This is possible because of the ability to discriminate against the contribution from insensitive and partially bleached grains.

Chapters 4 and 5 review some OSL characteristics of quartz and feldspars. It is demonstrated that doses in the order of 1 mGy can be measured using blue-light stimulation on some fired (archaeological) quartz samples. A comprehensive investigation of the sensitivity changes occurring in sedimentary quartz as a function of annealing was carried out and the results show that distinct sensitivity changes occur at temperatures related to the known phase changes in quartz. It is further concluded that the results do not support the idea that any prior dose (pre-dose) is responsible for the annealing-induced sensitivity changes.

Feldspars have not been used intensively in retrospective dosimetry so far. This is mainly due to the anomalous fading of this material. However, the high IRSL brightness, wide dose range and the widespread availability of a variety of feldspars in nature make this material a potential candidate for use in retrospective dose assessment. The known excitation resonance found for feldspars in the infrared range makes OSL equipment for this material very simple, and opens

up the possibility of using portable instrumentation for measuring OSL from feldspars directly on location at the field site.

Chapters 6 and 7 review some OSL characteristics of  $\text{Al}_2\text{O}_3:\text{C}$  and porcelain. OSL from  $\text{Al}_2\text{O}_3:\text{C}$  gives a potentially higher yield than TL. This is mainly because of a dramatic loss of luminescence when heating the material (thermal quenching). The energy response (matches that of quartz) and the high sensitivity has made  $\text{Al}_2\text{O}_3:\text{C}$  an attractive OSL dosimeter for short-term determination of the environmental dose rates. This is a further potential application of portable OSL instrumentation directly at the field site.

The OSL characteristics of porcelain materials have been shown in several cases to be dominated by the small contents of quartz and  $\text{Al}_2\text{O}_3$  found in most porcelain matrixes. This has made OSL a potential method for measuring doses from porcelain items collected in nuclear accident areas. However, the limitation in the use of porcelain for dosimetry lies in the transparency of most crockery. This makes it necessary to extract samples suitable for OSL measurements from depths greater than 2 mm, because of the optical bleaching of the outer layers. A similar bleaching effect was found for the TL signal from porcelain.

Chapter 8 gives a description of the different OSL methods studied at Risø for applications in retrospective accident dosimetry. Due to its generally high OSL sensitivity, quartz extracted from fired bricks has been used to determine the fallout doses. New measurement protocols based on the single-aliquot regenerative-dose method have been developed which effectively correct for any sensitivity changes occurring during the regeneration cycle. In combination with the recently developed blue LED stimulation light sources, these protocols have enabled equivalent doses lower than 20 mGy to be measured with very low measurement uncertainty. A precision of the order of 1% can usually be obtained in the determination of the equivalent dose (at the 100 mGy level) when using 15 different aliquots.

The new single grain OSL technique developed in the last 12 months has opened up the possibility of including a variety of new materials potentially useful for retrospective dosimetry. Such materials are e.g. mortar and concrete where single grain analysis of imbedded sand (quartz) can be used to discriminate the emission from partially bleached (poorly zeroed) grains and thereby facilitate a reliable dose determination. It is envisaged that single grain measurement methods and analysis techniques will be intensively studied at many dosimetry laboratories in the near future.

The readers' attention should be drawn to the "Preface and Acknowledgement" at the beginning of this thesis.

## 10 References

- Aitken M.J., Tite M.S. and Reid J. (1964) Thermoluminescent dating of ancient ceramics. *Nature* 202, 1032-1033.
- Aitken M.J., Zimmerman D.W. and Fleming S.J. (1968) Thermoluminescent dating of ancient pottery. *Nature* 219, 442-444.
- Aitken M.J. (1985) *Thermoluminescence Dating*. Academic Press. London.
- Aitken M.J. and Smith B.W. (1988) Optical dating: recuperation after heating. *Quat. Sci. Rev.* 7, 387-393.
- Aitken M.J. (1990) Optical dating of sediments: Initial results from Oxford. *Archaeometry* 32, 19-31.
- Aitken M.J. (1998) *An introduction to optical dating*. Oxford University Press. Oxford.
- Akber R.A., Prescott J.R., and Robertson G.B. (1988). The 100°C Thermoluminescence emission from high-fired ceramics: A three dimensional view. *Nucl. Tracks. Radiat. Meas.* 14, 21-25.
- Akselrod M.S., Kortov V.S., Kravetsky D.J. and Gotlib V.I. (1990) Highly sensitive thermoluminescent anion-defective Al<sub>2</sub>O<sub>3</sub>:C single crystal detector. *Radiat. Prot. Dosim.* 32, 15-29.
- Akselrod M.S. and Kortov V.S. (1990) Thermoluminescent and exoemission properties of new high-sensitivity TLD  $\alpha$ -Al<sub>2</sub>O<sub>3</sub>:C crystals. *Radiat. Prot. Dosim.* 33, 123-126.
- Akselrod M.S., Kortov V.S. and Gorelova E.A. (1993) Preparation and properties of  $\alpha$ -Al<sub>2</sub>O<sub>3</sub>:C. *Radiat. Prot. Dosim.* 47, 159-164.
- Akselrod M.S., Lucas A.C., Polf J.C. and McKeever S.W.S. (1998) Optically stimulated luminescence of Al<sub>2</sub>O<sub>3</sub>. *Radiat. Meas.* 29, 391-400.
- Bailey R.M., Smith B.W. and Rhodes E.J. (1997) Partial bleaching and the decay form characteristics of quartz OSL. *Radiat. Meas.* 27, 123-136.
- Bailey R.M. (1998) Depletion of the quartz OSL signal using low photon energy stimulation. *Ancient TL*, 16, 33-36.
- Bailiff I.K., Morris D.A. and Aitken M.J. (1977) A rapid interference spectrometer: Application to low level thermoluminescence emission. *J. Phys. E: Sci. Instrum.* 10, 1156-1160.
- Bailiff I.K. and Poolton N.R.J. (1991) Studies of charge transfer mechanisms in feldspars. *Nucl. Tracks Radiat. Meas.* 18, 111-118.
- Bailiff I.K. (1993) Measurement of the stimulation spectrum (1.2-1.7 eV) for a specimen of potassium feldspar using a solid state laser. *Radiat. Prot. Dosim.* 47, 649-653.
- Bailiff I.K. and Barnett S.M. (1994) Characteristics of infrared-stimulated luminescence from a feldspar at low temperatures. *Radiat. Meas.*, 23, 541-545.
- Bailiff I.K. (1995) The use of ceramics for retrospective dosimetry in the Chernobyl exclusion zone. *Radiat. Meas.* 24, 507-512.
- Bailiff I.K. and Stepanenko V. (1996) Final Report, Experimental Collaboration Project ECP10. In: *Retrospective Dosimetry and Dose Reconstruction* (eds. Bailiff I.K. and Stepanenko V.), EUR 16540EN, p. 115. European Commission.
- Bailiff I.K. (1997) Retrospective dosimetry with ceramics. *Radiat. Meas.* 27, 923-941.
- Baker R. (1991): Recent developments in firing whitewares. *Br. Ceram. Trans. J.* 90 36-38

- Banerjee D., Bøtter-Jensen L. and Murray A.S. (1999a) Retrospective dosimetry: Preliminary use of the single aliquot regeneration (SAR) protocol for the estimation of the equivalent dose in quartz from young house bricks. *Radiat. Prot. Dosim.* 84, 421-427.
- Banerjee D., Bøtter-Jensen L. and Murray A.S. (1999b) Estimation of the quartz equivalent dose in retrospective dosimetry using the single-aliquot regenerative-dose protocol. *Appl. Radiat. Isotop.* (in press).
- Banerjee D., Murray A.S., Bøtter-Jensen L. and Lang A. (1999c) Equivalent dose estimation from single aliquots of polymineral fine grains. (Submitted by April 1999 to *Radiat. Meas.*).
- Berggraaf D. and Haskell E.H. (1994) A software package for TL/OSL spectrometry and extraction of glow curves from individual grains. *Radiat. Meas.* 23, 537.
- Bluszcz A. and Bøtter-Jensen L. (1993) Calibration of a beta source using TL and OSL on quartz. *Risø-I-Report No.* 725(EN).
- Bluszcz, A.; Bøtter-Jensen, L. (1995) Dosimetric properties of natural quartz grains extracted from fired materials. *Radiat. Meas.* 24, 465-468.
- Braünlich P., Gasiot J., Fillard J.P. and Castagné M. (1981) Laser heating of thermoluminescent dielectric layers. *Appl. Phys. Phys. Lett.* 39 (9), 769-771.
- Briesmeister J.F. (Ed.) (1986) MNCP – A general Monte Carlo code for neutron and photon transport. Version 3A. Los Alamos National Laboratory.
- Bøtter-Jensen L. and Bechmann (1968) A versatile automatic sample changer for reading of thermoluminescence dosimeters and phosphors. *Proc. 2nd Int. Conf. on Luminescence Dosimetry, Gatlinburg, CONF-680920*, 281-290. U.S. National Bureau of Standards, Washington D.C.
- Bøtter-Jensen, L. (1978) A simple, hot N<sub>2</sub>-gas TL reader incorporating a post-irradiation annealing facility. *Nucl. Instrum. Methods* 153, 413-418.
- Bøtter-Jensen L. and Bundgaard J. (1978) An automatic reader for TL dating. *PACT* 2, 48-56.
- Bøtter-Jensen L. and Mejdahl V. (1980) Determination of archaeological doses for TL dating using an automated TL apparatus. *Nucl. Instrum. and Methods*, 175, 213-215.
- Bøtter-Jensen L., Bundgaard J. and Mejdahl V. (1983) An HP-85 microcomputer-controlled automated reader system for TL dating. *PACT* 9, 343-349.
- Bøtter-Jensen L. and Mejdahl V. (1985) Determination of potassium in feldspars by beta counting using a GM multicounter system. *Nucl. Tracks Radiat. Meas.*, 10, 663-666.
- Bøtter-Jensen L. and Mejdahl V. (1988) Assessment of beta dose-rate using a GM multicounter system. *Nucl. Tracks Radiat. Meas.* 14, 187-191.
- Bøtter-Jensen L. (1988) The automated Risø TL dating reader system. *Nucl. Tracks Radiat. Meas.* 14, 177-180.
- Bøtter-Jensen L., Ditlevsen C. and Mejdahl V. (1991) Combined OSL (infrared) and TL studies of feldspars. *Nucl. Tracks Radiat. Meas.* 18, 257-263.
- Bøtter-Jensen L. and Duller G.A.T. (1992) A new system for measuring OSL from quartz samples. *Nucl. Tracks. Radiat. Meas.* 20, 549-553.
- Bøtter-Jensen L., Jungner H. and Mejdahl V. (1993) Recent developments of OSL techniques for dating quartz and feldspars. *Radiat. Prot. Dosim.*, 47, 16, 643-648.
- Bøtter-Jensen L., Poolton N.R.J., Willumsen F. and Christiansen H. (1994a) A compact design for monochromatic OSL measurements in the wavelength range 380-1020 nm. *Radiat. Meas.* 23, 519-522.
- Bøtter-Jensen L., Duller G.A.T. and Poolton N.R.J. (1994b) Excitation and emission spectrometry of stimulated luminescence from quartz and feldspars. *Radiat. Meas.* 23, 613-616.

- Bøtter-Jensen L. (1995) Retrospective radiation dose reconstruction using optically stimulated luminescence on natural materials. In Proceedings of the International Workshop on Scientific Bases for Decision Making after a Radioactive Contamination of an Urban Environment, Rio de Janeiro and Goiania, Brazil, Aug. 29 – Sept. 2, 1994. IAEA TECDOC.
- Bøtter-Jensen L. and Thompson I.M.G. (1995) An international intercomparison of passive dosimeters, electronic dosimeters and dose rate meters used for environmental radiation measurements. *Radiat. Prot. Dosim.* 60, 201-211.
- Bøtter-Jensen L., Agersnap Larsen N., Mejdahl V. Poolton N.R.J., Morris M.F. and McKeever S.W.S. (1995a) Luminescence sensitivity changes in quartz as a result of annealing. *Radiat. Meas.* 24, 535-541.
- Bøtter-Jensen L., Jungner H. and Poolton N.R.J. (1995b) A continuous OSL scanning method for analysis of radiation depth-dose profiles in bricks. *Radiat. Meas.*, 24, 525-529.
- Bøtter-Jensen, L. (1996) Retrospective radiation dosimetry using optically stimulated luminescence on natural materials and ceramics for assessing population doses in nuclear accidental areas. In: Proceedings. The Nordic Society for Radiation Protection Seminar, 26-29 Aug 1996, Reykjavik, Iceland. Walderhaug, T.; Gudlaugsson, E.P. (eds.), (Nordic Radiation Protection Society, Reykjavik, 1997) p. 273-278
- Bøtter-Jensen L., Markey B.G., Poolton N.R.J. and Jungner H. (1996) Luminescence properties of porcelain ceramics relevant to retrospective radiation dosimetry. *Radiat. Prot. Dosim.*, 65, 1-4, 369-372.
- Bøtter-Jensen L. and McKeever S.W.S. (1996) Optically stimulated luminescence dosimetry using natural and synthetic materials. *Radiat. Prot. Dosim.* 65, 1-4, 273-280.
- Bøtter-Jensen L., Agersnap Larsen N., Markey B.G. and McKeever S.W.S. (1997)  $\text{Al}_2\text{O}_3:\text{C}$  as a sensitive OSL dosimeter for rapid assessment of environmental photon dose rates. *Radiat. Meas.*, 27, 295-298.
- Bøtter-Jensen L. (1997) Luminescence techniques: instrumentation and methods. *Radiat. Meas.* 17, 749-768.
- Bøtter-Jensen L. and Murray A.S. (1999) Developments in optically stimulated luminescence techniques for dating and retrospective dosimetry. *Radiat. Prot. Dosim.* 84, 307-316.
- Bøtter-Jensen L., Mejdahl V. and Murray A.S. (1999a) New light on OSL. *Quat. Sci. Rev.* 18/2, 303-309.
- Bøtter-Jensen L., Duller G.A.T., Murray A.S. and Banerjee D. (1999b) Blue light emitting diodes for optical stimulation of quartz in retrospective dosimetry and dating. *Radiat. Prot. Dosim.* 84, 335-340.
- Bøtter-Jensen L., Banerjee D., Jungner H. and Murray A.S. (1999c) Retrospective assessment of environmental dose rates using optically stimulated luminescence from  $\text{Al}_2\text{O}_3:\text{C}$  and quartz. *Radiat. Prot. Dosim.* 84, 537-542.
- Bøtter-Jensen L. and Jungner H. (1999) Application of luminescence techniques in retrospective dosimetry. *Acta Physica Polonica A*, 95/2, 275-286.
- Bulur E., An alternative technique for optically stimulated luminescence (OSL) experiments. *Radiat. Meas.*, 26, 701-7009 (1996).
- Chen R. and Fogel G. (1993). Superlinearity in thermoluminescence revisited. *Rad. Protect. Dosim.* 47 (1/2), 23-26.
- Chen R., Fogel G., and Kristianpoller N. (1994). Theoretical account of the sensitisation and de-sensitisation in quartz. *Rad. Meas.* 23, 277-279.
- Chen R., Yang X.H., and McKeever S.W.S. (1988). Strongly supralinear dose dependence of thermoluminescence in synthetic quartz, *J. Phys. D: Appl. Phys.* 21, 1452-1457.

- Clark R.J. and Sanderson D.C.W. (1994) Photostimulated luminescence excitation spectroscopy of feldspars and micas. *Radiat. Meas.*, **23**, 641-646.
- Colyott L.E., Akselrod M.S. and McKeever S.W.S. (1996) Phototransferred thermoluminescence in  $Al_2O_3:C$ . *Radiat. Prot. Dosim.*, **65**, 185-189.
- Daniels F., Boyd C.A. and Saunders D.F. (1953) Thermoluminescence as a research tool. *Science* **117**, 343-349.
- Deer W.A., Howie R.A., and Zussman J. (1992) *An Introduction to the Rock Forming Minerals*, 457-472, 2nd Edition Longman Scientific and Technical.
- Ditlevsen C. and Huntley D.J. (1994) Optical excitation of trapped charges in quartz, potassium feldspars and mixed silicates: the dependence on photon energy. *Radiat. Meas.*, **23**, 675-682.
- Duller G.A.T. (1991) Equivalent dose determination using single aliquots. *Nucl. Tracks Radiat. Meas.* **18**, 371-378.
- Duller G.A.T. and Wintle A.G. (1991) On infrared stimulated luminescence at elevated temperatures. *Nucl. Tracks Radiat. Meas.* **18**, 379-384.
- Duller, G.A.T. and Bøtter-Jensen, L. (1993) Luminescence from potassium feldspars stimulated by infrared and green light. *Radiat. Prot. Dosim.* **47**, 683-688.
- Duller G.A.T. (1995) Luminescence dating using single aliquots: methods and applications. *Radiat. Meas.* **24**, 217-226.
- Duller G.A.T. and Bøtter-Jensen L. (1996) Comparison of optically stimulated luminescence signals from quartz using different stimulation wavelengths. *Radiat. Meas.* **26**, 603-609.
- Duller G.A.T. (1997) Behavioural studies of stimulated luminescence from feldspars. *Radiat. Meas.* **27**, 663-694.
- Duller G.A.T. and Bøtter-Jensen L. (1997) Optically stimulated luminescence emission spectra from feldspars as a function of sample temperature. *Radiat. Meas.*, **27**, 145-151.
- Duller G.A.T., Bøtter-Jensen L. and Markey B.G. (1997) A luminescence imaging system based on a charge coupled device (CCD) camera. *Radiat. Meas.*, **27**, 91-99.
- Duller G.A.T., Bøtter-Jensen L., Kohsiek P. and Murray A.S. (1999a) A high-sensitivity optically stimulated luminescence scanning system for measurement of single sand-sized grains. *Radiat. Prot. Dosim.* **84**, 325-330.
- Duller G.A.T., Bøtter-Jensen L., Murray A.S. and Truscott A.J. (1999b) Single grain laser luminescence (SGLL) measurements using a novel automated reader. *Nucl. Instr. Methods B* (in press).
- Duller G.A.T., Bøtter-Jensen L. and Mejdahl V. (1999c) An automated iterative procedure for determining palaeodoses using the SARA method. *Quat. Sci. Rev.*, **18/2**, 293-301.
- Galloway R.B. (1993) Stimulation of luminescence using green light emitting diodes. *Radiat. Prot. Dosim.* **47**, 679-682.
- Galloway R.B. (1994) On the stimulation of luminescence with green light emitting diodes. *Radiat. Meas.* **23**, 2/3, 547-550.
- Galloway R.B. (1996) Equivalent dose determination using only one sample: alternative analysis of data obtained from infrared stimulation of feldspars. *Radiat. Meas* **26**, 103-106.
- Galloway R.B., Hong D.G. and Napier H.J. (1997) A substantially improved green light emitting diode system for luminescence stimulation. *Meas. Scien. and Techn.* (in press).
- Godfrey-Smith D.I., Huntley D.J. and Chen W.-H. (1988) Optical dating studies of quartz and feldspar sediment extracts. *Quat. Sci. Rev.* **7**, 373-380.
- Godfrey-Smith D.I. (1991) Optical dating studies of sediment extracts. D.Phil. thesis, Simon Fraser University, Burnaby, Canada.

- Godfrey-Smith D.I. and Haskell E.U. (1993) Application of optically stimulated luminescence to the dosimetry of recent radiation events monitoring low total absorbed dose. *Health Phys.* 65, 396-404.
- Godfrey-Smith D.I. and Cada M. (1996) IR stimulation spectroscopy of plagioclase and potassium feldspars, and quartz. *Radiat. Prot. Dosim.*, 66, 379-385.
- Harris A.M. and Jackson J.H. (1970) A rapid scanning spectrometer for the region 200-850 nm: application of thermoluminescent emission spectra. *J. Phys.* E3, 374.
- Hashimoto T., Hayashi Y., Koyanagi A., Yokosaka K. and Kimura K. (1986) Red and blue coloration of thermoluminescence from natural quartz sands. *Nucl. Tracks Radiat. Mes.* 11, 229-235.
- Hashimoto T., Sakaue S., and Ichino M. (1994). Dependence of TL-property changes of natural quartzes on aluminium contents accompanied by thermal annealing treatment. *Radiat. Meas.* 23, 293-299.
- Hashimoto T., Notoya S., Ojima T. and Hoteida M. (1995) Optically stimulated luminescence (OSL) and some other luminescence images from granite slices exposed with radiations. *Radiat. Meas.*, 24, 227-237.
- Haskell E.H. (1993a). Retrospective accident dosimetry using environmental materials: the role of thermoluminescence. *Nucl. Tracks Radiat. Meas.* 21, 87-93.
- Haskell E.H. (1993b) Accident dosimetry using environmental materials. *Radiat. Prot. Dosim.* 47, 297-303.
- Huntley D.J. Godfrey-Smith D.I. and Thewalt M.L.W. (1985) Optical dating of sediments. *Nature* 313, 105-107.
- Huntley D.J., Godfrey-Smith D.I., Thewalt M.L.W. and Berger G.W. (1988) Thermoluminescence spectra of some mineral samples relevant to thermoluminescence dating. *Journ. Lum.* 39, 123-136.
- Huntley D.J., Godfrey-Smith D.I. and Haskell E.H. (1991) Light-induced emission spectra from some quartz and feldspars. *Nucl. Tracks Radiat. Meas.* 18, 127-131.
- Huntley D.J., Short M.A. and Dunphy K. (1996) Deep traps in quartz and their use for optical dating. *Canadian Journal of Physics* 74, 81-91.
- Hübner S. and Göksu H.Y. (1997) Retrospective dosimetry using the OSL-predose effect in porcelain. *Appl. Radiat. Isot.* 48, 1231-1235.
- Hütt G., Jaek I. and Tchonka J. (1988) Optical dating: Feldspars' optical response stimulation spectrum. *Quat. Sci. Rev.* 7, 381-386.
- Hütt G. and Jaek I. (1989) Infrared stimulated photoluminescence dating of sediments. *Ancient TL*, 7, 48-51.
- Hütt G. and Jaek I. (1990) Photoluminescence dating on alkali feldspars: Physical ground, equipment and some results. *Radiat. Prot. Dosim.* 34, 73-74.
- Hütt G., Brodski L., Bailif I.K., Göksu Y., Haskell E.H., Junger H., and Stoneham D. (1993). Accident dosimetry using environmental materials collected from regions downwind of Chernobyl: a preliminary evaluation. *Radiat. Protect. Dosim.* 47 (1/4), 307-313.
- Jaek I., Hütt G., Seeman V. and Brodski L. (1995) Luminescence and ESR of the natural alkali feldspars, extracted from sediments, doped by probe impurities. *Radiat. Meas.* 24, 557-563.
- Jungner, H. and Bøtter-Jensen, L. (1993). A study of sensitivity change of OSL signals from quartz and feldspars. *Radiation Measurements* 23, 621-624.
- Kortov V.S., Milman I.I., Kirpa V.I. and Lesz J. (1994) Some features of Al<sub>2</sub>O<sub>3</sub>:C dosimetric thermoluminescent crystals. *Radiat. Prot. Dosim.* 55, 279-283.
- Krause W.E., Krbetschek M.R. and Stolz W. (1997) Dating of quaternary lake sediments from the Schirmacher Oasis (East Antarctica) by infra-red stimulated luminescence (IRSL) detected at the wavelength of 560 nm. *Quat. Geochron.* 16, 387-392.

- Kristianpoller N., Chen R., and Israeli M. (1974). Dose dependence of thermoluminescence peaks. *J. Phys. D: Appl. Phys.* **7**, 1063-1072.
- Lamothe M., Balescu S. and Auclair M. (1994) Natural IRSL intensities and apparent luminescence ages of single feldspar grains extracted from partially bleached sediments. *Radiat. Meas.* **23**, 555-562.
- Landolt-Bornstein (1982) Physical properties of rocks, Group V. *Geophys. Space Res.* 1b, 254.
- Lapraz D., Iacconi P., Paviller D., and Guilhot B. (1991) Thermostimulated luminescence and fluorescence of  $\alpha$ -Al<sub>2</sub>O<sub>3</sub>:Cr<sup>3+</sup> samples (ruby). *Phys. Stat. Solidi A* 126, 521-531.
- Larsen Agersnap N. (1999) Dosimetry based on thermally and optically stimulated luminescence. Risø-R-Report no. 1090 (EN).
- Lee K.H. and Crawford J.M. (1979) Luminescence of the F-centre in sapphire. *Phys. Rev. BR*, 3217-3229.
- Leonard R.S. (1992): Silica sand - its development and use in clay bodies. *Br. Ceram. Trans. J.* **91** 131-133
- Li S.-H. and Wintle, A.G. (1992). Luminescence sensitivity changes due to bleaching of sediments. *Nuclear Tracks and Radiation Measurements* **20**, 567-573.
- Li S-H. (1994) Optical dating: insufficiently bleached sediments. *Radiat. Meas.* **23**, 563-567.
- Lloyd D.C., Edwards A.A., Sevankaev A.V., Bauchinger M., Braselmann H., Georgiadou-Smacher V., Salassidus k., Darroudi F., Natajan A.T., vander Berg M., Fedortseva R., Mfomina Z., Maznik N.A., Melnov S., Politti F., Pantelias G., Pibuskaja M. and Vorobtsova I.E. (1996) Retrospective dosimetry by chromosomal analysis. In Proceedings of the EU Conference on the Radiological Consequences of the Chernobyl Accident (EUR 16544EN), 965-974.
- Luff B.J. and Townsend P.D. (1993) High sensitivity thermoluminescence spectrometer. *Meas. Sci. Technol.* **4**, 65-71.
- Majumdar R., Gilbert E. and Brook R.J. (1986): Kinetics of densification of alumina-zirconia ceramics. *Br. Ceram. Trans. J.* **85** 156-160
- Markey B.G., Bøtter-Jensen L., Poolton N.R.J., Christiansen H.E. and Willumsen F. (1996) A new sensitive system for measurement of thermally and optically stimulated luminescence *Radiat. prot. Dosim.* **66**, 1/4, 413-418.
- Markey B.G., McKeever S.W.S., Akselrod M.S., Bøtter-Jensen L. Agersnap Larsen N. and Colyott L.E. (1996) The temperature dependence of optically stimulated luminescence from  $\alpha$ -Al<sub>2</sub>O<sub>3</sub>:C. *Radiat. Prot. Dosim.* **65**, 185-189.
- Markey B.G., Bøtter-Jensen L. and Duller G.A.T. (1997) A new flexible system for measuring thermally and optically stimulated luminescence *Radiat. Meas.*, **27**, 83-89.
- Martini M., Paravisi S. and Liguori C. (1996) A new high sensitive spectrometer for 3-D thermoluminescence analysis. *Radiat. Prot. Dosim.* **66**, 447-450.
- Mattern P.L., Lengweiler K. and Levy P.W. (1971) Apparatus for the simultaneous determination of thermoluminescent intensity and spectral distribution. *Mod. Geol.*, **2**, 293.
- McFee C.J. and Tite M.S. (1994) Investigations into the thermoluminescence properties of single quartz grains using an imaging photon detector. *Radiat. Meas.*, **23**, 355-360.
- McKeever S.W.S., Strain J.A., Townsend P.D., and Udval P. (1983). Effects of thermal cycling on the thermoluminescence and radioluminescence of quartz, *PACT* **9**, 123-132.
- McKeever S.W.S., Chen C.Y., and Halliburton L.E. (1984). Point defects and the predose effect in natural quartz. *Nucl. Tracks Radiat. Meas.* **10**, 489-495.

- McKeever S.W.S. and Morris M.F. (1994) Computer simulations of optical bleaching of TL and OSL signals. *Radiat. Meas.* **23**, 301-306.
- McKeever S.W.S., Moscowitch M. and Townsend P. (1995) Thermoluminescence dosimetry materials: properties and uses. Nuclear Technology publishing, Kent, UK.
- McKeever S.W.S., Markey B.G. and Akselrod M.S. (1996a) Pulsed optically-stimulated luminescence dosimetry using  $\alpha$ -Al<sub>2</sub>O<sub>3</sub>:C. *Radiat. Prot. Dosim.* **65**, 267-272.
- McKeever S.W.S., Bøtter-Jensen, L., Agersnap Larsen, N. Mejdahl, V. and Poolton, N.R.J. (1996b). Optically stimulated luminescence sensitivity changes in quartz due to repeated use in single aliquot readout: experiments and computer simulations. *Radiation Protection Dosimetry*, **65**, 49-54.
- McKeever S.W.S., Bøtter-Jensen L., Agersnap Larsen N. and Mejdahl V. (1997a). OSL sensitivity changes during single aliquot procedures. Computer simulations. *Radiat. Meas.*, **27**, 75-82.
- McKeever S.W.S., Bøtter-Jensen L., Agersnap Larsen N. and Duller, G.A.T. (1997b) Temperature dependence of OSL decay curves: Experimental and theoretical aspects. *Radiat. Meas.* v. 27 p. 161-170.
- Meckbach R. and Chumak V. (1996) Reconstruction of the external dose of evacuees from the contaminated areas based on simulation modelling. In Proceedings of the EU Conference on the Radiological Consequences of the Chernobyl Accident (EUR 16544EN), 965-974.
- Mejdahl V. (1969) Thermoluminescence dating of ancient Danish ceramics. *Archaeometry* **11**, 99-104.
- Mejdahl V. (1983) Feldspar inclusion dating of ceramics and burnt stones. *PACT* **9**, 351-364.
- Mejdahl V. (1985) Thermoluminescence dating based on feldspars. *Nucl. Tracks Radiat. Meas.* **10**, 133-364.
- Mejdahl V. (1986) Thermoluminescence dating of sediments. *Radiat. Prot. Dosim.* **17**, 219-222.
- Mejdahl V. (1990) Thermoluminescence dating. *Norw. Arch. Rev.*, **23**, 21-29.
- Mejdahl V. and Bøtter-Jensen L (1994) Luminescence dating of archaeological materials using a new technique based on single aliquot measurements. *Quat. Sci. Rev. (Quat. Geochr.)* **13**, 551-554.
- Mejdahl V. and Christiansen H. (1994). Procedures used for luminescence dating of sediments. *Quat. Geochron.* **13**, 403-406.
- Mejdahl V. and Bøtter-Jensen L. (1997) Experience with the SARA OSL method. *Radiat. Meas.*, **27**, 291-294.
- Mejdahl (1997) Private communication.
- Mische E.F. and McKeever S.W.S. (1990). Mechanisms of supralinearity in LiF thermoluminescence dosimeters. *Radiat. Protect. Dosim.* **29**, 237-244 .
- Murray A.S., Martin R., Johnston A. and Martin P. (1987) Analysis for naturally occurring radionuclides at environmental concentrations by gamma spectrometry. *Journ. of Radioan. And Nucl. Chem., Artikels* **115**, 263-281.
- Murray A.S., Olley J.M. and Caitcheon G.C. (1995) Measurement of equivalent doses in quartz from contemporary water-lain sediments using optically stimulated luminescence. *Quat. Sci. Rev. (Quat. Geochr.)* **14**, 365-371.
- Murray A.S. (1996) Developments in optically stimulated luminescence and photo-transferred thermoluminescence dating of young sediments. Application to a 2000-year sequence of flood deposits. *Geochim. et Cosmochim. Acta*, **60**, 565-576.
- Murray, A.S. (1996). Incomplete stimulation of luminescence in young quartz sediments and its effect on the regenerated signal. *Radiation Measurements* **26/2**, 221-231.

- Murray A.S., Roberts R.G. and Wintle A.G. (1997) Equivalent dose measurement using a single aliquot of quartz. *Radiat. Meas.*, 27, 171-184.
- Murray A.S. and Roberts R.G. (1997) Determining the burial time of single grains of quartz using optically stimulated luminescence. *Earth Planet. Sci. Lett.* 152, 163-180.
- Murray A.S. and Wintle A.G. (1998) Factors controlling the shape of the OSL decay curve in quartz. *Radiat. Meas.* 29, 65-80.
- Murray A.S. and Roberts R.G. (1998) Measurement of the equivalent dose in quartz using a regenerative-dose single-aliquot protocol. *Radiat. Meas.* 29, 503-515.
- Murray A.S. and Mejdahl V. (1999) Comparison of regenerative-dose single-aliquot and multiple-aliquot (SARA) protocols using heated quartz from archaeological sites. *Quat. Sci. rev.* 18/2, 223-230.
- Murray A.S. and Wintle A.G. (1999) Isothermal decay of optically stimulated luminescence in quartz. *Radiat. Meas.* 30, 119-126.
- Olley J.M., Murray A.S. and Roberts R.G. (1996) The effects of disequilibria in the uranium and thorium decay chains on burial dose rates in fluvial sediments. *Quat. Geochron.* 15, 751-760.
- Olley, J.M., Caitcheon G.C and Murray A.S. (1998) The distribution of apparent dose as determined by optically stimulated luminescence in small aliquots of fluvial quartz: implications for dating young sediments. *Quat. Sci. Rev. (Quat. Geochron.)*, 17, 1033-1040.
- Pierson J., Forman S.L., Lepper K. and Conley G. (1994) A variable narrow bandpass optically stimulated luminescence system for Quaternary geochronology. *Radiat. Meas.*, 23, 533-535.
- Poolton N.R.J. and Bailiff I.K. (1989) The use of LEDs as an excitation source for photoluminescence dating of sediments. *Ancient TL* 7, 18-20.
- Poolton N.R.J., Bøtter-Jensen L., Wintle A.G., Jakobsen J., Jørgensen F., and Knudsen K.L. (1994a) A portable system for the measurement of sediment OSL in the field. *Radiat. Meas.* 23, 529-532.
- Poolton N.R.J., Bøtter-Jensen L., Ypma P.J.M. and Johnsen O. (1994b) Influence of crystal structure on the optically stimulated luminescence properties of feldspars. *Radiat. Meas.* 23, 551-554.
- Poolton N.R.J., Bøtter-Jensen L. and Duller G.A.T. (1995a) Thermal quenching of luminescence processes in feldspars. *Radiat. Meas.* 24/1, 57-66.
- Poolton N.R.J., Bøtter-Jensen L. and Johnsen O. (1995b) Thermo-optical properties of optically stimulated luminescence in feldspars. *Radiat. Meas.*, 24, 531-534.
- Poolton N.R.J., Bøtter-Jensen L. and Jungner H. (1995c) An optically stimulated luminescence study of porcelain related to radiation dosimetry. *Radiat. Meas.* 24, 543-549.
- Poolton N.R.J., Bøtter-Jensen L., Wintle A.G., Ypma P.J., Knudsen K.L., Mejdahl V., Mauz B., Christiansen H.E., Jakobsen J., Jørgensen F. and Willumsen F. (1996) A scanning system for measuring the age-related luminescence of split sediment cores. *Boreas*, 195-207.
- Poolton N.R.J., Bøtter-Jensen L. and Johnsen O. (1996) On the relationship between luminescence excitation spectra and feldspar mineralogy. *Radiat. Meas.* 26, 93-101.
- Poolton N.R.J., Bøtter-Jensen L. and Johnsen (1997) A search for IRSL-active dosimeters with enhanced sensitivity: a spectroscopic survey. *Radiat. Meas.* 27, 279-290.
- Prescott J.R. and Stephan L.G. (1982) Contribution of cosmic radiation to environmental dose. *PACT* 6, 17-25.
- Prescott J.R. and Hutton J.T. (1988) Cosmic ray and gamma ray dosimetry for TL and ESR. *Nucl. Tracks Radiat. Meas.* 14, 223-227.

- Prescott J.R., Fox P.J., Akber R.A. and Jensen H.E. (1988) Thermoluminescence emission spectrometer. *Appl. Phys.* **27**, 16, 3496-3502.
- Prescott J.R., Akber R.A. and Gartia R.K. (1990) Three-dimensional thermoluminescence spectroscopy of minerals. In: *ACS Symposium Series (415). Spectroscopic Characterization of Minerals and their Surfaces* (eds. Coyne L.M., McKeever S.W.S. and Blake D.F.) 180-189. American Chemical Society, Washington D.C.
- Richardson, C.A. (1993). Effects of bleaching on the sensitivity to dose of the infra-red stimulated luminescence of potassium-rich feldspars from Ynyslas, Wales. *Radiation Measurements* **23**, 587-591.
- Rees-Jones J., Hall S.J.B. and Rink W.J. (1997) A laboratory inter-comparison of quartz optically stimulated luminescence (OSL) results. *Quat. Sci. Rev. (Quat. Geochr.)* **16**, 275-280.
- Rendell H.M., Townsend P.D., Wood R.A. (1994). Thermal treatment and emission spectra of TL from quartz. *Radiat. Meas.* **23**, 441-449.
- Rhodes E.J. (1988) Methodological considerations in the optical dating of quartz. *Quat. Sci. Rev.* **7**, 359-400.
- Rhodes E.J. (1990) Optical dating of quartz sediments. Unpublished D.Phil. thesis, University of Oxford.
- Rhodes E.J. and Pownall L. (1994) Zeroing of the OSL signal in quartz from young glaciofluvial sediments. *Radiat. Meas.* **23**, 581-585.
- Rieser U., Kriebetcheck M.R. and Stolz W. (1994) CCD-camera based high sensitivity TL/OSL-spectrometer. *Radiat. Meas.* **23**, 523-528.
- Roberts R., Walsh G., Murray A.S., Olley J., Jones R., Morwood M., Tuniz C. Lawson E., Macphail M., Bowdery D. and Naumann I. (1997) Luminescence dating of rock art and past environments using mudwasp nests in northern Australia. *Nature* **387**, 696-699.
- Sainamthip P. and Reed J.S. (1989) Glazes for fast-fired wollastonite wall tile. *Ceramic Bulletin* **68** 103-106.
- Smith B.W., Aitken M.J., Rhodes E.J., Robinson P. and Geldard D.M. (1986) Optical dating: Methodological aspects. *Radiat. Prot. Dosim.* **17**, 229-233.
- Smith B.W., Rhodes E.J., Stokes S., Spooner N.A. and Aitken M.J. (1990) Optical dating of sediments: initial results from Oxford. *Archaeometry* **32**, 19-31.
- Smith B.W., Wheeler G.C.W.S., Rhodes E.J. and Spooner N.A. (1991) Luminescence dating of zircon using an imaging photon detector. *Nucl. Tracks Radiat. Meas.* **18**, 273-278.
- Smith B.W. and Rhodes E.J. (1994) Charge movements in quartz and their relevance to optical dating. *Radiat. Meas.* **23**, 329-333.
- Spooner N.A., Prescott J.R. and Hutton J.T. (1988) The effect of illumination wavelength on the bleaching of thermoluminescence (TL) of quartz. *Quat. Sci. Rev.* **7**, 325-330.
- Spooner N.A., Aitken M.J., Smith B.W., Franks M. and McElroy C. (1990) Archaeological dating by infrared stimulated luminescence using a diode array. *Radiat. Prot. Dosim.* **34**, 83-86.
- Spooner N.A. and Questiaux D.G. (1990) Optical dating - Achenheim beyond the Eemian using green/infrared stimulation. In *Synopsis from a Workshop on Long and Short Range Limits in Luminescence Dating*, Oxford, April 1989. RLAHA Occasional Publication Publication No. 9, 97-103.
- Spooner N.A. (1994) On the optical dating signal from quartz. *Radiat. Meas.* **23**, 2/3, 593-600.
- Stoneham D. and Stokes S. (1991). An investigation of the relationship between the 110°C TL peak and optically stimulated luminescence in sedimentary quartz. *Nucl. Tracks Radiat. Meas.* **18**, 119-123.

- Strickertsson K. and Murray A.S. (1998) Optically stimulated luminescence dates for late Pleistocene and Holocene sediments from Nørre Lyngby, Northern Jutland, Denmark. *Quat. Sci. Rev. (Quaternary Geochronology)* **18**, 169-178.
- Sunta C.M., Yoshimura E.M., and Okuno E. (1994a). Sensitization and supralinearity of CaF<sub>2</sub>: natural thermoluminescence phosphor. *Phys. Stat. Sol. (a)* **142**, 253-64.
- Sunta C.M., Yoshimura E.M., and Okuno E. (1994b). Supralinearity and sensitisation factors in thermoluminescence. *Radiat. Meas.* **23**, 655-666.
- Sunta C.M., Yoshimura E.M., and Okuno E. (1994c). Supralinearity and sensitization of thermoluminescence .Part I: A theoretical treatment based on an interactive trap system., *J. Phys. D: Appl. Phys.* **27**, 852-860.
- Tavcar A., Kosec M., Prelec M. and Kolar D. (1990): Microstructural, mechanical and electrical properties of zircon porcelain. *Br. Ceram. Trans. J.* **89** 135-138
- Telfer D.J. and Walker D. (1975) Optical detection of Fe<sup>3+</sup> in lunar plagioclase. *Nature* **258**, 694-695.
- Templer R. and Walton A. (1983) Image intensifier studies of TL in zircons. *PACT* **9**, 299-308.
- Templer R.H. (1985) The localised transition model of anomalous fading. *Radiat. Prot. Dosim.* **17**, 493-497.
- Tkalcec E., Prodanovic D., Falz W. and Hennicke H.W. (1984): Microstructure and properties of aluminous electrical porcelain doped with talc. *Br. Ceram. Trans. J.* **83** 76-80
- Visocekas R. (1993) Tunnelling radiative recombination in K-feldspar sanidine. *Nucl. Tracks Radiat. meas.* **21**, 175-178.
- Wieser A., Egersdörfer S., Koshta A.A. and Romanyukha A.A. (1999) Dose reconstruction in tooth enamel by deconvolution of the EPR spectrum. *Appl. Radiat. Isotop.* (in press).
- White W.B., Matsumura M., Linnehan D.G., Furukawa T. and Chandrasekhar B.K. (1986) Absorption and luminescence of Fe<sup>3+</sup> in single-crystal orthoclase. *American Mineralogist* **71**, 1415-1419.
- Wintle A.G. (1973) Anomalous fading of thermoluminescence in mineral samples. *Nature* **245**, 143-144.
- Wintle A.G. (1974) Factors determining the thermoluminescence of chronologically significant materials. Unpublished D-Phil. Thesis. University of Oxford.
- Wintle A.G. (1975) Thermal quenching of thermoluminescence in quartz. *Geophys. J.R. Astr. Soc.* **41**, 107-113.
- Wintle A.G. and Huntley D.J. (1980) Thermoluminescence dating of ocean sediments. *Canadian Journal of Earth Sciences*, **17**, 348-360.
- Wintle A.G. and Murray A.S. (1997) The relationship between quartz thermoluminescence, photo-transferred thermoluminescence, and optically stimulated luminescence. *Radiat. Meas.* **27**, 611-624.
- Wintle A.G. (1997) Luminescence dating: Laboratory procedures and protocols. *Radiat. Meas.* **27**, 769-817.
- Wintle A.G. and Murray A.S. (1998) Towards the development of a preheat procedure for OSL dating. *Radiat. Meas* **29**, 81-94.
- Wintle A.G. and Murray A.S. (1999) Luminescence sensitivity changes in quartz. *Radiat. Meas.* **30**, 107-118.
- Yang X. H. and McKeever S.W.S. (1990). The pre-dose effect in crystalline quartz, *J. Phys. D: Appl. Phys.* **23**, 237-244.



Title and authors

Development of Optically Stimulated Luminescence Techniques using Natural Minerals and Ceramics, and their Application to Retrospective Dosimetry

Lars Bøtter-Jensen

ISBN		ISSN	
87-550-2755-5		0106-2840	
87-550-2756-3 (Internet)			
Department or group		Date	
Nuclear Safety Research and Facilities Department		September 2000	
Pages	Tables	Illustrations	References
185	13	112	206

Abstract (max. 2000 characters)

This thesis summarises research and development of optically stimulated luminescence (OSL) and its applications by the author at Risø National Laboratory, up to 1999. These developments have been directed primarily at retrospective accident dosimetry and luminescence dating. Experimental investigations include the studies of OSL properties of the natural minerals quartz and feldspars and the artificial materials porcelain and aluminium oxide ( $\text{Al}_2\text{O}_3$ ).

Blue light emitting diodes and infrared laser diodes are shown to provide simple and practical alternatives to broad-band light and visible laser stimulation. The development of OSL apparatus designed for the rapid measurement of single grains of phosphors also opens up a new area of luminescence measurement, allowing the detailed examination of dose distributions within a multiple-grain sample. This is of particular importance to the studies of incompletely reset geological sediments, and to accident dosimetry measurements using unheated materials.

$\text{Al}_2\text{O}_3\text{:C}$  single crystals are tested as environmental OSL dosimeters for assessing both the natural background photon radiation dose rates in the field and the natural dose rates inside bricks collected for accident dose evaluation. Environmental doses of the order of few  $\mu\text{Gy}$  are measured with high precision. UV photo-stimulated luminescence spectra obtained from porcelain samples are used to confirm that the main component responsible for the OSL signal from porcelain is  $\text{Al}_2\text{O}_3$ .

OSL single-aliquot regenerative-dose (SAR) techniques are used with quartz extracted from Chernobyl bricks to determine the accrued dose after the accident. This has improved the measurement precision significantly, from about 5-6 % using traditional methods to now less than 2 %. Depth-dose profiles measured in Chernobyl bricks are compared with those obtained in the laboratory using different gamma sources and these comparisons show that the average energy of the accident radiation was lower than that of  $^{137}\text{Cs}$  photons. It is further demonstrated that doses lower than 50 mGy can be measured using the SAR method with a precision in the order of 2 %.

This thesis was submitted to the University of Copenhagen in September 1999.